

# Remote synchronization method for the quasi-zenith satellite system

**Author:**

Tappero, Fabrizio

**Publication Date:**

2008

**DOI:**

<https://doi.org/10.26190/unsworks/19360>

**License:**

<https://creativecommons.org/licenses/by-nc-nd/3.0/au/>

Link to license to see what you are allowed to do with this resource.

Downloaded from <http://hdl.handle.net/1959.4/41467> in <https://unsworks.unsw.edu.au> on 2024-05-05

THE UNIVERSITY OF NEW SOUTH WALES

SCHOOL OF SURVEYING  
&  
SPATIAL INFORMATION SYSTEMS

**Remote Synchronization Method  
for the Quasi-Zenith Satellite  
System**

**Fabrizio Tappero**

A thesis submitted to the University of New South Wales  
for the degree of Doctor of Philosophy

April 2008

*Supervisors:* A/Prof. Andrew G. Dempster  
Dr. Toshiaki Iwata

## **Note From the Author**

© 2008 Fabrizio Tappero and the University of New South Wales. The research presented in this dissertation is the result of an intensive research collaboration between the School of Surveying & Spatial Information Systems, University of New South Wales, Sydney Australia and the Space Technology Research Group at the National Institute of Advanced Industrial Science and Technology (AIST), Tsukuba, Japan. Fabrizio Tappero's PhD dissertation is the compendium of the research activity that took place within this research collaboration. Accordingly, the following dissertation is concerned with his research work from 2004 onwards. Research activities derived from this same research project by others, colleagues or collaborators, is intentionally omitted from the main text of the thesis or, where necessary, it is referenced. Furthermore, the originality and ownership of Tappero's contribution is proven by the published material he wrote as part of the research activity. A significant part of Tappero's PhD work, being based on a collaborative activity, draws upon the research effort of other AIST employees and Japanese companies which have been involved, as contractors, in the development of related hardware and/or software. This manuscript was typeset in 11pt Times with L<sup>A</sup>T<sub>E</sub>X.

*dedicated to my dear friend Atsuko*

# Acknowledgments

I want to thank Dr. Yoshiyuki Abe, Prof. Giovanni Maizza and Prof. Mauro Boero for the technical and personal support they have provided to me through the past eight years. The advice and assistance they have given me as colleagues and as friends have been immensely useful for the development of my research career as well as for my personal life.

I would also like to thank my former boss, Dr. Toshiyaki Iwata and my supervisor A/Prof. A. G. Dempster for the technical support and experienced advice they have given me throughout the development of this research work.

Fabrizio Tappero

# Abstract

This dissertation presents a novel satellite timekeeping system which does not require on-board atomic clocks as used by existing navigation satellite systems such as GPS, GLONASS or the planned GALILEO system. This concept is differentiated by the employment of a synchronization framework combined with lightweight steerable on-board clocks which act as transponders re-broadcasting the precise time remotely provided by the time synchronization network located on the ground. This allows the system to operate optimally when satellites are in direct contact with the ground station, making it suitable for a system like the Japanese Quasi-Zenith Satellite System, QZSS. Low satellite mass and low satellite manufacturing and launch cost are significant advantages of this novel system.

Two possible implementations of the time synchronization network for QZSS are presented. Additionally, the problem of satellite communication interruption is analyzed and a solution is presented. Finally a positioning and timing quality analysis, aimed to provide understanding of the actual timing quality requirements for QZSS, is presented.

# Contents

<b>List of Acronyms</b>	<b>xiv</b>
<b>1 Introduction</b>	<b>1</b>
1.1 Global Navigation Satellite Systems . . . . .	1
1.1.1 GPS and Satellite On-Board Timing . . . . .	3
1.1.2 Quasi-Zenith Satellite System . . . . .	5
1.2 Motivation of This Study . . . . .	7
1.3 Research Objective and Contribution . . . . .	8
1.4 Structure of This Dissertation . . . . .	10
1.5 Keywords . . . . .	12
<b>2 Timekeeping in Satellite and Navigation Systems</b>	<b>13</b>
2.1 Purpose of this Review . . . . .	13
2.2 Global Navigation Satellite Systems . . . . .	14
2.2.1 Global Positioning System, GPS . . . . .	14
2.2.2 GLONASS . . . . .	22
2.2.3 GALILEO . . . . .	24
2.3 Quasi-Zenith Satellite System, QZSS . . . . .	28
2.3.1 Introduction . . . . .	28
2.3.2 Overview of QZSS . . . . .	29
2.4 MILSTAR Communications System . . . . .	36
2.4.1 DFS-1 and DFS-2 Clock Performance . . . . .	38
2.4.2 Autonomous Synchronization . . . . .	39
2.4.3 Final Remarks . . . . .	42
2.5 Two-way Satellite Time and Frequency Transfer System . . . . .	43
2.5.1 Two-Way Satellite Time and Frequency Transfer Theory . . . . .	43
2.5.2 Influence of Satellite Motion on TWSTFT . . . . .	45
2.5.3 Dynamic Two-way Time Transfer . . . . .	48
2.6 Final Remarks and Summary . . . . .	49
<b>3 RESSOX System</b>	<b>53</b>
3.1 Introduction . . . . .	54
3.2 The RESSOX System . . . . .	58
3.2.1 Structure and Functioning . . . . .	58
3.2.2 Transmitting Time Adjuster (TTA) . . . . .	60

3.2.3	PN Code Generator . . . . .	61
3.2.4	QZS Signal Receiver . . . . .	61
3.2.5	VCXO . . . . .	61
3.2.6	Time Comparator . . . . .	62
3.3	Delays and Error Estimation Models . . . . .	62
3.3.1	Delays at the Ground Station and in the QZS . . . . .	63
3.3.2	Delay in the Troposphere . . . . .	64
3.3.3	Delay in the Ionosphere . . . . .	65
3.3.4	Satellite Orbit Estimation Error . . . . .	68
3.3.5	Geometric Delay . . . . .	72
3.3.6	Relativistic Effect . . . . .	73
3.4	Ground Station . . . . .	75
3.5	RESSOX Feedback/Feed-forward Development . . . . .	76
3.5.1	Introduction . . . . .	76
3.5.2	TTA and UDS Behavior . . . . .	76
3.5.3	Time Synchronization Performance . . . . .	79
3.5.4	L1/L2/L5 Error Adjustment . . . . .	80
3.6	Conclusions . . . . .	83
<b>4</b>	<b>Remote Timekeeping System</b>	<b>85</b>
4.1	Introduction . . . . .	85
4.2	Remote Timekeeping System for QZSS . . . . .	87
4.2.1	RESSOX Architecture and its Limitations . . . . .	87
4.2.2	Remote Timekeeping System . . . . .	88
4.2.3	TWSTFT Method for QZSS . . . . .	89
4.2.4	Additional Note About TWSTFT Delay . . . . .	90
4.3	Remote Timekeeping System Design . . . . .	90
4.3.1	Ground Station Atomic Reference . . . . .	92
4.3.2	Telemetry Interface Blocks . . . . .	93
4.3.3	Voltage-Controlled Crystal Oscillator (VCXO) . . . . .	93
4.3.4	Phase-Error Measurement . . . . .	94
4.3.5	RTKS Loop Controller . . . . .	96
4.3.6	RTKS Scheme . . . . .	102
4.4	Long-term Stability of RTKS . . . . .	110
4.5	Conclusions . . . . .	111
<b>5</b>	<b>QZSS Satellite Communication Interruption</b>	<b>115</b>
5.1	Introduction . . . . .	116
5.2	Optimal Clock Prediction . . . . .	117
5.3	Clock Synchronization Network . . . . .	118
5.3.1	Atomic Reference . . . . .	119
5.3.2	Telemetry Interface, Modem Transmitter and Communication Blocks . . . . .	119
5.3.3	Closed-Loop VCXO Controller . . . . .	119
5.3.4	Voltage-Controlled Crystal Oscillator (VCXO) . . . . .	119
5.4	VCXO Indirect Phase Drift Prediction . . . . .	120

5.4.1	The $CV_{apr}(m)$ Array and Its Structure . . . . .	123
5.4.2	The Matrix $\overline{CV}_{apr}(m, h)$ and Its Structure . . . . .	123
5.4.3	Construction of the Free-run VCXO Voltage, $V'_{apr}(t)$ . . . . .	126
5.4.4	Choice of the Coefficients $K_n$ . . . . .	127
5.4.5	Algorithm Performance . . . . .	129
5.5	VCXO Phase Compensation, Experimental Results . . . . .	131
5.5.1	Closed-loop Case . . . . .	132
5.5.2	Open-loop Case . . . . .	132
5.5.3	On-board Computer Requirements . . . . .	133
5.6	Hardware-in-the-loop Experiment . . . . .	134
5.6.1	Experimental Setup . . . . .	134
5.6.2	Free-run Experiment . . . . .	135
5.7	Simulation Results and Conclusions . . . . .	136
<b>6</b>	<b>RESSOX and RTKS, Positioning Quality and Timing</b>	<b>141</b>
6.1	Introduction . . . . .	142
6.2	RESSOX/RTKS Software Simulator . . . . .	143
6.3	Constant Phase Error . . . . .	144
6.3.1	RESSOX/RTKS Hardware Simulator . . . . .	148
6.4	Satellite Communication Interruption . . . . .	152
6.4.1	QZSS Satellite On-board VCXO Model . . . . .	152
6.5	Positioning Performance Analysis . . . . .	154
6.5.1	Experiment One: Long-term Study . . . . .	155
6.5.2	Experiment Two: Short-term Study . . . . .	156
6.6	Results and Conclusions . . . . .	158
<b>7</b>	<b>Regional Synchronized GNSS</b>	<b>163</b>
7.1	Introduction . . . . .	163
7.2	Regional Synchronized GNSS . . . . .	164
7.2.1	Orbit Design and LEO Satellite Visibility . . . . .	164
7.2.2	LEO Satellite Velocity and Doppler Shift . . . . .	166
7.2.3	Advantages of the Proposed System . . . . .	167
7.3	Experimental Synchronization Payload . . . . .	168
7.3.1	Host Satellite, ALMASat-I . . . . .	168
7.3.2	Payload and Ground Station Synchronization Test . . . . .	170
7.4	Conclusions . . . . .	170
<b>8</b>	<b>Conclusions and Future Works</b>	<b>173</b>
8.1	The Context of the Results . . . . .	173
8.2	Summary of the Results . . . . .	174
8.3	Regional Synchronized GNSS . . . . .	177
8.4	Future Work . . . . .	177

---

<b>A Appendix - RESSOX/RTKS Hardware Simulator</b>	<b>179</b>
A.1 RESSOX/RTKS Hardware Simulator . . . . .	179
A.1.1 Transmitting Timing Adjuster and Timing Controller . . . . .	180
A.1.2 Modems (PN-Code Generator and Time Comparator) . . . . .	181
A.1.3 Uplink Delay Simulator (UDS) . . . . .	182
A.1.4 QZS Signal Generator and Controller . . . . .	183
A.1.5 QZS Signal Receiver and Controller . . . . .	183
A.1.6 VCXO . . . . .	184
A.1.7 Time Interval Counter (TIC) . . . . .	184
A.1.8 VCXO Controller Interface . . . . .	185
A.1.9 Additional Note . . . . .	185
A.1.10 Contribution from the Author . . . . .	186
<b>B Appendix - RESSOX/RTKS Software Simulator</b>	<b>187</b>
B.1 RESSOX/RTKS Software Simulator . . . . .	187
B.1.1 RTKSsim Structure . . . . .	187
B.1.2 Satellite Trajectory Generator - SatTrjGen . . . . .	192
B.1.3 Pseudorange Generator - PseudoGen . . . . .	195
B.1.4 Positioning Generator - PosGen . . . . .	197
B.1.5 How to Run RTKSsim . . . . .	201
B.1.6 VCXO TKS Controller Implementation . . . . .	201
B.1.7 RTKSsim Tool Used for Subsystem Development . . . . .	203
B.1.8 Contribution from the Author . . . . .	203
<b>C Appendix - Feedback Interruption, Experimental Results</b>	<b>205</b>



# List of Acronyms

AIST	National Institute of Advanced Industrial Science and Technology
ATC	Adaptive Time Constant
BPF	Band Pass Filters
CAN	Controller Area Network
C/A	Course/Acquisition
CDMA	Code Division Multiple Access
CS	Control Segment
Cs	Cesium
DoD	US Department of Defence
DTWTT	Dynamic Two-Way Time Transfer
EGNOS	European Geostationary Navigation Overlay Service
EQM	Engineering Qualification Model
ERD	Estimated range deviation
ESA	European Space Agency
EU	European Union
FDMA	Frequency Division Multiple Access
FIR	Finite Impulse Response
FM	Flight Model
GDOP	Geometric Dilution of Precision
GJU	GALILEO Joint Undertaking
GLONASS	Global'naya Navigatsionnaya Sputnikovaya Sistema
GNSS	Global Navigation Satellite System
GPIB	General Purpose Interface Bus
GPS	Global Positioning System
GSTB	GALILEO System Test Bed
HEO	High Earth Orbit
HP	High Precision
IGS	International GPS Service
JAXA	Japan Aerospace Exploration Agency
L1C	L1 Civil
L2C	L2 Civil
LSB	Least Significant Bit

MA	Moving Average
MCS	Master Control Station
MDU	Mission Data Unit
MEO	Medium Earth Orbit
MS	Monitoring Stations
MSAS	MTSAT Satellite-Based Augmentation System
MTSAT	Japanese Multifunctional Transport Satellites
NAVSTAR	Navigation System with Timing And Ranging
NICT	National Institute of Information and Communications Technology
NIST	National Institute of Standards and Technology
NSC	Non-Standard Code
OVCXO	Oven Voltage-Controlled Crystal Oscillator
PFM	Proto-Flight Mode
PHM	Passive Hydrogen Maser
PD	Proportional Derivative
PI	Proportional Integral
PLL	Phase-Locked Loop
PN	Pseudo Noise
PPM	Pulse Per Minute
PRN	Pseudo Random Noise
QZS	Quasi-Zenith Satellite
QZSS	Quasi-Zenith Satellite System
RAFS	Rubidium Atomic Frequency Standard
Rb	Rubidium
RESSOX	Remote Synchronization System for the On-Board Crystal Oscillator
RMS	Root Mean Square
RNSS	Regional Navigation Satellite System
RTKS	Remote Timekeeping System
SA	Selective Availability
SADBCE	SA Database Control Element
SBAS	Satellite-Based Augmentation Systems
S/C	Spacecraft
SIS	Signal In Space
SMC	Serial Magnitude Command
SP	Standard Precision
SV	Space Vehicle
SVN	Space Vehicle Number
TAI	International Atomic Time
TCS	Tracking Control Station
TIC	Time Interval Counter
TKS	Timekeeping System
TMS	Time Management Station
TTA	Transmitting Timing Adjuster

---

TWSTFT	Two-Way Satellite Time and Frequency Transfer
TWTT	Two-Way Time Transfer
UDS	Uplink Delay Simulator
UHF	Ultra-High Frequency
US	United States
UTC	Coordinated Universal Time
VCXO	Voltage-Controlled Crystal Oscillator
WAAS	Wide Area Augmentation System

# List of Figures

1.1	Frequency stability comparison of a typical space-borne Rb clock and a space-borne VCXO. . . . .	3
2.1	GPS Block IIR timekeeping system [88]. . . . .	16
2.2	Ranking of GPS clocks by Hadamard deviation (The Hadamard Variance is a 3-sample variance with binomially-weighted coefficients that is similar to the 2-sample Allan Variance) for one day (Q1-2002) [29]. . . . .	20
2.3	GPS II/IIA ERD January 2001 through April 2002 [29]. . . . .	21
2.4	Picture of the GSTB-V2 RAFS [37]. . . . .	25
2.5	Allan deviation obtained from all signals using GUSN station for RAFS-FM4 clock on board GIOVE-A, [45]. . . . .	26
2.6	Engineering Model of GALILEO Passive Hydrogen Maser (PHM) atomic clock [36]. . . . .	27
2.7	Quasi-Zenith Satellite System (QZSS) overview [65]. . . . .	29
2.8	QZSS orbital ground track. . . . .	31
2.9	QZS elevation and azimuth (26.12.2009, 12:00 UTC) for several major Asian cities [65]. . . . .	32
2.10	Relative velocity of signals for several cities (26.12.2009 12:00 UTC) [65]. Data outages are due to satellite visibility issues. . . . .	33
2.11	Variation of QZS elevation angle for several major cities (26.12.2009 12:00 UTC) [65]. . . . .	35
2.12	Average number of QZS that can be seen at an elevation angle of 10 deg or more [65]. . . . .	36
2.13	a) Raw time-offset history of the crystal oscillator onboard DFS-1 (thick line). b) Raw time-offset history of the Rb atomic clock onboard DFS-2 (thick line). Thin lines correspond to least squares quadratic fits to the data, and minor divisions of the horizontal axis correspond to seven day intervals [42]. . . . .	38
2.14	Allan deviation, $\sigma_y(\tau)$ , versus averaging time, for the DFS-1 crystal oscillator (gray) and the DFS-2 Rb atomic clock (black). The short dashed curve is the anticipated $\sigma_y(\tau)$ based on satellite to ground-station time-transfer noise and the Rb clock's random-walk of frequency noise. The long dashed line corresponds to the crystal oscillator's random-walk noise [42]. . . . .	40

2.15	Raw time-offset of the DFS-1 crystal oscillator (black line) while it was slaved to the DFS-2 Rb atomic clock. The thin curve is a least squares quadratic fit to the data [42]. . . . .	41
2.16	Raw time-offset measurements of the DFS-1 crystal oscillator clock (filled circles) and the DFS-2 Rb atomic clock (open circles) by the same ground station. The solid line is a quadratic fit to all the data [42].	42
2.17	Basic two-way time transfer method [110]. . . . .	44
2.18	Schematic view of the positions of an Earth station (E) and a non-geostationary satellite (S1 and S2) moving counterclockwise around the Earth [129]. . . . .	47
2.19	DTWTT performance in the test flight described in [25]. . . . .	50
3.1	RESSOX system. The QZSS works as complementary system for the present GPS and also provides augmentation features. . . . .	55
3.2	Conceptual comparison of the GPS Block-IIR (a) and a remote synchronization scheme (b) where no on-board atomic clock is used. . . .	56
3.3	RESSOX system, basic schematic. . . . .	58
3.4	Flowchart of double RESSOX control. The orbit calculation and the delay calculations are used to drive the feed-forward control through the TTA. The feedback control is used to refine the correction signal, taking advantage of the feedback time information available at the QZS signal receiver. . . . .	60
3.5	Delay due to the troposphere vs the satellite elevation angle $E$ ( $5 < E < 90$ ). The meteorological conditions considered here are temperature=15 °C, humidity=70 % and atmospheric pressure=1013 hPa. The implemented models and mapping functions shown here are the Saastamoinen model (SA), Hopfield model (HP), Marini & Murrain mapping function (MM), Niell mapping function (NM) and the Saastamoinen mapping function (SM). Under the above conditions, all implemented models give the same result. Location: Tsukuba, Japan. . . . .	65
3.6	Delay due to the troposphere during a one-day simulation. The simulation date was January 1 <sup>st</sup> 2000. Location: Tsukuba, Japan. . . . .	66
3.7	Ionosphere electron content distribution. The simulation starting date was January 1 <sup>st</sup> 2000 at 23:59. . . . .	67
3.8	Delay due to the ionosphere during a one-day simulation. The simulation start date was January 1 <sup>st</sup> 2000. Uplink Ku band, 14 GHz signal, location: Tsukuba, Japan. The visible discontinuities are due to the 2 hour sampling in the original data downloaded from the Centre of Orbit Determination (CODE) website [2]. The no-data region is due to a 5 deg threshold cut off implemented in the QZS orbit simulator. . . . .	67
3.9	Error introduced by the two geopotential models (JGM3, EGM96) employed in the simulator. Some different grades of approximations were tested: 2X2, 6X6, 8X8, 10X10, 12X12. Results are for a two-day simulation, start date January 1 <sup>st</sup> 2000. . . . .	69

3.10	Error contributions for the third-body forces of Sun, Moon and other planets on the satellite orbit estimated for a two-day simulation. The simulation start date was January 1 <sup>st</sup> 2000. . . . .	70
3.11	Error introduced by the effect of the solar radiation pressure on the satellite orbit. The simulation start date was January 1 <sup>st</sup> 2000. . . . .	71
3.12	Error introduced by the variation of the Earth's gravitational field due to the tidal deformation of the Earth's shape caused by the gravitational effect of the Moon and Sun. The simulation start date was January 1 <sup>st</sup> 2000. . . . .	72
3.13	(a) Representation of the cause of the delay due to the QZS speed (geometric delay). (b) Simulated results of the geometric delay during a period of 26 hours. The no-data region is due to a 5 deg threshold cut off implemented in the QZS orbit simulator. The simulation start date was January 1 <sup>st</sup> 2000. Location: Tsukuba, Japan. . . . .	73
3.14	a) QZS elevation angle and b) geometric range for a ground station located on the Marshall Islands (geodetic latitude= 8.7 deg north, longitude=167.7 deg east). The simulation is relative to one complete orbital period (24 hours). . . . .	76
3.15	Hardware setup for testing the performance of the TTA and the UDS for different values of the imposed time delay $a$ . . . . .	77
3.16	a) Time difference variation, over two channels, during a 700 s period when the value of $a$ is equal to 0. b) Allan deviation of the time difference variation of channel 1. Refer to the experimental setup of Fig. 3.15. . . . .	78
3.17	Variation of the time difference due to the variation of $a$ . Refer to the experimental setup of Fig. 3.15. . . . .	79
3.18	a) $UTC_{phase} - VCXO_{phase}$ when the proportional control on the satellite side is active. b) VCXO input voltage. The experiment is relative to a 25 minutes period. . . . .	80
3.19	Synchronization performance of the RESSOX feedback/feed-forward system. a) Overall synchronization error over 90000 s (25 hours). b) Allan deviation of the synchronization error. The dashed line indicates the $\sigma = 2$ ns white noise. . . . .	83
4.1	Simplified version of the RESSOX synchronization scheme. . . . .	87
4.2	Simplified version of the RTKS synchronization scheme. . . . .	89
4.3	Two-way satellite time and frequency transfer scheme for QZSS. . . . .	90
4.4	QZSS TWSTFT apparatus and its delays. . . . .	91
4.5	RTK Phase-Locked Loop. . . . .	91
4.6	Frequency stability of the Anritsu hydrogen maser RH401A and frequency stability of the Cs. Agilent 5071A, now Symmetricom 5071A (planned QZSS ground station clock). Curves are generated accordingly to the specification sheet of both clocks. . . . .	92
4.7	Schematic of the RTKS combined with the TWSTFT infrastructure. . . . .	93

4.8	Frequency stability (Allan deviation) of the VCXO Oscilloquartz 8607-BM measured against two different reference clocks, the Anritsu hydrogen maser RH401A and an VCXO with similar quality as the 8607-BM. Manufacture's curve is also provided. . . . .	95
4.9	Mathematical model for the locked state of the RTKS PLL . . . . .	99
4.10	RTKS PLL response to a 20 ns phase error step. . . . .	101
4.11	RTKS PLL response to a 50 ns phase error step when four different delay scenarios are considered. 1 epoch is equivalent to 1 s delay. . . . .	102
4.12	Five cases of RTKS PLL settling time versus the length of the delay introduced to the PLL. This particular case refers to a 50 ns phase step. Straight line segments represent the linear fit. . . . .	103
4.13	a) VCXO phase error over 1000 s when different length N of optimally unbiased MA filters are used. b) Average absolute VCXO phase error as a function of the optimally unbiased MA filter length. . . . .	104
4.14	Experimental measured phase error of the RTKS VCXO, Oscilloquartz 8607-BM, when left uncontrolled for 300 s. . . . .	105
4.15	A) Oven VCXO phase error over 9000 s for different lengths N of optimally unbiased MA filters. At t=1000 s a linear phase drift is introduced in to the RTKS loop. . . . .	106
4.16	VCXO phase error settle (phase error within 0.5 ns) time versus optimum Moving Average length N. The two lines show the settle time of the GPS TKS for the two modes, slow-loop mode and fast-loop mode. . . . .	108
4.17	QZSS RTKS schematic. . . . .	109
4.18	Modified version of the RESSOX Hardware Simulator for testing of the RTKS PI filter. . . . .	111
4.19	A) Frequency stability of the uncontrolled VCXO Oscilloquartz 8607-BM measured against two different reference clocks, the Anritsu hydrogen maser RH401A and an VCXO with similar quality as the 8607-BM. Manufacture's curve is also provided. as in Fig. 4.8. B) Allan deviation for the long-term stability of the RTKS VCXO when the Cs atomic clock and the hydrogen maser were used as references. Stability at 100,000 s was less than $10^{-14}$ . . . . .	112
5.1	Simplified representation of the RTKS for the remote synchronization of QZSS clocks. . . . .	118
5.2	Method to generate the the approximation curves $CV_{apr}(n)$ . Out of the $t_c$ available samples, a sub-series of them is used to produce approximation curves using the Least Square Method. . . . .	121
5.3	Three examples (a, b and c) of VCXO phase error compensation. The algorithm presented has been implemented as a non real-time routine and applied to the phase error shown in Fig. 5.11. Three feedback interruptions have been simulated and 100,000 past samples have been used to create the vector $CV_{apr}(m)$ and then used to steer the VCXO without feedback. The overall phase error was kept below about 2 ns for feedback interruptions of up to 1 h in length. . . . .	124

5.4	a) VCXO phase error, and b) VCXO voltage during a closed-loop controlling period of about 50,000 s. . . . .	127
5.5	VCXO voltage and straight line approximations during a closed-loop controlling period. . . . .	128
5.6	Coefficients $K_n$ calculated by the optimum mean value algorithm. . .	129
5.7	Two examples (a and b) of VCXO phase error compensation. The algorithm presented (named CV interpolator) has been compared against the a linear interpolation method. Both methods have been implemented as a non real-time routine and applied to the phase error shown in Fig. 5.11. Two 36000 s feedback interruptions have been simulated and 100,000 past samples have been used to create the vector $CV_{apr}(m)$ and then used to steer the VCXO without feedback. The linear interpolator method, was able to compensate the VCXO phase error, limiting the overall phase error within 1.5 ns (with an interruption period of 3600s). For the same scenario, the proposed method could limit the VCXO phase error within 0.4 ns (interruption period of 3600 s). . . .	130
5.8	Optimum $V'_{apr}$ . . . . .	130
5.9	Maximum phase error and integral of the phase error for a 3600 s interruption. . . . .	131
5.10	Results of a 20,000 s experiment using the Oscilloquartz VCXO 8607-BM with no PLL feedback control. a) The VCXO phase error when no controlling method is applied. b) The VCXO phase error when the proposed algorithm is applied using the approximation function $CV_{apr}(m)$ . . . . .	133
5.11	Phase error of the VCXO Oscilloquartz 8607-BM left in free-run mode for about 70 hours (250,000 s). After being accurately synchronized (same phase and same frequency) with the atomic standard used as reference, the VCXO has been left to free-run without any control and with a constant voltage of 5.0910 V. . . . .	134
5.12	RESSOX/RTKS Software Simulator with the space-borne Oscilloquartz VCXO 6607-BM and its phase error compensation algorithm embedded in it. . . . .	135
5.13	Sky-view of the simulated scenario for the combined system GPS&QZSS. . . . .	137
5.14	Positioning error of the combined system QZSS&GPS over 5 hours. The QZSS on-board clock is an ideal time reference (no drift assumed). 0 m is the true user position. . . . .	138
5.15	Positioning error of the combined system QZSS&GPS over 5 hours. The QZSS on-board clock is the Oscilloquartz VCXO 6607-BM with no drift control. 0 m is the true user position. . . . .	138
5.16	Positioning error of the combined system QZSS&GPS over 5 hours. The QZSS on-board clock is the Oscilloquartz with drift compensation control. 0 m is the true user position. . . . .	138
6.1	RESSOX/RTKS Software Simulator. . . . .	144

---

6.2	Position calculation results of the RESSOX/RTKS Software Simulator. Four scenarios are considered: GPS-only, and 3 cases where GPS is used together with QZSS with 3 different values of phase shift (0 ns, 20 ns and 50 ns). Data is relative to a simulation started at UTC 23:15, 31st of December 2004, and ending at UTC 08:15, 1st of January 2005. Note the scale for the 50 ns case is considerably larger. . . . .	146
6.3	Position calculation results of the RESSOX/RTKS Software Simulator represented by histograms. Four scenarios are considered: GPS-only and 3 cases where GPS is used together with QZSS with 3 different values of phase shift (0 ns, 20 ns and 50 ns). Data is relative to a simulation started at UTC 23:15, 31st of December 2004, and ending at UTC 08:15, 1st of January 2005. . . . .	147
6.4	Representation of the mean x position (Earth-fixed coordinate system) and its standard deviation for four different level of phase shift (0 ns, 20 ns, 50 ns and 100 ns) over a 9 hour period. The 6.24 m wide dark region centered at 0.52 m represents the GPS-only simulation. . . . .	148
6.5	Schematic of the Hardware Simulator employed to simulate four GPS satellites and one QZS. The two Spirent GSS4730 devices are independently driven by two different time references (a high-stability VCXO and a hydrogen maser). . . . .	149
6.6	Sky-view at the beginning of the 30 minute simulation of the combined GPS and QZSS. Four GPS satellites are combined with one QZSS satellite (QZSS-1). Time : UTC 03:00, 1st of January, 2005. User location, Okinawa, Japan (lat:26.1946 deg, long:127.67763 deg). . . . .	150
6.7	Estimated position data obtained during the three periods of the simulation of the combined GPS&QZSS when the phase shift is 0 ns (case a), 20 ns (case b) and 50 ns (case c). Results were obtained using the RESSOX Hardware Simulator. The simulation length was about 30 minutes. Note the larger scale for the 50 ns case. . . . .	151
6.8	Schematic of the RESSOX/RTKS Software Simulator employed for the evaluation of the positioning performance of GPS plus QZSS when QZSS clocks are controlled by two-state model VCXOs. . . . .	153
6.9	RESSOX/RTKS Software Simulator modified to accommodate the two-state error model used to simulate the on-board QZS clock behavior. . . . .	154
6.10	Allan deviation of the simulated VCXO. The two dark regions represent the Allan deviation of a typical space-borne Rb clock and the Allan deviation of a space-borne VCXO. . . . .	155
6.11	Positioning performance of GPS&QZSS when an ideal RESSOX is employed; no synchronization interruptions. a) The error in north direction over time, b) the error in east direction over time, c) the distribution of the RMS positioning error, and d) the scattering plot. . . . .	156

6.12	Positioning performance of GPS&QZSS when RESSOX is employed and the satellite QZS-3 clock, Fig. 6.13, is left in free running mode. a) The error in north direction over time, b) the error in east direction over time, c) the distribution of the RMS positioning error and d) the scattering plot. . . . .	157
6.13	Sky-view of the GPS plus QZSS scenario. a) Sky-view starting configuration, b) sky-view end configuration. GPS satellites and QZSSs are visible above a 40 deg mask angle. The dark area represents the period (approximately 4h) when the QZS-3 on-board VCXO is left in free-run mode. . . . .	157
6.14	Positioning performance of the GPS&QZSS when an ideal RESSOX is employed; no synchronization interruptions. From top left to bottom right: the northings error sigma over time, the eastings error sigma over time, the RMS positioning error sigma over time and the 2DRMS sigma over time. Values of sigma are calculated using the last 10 minutes worth of data at each time. . . . .	158
6.15	Positioning performance of the GPS&QZSS when RESSOX is employed and the satellite QZS-3 clock is left in free-run mode. From top left to bottom right: the northings error sigma over time, the eastings error sigma over time, the RMS positioning error sigma over time and the 2DRMS sigma over time. Values of sigma are calculated using the last 10 minutes worth of data at each time. . . . .	160
7.1	Simplified bi-dimensional representation of synchronization ground station, user and satellite for the proposed system. . . . .	165
7.2	Australian territory and six ground stations. . . . .	166
7.3	Drawing of the microsatellite ALMASat-I developed by the microsatellite laboratory, in the II School of Engineering, University of Bologna, Italy. . . . .	169
A.1	RESSOX/RTKS Hardware Simulator. . . . .	180
A.2	Block diagram of the TTA. . . . .	181
A.3	Block diagram of the UDS. . . . .	182
A.4	Block diagram of the QZS signal generator. . . . .	183
A.5	Block diagram of the QZS signal receiver. . . . .	184
A.6	VCXO Controller interface running on a standard PC. . . . .	185
A.7	RESSOX/RTKS Hardware Simulator. . . . .	186
B.1	Basic schematic of the RTKSsim Software Simulator. . . . .	188
B.2	Directory structure of RTKSsim. . . . .	190
B.3	Example of SatTrjGen.cnf. . . . .	193
B.4	Example of PseudoGen.cnf. . . . .	196
B.5	RTKSsim graphical user interface, GUI. . . . .	201
B.6	Block scheme of the VCXO TKS developed in ANSI-C. . . . .	202
B.7	Structure of the VCXO RTKS simulator. . . . .	203

# Chapter 1

## Introduction

This study investigates an innovative satellite timekeeping system which does not require on-board atomic clocks as used by existing navigation satellite systems such as Global Positioning System (GPS), the Global'naya Navigatsionnaya Sputnikovaya Sistema (GLONASS), or the planned GALILEO system. This novel concept employs, instead, a synchronization network combined with a lightweight steerable on-board Voltage-Controlled Crystal Oscillator (VCXO). A ground-based synchronization network will keep on-board clocks locked to a master time reference located on the ground. This allows the system to operate optimally when satellites are in direct contact with the ground station, making it suitable for a system such as the Japanese Quasi-Zenith Satellite System (QZSS). Low satellite mass and low satellite manufacturing and launch costs are advantages of this novel system. This thesis presents a feasibility study of the proposed system and will address its practical implementation. This study was carried out in conjunction with the Space Technology Research Group at the National Institute of Advanced Industrial Science and Technology (AIST) in Japan [1].

### 1.1 Global Navigation Satellite Systems

Global Navigation Satellite System (GNSS) is the standard generic term for satellite navigation systems that provide autonomous geo-spatial positioning with global cover-

age. A GNSS allows small electronic receivers to determine their location (longitude, latitude, and altitude) to within a few meters using timing of radio signals transmitted along lines of sight from satellites. A receiver on the ground with a fixed position can also be used to calculate the precise time as a reference for scientific experiments [51].

As of 2008, the United States Navigation System with Timing And Ranging (NAVSTAR) GPS is the only fully operational GNSS. The Russian GLONASS is a GNSS in the process of being restored to full operation. The European Union's GALILEO positioning system is a next generation GNSS in the initial deployment phase and is scheduled to be operational in 2013. China has indicated it may expand its regional BEIDOU navigation system into a global system. India's regional IRNSS, a next generation Regional Navigation Satellite System (RNSS), is in the developmental phase and is scheduled to be operational by approximately 2012.

Early predecessors to these were the ground based DECCA, LORAN and Omega systems, which used terrestrial radio transmitters instead of satellites. These systems broadcast a radio pulse from a known master location, followed by repeated pulses from a number of slave stations. The delay between the reception and transmission of the signal at the slaves was carefully controlled, thereby allowing the receivers to compare the delay between reception and the delay between sending. From this the distance to each of the slaves could be determined, hence providing data to determine a navigation fix.

The first satellite navigation system was Transit, a system deployed by the US military in the 1960s. Transit's operation was based on the Doppler effect: the satellites travelled on well-known paths and broadcast their signals on a known frequency. The received frequency differed slightly from the broadcast frequency because of the movement of the satellite with respect to the receiver. By monitoring this frequency shift over a certain time interval, the receiver could determine its location given a precise knowledge of the satellite's orbit.

Part of an orbiting satellite's broadcast included its precise orbital data. In order to ensure accuracy, the US Naval Observatory (USNO) continuously determined precisely the orbits of these satellites. As a satellite's orbit deviated from the computed one,

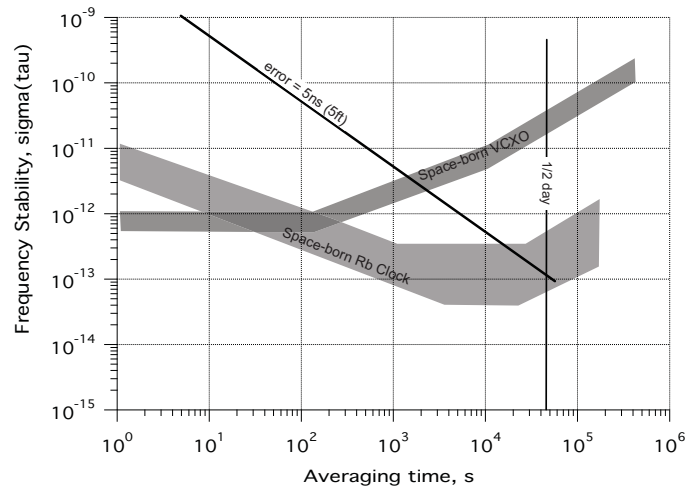


Figure 1.1: Frequency stability comparison of a typical space-borne Rb clock and a space-borne VCXO.

the USNO would send the updated information to the satellite.

Modern systems are more direct [85]. The satellite broadcasts a signal that contains information on the orbit of the satellite and the precise time the signal was transmitted. The position and orbit of the satellite is transmitted in a data message that is superimposed on a code that serves as a timing reference. The satellite uses an atomic clock to maintain synchronization of all the satellites in the constellation. The receiver compares the time of the broadcast encoded in the transmission with the time of reception measured by an internal clock, thereby measuring the time-of-flight to the satellite. Several such measurements can be made at the same time to different satellites, allowing a continual navigation fix to be generated in real-time.

### 1.1.1 GPS and Satellite On-Board Timing

When GPS was conceived, the most difficult technological problem facing the developers was the need to fly accurate timing standards ensuring that all satellite clocks remained synchronized to a single time system. GPS uses the one-way ranging principle based on comparing the time-of-transmission of a signal (as determined by a satellite clock) to the time-of-reception (as determined by a ground-based receiver

clock), to compute the time-of-flight of the satellite-to-receiver signal. Simultaneous distance measurements (converting time-of-flight to ranges) to four satellites permits the 3D coordinates and the receiver clock error (relative to the synchronized satellite time scale) to be determined to an accuracy of a few meters (where clock error can be considered to be the distance light travels in the clock error period).

Considering that light travels at approximately  $3 \times 10^8$  m/s, if the system can tolerate an error buildup caused by the on-board clocks of 1.6 m, the on-board clock frequency stability should guarantee a drift of less than 5 ns between periodic telemetry uploads, when the accumulated clock error can be effectively reset to zero. For GPS satellites, such an upload is typically performed every half day. Therefore the required frequency stability should be about  $(5 \times 10^9)/(4 \times 10^4) = 1.25 \times 10^{-13}$  over 12 hours [85]. Such a stringent requirement can be met only by atomic clocks such as Cesium (Cs) and high quality Rubidium (Rb) frequency standards.

GPS satellite clocks, or more generally satellite positioning system clocks, run independently (free-run) between timing updates that occur when a given GPS satellite becomes visible to the GPS control station located in Colorado (US). During those free-run periods, GPS clocks will drift away from their common time. Fig. 1.1 shows through a frequency stability representation, the performance of a typical space-borne Rb clock during a period of about 12 hours. Under the hypothesis that the acceptable build up error (on a single pseudorange) due to clock drift is 5 ft (1.5 m), a good space borne Rb atomic clock would in fact meet the stability requirements. The same plot shows also a typical build up error if the clock on board the satellite was a space-borne VCXO. As is noticeable, after about 1000 s (16 minutes) a VCXO would give a single pseudorange error which would exceed the 5 ft limit, making VCXOs inappropriate clocks for a system like GPS. However, the drift that the VCXO would show for an interruption that is no longer than 1000 s would cause a build-up pseudorange error smaller than 5 ft and therefore still be acceptable.

The great research effort in the study of space-borne atomic clocks that followed the development of GPS has led to a great employment of those clocks for space applications. Twenty years after GPS, Europe decided to realize its own global satellite-based

positioning system that would eventually ensure the reliability of those applications which currently rely on GPS. On December 28, 2005 the first GALILEO test satellite was launched. GALILEO is not the only alternative satellite positioning system; Russia's GLONASS also provides alternative GNSS signals. This system was only fully operational for a short period in the mid-1990s, but in the last few years GLONASS has been progressively revitalized. Both GLONASS and GALILEO have similar requirements for precise clocks as GPS does. Moreover, GALILEO will be the first GNSS with an on-board hydrogen maser clock [51].

Other satellite-based systems have been designed as regional augmentations to GNSS, such as the European Geostationary Navigation Overlay Service (EGNOS), the American Wide Area Augmentation System (WAAS) and the Japanese Multifunctional Transport Satellites (MTSAT). In these cases, their main objective is to provide GPS with the integrity to be used for aviation applications such as en-route and terminal navigation. Such augmentation systems mimic GNSS and atomic frequency standards are again the technology employed for the satellite clock. Other regional systems have also been proposed. The Japanese QZSS is a regional system which aims to provide extra GPS-like signals to users in Japan and Australasia.

### 1.1.2 Quasi-Zenith Satellite System

The Quasi-Zenith Satellite System (QZSS) is a regional space-based positioning system that uses a constellation of three geosynchronous satellites placed in multiple orbital planes. The system provides coverage over East Asia, Australasia and Japan, and is designed to ensure that users in these regions are able to receive positioning signals from one high elevation satellite at all times. QZSS enhances GPS services in two ways: first, availability enhancement, whereby the availability of GPS signals is improved, second, performance enhancement whereby the accuracy and reliability of GPS derived navigation solutions is increased [65].

Because the GPS availability enhancement signals transmitted from Quasi-Zenith Satellites (QZSSs) are compatible with modernized GPS signals, and hence interoperability is ensured, the QZSSs will transmit the L1C/A signal, L1C signal, L2C signal

and L5 signal. This minimizes changes to specifications and receiver designs.

Compared to standalone GPS, the combined system GPS plus QZSS delivers improved positioning performance via ranging correction data provided through the transmission of submeter-class performance enhancement signals L1-SAIF and LEX from QZS. It also improves reliability by means of failure monitoring and system health data notifications. QZSS also provides other support data to users to improve GPS satellite acquisition [65].

Despite similarities in the signals, the QZSS orbit design greatly differs from that of GPS, and if an appropriate location is chosen (for example Marshall Islands), permanent QZSSs view can be achieved. Furthermore QZSS is a civil system with different basic requirements to GPS. QZSS positioning capabilities therefore represent a new-generation civil GPS space augmentation system with limited navigation capabilities [87]. In other words, although the QZSS is seen primarily as an augmentation to GPS, without requirements or plans for it to operate in standalone mode, QZSS can provide limited accuracy positioning on its own. The service also could be augmented with geostationary satellites from Japan's MTSAT Satellite-based Augmentation System (MSAS), which features a geostationary satellite-based design similar to the US Federal Aviation Administration's WAAS and the European Geostationary Navigation Overlay Service. Details of the QZSS orbit design and signal structure can be found in Chapter 2.

According to its original plan, QZSS was to carry two types of space-borne atomic clocks; a hydrogen maser and a Rb atomic clock [65, 87]. The development of a passive hydrogen maser for QZSSs was abandoned in 2006. The positioning signal will be generated by a Rb clock and an architecture similar to the GPS timekeeping system will be employed. QZSS will also be able to use a Two-Way Satellite Time and Frequency Transfer (TWSTFT) scheme, which will be employed to gain some fundamental knowledge of satellite atomic standard behavior in space as well as for other research purposes [65, 129, 54].

Although the first generation QZSS timekeeping system is based on the Rb clock, the first QZS, scheduled to be launched in 2009, will carry a basic prototype of the

---

crystal clock synchronization system described here. During the first half of the two year in-orbit test phase, preliminary tests will investigate the feasibility of the atomic clock-less technology which might be employed in the second generation QZSS.

## 1.2 Motivation of This Study

The cost of building and launching a satellite is very high, of the order of hundreds of millions of dollars. Often the projected commercial gain may not justify such expense, especially in the case of multi-satellite systems such as global or regional satellite-based positioning systems. In the satellite navigation business, it is often taken for granted that the satellites are provided as free infrastructure. It is in fact true that worldwide satellite-based positioning is possible only because the US and Russia (and over the next five years also Europe) have invested in the satellite constellations that permit GNSS receivers to operate anywhere in the world.

In recent publications, scientists and engineers have begun to consider new ways to build cheaper satellite-based positioning systems using smaller and lighter satellites. This would reduce the costs associated with building and launching complex and heavy payloads (refer to Chapter 2). Modern rocket launch costs run into thousands of \$US per kg for transfer to low Earth orbit, and of the order of \$US20,000 per kg for transfer to geosynchronous orbit. For example, each GALILEO satellite will carry two Rb Atomic Frequency Standards (RAFS) and two Passive Hydrogen Masers (PHM) for a total weight of about 36 kg (3.3 kg for each RAFS and 18 kg for each PHM).

The Japanese government is investigating the feasibility of an alternative low-cost technology for satellite-based positioning. An initial investment in research and development of 625M Yen (\$US 5.5M) over a five year period was made, and in 2003 the Space Technology Group in the National Institute of Advanced Industrial Science and Technology (AIST) [1] and the Japan Aerospace Exploration Agency (JAXA) [3] began investigating an alternative solution for the QZSS timekeeping system. An alternative that would not require QZSSs to carry atomic clocks.

### 1.3 Research Objective and Contribution

The novelty of the QZSS proposal rests on the orbit design and its high satellite visibility. Such a peculiar feature makes it possible to recast the classic on-board atomic clock scheme as a remote synchronization system where the main time reference (atomic clock) is located on the ground, and a correction/synchronization infrastructure keeps the on-board time reference continuously aligned with a high accuracy time scale. The main objective of this project is to assess the feasibility of a low-cost timekeeping system which would reduce manufacturing costs of QZSSs and spacecraft launching costs. As a result of a collaborative research program, the Space Technology Group of AIST, Japan, and the University of New South Wales, Australia, investigated the feasibility of a remote synchronization scheme for the QZSS.

The use of synchronization methods for the QZSS on-board clocks would reduce the gap for a low-cost technology for satellite-based positioning. Aside from the economic benefits mentioned above, a remotely synchronized satellite-based positioning/augmentation system which does not require a high quality on-board atomic frequency standard is in itself a very interesting system, both from the research and the engineering points of view. Such a revolutionary system may lead to research achievements that could have applicability in fields such as clock design, network synchronization and time transfer.

This dissertation contributes to the field by presenting a feasibility study of a synchronization architecture, known as the Remote Synchronization System for the On-Board Crystal Oscillator (RESSOX), aimed to realize the atomic clock-less concept for the QZSS. An analysis of the delays that the proposed system has to account for is presented. The design and testing of components for the Hardware Simulator have also been carried out.

The RESSOX synchronization scheme described in Chapter 3 is characterized by a high level of complexity. Its operation depends heavily on the precise satellite position prediction algorithm and on precise delay prediction calculations. In Chapter 4 a novel alternative architecture alternative to RESSOX, known as Remote Timekeeping System (RTKS), is presented. Based on the TWSTFT system, RTKS is a simpler and

more reliable architecture. Contributions include the novel idea behind the system and its implementation.

One of the critical issues regarding the RESSOX architecture and RTKS architectures is the effect of the loss of synchronization during satellite communication interruptions.

A significant contribution is the study presented in Chapter 5 of the effects on positioning when a space-borne VCXO is employed in the atomic clock-less RESSOX and RTKS architectures. Particular attention is given to the effects of faulty synchronization on positioning. Furthermore, a method for solving the free-run VCXO problem is proposed. The study of the relationship between positioning quality and synchronization quality defines the requirements for the whole synchronization method. It also assesses the delicate issue of synchronization loss, which is, technically, the main drawback of this system. Studying the relationship between QZSS time quality and QZSS plus GPS positioning capabilities with the focus on time synchronization loss addresses some of the problems for the specification of the crystal clock to be employed for the proposed scheme. Along with the development of this study, a contribution has been made to the development of the Software Simulator described in the Appendix.

Aside from the strictly technical contributions, this study has been an opportunity to strengthen the international research relationship between the School of Surveying and Spatial Information Systems at the University of New South Wales and the Space Technology Group of AIST.

The contribution of this thesis can therefore be summarized in the following five main points:

**RESSOX feasibility study.** An optimal architecture for realizing the atomic clock-less concept for QZSS. Design definition and feasibility is presented. Design of the feed-forward and feedback commands are presented.

**Remote timekeeping system, RTKS.** A synchronization scheme known as RTKS, an alternative to RESSOX, is presented. A VCXO Phase-Locked Loop (PLL) controller for RTKS is also described. Considerations on the overall system design are

given.

**QZSS clock, the free-run problem.** The timing accuracy degradation problem due to lack of ground communication is addressed by presenting a VCXO control method which reduces the satellite on-board time error.

**QZSS, positioning quality and timing.** The relationship between QZSS timing quality and QZSS plus GPS positioning quality is investigated. RESSOX and RTKS subsystems requirements are derived.

**Simulation tool development.** Along with the research activity, direct contributions in the development of the RESSOX/RTKS Hardware Simulator as well as of the RESSOX/RTKS Software Simulator have been made.

During the last four years, this research activity directly led to the development and improvement of the RESSOX/RTKS Software Simulator and the RESSOX/RTKS Hardware Simulator (refer to Appendix A), two pivotal research tools used by the RESSOX team.

## 1.4 Structure of This Dissertation

The dissertation is structured as follows:

**Chapter 2:** Presents a review of the literature relevant to GPS with particular focus on its timekeeping system. The Japanese QZSS is then introduced. An example of where a similar remote synchronization technology is adopted, the MILSTAR satellite system, is presented. The final sections present an overview of the TWSTFT and Clock stability theory.

**Chapter 3:** Introduces the first practical implementation, known as RESSOX, of the synchronization method for the QZSS. The basic RESSOX concept, originally presented by Iwata *et. al* [59], is presented here. Design definition and feasibility is examined and design of the feed-forward and feedback commands is presented.

**Chapter 4:** Introduces a second implementation, known as RTKS, of the synchronization method suitable for the QZSS. The concept is described and a study of its feasibility is presented.

**Chapter 5:** Examines a common problem that affects the RESSOX scheme as well as the RTKS scheme, namely the problem of guaranteeing synchronization during a break in satellite communications. The synchronization interruption problem is presented together with a solution based on satellite on-board drift prediction during hold-over directly applied to the VCXO control voltage.

**Chapter 6:** Presents a positioning-oriented study where QZSS is combined with GPS, and from which the relationship between QZSS timing quality and QZSS plus GPS overall positioning quality and capability is derived. Particular attention is given to the effects of faulty synchronization on positioning, specifically when the QZS clock has to function without remote control due to unavoidable communication interruptions.

**Chapter 7:** Examines the concept of a constellation of compact low-Earth orbit positioning satellites that are equipped with on-board steerable clocks. Key issues such as number and spatial location of required synchronization stations, clock desynchronization issues and positioning accuracy are discussed.

**Chapter 8:** Draws conclusions about the results of the study. The future work required by the project is mapped out.

**Appendix:** Contains detailed information about the Hardware Simulator and the Software Simulator which have been developed along this research. The Hardware Simulator has been developed in collaboration with several Japanese companies at the laboratories of AIST [1]. The Software Simulator has been developed in collaboration with Mitsubishi Space Software Incorporated [4].

## 1.5 Keywords

Quasi-Zenith Satellite System, Global Positioning System, Timekeeping System, Synchronization, Atomic Clock, Timing, Phase Shift.

## Chapter 2

# Timekeeping in Satellite and Navigation Systems

### 2.1 Purpose of this Review

This Chapter will review the literature relevant to the subject of this dissertation. The first Section reviews the GPS design and its Timekeeping System (TKS). Currently the only fully operational GNSS, GPS presents the best example of TKS architecture for a satellite positioning system. The Japanese QZSS is very likely to have similar features and must face similar challenges as the ones involved in the design and deployment of GPS. The Russian GLONASS is also examined in this review. The second Section presents an overview of GIOVE-A, the first element of the GALILEO in-orbit validation phase. Launched in December 2005, GALILEO (and specifically GIOVE-A) represent an alternative engineering development of a satellite-based system. In the third section, QZSS is introduced and details of the satellite segment are given. The QZSS is the satellite positioning and augmentation platform for which the synchronization system described in this thesis was designed for. The penultimate Section presents an overview of the MILSTAR mission. This three satellite military system has successfully implemented satellite time synchronization of clocks on board the satellites. MILSTAR is the most successful documented engineering implementation of a real-time synchronization of satellite clocks.

In the last section, an overview of the two-way time transfer (TWTT) system, is presented. Particular focus on the application of TWSTFT system for non-geostationary satellites such as QZSS is given. This Section represents an introduction to the alternative synchronization scheme presented in Chapter 4, specifically developed for the QZSS.

Due to the broad research objective of this project, this literature review tries to bring together a large body of knowledge. Details of the systems presented here which are not relevant to this project have been omitted.

## 2.2 Global Navigation Satellite Systems

### 2.2.1 Global Positioning System, GPS

The NAVSTAR GPS is a satellite-based radio positioning and precise time transfer system that has been developed, maintained and operated by the US Department of Defense (DoD). The system nominally consists of 24 satellites in almost circular orbital planes, with altitudes above the Earth's surface of about 20,000 km. The satellites continuously transmit their signals to users on or above the Earth, and in all weather conditions. This allows users to ascertain the position of their GPS receivers anywhere on land, at sea, in the air or in low-Earth orbit [51].

Currently, GPS satellites continuously transmit two carrier frequencies in the L-band, a subset of the ultra-high frequency (UHF) band. The primary frequency is known as L1 ( $f_{L1}=1575.42$  MHz), and the secondary frequency as L2 ( $f_{L2}=1227.6$  MHz). The GPS satellites transmit additional radio frequency signals at frequencies referred to as L3 and L4, which have been reserved for other DoD purposes. Future satellites will transmit another civilian frequency L5 ( $f_{L5}=1176.45$  MHz).

L1 is modulated by two Pseudo-Random Noise (PRN) ranging codes, one for civil users and another for DoD authorized users. On the Block IIA/IIR satellites, L2 is modulated by only one PRN code whose use is restricted to DoD authorized users. The two codes are known as the Coarse Acquisition or Clear Access (C/A) code, which is available on L1 only, and Precise (P/Y) code available on L1 and L2. Eight

Block IIR satellites have been modified (Block IIR-M) to use the new military M-code modulated on both the L1 and L2 frequencies, as well as the more robust civil signal L2C modulated on the L2 frequency. The M-code signal was developed to enable GPS operations in a higher jamming environment and to reduce the vulnerability of military GPS-based systems. The first modified Block IIR (or 2R-M) satellite was launched in September 2005. Details about the GPS signal code structure can be found in [85].

### GPS Timekeeping System

The TKS in the GPS Block IIR satellites provides an accurate 10.23 MHz signal to the code generators and to the L-Band subsystem of the navigation payload. This system implements a control loop in software that continuously tunes a voltage controlled crystal oscillator (VCXO). This allows it to follow the timing stability of a Rb atomic frequency standard (RAFS) located on board each GPS satellite. Due to the consistent comparison of two independent oscillators, the TKS is able to detect variances in either the RAFS or in the VCXO which can degrade the signal. If an anomaly is identified, the TKS protects users by rapidly switching to non-standard codes (NSC) within seconds.

The GPS Block IIR TKS (Fig. 2.1) tunes the 10.23 MHz digitally controlled VCXO in order to produce the GPS navigation signal with the timing accuracy of RAFS. By linking the VCXO to the RAFS using a software-controlled loop, it is possible to accurately adjust the frequency and phase of the TKS output, to cancel drift of the RAFS once it has been identified, and to detect anomalous RAFS frequency or phase excursions.

#### *TKS hardware and calculation of phase error*

Fig. 2.1 shows the frequency divider circuitry which produces a pulse once per epoch from the digitally controlled VCXO, and once per epoch from the fixed frequency RAFS. The phase difference between the reference epoch from the RAFS divider chain and the system epoch from the VCXO divider chain is measured by a phase meter. The phase meter uses a 600 MHz oscillator to make measurements of this phase difference with an accuracy of  $\pm 1.67$  ns. The additional processing shown in Fig. 2.1 is performed



*Large error detection and fast/slow loop switching*

Referring to Fig. 2.1, the computed phase error passes to the “Large Error Detect” function. If two consecutive phase errors greater than the “Failure Threshold” are detected, the software causes Non-Standard Codes (NSC) to be transmitted by the satellite in order to prevent users from locking to the erroneous L-band transmission. If this happens, it causes an outage of service which can only be corrected by Control Segment (CS) intervention. The “Failure Threshold”, one of the fields in the Selective Availability Database Control Element (SADBCE), determines whether errors are large enough to cause NSC. The NSC decision has two other effects [88]. First, the control loop switches to a faster time constant (15 seconds), referred to as “Fast Loop”. The original time constant will be restored when 50 consecutive errors less than a smaller threshold, the “Clipping Threshold”, have occurred. The mode which uses the longer time constant is referred to as the “Slow Loop”. Switching to the “Fast Loop” mode also has the effect of disabling “Gain-Tracking” and “Adaptive Time Constant”. This happens because it is not possible to successfully adjust the VCXO gain when large phase errors are present and the mean phase error is very different from zero [88].

*Adaptive time constant, ATC*

If ATC is enabled via a Serial Magnitude Command (SMC) from the CS, the phase error is weighted by a function which depends on the magnitude of the phase error. A number between 1 and 6 weights larger phase errors, and a number between 0.7 and 1 weights smaller phase errors ( $< 1$  ns). Thus, ATC has the effect of correcting large phase errors more quickly. The time constant of the filter is shortened by a factor of about 6 if a phase error greater than a few ns occurs. In regular operation, the time constant selected by the CS (usually 150-200 seconds) is used. Note that the ATC weighting does not occur if the system is in the “Fast Loop” mode.

*Loop filter*

The phase error, possibly weighted by a factor between 0.7 and 6, is applied to either the Fast Loop filter or the Slow Loop filter depending on the current mode of the

TKS. The time constant in the Fast Loop mode is fixed at 15 seconds, while the time constant in the Slow Loop mode is derived from the SADBCE uploaded by the CS. Generally, if the VCXO is showing instability, the ATC mode or shorter time constants are preferred. As the initialization process may result in initial phase errors which need to be eliminated, the TKS starts with the mode set to Fast Loop.

*Adding dither and scaling by reciprocal of VCXO gain*

The output of the filter represents the desired frequency of the VCXO. However, to generate dither as, for example, in the case of Selective Availability (SA), a pseudo-random frequency change must be applied to the VCXO each epoch. This adds dither frequency to the filter output. By adding the dither, the desired fractional frequency offset of the VCXO from its center value, nominally 10.23 MHz is produced. To get the VCXO to produce this desired frequency, however, the frequency change produced by a 1 Least Significant Bit (LSB) change to the digital control input of the VCXO must be known. If it is known, for example, that the VCXO changes frequency by  $2.5 \times 10^{-12}$  for each LSB change of the control word (the VCXO gain), then the desired fractional frequency change must be multiplied by  $4 \times 10^{11}$  ( $1/(2.5 \times 10^{-12})$ ) to compute the control word for the VCXO. This is indicated by the multiplier function in Fig. 2.1.

*VCXO gain-tracking*

To compensate for the fact that the sensitivity of the VCXO to changes in control word (i.e. the VCXO gain) may change over time, the TKS software continuously estimates the VCXO gain. To do this certain conditions must be met. First, the TKS must be generating dither, and second, it must be operating in the Slow Loop mode. If the TKS is not generating dither, then it is not necessary for the VCXO slope to be estimated with an accuracy greater than about 5 %, and the initial calibration of the VCXO slope is accurate enough. This has been the case since 5 February 2000 when SA dither was turned off [88].

### GPS TKS Clocks

In the GPS Block IIR TKS shown in Fig. 2.1, the source of signal timing for a given satellite is the on-board Rb atomic frequency standard, RAFS. For redundancy, there are three RAFS in the TKS, one is active and two are backups. The RAFS is a free-running clock at approximately 13.4 MHz with no controls. The 13.4 MHz signal is passed through the on-board TKS. This phase locks a voltage-controlled crystal oscillator to it in order to generate a 10.23 MHz transmitted clock, which is broadcast to all the GPS users as an L-band signal. Ground control can send commands to the TKS in order to adjust the phase, frequency, and frequency drift in the 10.23 MHz signal [29].

#### *Current GPS IIR on-orbit performance*

Data is uploaded to each GPS satellite daily by the Master Control Station (MCS). Amongst this data, the GPS IIR upload contains a 210-day prediction of satellite clock residuals. The GPS satellite broadcasts these residuals to the users in the L-band signal (as coefficients of a second order polynomial function). Since the upload occurs daily, the age of the broadcast clock residuals is zeroed roughly every 24 hours. It follows that the performance of a given GPS satellite is highly dependent on the stability of its atomic clock, particularly its stability over one day [29].

Fig. 2.2 shows a ranking of GPS clocks by frequency stability for one day for the first quarter of 2002. The SVs with the most stable clocks contain Rb atomic frequency standards. The five most stable clocks are the GPS IIR PerkinElmer RAFS on SVNs 41, 43, 46, 51, and 54. The RAFS on SVN 44 appears to be out of character with respect to the other five GPS IIR RAFS.

Estimated range deviation (ERD) is defined to be the difference between the predicted ephemeris/clock and the MCS Kalman filter current state estimate rmsd over a continuum of geodetic locations visible to the SV. Fig. 2.3 are plots of the maximum ERD for some GPS satellites for every day over the period from January 2001 through April 2002. In these plots, ERD is dominated by the stability of the RAFS. As expected, the best ERD performance is found in the most stable clocks. Random

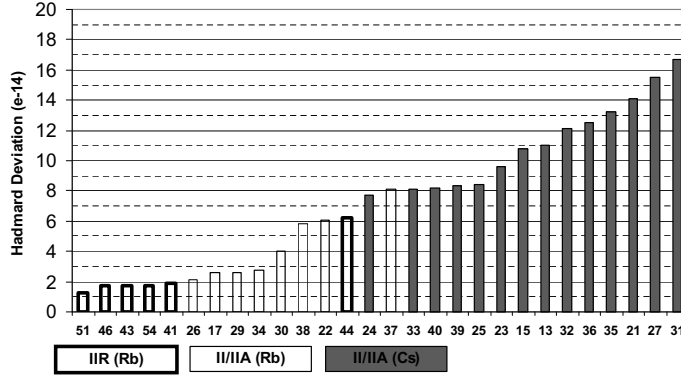


Figure 2.2: Ranking of GPS clocks by Hadamard deviation (The Hadamard Variance is a 3-sample variance with binomially-weighted coefficients that is similar to the 2-sample Allan Variance) for one day (Q1-2002) [29].

frequency breaks of  $10^{-13}$  magnitude in the RAFS caused the outliers visible in the ERD plots for SVNs 41, 46, 51, and 54. In addition, the early data for SVN 54 show MCS Kalman filter convergence during beginning-of-life RAFS frequency stabilization.

The GPS IIR has three RAFS per SV. The least stable of the RAFS is in slot 2 of SVN 44, which is the currently active clock on that SV. Therefore, the ERD plot for SVN 44 sets the standard for the worst-case performance for any IIR SV. Independent measurements, [29], show that the PerkinElmer RAFS data (SVNs 41, 43, 46, 51 and 54) are a good predictor of on-orbit performance.

#### *GPS Enhanced RAFS, ERAFS*

The stability specification for the PerkinElmer RAFS-IIR Rb standard is  $\sigma_y(\tau) < 3 \times 10^{-12}/\sqrt{\tau} + 5 \times 10^{-14}$ . This places an upper stability limit of  $\sigma_y < 6 \times 10^{-14}$  at an averaging time of 1 day on the RAFS-IIR. Five of the six RAFS-IIR standards now in service have significantly better performance than the current requirement. This has raised performance expectations of the overall system and has highlighted the poorer performance of RAFS-IIR SVN 009, currently in service on board SVN 44. RAFS-IIR SVN 009's factory test data were near the upper limit of  $\sigma_y < 6 \times 10^{-14}$  at shipment, and this RAFS has exhibited out-of-specification performance in service.

The overall performance of the PerkinElmer RAFS-IIR has also drawn attention

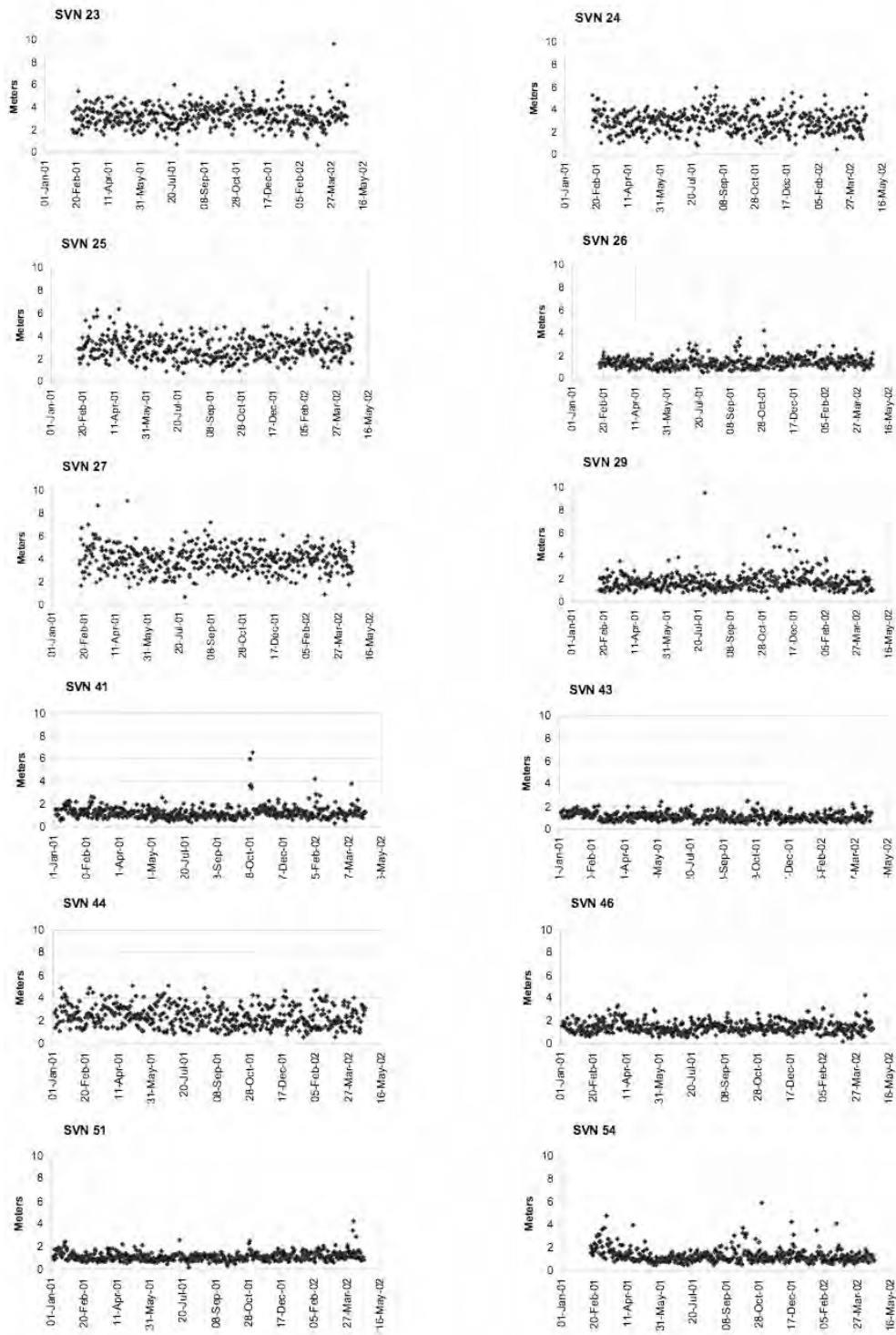


Figure 2.3: GPS II/IIA ERD January 2001 through April 2002 [29].

to frequency jumps or breaks. The low noise of the RAFS means that features as small as  $\sigma_y < 5 \times 10^{-14}$  are observable. Frequency jumps or breaks of various magnitudes, some of which are quasi-periodic, have been attributed to the in-service RAFSs. Some frequency breaks have been large enough to require ground intervention.

#### *Precise Phase Meter, PPM*

The precise phase meter (PPM) compares the phase of the reference epoch, which occurs every given cycle of the on-board RAFS, to the timing of the VCXO epoch. This occurs every 15,345,000 cycles of the code clock produced by the VCXO. The phase meter measures this phase with a resolution of  $\pm 1.67$  ns. The RMS error of the Block IIR phase meter is no better than 0.68 ns, more typically 0.8 ns. To meet the short-term Allan deviation specification of Block IIR, it is necessary to smooth phase errors over a time period of about 150 seconds with a second-order filter in order to generate frequency correction commands to the VCXO. Even so, the primary cause of short-term ( $t < 100$  seconds) timing instability in the Block IIR TKS is the phase meter. Any attempt to improve short-term stability would be nearly impossible with the existing phase meter [29]. A recently built a PPM with an RMS measurement error of  $0.8 \times 10^{-12}$  seconds is about 1,000 times more accurate than the existing design. Resolution (quantization) is typically less than  $10^{-14}$  seconds. The design and implementation of the PPM is covered by US Patent 6,441,601 B1.

#### **2.2.2 GLONASS**

The Global'naya Navigatsionnaya Sputnikovaya Sistema, GLONASS, is the Russian Space Forces counterpart to the United States GPS. Both systems share the same principles in data transmission and positioning methods. The operational space segment of GLONASS consists of 21 satellites in and additional three orbital planes, with three on-orbit spares. The three orbital planes are separated by 120 deg, and the satellites within the same orbit plane are separated by 45 deg. Each satellite operates in circular 19,100 km orbits at an inclination angle of about 64.8 deg and completes an orbit in approximately 11 hours 15 minutes. The system has not been fully available since the mid-90s, however it is maintained and remains partially operational. Russia's First

Deputy Prime Minister Sergei Ivanov stated that the system will have the 24 satellites required for worldwide coverage by 2010 [51, 5].

GLONASS satellites transmit two types of signals: a standard precision (SP) signal and an obfuscated high precision (HP) signal. All satellites transmit the same code on their SP signal, however each transmits on a different frequency using a channel frequency division multiple access (FDMA) technique spanning from 1602.5625 MHz to 1615.5 MHz. This is known as the L1 band. The Equation to calculate the exact center frequency is  $1602MHz + n \times 0.5625MHz$ , where n is a satellite's frequency channel number (n=0,1,2,...24). Signals are transmitted in a 38 deg cone, using right-hand circular polarization, at an EIRP between 25 to 27 dBW (316 to 500 watts) [51, 5].

Regarding the satellite on-board timekeeping system, GLONASS SVs generate time information in the same way GPS satellites do. An on-board atomic time reference is locally linked to a VCXO with a TKS monitored from the ground station. Necessary time corrections are periodically provided to the on-board TKS when satellites come in view. GLONASS Block IIC satellites have three Cs frequency standards. The stability of the on-board synchronizing system has increased the accuracy of navigation signal phase synchronization by as much as a factor of two (7.5 ns).

Unlike GPS, where its time is continuous and therefore differs by an integer number of leap seconds from UTC (the difference between UTC and GPS time is included in the almanac message), the GLONASS time is kept synchronized to UTC. GLONASS uses more conventional time units such as days, hours, minutes and seconds. The day count begins with a leap year (1992) and counts up to 1461 days before returning back to zero.

In respect to the GPS architecture, GLONASS appears to have other small differences. For example, the clocks in the GLONASS satellites have satellite orbit eccentricity correction applied before broadcasting. However, the overall system remains similar to GPS, for more information refer to Section 2.2.1.

### 2.2.3 GALILEO

GALILEO is a joint initiative of the European Commission and the European Space Agency (ESA) for a state-of-the-art global navigation satellite system. It aims to provide a highly accurate, guaranteed global positioning service under civilian control. It is planned to be compatible and interoperable with GPS and GLONASS with the announced CDMA signals on L1 and L5. The fully deployed GALILEO system will consist of 30 satellites (27 operational and 3 active spares), in three circular Medium Earth Orbit (MEO) planes at an altitude of 23,222 km with an inclination of about 56 deg. Atomic clocks are critical equipment for the satellite navigation system. The Rubidium Atomic Frequency Standard (RAFS) and Passive Hydrogen Maser (PHM) are the present clock technologies planned for the GALILEO navigation payload [51]. According to the present baseline clock technology, every satellite will carry two RAFSs and two PHMs. The need for reliability through technological diversity and compliance with the GALILEO mission life requirement (12 years) has necessitated the adoption of a dual technology plan for the on-board clocks. Both developments are based on early studies performed at the Observatory of Neuchatel from the end of the 1980s and Temex Neuchatel Time (TNT) since 1995. The activities related to the GALILEO System Test Bed (GSTB-V2) experimental satellite as well as the implementation of the In Orbit Validation phase are in progress. The first experimental satellite, GIOVE-A, launched 28th December 2005, is working to secure the GALILEO frequency filings, test some of the critical technologies such as the atomic clocks, allow experimentation on GALILEO signals, and to characterize the MEO environment. The two RAFS' on the GIOVE-A satellite are supplied by Surrey Satellite Technologies Ltd. The launch of the second GALILEO test satellite, GIOVE-B, took place on April 26, 2008.

#### **GIOVE-A Rubidium Atomic Frequency Standard**

The RAFS development milestones are chronologically listed below.

The first development activity was completed in 2000 with one Engineering Model (EM) RAFS produced. The result of the development was applied clock design used for qualification and lifetime testing. The delivery of EM, the baseline unit for the



Figure 2.4: Picture of the GSTB-V2 RAFS [37].

Parameter	Measurement
Frequency stability	$< 4 \cdot 10^{-14}$ @ 10'000 sec
Flicker floor	$< 3 \cdot 10^{-14}$ (drift removed)
Thermal sensitivity	$< 5 \cdot 10^{-14}$ /°C
Magnetic sensitivity	$< 1 \cdot 10^{-13}$ / Gauss
Mass and volume	3.3 kg and 2.4 liter

Table 2.1: RAFS GSTB-V2 general achieved performance [37].

development of the flight models for GSTB-V2 (Fig. 2.4), was the last development and qualifications step initiated at the end of 2001 and completed by the beginning of 2003.

In the frame of GSTB-V2, one Engineering Qualification Model (EQM), one Proto-Flight Model (PFM) and five Flight Model (FM) units have been delivered. The PFM and FM1 were integrated in GIOVE-B. The FM4 and FM5 were integrated in GIOVE-A and have been in orbit since 28th December 2005. In addition, the FM2 and FM3 are available as FM spare units. RAFS for GSTB-V2 performance achieved are given in the Table 2.1. A detailed description of these units was published in [38]. In space, the performance of the GIOVE-A on-board RAFS is shown in Fig. 2.5.

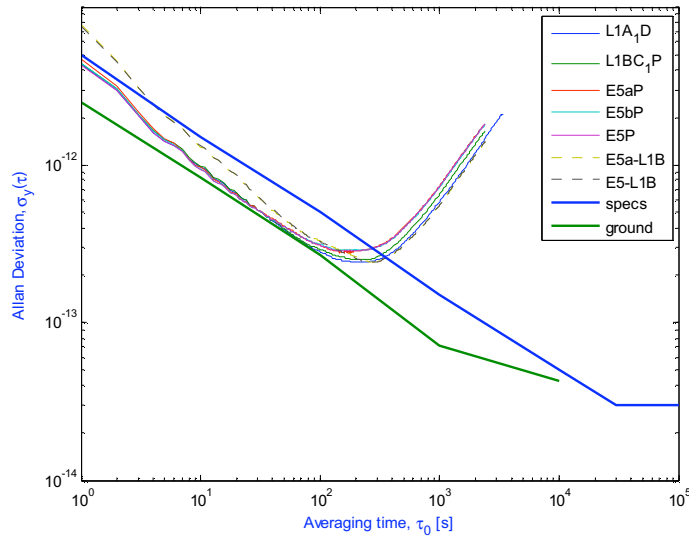


Figure 2.5: Allan deviation obtained from all signals using GUSN station for RAFS-FM4 clock on board GIOVE-A, [45].

### GALILEO Passive Hydrogen Maser

The space hydrogen maser will be GALILEO's master clock. The year 1998, at the Observatory of Neuchatel, saw the first maser development for navigation applications. However, the GALILEO definition phase indicated that the active maser was too heavy and too large, whilst its excellent frequency stability was not required. Therefore, in 2000, development was re-orientated towards building a PHM. The development of the PHM Engineering Model (Fig. 2.6) was completed in early 2003. The instrument has been continuously tested since June 2003 to assess its long-term performance and for the early identification of reliability and lifetime problems. The instrument was redesigned to increase compactness, ease of assembly, integration and on-satellite testing by the inclusion of an external vacuum envelope [36]. Main efforts now focus on repeatable and reliable manufacturing. Two technological models were built.



Figure 2.6: Engineering Model of GALILEO Passive Hydrogen Maser (PHM) atomic clock [36].

## 2.3 Quasi-Zenith Satellite System, QZSS

### 2.3.1 Introduction

The QZSS is a regional space-based positioning system that uses a constellation of satellites placed in multiple orbital planes. The satellites have the same orbital period as a traditional equatorial geostationary orbit, however, they have a large orbital inclination and therefore move with respect to the Earth's surface. QZS orbits are also elliptical and are known as highly-inclined elliptical orbits. The system covers a region in East Asia and Asia-Pacific and is designed to ensure that Japanese users are able to receive positioning signals from a high elevation at all times [87, 65]. QZSS enhances GPS services in the following two ways:

- Availability enhancement (improving the availability of GPS signals)
- Performance enhancement (increasing the positioning accuracy and reliability of GPS).

QZSS enhances standalone GPS availability for any user that has visibility to, and can track, one or more QZS. This enhancement will be the greatest for users in Japan because the constellation design is optimized for that area. However, users elsewhere in the Asia-Pacific region will also benefit from the enhanced geometric arrangement made possible by QZSS. This increases the locations and times at which positioning is possible in both urban and mountainous areas [87].

The system uses modernized GPS signals as a base and will transmit the L1C/A signal, L1C signal, L2C signal and L5 signal. This minimizes the need for changes to specifications and receiver designs.

QZSS provides range correction data through the transmission of performance enhancement signals that improves overall positioning quality when GPS plus QZSS receiver is employed [65, 126].

Three satellites placed in three separated elliptic orbits with an orbital inclination of about 45 deg and a right ascension of the ascending node of 120 deg constitute the QZSS space segment. All three orbits are geosynchronous with a semi-major axis of about 42,164 km. This constellation guarantees the presence of at least one satellite,

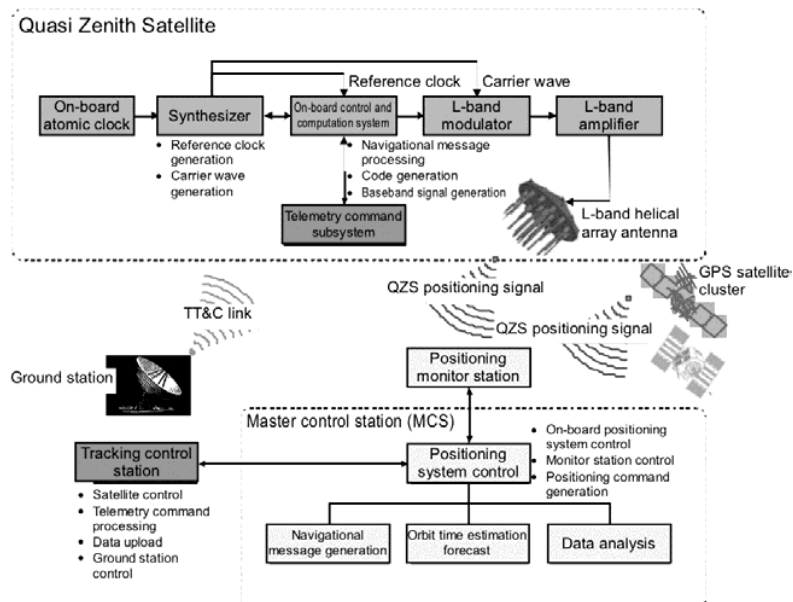


Figure 2.7: Quasi-Zenith Satellite System (QZSS) overview [65].

periodically replaced (with hand-over) every eight hours, situated approximately over the perpendicular (Zenith) of Japan, 24 hours a day. Fig. 2.8 shows the orbital ground track common for all three QZSSs.

### 2.3.2 Overview of QZSS

#### System Overview

QZSS consists of: (a) the QZSS Space Segment comprising a constellation of QZSSs orbiting the Earth, and (b) the QZSS Ground Segment comprised of Monitoring Stations (MS), a MCS and Tracking Control Stations (TCS). A system diagram is provided in Fig. 2.7.

QZS signals are monitored by the MS. The MCS then collects the MS monitoring results, and estimates and predicts the QZS time and QZS orbits. The MCS also gathers other data to generate navigation messages, and uplinks to the QZSSs via the TCS.

The TCSs constantly monitor the status of the QZSSs. They function in cooperation

with the MCS to provide any necessary services. In addition, approximately once per year, the TCS exercises orbital control to ensure that the QZSS maintains their correct orbital positions [65].

### QZSS Constellation and Orbit

The baseline QZSS constellation is comprised of three satellites. All QZSSs are in orbits that have the same “figure eight” ground track (passing over Southeast Asia, Australia, etc.). The orbit tracks of the three satellites are shown in Fig. 2.8. Fig. 2.9 shows the variation of QZS elevation angle for some major Asian cities where the QZSS service will be available [65].

The parameters defining the QZS nominal orbits are provided below. The satellites have the same orbital period (one day) as a traditional equatorial geostationary satellite, however, they have a large orbital inclination so they do not remain in the equatorial plane and therefore move with respect to the Earth’s surface. The QZSS orbits are also elliptical and are sometimes known as highly-inclined elliptical orbits. The QZS will orbit somewhat further from the Earth in the northern hemisphere than in the southern hemisphere, resulting in a longer period of high elevation angle service for the region of Japan. Ultimately a single satellite will be deployed in each of the three orbital planes, thereby providing continuous coverage at high elevation angles for the primary service areas (including all Japanese territory). The average central longitude of the QZS ground track is 135 deg East. Planned orbital parameters are:

Semi-Major Axis,  $a = 42164$  km (average)

Eccentricity,  $e = 0.099$  max

Orbital inclination,  $i = 45$  deg  $\pm$  5 deg

Right ascension of ascending node,  $\Omega = 120$  deg

Argument of perigee,  $\omega = 270$  deg  $\pm$  1 deg

Longitude of ascending node = 146.3 deg East  $\pm$  5 deg

The average number of QZSSs over the world is plotted in Fig. 2.8.

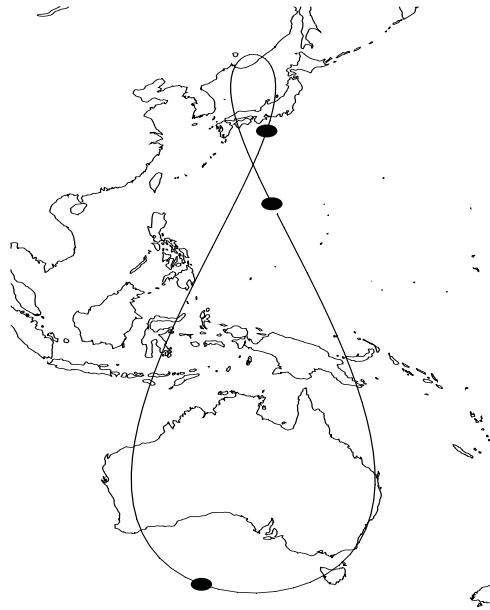


Figure 2.8: QZSS orbital ground track.

### Transmission Signals

QZSSs will transmit six positioning signals: L1C/A signal, L1-SAIF signal, L1C signal, L2C signal, LEX signal and L5 signal. Four of these, L1C/A, L1C, L2C and L5, are known as positioning availability enhancement signals (or simply availability enhancement signals) in the sense that they complement the existing GPS. The remaining two signals L1-SAIF and LEX are known as positioning performance enhancement signals (or simply performance enhancement signals) in the sense that they enhance performance through the transmission of existing GNSS differential data and integrity data [65].

The expected Doppler values for QZS signals received at some reference locations are shown in Fig. 2.10 as a function of time as they vary over the course of the QZS orbit. These values have been multiplied by the Doppler coefficients for each positioning signal frequency listed in Table 3.2. Note that these Doppler values are significantly smaller than for standard GPS satellite orbits.

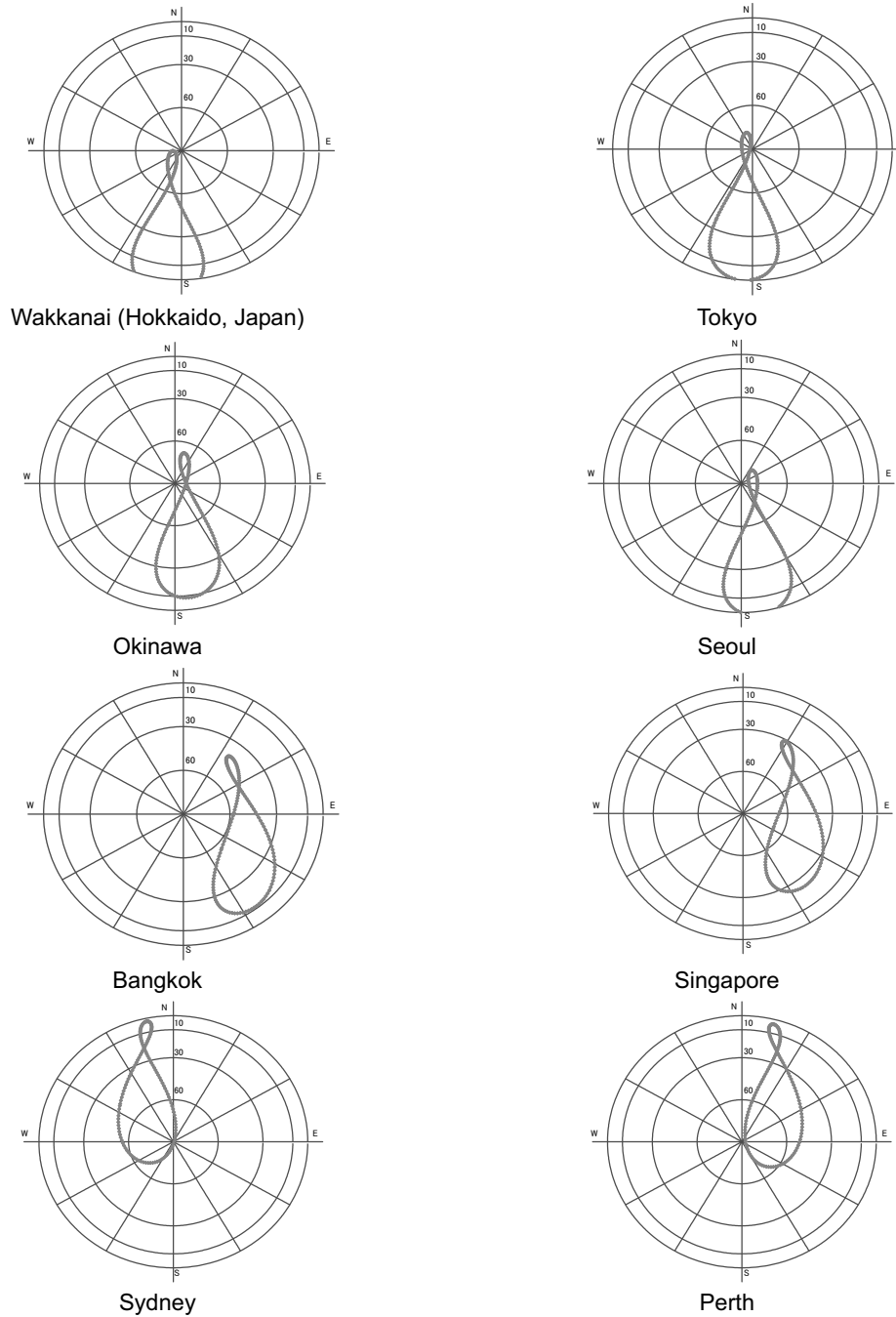


Figure 2.9: QZS elevation and azimuth (26.12.2009, 12:00 UTC) for several major Asian cities [65].

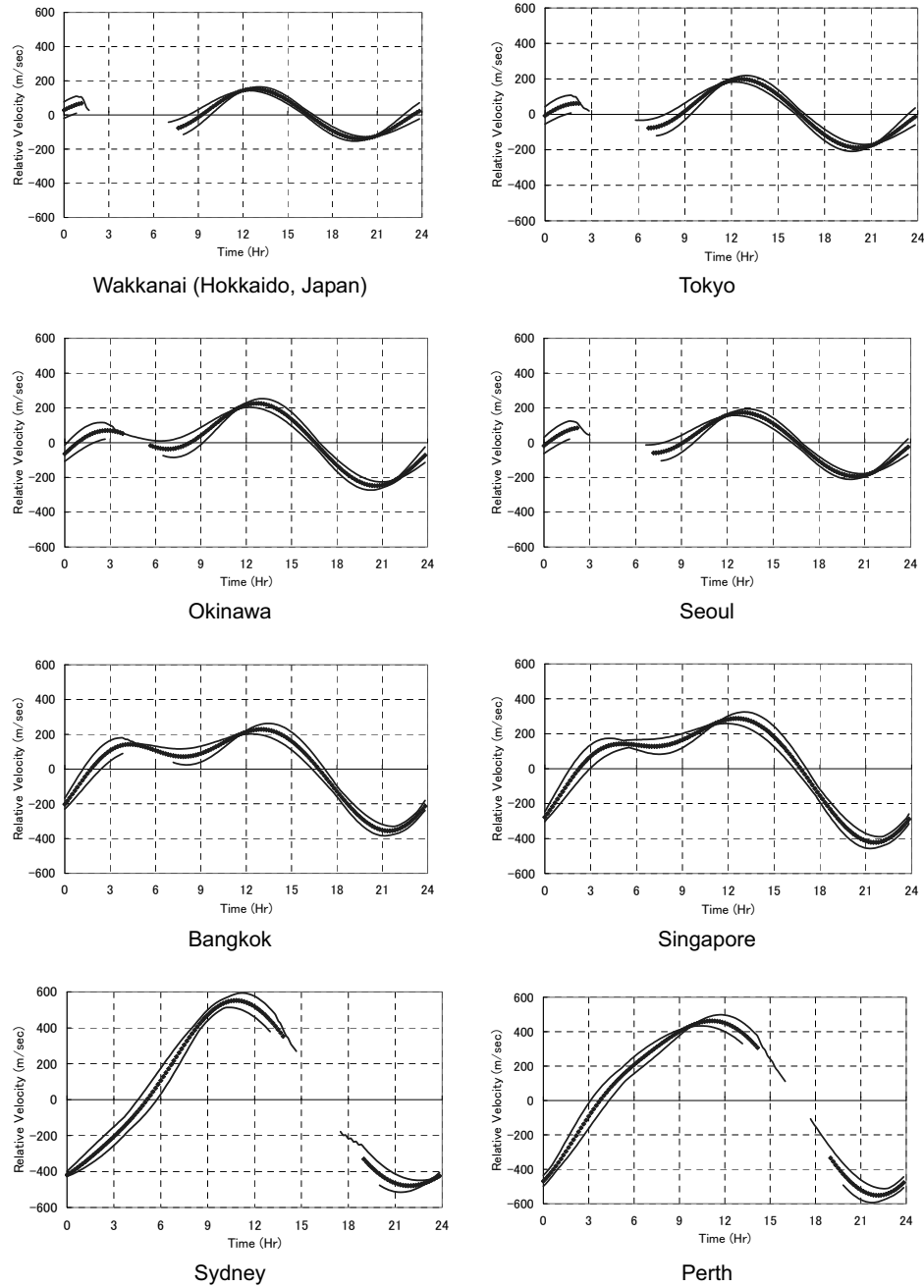


Figure 2.10: Relative velocity of signals for several cities (26.12.2009 12:00 UTC) [65]. Data outages are due to satellite visibility issues.

### **Elevation and Azimuth**

Plots of expected Elevation and Azimuth angles of QZSSs for each reference location are shown in Fig. 2.11 as they vary over the course of the QZSS orbit.

### **Time Scale**

The QZSS time scale is known as QZSSST, and will conform to UTC (NICT), and the offset with respect to the GPS time scale, GPST, will be controlled.

- One-second length. The length of one second is identical to International Atomic Time (TAI). It is also the same for GPS and GALILEO.
- Integer second offset for TAI. The integer second offset for TAI is the same as GPS, and TAI is 19 seconds ahead of QZSSST.

The difference between QZSSST and GPST will be accounted for in the QZSS data message so that QZSSs will appear as GPS ones as far as the user equipment algorithm is concerned.

### **QZSS Satellite Availability**

For the 3-satellite QZSS constellation, Fig. 2.12 shows the average number of QZSS visible from the Earth. Note that two or more satellites are always visible not only from Japan but throughout the Southeast Asia and Oceania regions.

Each QZSS transmits ionospheric parameters that are effective in relevant geographical regions. The accuracy of these parameters is detailed in [65].

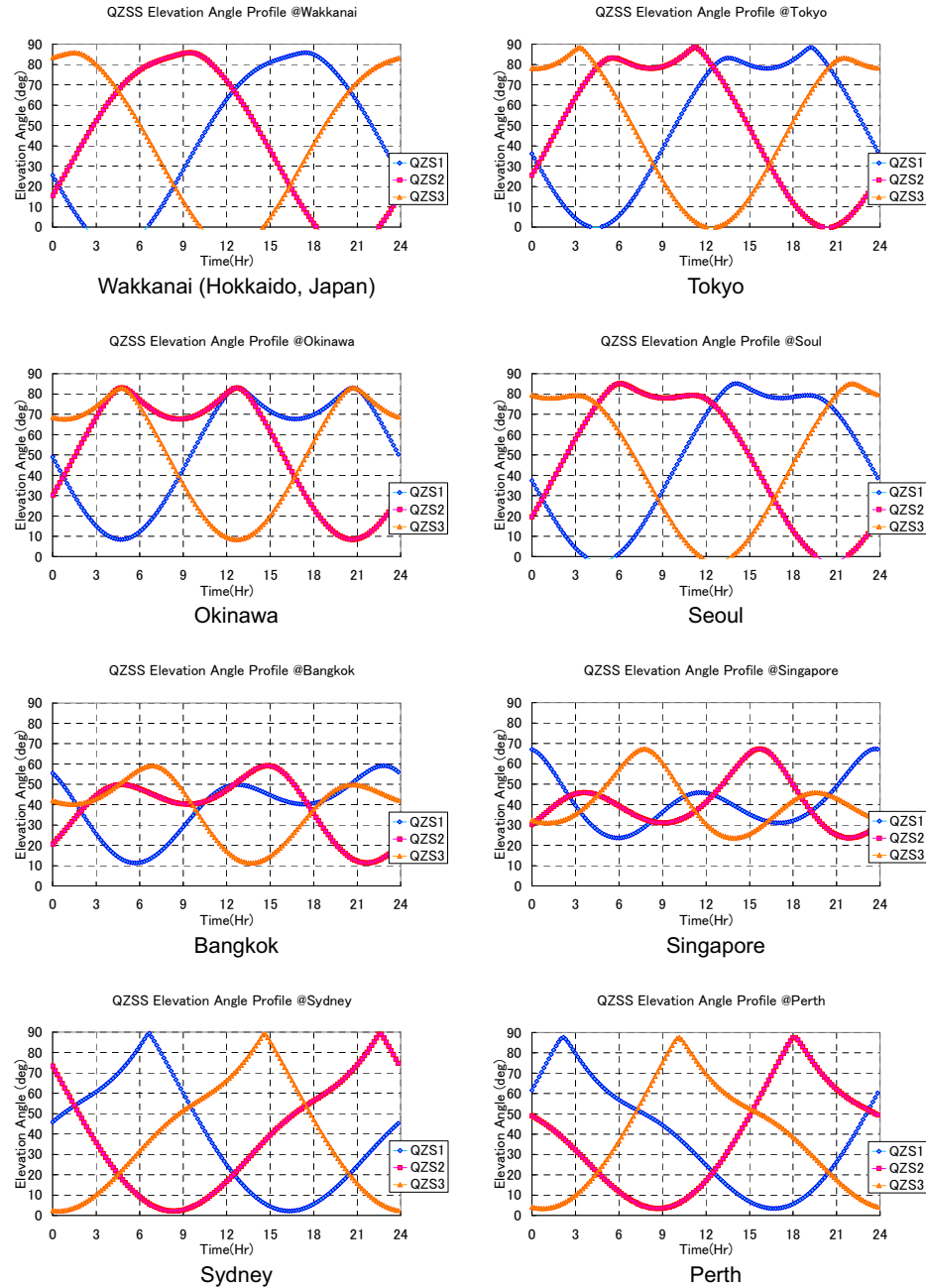


Figure 2.11: Variation of QZS elevation angle for several major cities (26.12.2009 12:00 UTC) [65].

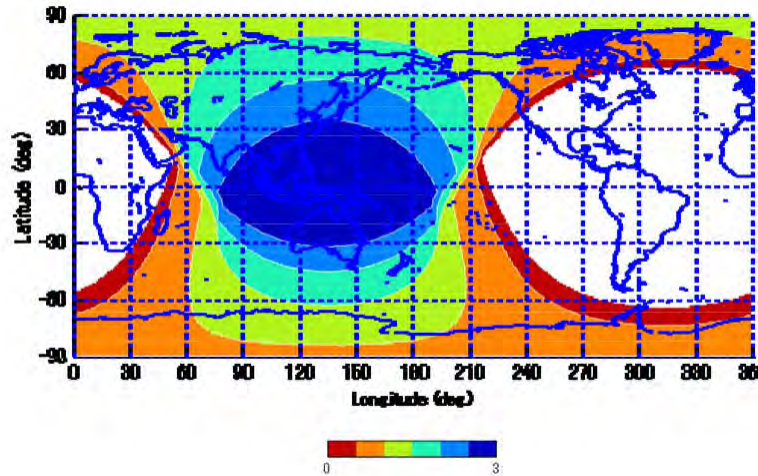


Figure 2.12: Average number of QZS that can be seen at an elevation angle of 10 deg or more [65].

## 2.4 MILSTAR Communications System

The MILSTAR system is a space-borne, multi-service communications system which provides the US Army, Navy, and the Air Force with command and control of strategic and tactical forces. The system is comprised of three segments: Terminal, Mission Control, and Space. The space segment consists of low data rate, medium data rate and crosslink communications payloads on geosynchronous satellites [23, 22].

The low data rate payload provides secure and jam-resistant teletype and voice communications. The satellites communicate with the ground through a suite of antennas, and have a crosslink capability. On-board signal processing allows the satellites to act as switchboards. Secure communications are achieved with standard techniques, including frequency hopping, permutation, interleaving and error correction [16].

Despite the different mission objective of MILSTAR when compared with QZSS, MILSTAR represents a good example of remote time synchronization implementation of satellite on-board clocks.

Satellite navigation and communication often require fairly precise synchronization (same phase) and syntonization (same frequency) among spacecraft clocks. The traditional method for achieving synchronization is by using a ground station to make

time-offset measurements to the various spacecraft clocks, and then update the time and frequency of each satellite as needed. Though it is easily implemented, there are disadvantages to this traditional approach. These include the large workload placed on the ground station, the need to have several ground stations to cover satellites in different orbital locations, and errors due to unaccounted-for delays due to atmospheric propagation [42, 15].

The MILSTAR communications system has chosen an alternative method for spacecraft synchronization and syntonization. MILSTAR's mission is to provide secure anti-jam communication capabilities for US DoD operations [35]. In order to accomplish that task MILSTAR employs precise timekeeping on its satellites and at its ground control stations [35, 40]. A MILSTAR ground station makes time-offset measurements to an in-view geosynchronous satellite, which for this illustrative discussion we will call the Master, and as a result of information passed along the satellite crosslinks, other satellites in the constellation (e.g. Slaves) autonomously synchronize and syntonize themselves to the Master. Since the ground station only needs to steer the time and frequency of a single satellite, its workload, and hence the timekeeping-related operational costs of the system, are minimised. Moreover, the synchronization among the satellites, without transmission through the ionosphere, means that atmospheric propagation delays cannot perturb the synchronization between spacecraft clocks [42].

The first of six MILSTAR satellites, DFS-1, was launched on 7 February 1994, while DFS-2, the second MILSTAR satellite, was launched on 6 November 1995. Each satellite carries a set of precise clocks: DFS-1 carries crystal oscillators, while DFS-2 carries Rb atomic clocks [42]. The ground stations maintain precise time with Cs atomic clocks. Following the launch of the second MILSTAR satellite, crosslinks between DFS-2 and DFS-1 were activated and DFS-1's time and frequency was slaved to DFS-2. In the slaving procedure, DFS-1 uses satellite crosslink information to rapidly correct its time in order to remain synchronized to DFS-2 and to periodically correct its oscillator frequency. DFS-2 is synchronized to UTC by a ground station that periodically collects timing information from the satellite, and, after a number of

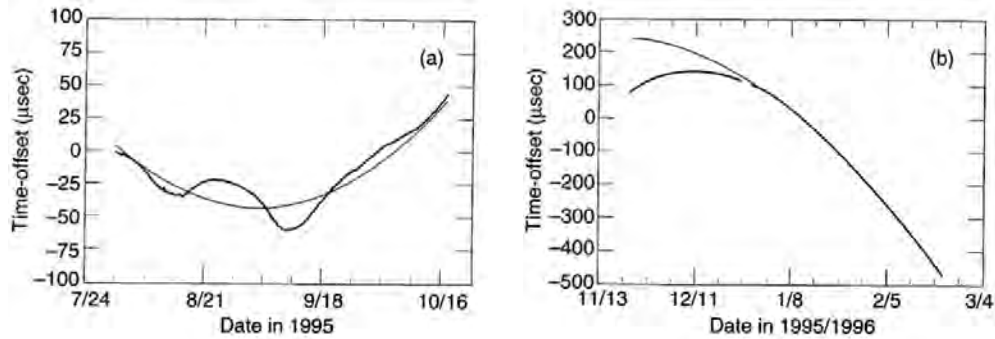


Figure 2.13: a) Raw time-offset history of the crystal oscillator onboard DFS-1 (thick line). b) Raw time-offset history of the Rb atomic clock onboard DFS-2 (thick line). Thin lines correspond to least squares quadratic fits to the data, and minor divisions of the horizontal axis correspond to seven day intervals [42].

days, commands time and frequency modifications to the DFS-2 satellite clock [24]. Timekeeping data can be collected by ground stations for both satellites. This data is archived along with any commanded time and frequency corrections. Using the archived data the reconstructed raw time offsets for the DFS-1 and DFS-2 clocks were obtained Fig. 2.13; that is, the time offsets that would have been observed on the ground had the ground station made no time or frequency corrections to the satellite clocks. The analysis of these raw time offsets using the Allan variance indicates that each clock is performing well and that when cross-link synchronization is initiated DFS-1 achieves a (150 ns or better) synchronization of DFS-2 without assistance from the ground.

#### 2.4.1 DFS-1 and DFS-2 Clock Performance

##### Deterministic Timekeeping Variations

The reconstructed raw time-offset measurements of DFS-1 and DFS-2 are displayed by the thick lines in Fig. 2.13 a) and b) respectively; thin lines show quadratic fits to the data. (In both figures, initial time and frequency offsets were subtracted from the data sets to better display the quadratic variation of time offset.) For DFS-1, the quadratic fit yields a  $+9.8 \times 10^{-13}$  /day drift rate, which is quite good for a crystal oscillator

clock [95]. Moreover, DFS-1 has exhibited this same drift rate since October 1994. Analysis of the data in Fig. 2.13 b) indicates that DFS-2 has a  $-1.5 \times 10^{-12}$  /day drift rate. The magnitude of this drift rate is consistent with pre-launch expectations for the DFS-2 atomic clock, at this point in its operating life, despite being slightly larger than that of the crystal oscillator clock. With continued operation, the slowly varying frequency drift rate should drop below the  $10^{-12}$  /day level and should ultimately become constant. The deviation of the raw time-offset data from the quadratic for the early part of DFS-2's time-offset history is a consequence of the atomic clock's warm-up behavior [121]. The important thing to note from Fig. 2.13 for future discussion is that the aging rate of the DFS-1 clock is distinctly different from that of the DFS-2 clock.

### MILSTAR Clock Allan Variance

Fig. 2.14 shows the resulting Allan deviation,  $\sigma_y(\tau)$ , versus  $\tau$  for the DFS-1 crystal oscillator and the DFS-2 Rb atomic clock. The dashed lines correspond to estimates of the Allan deviation based on a simple model: satellite to ground-station time-transfer noise dominates the Allan variance for  $T$  less than 10,000 seconds, while random-walk frequency noise dominates  $\sigma_y(\tau)$  for longer averaging times (satellite to ground-station time-transfer noise is associated with randomly varying delays at the transmitter, at the receiver and along the transmission path). For the crystal oscillator the long-term Allan deviation is well modeled by  $\sigma_y(\tau) = 1.6 \times 10^{-14} \times \tau^{1/2}$ , a value consistent with a high-performance crystal oscillator [17]. For the Rb atomic clock the long-term Allan deviation is well modeled by  $\sigma_y(\tau) = 2.2 \times 10^{-15} \times \tau^{1/2}$ , again a value consistent with a well-functioning device [49].

### 2.4.2 Autonomous Synchronization

Following the launch of DFS-2 the DFS-1 satellite became a slave to DFS-2. This meant that DFS-1 tied its crystal oscillator to the DFS-2 atomic clock using cross-link timing information. It is possible to reconstruct the timekeeping behavior of DFS-1 while it was slaved to DFS-2 using the archived data of DFS-1's time offset during the

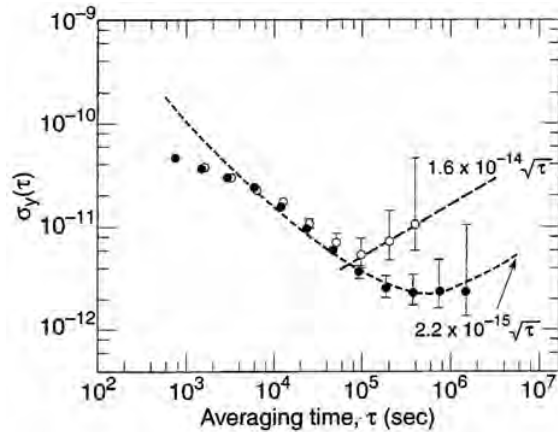


Figure 2.14: Allan deviation,  $\sigma_y(\tau)$ , versus averaging time, for the DFS-1 crystal oscillator (gray) and the DFS-2 Rb atomic clock (black). The short dashed curve is the anticipated  $\sigma_y(\tau)$  based on satellite to ground-station time-transfer noise and the Rb clock's random-walk of frequency noise. The long dashed line corresponds to the crystal oscillator's random-walk noise [42].

slaving period along with ground station corrections to DFS-2 and DFS-1. The black data points of Fig. 2.15 shows the raw time-offset of DFS-1 clock during a period in which DFS-1 is slaved to DFS-2. The curve is a quadratic least squares fit to the data. DFS-1 slaving to DFS-2 was deactivated for several days during this period (lack of black data points). Collected data yields a  $-2.3 \times 10^{-12}$  /day fractional frequency drift rate. This is to be compared with the DFS-1 crystal oscillator's intrinsic drift rate of  $-9.8 \times 10^{-13}$  /day. The  $-3 \times 10^{-12}$  change observed in DFS-1 drift is due to the fact that during this period DFS-1 maintained tight synchronization and syntonization to the DFS-2 Rb atomic clock, which had a negative drift rate. The incongruity between DFS-1's (apparent)  $-2.3 \times 10^{-12}$  /day drift rate and DFS-2's  $-1.5 \times 10^{-12}$  /day drift rate is a consequence of the few days during this period when slaving was turned off. If an attempt is made to account for those few days, the DFS-1 and DFS-2 drift rates become almost identical.

An estimate of the synchronization between DFS-1 and DFS-2 may be obtained from raw time-offset measurements made to both satellites by a single ground station. As illustrated in Fig. 2.16 this occurred in early February 1996. On 8 February 1996 a

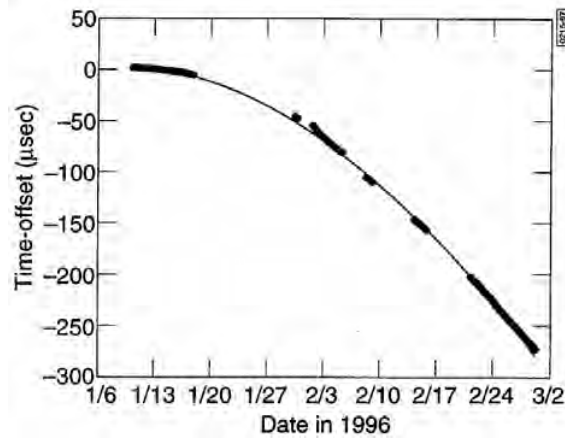


Figure 2.15: Raw time-offset of the DFS-1 crystal oscillator (black line) while it was slaved to the DFS-2 Rb atomic clock. The thin curve is a least squares quadratic fit to the data [42].

ground station commanded a time and frequency correction to the DFS-2 atomic clock and began making time-offset measurements to DFS-1 clock (filled circles). Then, on 9 February 1996 the same ground station began making time-offset measurements to DFS-2 clock (open circles). The solid line of Fig. 2.16 is a quadratic fit to all the data. It clearly indicates that the ground station synchronized DFS-2. DFS-1 was not corrected by any ground command, but rather by autonomous cross-link synchronization to DFS-2. Based on the deterministic and stochastic variations of the crystal oscillator's fractional frequency, and the fact that DFS-1 received its last correction from the ground on 4 February, DFS-1's time offset should have been appreciable on the scale of Fig. 2.16 (i.e., at the 1 sigma level somewhere within  $\pm 3\mu\text{s}$ ). However, as a consequence of cross-link synchronization to DFS-2, DFS-1's time offset was near zero.

The standard deviation of time-offset residuals from the quadratic regression line, are  $\sigma_{DFS-1} = 141$  ns and  $\sigma_{DFS-2} = 207$  ns. These variations about the regression line are a consequence of three factors. First, satellite to ground station time-transfer noise; second, diurnal oscillations due to the satellite clocks' temperature sensitivities, and third; crystal oscillator and atomic clock noise processes. In addition to this, the DFS-1 variations must include the residuals associated with the slaving process. As a

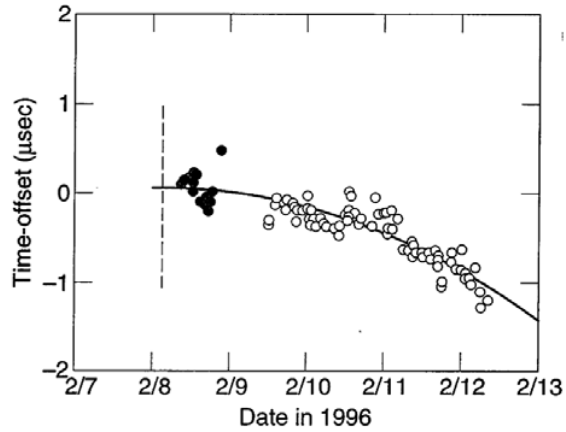


Figure 2.16: Raw time-offset measurements of the DFS-1 crystal oscillator clock (filled circles) and the DFS-2 Rb atomic clock (open circles) by the same ground station. The solid line is a quadratic fit to all the data [42].

result, we can obtain an upper bound on the slaving process's error in synchronizing DFS-1 to DFS-2 by combining these two standard deviation values:

$$\sigma_{slaving} = \sqrt{\sigma_{DFS-2}^2 - \sigma_{DFS-1}^2} = 152 \text{ ns} \quad (2.1)$$

Thus, the data demonstrates that the two spacecraft were synchronized to within  $\pm 150$  ns, without ground station intervention.

### 2.4.3 Final Remarks

MILSTAR is the first satellite system to employ cross link synchronization for geosynchronous spacecraft. The results reported here demonstrate the efficacy of that method. In particular, results show that cross-link synchronization has allowed DFS-1 and DFS-2 to achieve a 150 ns (or better) level of synchronization without control from the ground.

## 2.5 Two-way Satellite Time and Frequency Transfer System

TWSTFT via geostationary satellites [70] is a particularly useful technique for remote and accurate time and frequency transfer. Primary timing laboratories in Europe, North America and the Asia-Pacific region have established TWSTFT links through geostationary communication satellites for the calculation of International Atomic Time (TAI) and Coordinated Universal Time (UTC). By means of a simultaneous two-way transmission scheme, the time synchronization error introduced by the various systematic errors in Earth station coordinates, satellite coordinates and ionospheric and tropospheric delays are considerably reduced by TWSTFT. Delay instabilities remain within Earth station instruments which limit the stability of TWSTFT. Measurement and stabilization techniques and calibration systems of the delay instabilities have advanced, and have achieved sub-nanosecond accuracy [30, 9, 54].

The constant satellite position in relation to Earth stations means that geostationary communication satellites are particularly well suited to TWSTFT. However, the disadvantage of using geostationary satellites is that at high latitudes the satellites are at low elevation angles. Moreover, the number of satellites in geostationary orbit should be considered finite resources. Non-geostationary satellites, for example polar orbiters, are expected to open up new opportunities for TWSTFT links, especially at high latitudes. The relative motion of the satellites, as seen from Earth stations, is the major difference between TWSTFT via geostationary and non-geostationary satellites. The satellite motion produces non-reciprocal paths in TWSTFT, thus degrading the time transfer accuracy. In addition, geostationary satellites change their path length from Earth stations. The error owing to the non-reciprocal path in TWSTFT via geostationary satellites might be at most a few hundred picoseconds [50].

### 2.5.1 Two-Way Satellite Time and Frequency Transfer Theory

The TWSTFT method is one of the most accurate techniques for comparing distant clocks. The first satellite-based TWSTFT took place between the United States and the United Kingdom in 1962 using the Telstar satellite [47]. These early experiments

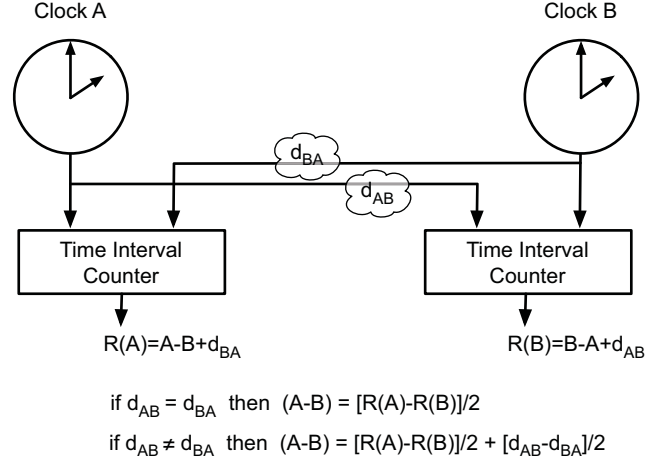


Figure 2.17: Basic two-way time transfer method [110].

led to an accuracy of  $0.1 \mu\text{s}$ . The discovery of the Sagnac effect, together with the employment of the PN sequences and several other enhancements, led to great improvements in terms of accuracy. Today, clocks are routinely compared world-wide using this technique through commercial communication satellites and commercial equipment. Accuracy greater than  $0.5 \text{ ns}$  at all times is now achievable [47].

The TWSTFT technique is illustrated in Fig. 2.17. Two clocks, clock A and clock B, are located far away from each other. Both clocks time information is sent through a double communication channel that can be a radio or phone channel, or a satellite communication channel.  $d_{AB}$  is the delay of the channel in one direction and  $d_{BA}$  is the delay of the channel in the other direction. Two time interval counters (TICs) are employed to estimate the phase shift  $R(A)$  and  $R(B)$  respectively. Once both  $R(A)$  and  $R(B)$  measurements are available, the difference is:

$$R(A) - R(B) = (A - B + d_{AB}) - (B - A + d_{BA}) = A - B + d_{AB} - B + A - d_{BA} \quad (2.2)$$

therefore:

$$A - B = \frac{R(A) - R(B)}{2} + \frac{d_{AB} - d_{BA}}{2} \quad (2.3)$$

which is the phase shift between the two clocks. Furthermore if we could assume that the two communication channels have the same delay, the phase shift between the two clocks would become simply half the difference of what the two TICs indicate:

$$A - B = \frac{R(A) - R(B)}{2} \quad (2.4)$$

Generally, the implementation of this method is via a geostationary satellite and the communication channel between the two clocks is a ground-satellite-ground link. Hence, the rotation of the Earth during satellite communications generates an additional delay, known as the Sagnac effect, that needs to be considered. Uncertainties below 1 ns are commonly achievable and time comparison of clocks located in different parts of the world is possible. The TWSTFT method is now a very common method for comparison of ultra-stable atomic standards located anywhere in the world [47].

### 2.5.2 Influence of Satellite Motion on TWSTFT

Non-geostationary satellite motion can cause different signal delays between uplinks and downlinks in TWSTFT [129]. The signal delays in uplinks and downlinks consist of geometric path delays and ionospheric and tropospheric delays. The geometric path delays are generally several orders of magnitude larger than the ionospheric and tropospheric delays. The temporal and spatial variation of the total electron count, air and moisture content along the line of sight varies only slightly within the typical round-trip propagation time of TWSTFT signals, while their daily and seasonal variations are considerable [129]. In other words, the ionospheric and tropospheric delays can be cancelled with TWSTFT via non-geostationary satellites to the same degree as TWSTFT via geostationary satellites. Accordingly, the differential ionospheric and tropospheric delays here have been intentionally omitted. Similarly, for TWSTFT via geostationary satellites, the dependence of the ionospheric delays on frequency produces a certain amount of differential ionospheric delay between uplinks and downlinks. Since the ionospheric delay is inversely proportional to the frequency squared, adoption of high-frequency Ku-band (10 GHz to 15 GHz) radiation in uplinks and downlinks reduces the differential ionospheric delay to several hundred picosec-

onds even at the solar maximum [129]. Several hundred picoseconds of differential ionospheric delay is a small but significant contribution to the subnanosecond time transfer. TWSTFT via geostationary satellites often corrects such ionospheric delays with an empirical model of the ionosphere, especially near the geomagnetic equatorial region. In the QZSs, since the QZS also transmits L-band signals, which have 100 times the sensitivity to electron density along the line of sight as Ku-band, ionospheric delays can be calculated to a higher accuracy than general TWSTFT via communication satellites, which use only Ku-band [129]. Yokota's [129] model investigated only the differential geometric path delay in the discussion of whether TWSTFT via non-geostationary satellites can achieve subnanosecond accuracy. However, when closely examining the accuracy within 1 ns of TWSTFT via either geostationary and non-geostationary satellites, the differential ionospheric and tropospheric delays and delays of Earth station instruments need to be taken into account. Note that the Sagnac effect also affects the path non-reciprocity in TWSTFT [70]. This was also omitted in the Yokota's model because computation of the Sagnac effect can be done more accurately than calculation of the differential geometric path delay by using the same estimated positions of the satellites and Earth stations. Here, the non-reciprocal geometric path delay will be examined using a simple two-dimensional model as shown in Fig. 2.18. A satellite orbits the Earth at the same altitude ( $h = 36\,000$  km) and speed ( $v = 3.1$  km/h) as geostationary orbiters. The Earth and an Earth station, labeled as E, are fixed.

Consider points S1 and S2 as satellite positions when the satellite transmits to and receives from the Earth station, respectively. The path length  $l(t)$  between the satellite and the Earth station at time  $t$  is given by:

$$l(t) = \sqrt{(R_E + h)^2 + R_E^2 - 2R_E(R_E + h)\cos\omega t} \quad (2.5)$$

where  $R_E$  denotes the approximate Earth radius (6380 km) and  $\omega$  denotes the angular frequency equal to  $v/R_E \approx 7.27 \times 10^{-5}$  rad/s. The time difference  $t$  between the transmission and reception of the satellite provides the non-reciprocal geometric path or the difference between the path lengths in uplinks  $l_u$  and downlinks  $l_d$ ;  $l(t)$

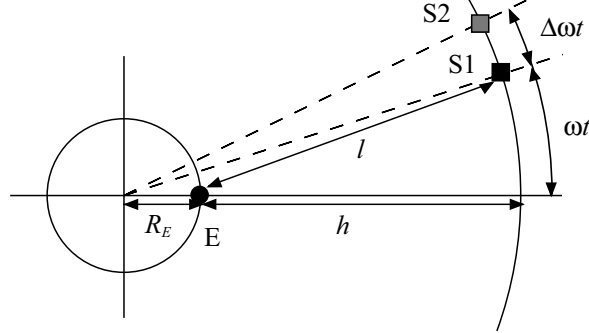


Figure 2.18: Schematic view of the positions of an Earth station (E) and a non-geostationary satellite (S1 and S2) moving counterclockwise around the Earth [129].

and  $l(t+\delta t)$  correspond to  $l_u$  and  $l_d$ . Note that  $t$  in TWSTFT can be up to the propagation time (0.1 s) or sampling time (typically 1s). Because  $\delta t \ll 2\pi/\omega$ , the differential geometric path length  $l(t+\delta t) - l(t)$  can be approximated by  $(dl(t)/dt)\delta t$ . As a result, assuming that the uplink and downlink propagate at the speed of light  $c \approx 3.0 \times 10^8$  m/s, the differential geometric path delay (in seconds) is expressed as:

$$\frac{|l_u - l_d|}{c} \cong \left| \frac{dl(t)}{dt} \frac{\Delta t}{c} \right| < \frac{\omega}{l} (R_E + h) R_E \frac{\Delta t}{c} \cong \Delta t \times 10^{-6} \quad (2.6)$$

Synchronization between the satellite transmission and reception within 1 ms is required for implementing TWSTFT via non-geostationary satellites to subnanosecond accuracy. Since such simultaneity is not constantly assured in the actual TWSTFT, where separated receivers work independently, corrections to the differential geometric path delay using the estimated satellite position will be considered. In Fig. 2.18, points S1 and S2 represent the actual and estimated positions of the satellite, respectively  $l(t)$  and  $l(t+\delta t)$  become the actual path length  $l$  and the estimated one  $\tilde{l}$ . The estimated accuracy of the satellite position  $\Delta r_s$  (meters) is given by  $\Delta r_s = \Delta t v$ . As a result, we obtain a residual of the geometric path delay correction (seconds) expressed as:

$$\frac{|l - \tilde{l}|}{c} \cong \frac{dl(t)}{dt} \frac{\Delta r_s}{c} < \Delta r_s \times 10^{-9} \quad (2.7)$$

The expression suggests that the satellite position should be known to an accuracy

of less than a meter for sub-nanosecond accuracy of TWSTFT via non-geostationary satellites. For example, the International GNS Service (IGS) provides estimated GPS satellite ephemerides with accuracies at the few decimeters or less. Even for one-way time and frequency transfer between a satellite and an Earth station, real-time correction of the influence of satellite motion possibly assures the sub-nanosecond accuracy, while  $\Delta r_s$  is confined to being peripheral to the satellite motion. Equation 2.7 indicates the accuracy better than one-way geometric path delay correction. There is a possibility that even some ephemerides with an accuracy of more than 1 m would ensure sub-nanosecond accuracy of the two-way geometric path delay correction  $|(l_u - l_d) - (\tilde{l}_u - \tilde{l}_d)|/c$ .

Recent studies, [129], demonstrate that the differential geometric path delay of microseconds is produced by the time difference (of seconds) between the satellites transmission and reception. Orbit estimation, even with 1 km accuracy, enables the correction of the differential geometric path delay with sub-nanosecond accuracy. TWSTFT via non-geostationary satellites can achieve the same accuracy as that via geostationary satellites. Similar to TWSTFT via geostationary satellites, the future challenges of TWSTFT via non-geostationary satellites which will need to be addressed for advancing the accuracy are the measurement, stabilization and calibration of the delay instabilities in Earth station instruments [129].

### 2.5.3 Dynamic Two-way Time Transfer

Unlike the Static TWTT which has been used for years over satellite links between static locations, the Dynamic Two-way Time Transfer (DTWTT) involves performing the same measurement where one (or both) may be moving. A characteristic example is a satellite channel used between a ground node and an air-borne node. This case is identical to the static one except one of the nodes is now moving over the measurement interval. The computation of the two-way clock difference is changed by the addition of platform motion. More details can be found in [25].

There are multiple effects that change the frequency of a clock in motion. Clock effects include gravitational potential, velocity and Sagnac effects, and depend on

altitude, speed, and/or direction. Each of these clock effects acts on the physical clock, altering its performance from its static state. While these effects are interesting, they are not corrected for in the DTWTT measurement. The fact that one or both of the clocks is running faster or slower due to relativistic effects will be measured using the two-way calculation and can be compensated for by the user of the two-way data.

### DTWTT Performance

[25] presents flight tests where two identical sets of DTWTT equipment were installed on an aircraft and the ground to make the timing measurements between two clocks.

The RF ground equipment was standard commercial hardware and the RF equipment on the aircraft was a custom terminal built for flight use. The modems were commercial satellite communications units that were modified to provide two-way measurements in the background of standard data transmission. The measurement chassis consisted of precision timing equipment including two-channel timers, amplifiers, and a controlling computer. The computer was used to control the measurement collection and process the two-way measurements. The aircraft also included multiple measurement devices (GPS and INS) to determine its location during flight. The data collected during a flight test over a Ku-band communications channel was used between the ground and the aircraft. A commercial satellite was used to create a data channel with 768 kbps user data rate and Viterbi coding. Fig. 2.19 shows the time difference of the two clocks before and after the experiment, the intermediate line is the DTWTT measurement. The real-time difference can only be inferred from its distribution before and after the experiment. However as reported in [25], a time error  $< 1$  ns (rms on a 30-second average) for the whole experiment duration is a reasonable assumption.

## 2.6 Final Remarks and Summary

The broad objective of this dissertation is to present the main problems associated with a TKS for the QZSS augmentation system which does not require any satellite on-board atomic reference and to provide some conceptual solutions to these problems.

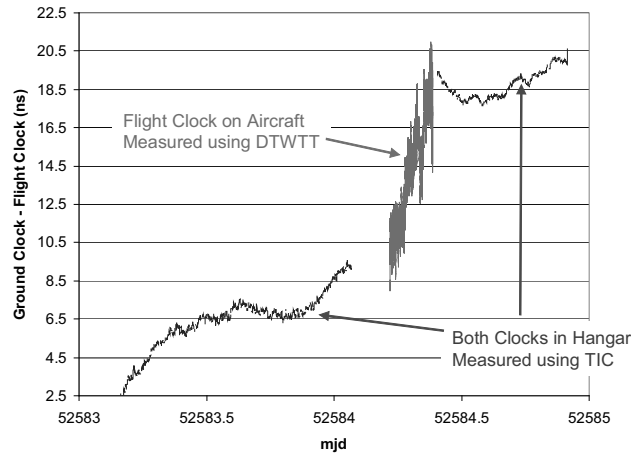


Figure 2.19: DTWTT performance in the test flight described in [25].

In order to understand what solutions have been successfully implemented and how to use the knowledge available in the literature, in this Section we presented the following architectures:

- The positioning system GPS and its TKS.
- The positioning system GALILEO and its first test satellite GIOVE-A.
- The Japanese QZSS for which the proposed system is designed.
- The military satellite system MILSTAR and its remote time inter-synchronization implementation for satellite on-board clocks.
- The TWSTFT system for QZSS as tool to measure the time difference between two moving clocks. In addition a DTWTT experimental setup with an air borne platform.

The QZSS augmentation system is very likely to have similar features and problems as those solved when designing the GPS TKS. GALILEO, and specifically GIOVE-A, represent an alternative development of a satellite-based system similar to GPS. The MILSTAR mission is a three satellite military system where satellite time synchronization is successfully implemented to synchronize clocks flying on board the

satellites. MILSTAR is the closest implementation, documented in literature, of time synchronization implemented for satellite clocks.

In the last section, an overview of TWTTs was presented with particular focus on TWTTs for non-geostationary satellites.



## Chapter 3

# RESSOX System

A feasibility study of the remote synchronization system for the on-board crystal oscillator (RESSOX) of the QZSS is proposed. Aimed at offering an alternative architecture to the classic GPS TKS, the RESSOX system consists of a synchronization framework where a voltage-controlled crystal oscillator, on board the QZS, is kept synchronized to an ultra-stable atomic clock, located at the ground station. Based on orbit calculations and delay predictions, feedback and feed-forward controls provide the correct synchronization correction to the remote time reference on board the satellite. Compared with the classic GPS TKS, the RESSOX scheme offers several advantages in terms of accuracy, cost, weight and power consumption.

In the following sections, a system-level design for RESSOX and its feasibility study is proposed. The RESSOX feedback and feed-forward architecture is presented together with its main subsystems. A delay budget used to generate the command signal for the RESSOX synchronization feed-forward subsystem is discussed. Synchronization performance study of the feed-forward sub-block is presented together with its coupling with the feedback sub-block. Synchronization results of a hardware experimental version of the feedback/feed-forward system is presented.

Differences and advantages of the proposed system are compared with the classic atomic clock scheme. Furthermore, the results of the study of the proposed on-board and ground-site subsystems are presented.

### 3.1 Introduction

The QZSS is a satellite augmentation system that will provide an improved positioning service over Japan and Australasia [65, 87]. Details of the QZSS can be found in Section 2.3.

QZSS consists of three satellites placed in three separate elliptic orbits with an orbital inclination of 45 deg and a right ascension of ascending node of 120 deg. All three orbits are geosynchronous with a semi-major axis of about 42,164 km. A constellation such as this would guarantee the presence of at least one satellite, periodically replaced (with hand-over) every eight hours over Japan, 24 hours a day. Fig. 2.8, in Section 2.3.2, shows the orbital ground track of QZSS.

Since time synchronization accuracy is a key issue, GPS satellites are equipped with very stable time references, the basis on which the positioning signal is generated. In the case of GPS, such a stable time reference signal is based on Rb and Cs on-board atomic clocks [85]. A sophisticated TKS couples the atomic clocks with an ultra-stable voltage-controlled crystal oscillator and allows time synchronization/correction between the satellite signals. Atomic clocks are employed as on-board time references because: 1) an atomic clock has very good long-term stability, 2) a single ground station cannot be continuously linked to the satellites as they orbit around the Earth, 3) being military-based, the system should be autonomous, that is, it does not rely on any ground station. In fact, in the case of war, the GPS must be fully station-independent, at least for a limited period of time [85, 84].

By contrast, the Japanese QZSS has a wholly different orbit system [87, 126]. First of all, being intended for civil use, it does not have the same military requirements as GPS. Furthermore, because of the QZSS orbit design, each QZS can remain visible to the ground station throughout its entire orbital period. Hence, it is conceptually feasible to locate a low-cost and low-weight time reference device on-board the satellite, and to keep it synchronized to a highly stable time reference located on the ground by adopting an uplink/downlink architecture. Hence the satellite itself would broadcast very precise time information that is actually generated on the ground by an atomic clock network.



Figure 3.1: RESSOX system. The QZSS works as complementary system for the present GPS and also provides augmentation features.

RESSOX represents an alternative solution to the classic TKS scheme. Fig. 3.1 shows the basic scheme of this novel synchronization system. It is also notable how the RESSOX satellite will be combined with the present GPS system to improve position accuracy.

To better explain the conceptual difference between the GPS Block-IIR and the RESSOX concept, Fig. 3.2(a) shows the GPS Block-IIR TKS scheme where the on-board crystal oscillator is locally synchronized with the on-board atomic clocks. The overall system will have the short-term stability of the crystal oscillator and the long-term stability of the atomic clock which acts as the on-board reference clock. On the other hand, in the RESSOX scheme (Fig. 3.2(b)), the QZS on-board clock, a highly stable VCXO, is remotely driven by the synchronization framework by taking advantage of the time reference located at the ground station. Therefore the satellite clock will act as a transponder. For the RESSOX system then, the overall short-term stability is expected to be at least as good as that of the GPS Block-IIR TKS and the long-term stability is guaranteed by the ground clock [59].

The main advantage of RESSOX with respect to the classic TKS is the absence

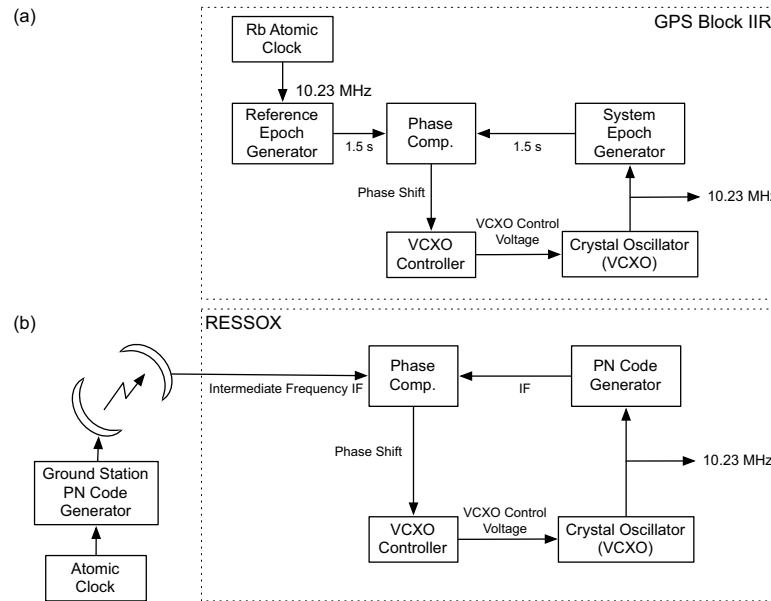


Figure 3.2: Conceptual comparison of the GPS Block-IIR (a) and a remote synchronization scheme (b) where no on-board atomic clock is used.

of the delicate, expensive and relatively heavy atomic clocks on-board each satellite. Moreover, because of the very good short-term frequency stability ( $t < 1000$  s) of the VCXO, similar or better performance to that of the classic GPS is expected. Table 3.1 presents a comparison of the Cs atomic clock, Rb atomic clock and the VCXO.

In the literature, there are similar examples of the satellite atomic clock being replaced by a sophisticated uplink/downlink synchronization network. For instance, in [42] Camparo *et al.* presented an inter-satellite synchronization system for the military telecommunication satellite system MILSTAR; the first satellite system to employ cross-links for precise satellite time synchronization. The first MILSTAR satellite has its time and frequency tied (i.e. slaved) to the Rb atomic clock carried onboard DFS-2, the second MILSTAR satellite. The DFS-2 Rb atomic clock was controlled by the ground, while the slaving of DFS-1 to DFS-2 was accomplished without ground intervention; all timing information required by the slaving algorithm was obtained through the DFS-1 to DFS-2 satellite cross-link. For more information refer to Section 2.4.

Table 3.1: Comparison of Cs atomic clock, Rb atomic clock and VCXO [85, 84].

Type	Short-term stability	Mass (kg)	Lifetime (years)	Volume (mm <sup>3</sup> )	Power (W)	Price (yen)
Cs atomic cl. (Datum)	1s $1 \times 10^{-11}$	15.1	$\sim 7.3$	159X191X419 12.7 liters	50 (warm up)	55M
	10s $6 \times 10^{-12}$				33 (steady state)	
	100s $2 \times 10^{-12}$					
	1000s $6 \times 10^{-13}$					
Rb atomic cl. (PerkinElmer)	1s $3 \times 10^{-12}$	5.8	$\sim 10$	127X216X147 4.03 liters	65 (warm up)	44M
	10s $1 \times 10^{-12}$				39 (steady state)	
	100s $3 \times 10^{-13}$				14(+45 base plate)	
	1000s $1 \times 10^{-13}$					
VCXO (Kernco)	1s $4 \times 10^{-13}$	1.4	20+	76X76X216 1.24 liters	5	30M
	10s $3 \times 10^{-13}$					
	100s $5 \times 10^{-13}$					
	1000s $2 \times 10^{-12}$					

Another example of a time synchronization technique similar to RESSOX, but based on the TWTT scheme, is reported in [110]. For more information refer to Section 4.

In the following sections, the implementation of the RESSOX scheme is presented. Given that RESSOX is a ground-satellite synchronization scheme, an analysis of all the signal delays that should be carefully considered in its implementation is presented.

Most of the material related to this Chapter has been published by the author in conference proceedings [118, 115, 110, 117, 116] and in international journal articles [114, 63]. The research activity related to this Chapter has led to the development, in collaboration with Mitsubishi Space Software Inc., of a Software Simulator, described in the Section B, and to a Hardware Simulator, by AIST, described in Section A. Both tools have been greatly improved during the RESSOX research. The RESSOX idea was originally presented by Iwata *et al.* in [59]. The research work presented in this Chapter, the simulations, the development of some of the models (refer to Section B) and the development of some of the hardware (refer to Section A) were carried out by the author. Essential assistance in this study was provided by Dr. Iwata, co-supervisor of this thesis and by Mr. Nakajima of Mitsubishi Space Software Inc..

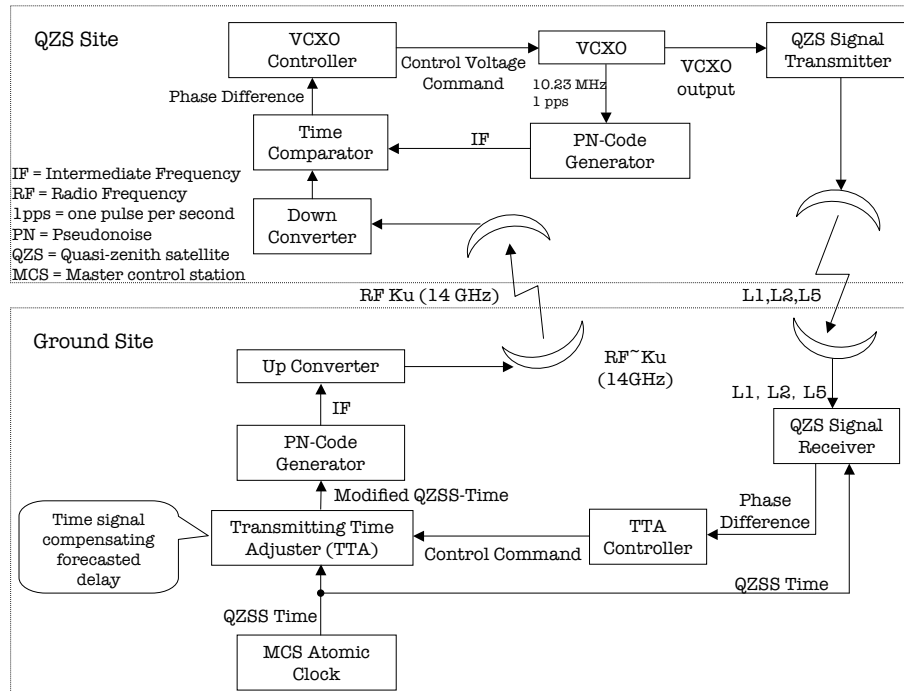


Figure 3.3: RESSOX system, basic schematic.

## 3.2 The RESSOX System

### 3.2.1 Structure and Functioning

A detailed representation of the RESSOX scheme is shown in Fig. 3.3. The top half represents the assembly on board the satellite. The bottom half is the representation of the equipment at the ground site. The uplink communication channel (RF, Ku-band,  $\sim 14$  GHz) is employed for the realization of the *feed-forward control* responsible for the direct synchronization/correction of the on-board VCXO with the local ground-site time reference. The downlink communication channel (L1, L2 and L5 band) is used as feedback to realize the *feedback control*. Together with the QZSS orbit estimation model and the QZSS delay estimation model, the feedback control evaluates/improves the synchronization quality between ground-site and satellite.

On board the satellite, the core of the TKS is the highly stable VCXO. With its high short-term stability, it provides the QZS with a stable time reference signal.

Such a signal is coupled, via a time comparator, to the correction signal coming from the ground station. The local time (satellite VCXO time) signal phase is changed by controlling the input voltage of the VCXO. The comparison of the phase difference by means of the time comparator is performed every epoch (1 s) through the comparison of the pseudonoise (PN) code of the local VCXO signal and the ground station signal. In order to successfully lock the VCXO output with the down converter output, a phase locked loop (PLL) scheme is employed and a dedicated control algorithm is used for the correct phase lock [92, 88]. The final VCXO output is sent back to Earth through a QZS L1/L2/L5 signal generator, that is, the usual navigation signal.

The other half of the system represents the ground site. Here, ultra-stable atomic clocks provide the QZSS time reference, synchronized to UTC(NICT) managed by the National Institute of Information and Communication Technology (NICT).

A comprehensive software model of the QZSS orbit and all of the delays that occur to the signal between the satellite and the ground station is employed in the feed-forward control to smoothly drive the Transmitting Time Adjuster (TTA) and produce a modified version of the QZSS time that is then broadcast to the QZS. The QZSS time is modified such that once it reaches the QZS, the phase difference between the ground-site time reference (QZSS time) and the modified version received by the time comparator (satellite time) is as close as possible to 0 ns.

The second control, the feedback control, is implemented through the use of the QZS signal receiver. Here the VCXO output signal is received at the ground station and compared to the local QZSS time. The resulting phase difference is used to verify and refine the correct synchronization of the VCXO with the QZSS time.

Fig. 3.4 shows how the two controls coexist and how they both drive the TTA, taking advantage of the orbit estimation and the delay calculation, as well as the feedback signal available from the QZS signal receiver.

The control of the TTA and the construction of the delay prediction model is performed in real-time and requires a significant amount of computational power (ionospheric and tropospheric delay calculation, QZS orbit estimation, relativistic effects and geometric delay calculations, etc.). Precise estimation of such delays is a key

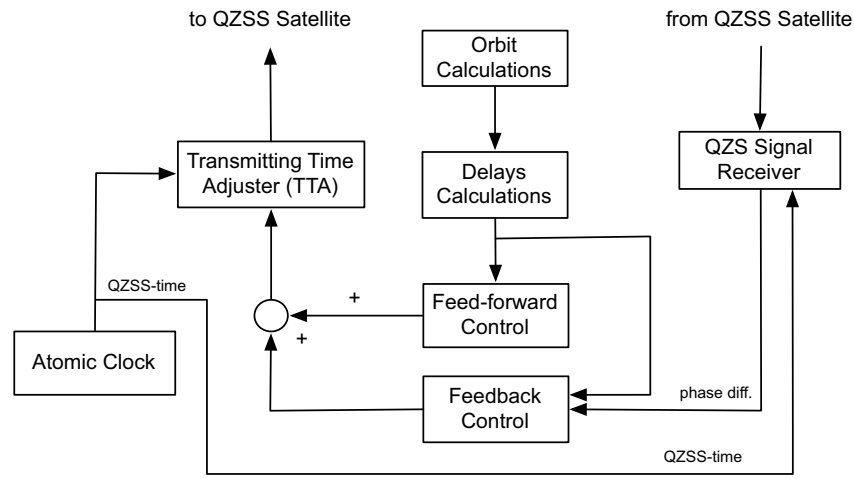


Figure 3.4: Flowchart of double RESSOX control. The orbit calculation and the delay calculations are used to drive the feed-forward control through the TTA. The feedback control is used to refine the correction signal, taking advantage of the feedback time information available at the QZS signal receiver.

requirement for the successful realization of RESSOX.

In the following sections, the main components of the RESSOX scheme will be described and the requirements and critical issues will be presented.

### 3.2.2 Transmitting Time Adjuster (TTA)

The TTA is responsible for compensating for the delays that occur during signal propagation between the ground station and the satellite. Furthermore, considering that the QZS travels at a variable speed of 0~300 m/s (with respect to the ground station), the TTA must be able to respond to this velocity (a real-time system constraint) and provide a delay compensation signal that has a maximum speed variation of  $1 \mu\text{s/s}$ . Moreover considering that the distance between the satellite and ground station is the predominant delay, the TTA must be able to provide roughly the same delay compensation value. Thus, a delay capability in the range of 0.1~0.2 s is required.

### 3.2.3 PN Code Generator

The time information necessary to correct and synchronize the on-board VCXO is transmitted to the QZS through a PN code using the Ku-band and is modulated using BPSK modulation. The PN code is a 5115-bit sequence and is repeated every 0.5 ms. The RESSOX control signal has a data overlay of 2000 bit/s to resolve the 0.5 ms ambiguity. The overlay data is dummy data with the pattern of 0s and 1s.

### 3.2.4 QZS Signal Receiver

At the ground-site, such signals are used as a feedback command to measure the signal travel delay by means of the QZS signal receiver. The QZS signal receiver reconstructs the VCXO time signal and compares it (through the PN code) with the QZSS time. The difference is used to drive the TTA via the timing controller. Therefore, the QZS signal receiver must be equipped with a stable phase comparator to generate the phase difference signal. Considering the fact that the total acceptable time discrepancy is 10 ns, a resolution of approximately 1 ns (10 % of the total error), or less, is required.

### 3.2.5 VCXO

As mentioned above, the allowed time discrepancy between the ground time reference (QZSS time) and the VCXO (RESSOX time accuracy) is about 10 ns. The relative user equivalent range error (UERE) would be about 3 m, similar to the basic requirement for the GPS on-board clock build-up error originally specified as 5 ft (about 1.52 m). On board the satellite, the phase difference measurement is performed by the time comparator and its accuracy is limited to approximately 0.1 ns (a hardware limitation). Therefore, it is reasonable to fix the requirement for the VCXO time accuracy to be approximately 0.1 ns for every epoch. On the other hand the QZS cannot be kept linked to the ground station 24 hours a day; in fact, when a QZS reaches the equatorial region, communication to the satellite must be shut down to avoid interference with local geostationary satellites. Such a “dark period” lasts for approximately 40 minutes (2400 s) and occurs twice a day. A VCXO free-run for a 2400 s period imposes a constraint for the VCXO frequency stability of less than

$(10 \text{ ns})/(2400 \text{ s}) = 4 \times 10^{-12}$  over the 2400 s period. Considering also that other errors will eventually contribute to the deterioration of the RESSOX accuracy, the final requirement for the VCXO frequency stability should be of the order of  $10^{-12}$  over a period of 2400 s. As shown in Table 3.1, the Kernco VCXO can satisfy such a requirement.

### 3.2.6 Time Comparator

On the QZS, the time comparator is one of the most important components because it is responsible for the correct VCXO output signal phase comparison. If a time interval counter (TIC) were adopted directly with the 10.23 MHz VCXO time signal, an ambiguity of about 100 ns would be introduced (cycle ambiguity). In order to avoid such a problem the phase evaluation is implemented using a PN code. The phase comparison between the local time (on-board VCXO time) and the time information uplinked from the ground station is then measured with an intrinsic time comparison ambiguity of 1 s.

## 3.3 Delays and Error Estimation Models

For the successful realization of RESSOX, estimation of signal delays and approximation errors is essential. The RESSOX numerical model includes the delay in the ground station equipment and in the satellite equipment, the delay in the ionosphere and troposphere, the satellite trajectory estimation error (including the gravity potential model, other celestial body effects, solar radiation pressure and the tidal effect) and the relativistic effect.

In the following sections, the delays that occur as the signal travels from the ground station to the satellite are analyzed. Moreover, the whole RESSOX synchronization loop, realized through the uplink/downlink connection between the QZS and the ground station, has such phase shift synchronization constraints that delays in the circuitry used on board the satellite and at the ground station must be carefully estimated and eventually taken into account. Any electronic equipment that is interposed inside the synchronization loop could be a cause of non-negligible delay. In order to

investigate the order of magnitude and the nature of these delays, some experiments were carried out. All the electronic instruments used in the synchronization loop were tested and the phase-shift error was measured. A numerical simulation tool has also been developed, by which the delays such as those due to the ionosphere, troposphere, tide effect, solar pressure, relativistic effects and geometric and orbit errors can be estimated.

### 3.3.1 Delays at the Ground Station and in the QZS

#### Delay in the Cables

The delay in the connection cables used for wiring the RESSOX Hardware Simulator was experimentally measured using a 5 MHz sinusoidal signal and the universal time interval counter Stanford Research Systems SR620. The results show an average delay of 5 ns per linear meter (with a measurement uncertainty of 0.4 ns). This value is confirmed by the empirical formula for calculating the phase delay,  $D_{cable}$ , in a coaxial cable:

$$D_{cable} = \frac{\ell_{cable} \sqrt{\mu_s \epsilon_s}}{c} \quad (3.1)$$

where  $\ell_{cable}$  is the cable length in meters,  $\mu_s$  and  $\epsilon_s$  specify the dielectric type and  $c$  is the speed of light in free space (299,792,458 m/s). For a polyester coaxial cable,  $\mu_s = 1$  and  $\epsilon_s = 2.3$ , the result is a delay of 5.06 ns/m.

#### Delay in the TTA-PN Code Generator-Time Comparator chain

The internal delay for the combined modules, TTA, PN Code Generator and Time Comparator (satellite side), was experimentally measured and an average delay of 2.96  $\mu$ s was estimated. The deviation of the distribution that represents the time delay is fairly small (0.4 ns) so the assumption of a constant time delay value is reasonable. The experimental setup employed for this measurement consisted of a Cs atomic clock as signal source and a universal time interval counter Stanford Research Systems SR620.

### Temperature Drift of the TTA Delay

The temperature drift of the delay in the TTA due to external temperature variations was experimentally measured, and it was discovered that a temperature fluctuation of 10 °C would cause a 600 ps (measurement uncertainty of 0.4 ns) time delay variation (0.06 ns/°C). This suggests that the temperature of the room where the ground-site devices are kept must be temperature stabilized, or carefully measured and considered in the utilization of the TTA.

### 3.3.2 Delay in the Troposphere

The troposphere produces delay effects of the order of 2~25 m. These effects vary with elevation angle; a lower elevation angle produces a longer path length through the troposphere, and also varies with the detailed atmospheric gas density profile versus altitude [85, 52]. For the evaluation of the tropospheric delay, the following models were implemented and compared:

- Saastamoinen Model (SA)
- Hopfield Model (HP)

These models were used in combination with the following mapping functions:

- Saastamoinen Mapping Function (SM)
- Niell Mapping Function (NM)
- Marini & Murrei Mapping Function (MM)

Fig. 3.5 shows an example of delay due to the tropospheric effect, for a temperature of 15 °C, a humidity of 70% and an atmospheric pressure of 1013 hPa.

In order to estimate the tropospheric delay for the QZSS orbital position during the entire day, the same models were integrated into the RESSOX simulation tool. A hypothetical ground station located in Tsukuba, Japan, was simulated. Fig. 3.6 shows the delay due to the troposphere during a one-day simulation. The delay values relative to elevation angles smaller than 10 deg were intentionally omitted.

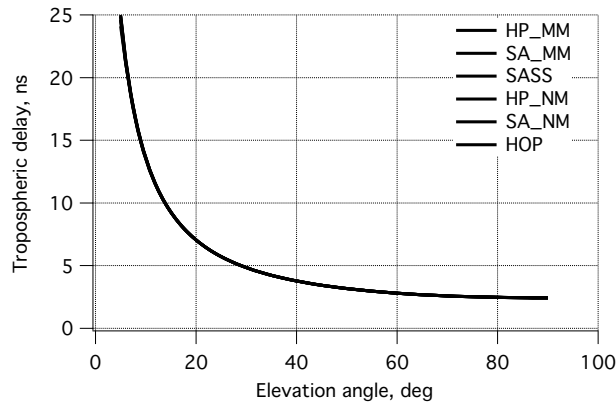


Figure 3.5: Delay due to the troposphere vs the satellite elevation angle  $E$  ( $5 < E < 90$ ). The meteorological conditions considered here are temperature=15 °C, humidity=70 % and atmospheric pressure=1013 hPa. The implemented models and mapping functions shown here are the Saastamoinen model (SA), Hopfield model (HP), Marini & Murrain mapping function (MM), Niell mapping function (NM) and the Saastamoinen mapping function (SM). Under the above conditions, all implemented models give the same result. Location: Tsukuba, Japan.

The implementation of the tropospheric delay compensation algorithm implies the necessity of a real-time weather database that can make humidity, temperature and atmospheric pressure data readily available. A simple meteorological station located in the vicinity of the RESSOX ground station would be necessary for this purpose.

### 3.3.3 Delay in the Ionosphere

Because of the free electrons in the ionosphere, electromagnetic waves do not travel at the speed of light (in free space) when they propagate through this region. By implementing the *Single Layer Model* [52] in the simulation tool it is possible to investigate the effect of the ionosphere. The required coefficients for the *Single Layer Model* were downloaded from the Centre of Orbit Determination (CODE) website [2]. By means of the *Single Layer Model*, a lat/long map of the Total Electron Content (TEC) is calculated (Fig. 3.7), the delay caused by the ionosphere can be estimated by the following formula:

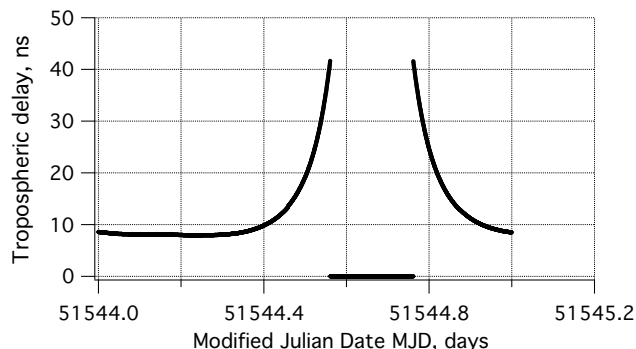


Figure 3.6: Delay due to the troposphere during a one-day simulation. The simulation date was January 1<sup>st</sup> 2000. Location: Tsukuba, Japan.

$$D_{ion} = \frac{40.4}{c \times f^2} \times TEC \quad (3.2)$$

where  $TEC$  represents the Total Electron Content along the signal path measured in  $\text{el}/\text{m}^2$ ,  $c$  is the speed of light in free space ( $299,792,458 \text{ m/s}$ ) and  $f$  is the uplink signal frequency. By computing the QZS position and by knowing the position of the ground station (in our case: Tsukuba, Japan), the satellite elevation and satellite distance is computed and the  $TEC$  for each given satellite position is calculated. For the RESSOX uplink signal (Ku band, 14GHz), the ionospheric delay was estimated to be between 0.08 ns and 0.30 ns (during a 24 hour period) whereas for the L1 and L2 downlink signals the delay was approximately 100 times greater. The ionospheric delay varies with the satellite elevation angle and, naturally, with the ionospheric conditions (which effect electron density). Fig. 3.8 shows the simulation delay due to the ionosphere for the uplink Ku band, 14 GHz signal.

Ultimately, the RESSOX real-time delay model of the ionosphere will require a real-time measurement of the ionosphere conditions, similar to that of the CODE [2]. The L1 and L2/L5 signals will instead be used separately to determine the ionospheric delay in the RESSOX feedback control loop.

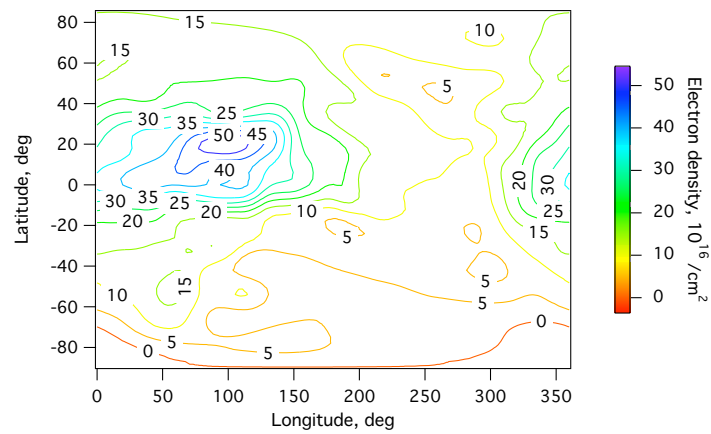


Figure 3.7: Ionosphere electron content distribution. The simulation starting date was January 1<sup>st</sup> 2000 at 23:59.

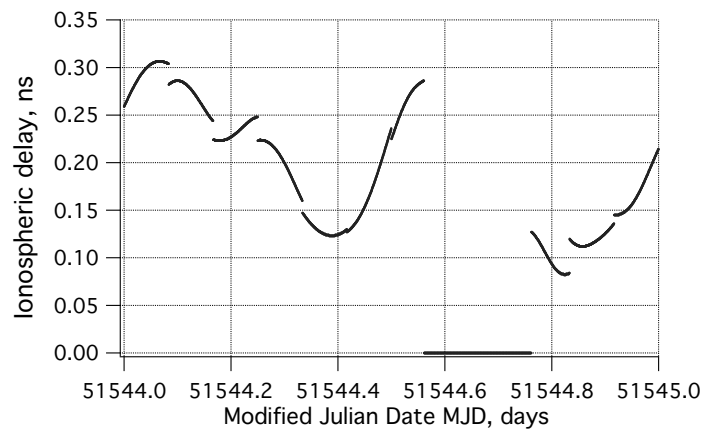


Figure 3.8: Delay due to the ionosphere during a one-day simulation. The simulation start date was January 1<sup>st</sup> 2000. Uplink Ku band, 14 GHz signal, location: Tsukuba, Japan. The visible discontinuities are due to the 2 hour sampling in the original data downloaded from the Centre of Orbit Determination (CODE) website [2]. The no-data region is due to a 5 deg threshold cut off implemented in the QZS orbit simulator.

### 3.3.4 Satellite Orbit Estimation Error

#### Non-spherical Gravity Field of Earth

The Equation that describes the gravity potential  $U$  for the Earth is:

$$U = \frac{GM_{\oplus}}{r} \sum_{n=1}^{maxN} \sum_{m=0}^n \left( \frac{R_{\oplus}^n}{r^n} \right) \bar{P}_{nm}(\sin \phi) \cdot (C_{nm} \cos m\lambda + S_{nm} \sin m\lambda) \quad (3.3)$$

where  $GM_{\oplus}$  is  $398,600.4405 \pm 0.001 \text{ km}^3\text{s}^{-2}$ ,  $R_{\oplus}$  is the approximate equatorial Earth radius of 6378 km and  $\lambda$ ,  $\phi$  and  $r$  are the longitude of point  $r$  (counted positive towards the east), the geocentric latitude and the geocentric satellite distance, respectively.  $\bar{P}_{nm}$  is the associated Legendre polynomial. Since Earth's internal mass distribution is complex, the geopotential coefficients  $C_{nm}$  and  $S_{nm}$  are used to model the non-spherical gravity field.

The JGM-3 and the EGM96 [80] are the Earth's gravity potential models implemented in the simulator, and define the coefficients for formula (3).

Fig. 3.9 shows some simulation results where the models JGM-3 and EGM96 were utilized with different values of degree and order  $N$  and  $M$  of the spherical harmonic model. The error relative to each model is derived as a difference with respect to the reference orbit. The reference orbit is the orbit model that takes into account all relevant perturbations and is based on a gravity model of the Earth complete to the degree and order  $N=M=360$  (EGM96). Table 3.2 lists the specifications of the reference model used for these simulations. In order to keep the error due to the geopotential model below 1 mm, EGM96  $M=N=8$  can already be considered a suitable model.

#### Third-Body Forces; the Sun, Moon and Other Planets

Satellite trajectories are influenced by the gravitational field of not only the Earth, but also of the Sun, the Moon and other planets. In order to study the effects of such gravitational fields on the QZS trajectory, the gravitational effects of third bodies

Table 3.2: Specifications of the QZSS reference orbit estimation model.

Orbit parameters	Values
Semimajor axis, m	42164170.0
Eccentricity, m	0.099
Inclination, deg	45.0
Right Ascension of Ascending Node, deg	120.0
Argument of perigee, deg	270.0
Mean motion, deg	120.0
Satellite mass, kg	3000.0
Satellite cross section, m <sup>2</sup>	30.0
Radiation pressure coefficient (Cr)	1.2
Geopotential model	EGM96, N=M=360
Included models	Moon, Sun, Mars, Venus, etc., solar pressure, solid Earth tide, atmospheric drag.

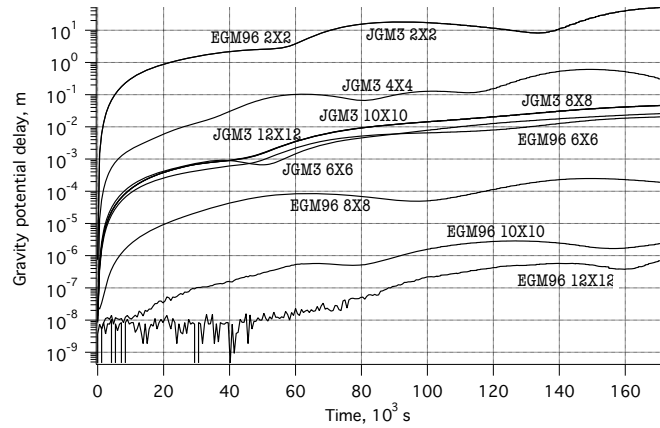


Figure 3.9: Error introduced by the two geopotential models (JGM3, EGM96) employed in the simulator. Some different grades of approximations were tested: 2X2, 6X6, 8X8, 10X10, 12X12. Results are for a two-day simulation, start date January 1<sup>st</sup> 2000.

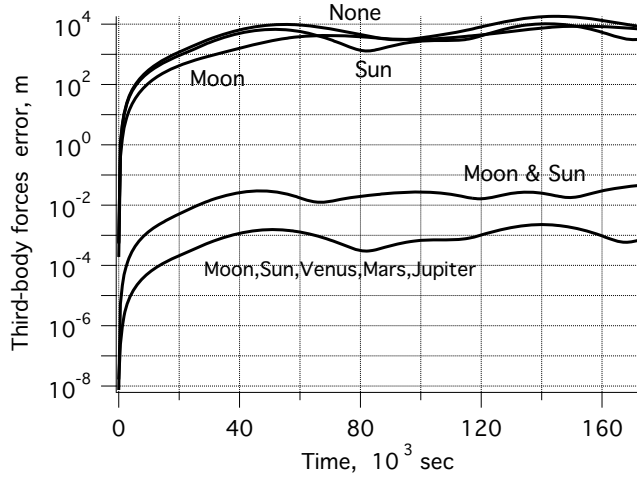


Figure 3.10: Error contributions for the third-body forces of Sun, Moon and other planets on the satellite orbit estimated for a two-day simulation. The simulation start date was January 1<sup>st</sup> 2000.

(Sun, Moon, Mercury, Venus, etc.) were implemented. They are described by

$$\ddot{\mathbf{r}} = \sum_{j=1, j \neq 3}^{11} \mu_j \left( \frac{\mathbf{r}_j - \mathbf{r}}{|\mathbf{r}_j - \mathbf{r}|^3} - \frac{\mathbf{r}_j}{|\mathbf{r}_j|^3} \right) \quad (3.4)$$

where  $\mathbf{r}$  is the satellite position vector,  $\mathbf{r}_j$  is the  $j$ -th celestial body position vector and  $\mu_j$  is the  $GM_j$ , where  $G$  is the gravitational constant and  $M_j$  is the mass of the  $j$ -th celestial body.

The Jet Propulsion Laboratory database of solar system ephemeris (JPL-DE405) was employed, and different approximation cases were analyzed. Fig. 3.10 gives an indication of the error introduced by each third-body model. The total contribution to the orbit estimation error when the Sun, Moon and all the planet models are not taken into account is estimated to be approximately  $10^4$  m (two-day simulation). The Moon and the Sun models, if neglected, give rise to the same order of error ( $\sim 10^4$  m). Therefore neither of them can be neglected.

The influence of Venus, Mars and Jupiter, if neglected, contributes an error of approximately  $10^{-3}$  m (for a two-day simulation), a value acceptably negligible for our purposes.

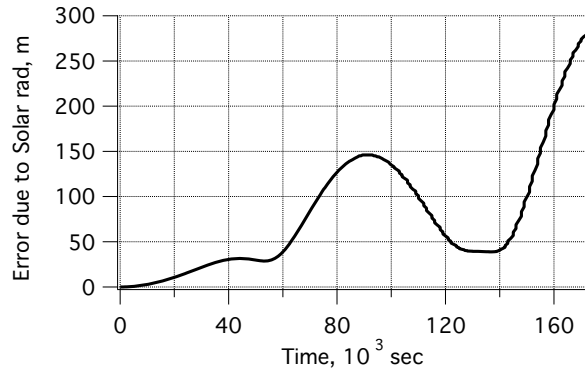


Figure 3.11: Error introduced by the effect of the solar radiation pressure on the satellite orbit. The simulation start date was January 1<sup>st</sup> 2000.

### Solar Radiation Pressure

A satellite that is exposed to solar radiation experiences a small force that arises from the absorption or reflection of photons. The intensity of this force depends on the satellite's mass and surface area. For our simulations, it was assumed that the solar radiation pressure coefficient  $C_r = 1.2$ , the satellite mass  $m$  is 3000 kg, and the satellite cross section  $S$  is 30 m<sup>2</sup>. The Equation that accounts for the solar radiation pressure is

$$\ddot{\mathbf{r}} = sP \frac{C_r S}{m} \frac{\mathbf{r}_j - \mathbf{r}}{|\mathbf{r}_j - \mathbf{r}|^3} AU^2 \quad (3.5)$$

where  $\mathbf{r}$  is the satellite position vector,  $\mathbf{r}_j$  is the Sun's position vector,  $s$  is the shadow function [80] ( $0 \leq s \leq 1$ ),  $P$  is the solar radiation pressure at 1 AU ( $4.56 \times 10^{-6}$  N/m<sup>2</sup>) and  $AU$  is the astronomic unit ( $\sim 149,600,000$  km).

Fig. 3.11 shows the solar radiation pressure effect during a two-day simulation. The maximum error is about 300 m and obviously cannot be neglected. This model is therefore included in the RESSOX control and the relative effect will be appropriately compensated.

### Tidal Effect

The gravitation of the Moon and the Sun express themselves as a direct attractive force on the satellite body, as in Equation 3.4. In addition, these forces also deform

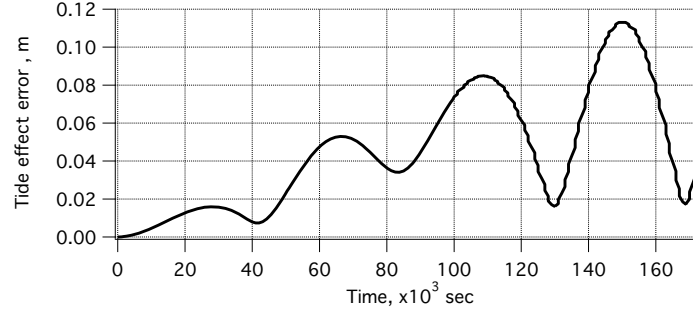


Figure 3.12: Error introduced by the variation of the Earth’s gravitational field due to the tidal deformation of the Earth’s shape caused by the gravitational effect of the Moon and Sun. The simulation start date was January 1<sup>st</sup> 2000.

the body of Earth and thus cause a time-varying deformation of Earth. The Equation that describes the tidal effect is:

$$\ddot{\mathbf{r}} = \frac{3}{2}k_2 \frac{\mu_d}{|\mathbf{r}_d|^3} \frac{a_e^5}{|\mathbf{r}|^4} \cdot \left[ 2 \left[ \frac{\mathbf{r}_d}{|\mathbf{r}_d|} \cdot \frac{\mathbf{r}}{|\mathbf{r}|} \right] \frac{\mathbf{r}_d}{|\mathbf{r}_d|} + \left[ 1 - 5 \left[ \frac{\mathbf{r}_d}{|\mathbf{r}_d|} \cdot \frac{\mathbf{r}}{|\mathbf{r}|} \right]^2 \right] \frac{\mathbf{r}}{|\mathbf{r}|} \right] \quad (3.6)$$

where  $\mathbf{r}$  is the satellite position vector,  $\mathbf{r}_d$  is the position vector of the celestial body that causes the tidal effect (Moon or Sun),  $\mu_d$  is the relative  $GM_d$  where  $G$  is the gravitational constant and  $M_d$  is the mass of the Moon or the Sun,  $a_e$  is the equatorial radius of the Earth and  $k_2$  is the Love’s number ( $\sim 0.3$ ).

Fig. 3.12 shows an estimation of the orbit error introduced by the tidal effect. It predominantly increases with time and can reach values up to 0.12 m after a two-day simulation. Therefore tidal effects cannot be neglected.

### 3.3.5 Geometric Delay

In accordance with the QZSS orbit design (Table 3.2), the distance between the satellite and the ground station (QZS range) varies from approximately 36,000 km to 39,000 km. In order to achieve a satisfactory synchronization between the on-board VCXO and the QZSS time at the ground station, the delay generated by the QZS range must be suitably compensated for. During the transmission of the synchronization signal from the ground station to the satellite (and vice versa), the satellite is moving at a speed that varies from 0 m/s to approximately 300 m/s (QZS speed relative to the Earth).

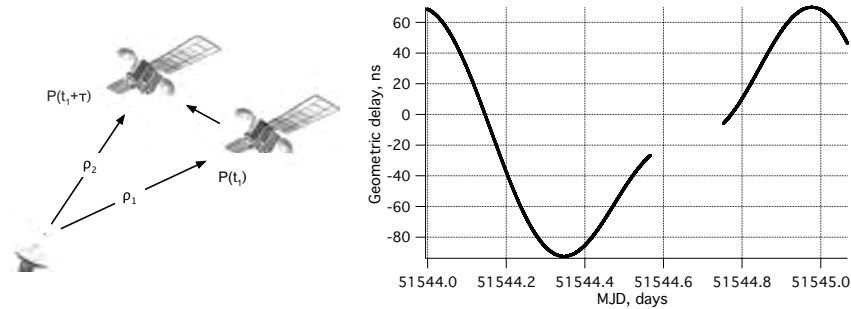


Figure 3.13: (a) Representation of the cause of the delay due to the QZS speed (geometric delay). (b) Simulated results of the geometric delay during a period of 26 hours. The no-data region is due to a 5 deg threshold cut off implemented in the QZS orbit simulator. The simulation start date was January 1<sup>st</sup> 2000. Location: Tsukuba, Japan.

Therefore, when the uplink signal leaves the ground station antenna at time  $t_1$ , the satellite is at position  $P(t_1)$  and the distance that the signal must travel is  $\rho_1$ . However, in the meantime, the satellite has moved and when the signal reaches the satellite antenna its new position is  $P(t_1 + T)$  and the new ground station/satellite distance is now  $\rho_2$ . The discrepancy  $(\rho_2 - \rho_1)$  implies a delay in the RESSOX compensation algorithm, referred to here as the geometric delay. This delay has been evaluated in the simulations, as shown in Fig. 3.13. When the QZS travels at its maximum speed, the geometric delay can reach values greater than 60 ns, so an appropriate compensation is essential.

### 3.3.6 Relativistic Effect

According to the theory of relativity, a moving clock appears to run slow with respect to a similar clock that is at rest. This effect is known as a second-order Doppler shift or transverse Doppler shift. In addition, a clock in a weaker gravitational potential appears to run fast in comparison to one that is in a stronger gravitational potential. This gravitational effect is known in general as gravitational redshift [85, 10].

Relativistic effects are much larger than one part in  $10^{13}$ , and because QZSs orbit the Earth with a velocity  $\nu$  of 3.874 km/s (inertial frame) at an orbital altitude of

35,736 km, for instance, its velocity would cause a time discrepancy of:

$$t' \approx \left(1 - \frac{\nu^2}{2c^2}\right) t \quad (3.7)$$

For the QZS orbit system,

$$\frac{\nu^2}{2c^2} \approx 8 \times 10^{-11} \quad (3.8)$$

where  $t$  is the reference time (on Earth),  $t'$  is the time reference on the satellite,  $c$  is the speed of light (299,792,458 m/s) and  $\nu$  is the QZS speed. Thus, on account of its velocity, a satellite clock appears to run slow by 7  $\mu$ s per day compared with a clock on the Earth's surface. The effects of gravitation are even larger. For an altitude of  $3.6 \times 10^4$  km, the satellite clock is less influenced by the Earth's gravitational field and therefore suffers a gravitational frequency shift given by

$$\frac{\Delta f}{f} = \frac{\Delta \Phi}{c^2} \quad (3.9)$$

where  $\Delta \Phi$  is the gravitational potential difference between the satellite and the geoid. This gravitational shift causes the satellite clock to run faster by approximately 30  $\mu$ s per day than an otherwise identical clock on the ground (on the geoid).

The net effect is that the satellite clock appears to run fast by approximately 23  $\mu$ s per day. This is a large rate difference for an atomic clock with a precision of a few nanoseconds. The time discrepancy due to time dilation (second order Doppler shift) and the redshift effects must therefore be included in the RESSOX compensation algorithm.

Furthermore, according to the theory of relativity, there are other effects [10]. The QZS orbit is not circular (Table 3.2), and the QZS speeds up and slows down to maintain its angular momentum while its distance from the Earth varies along its orbit. Thus, although the principal velocity and gravitational effects have been compensated for by a rate offset, there remains a slight residual variation that is proportional to the satellite orbit eccentricity. For instance, with an orbital eccentricity of 0.099 there is a relativistic sinusoidal variation in the apparent clock time having a peak-to-peak amplitude of approximately 500 ns. This correction must be taken into account and appropriately compensated for. Furthermore, because of the QZSS orbit eccentricity, the Keplerian variation periodically changes the second-order Doppler shift and the

gravitational frequency shift error contribution at the same time. Such variations must be taken into account through an appropriate compensation algorithm.

For the QZSS, relativistic effects related to the rotation of the Earth (the Sagnac effect) [10] can contribute with a periodic error that can easily reach 10 m, and therefore are not negligible.

Minor phenomena such as tidal effects on orbiting QZS clocks due to the Moon and Sun amount to less than one part in  $10^{15}$ , hence they can be ignored. For a theoretical analysis of relativistic phenomena refer to [85, 10].

### 3.4 Ground Station

A convenient location for the ground station is an important requirement for the realization of RESSOX. High visibility of satellites for the ground station location is vital. In accordance with the QZSS orbit design parameters (Table 3.2) some simulations were carried out and several locations were analyzed. Because of the nature of the QZSS orbit, the QZS yields good visibility anywhere within the region of East and South East Asia and Oceania. However, a centralized (with respect to the QZSS ground track) choice would guarantee high visibility 24 hours a day without the difficulty of establishing a connection if characterized by a low inclination angle and a long geometrical range. According to the simulations, among the several possible choices, the Marshall Islands (geodetic latitude= 8.7 deg north, longitude=167.7 deg east) were found to be a suitable location for the ground station. In fact, as can be seen in the simulation results shown in Fig. 3.14, the elevation angle never actually goes below 19 deg. Moreover, the geometric range variation is limited ( $3.67 \times 10^7 \sim 3.93 \times 10^7$  m). Under these circumstances the on-board time reference would be continuously linked to the ground station, with an exception for the equatorial region. Consequently, the Marshall Islands are a suitable location for the RESSOX ground station.

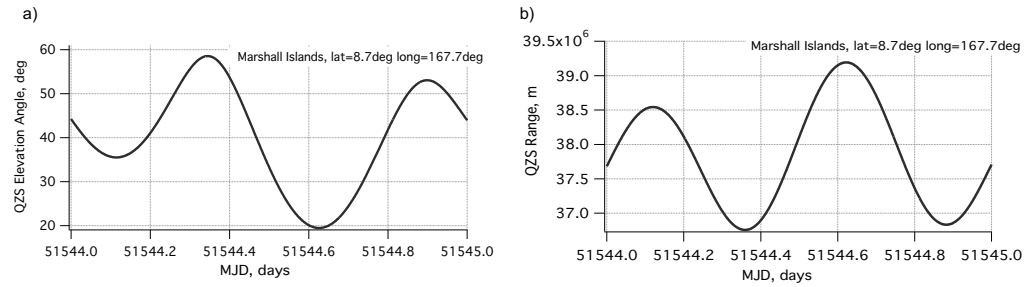


Figure 3.14: a) QZS elevation angle and b) geometric range for a ground station located on the Marshall Islands (geodetic latitude= 8.7 deg north, longitude=167.7 deg east). The simulation is relative to one complete orbital period (24 hours).

## 3.5 RESSOX Feedback/Feed-forward Development

### 3.5.1 Introduction

The RESSOX architecture shown in Fig. 3.3 and described in previous sections has been developed over the course of this study. The research and development of part of the ground-site and the satellite communication modules (e.g. Modem-Tx and Modem-Rx), have been carried out by the RESSOX team at AIST (of which the author was a member until early 2006), therefore its description has been left out of this dissertation. Details can however be found in [60, 59, 57, 58, 56, 53, 108].

In the following sections a description of the RESSOX feedback mechanism and its combination with the RESSOX feed-forward loop, described in [62], is presented. Additional technical information of this system is reported in Appendix A.

### 3.5.2 TTA and UDS Behavior

The TTA and the uplink delay simulator (UDS) described in Appendix A have been employed to form the simplest configuration possible so that the RESSOX feed-forward loop, described in Section 3.2.1, could be developed and evaluated.

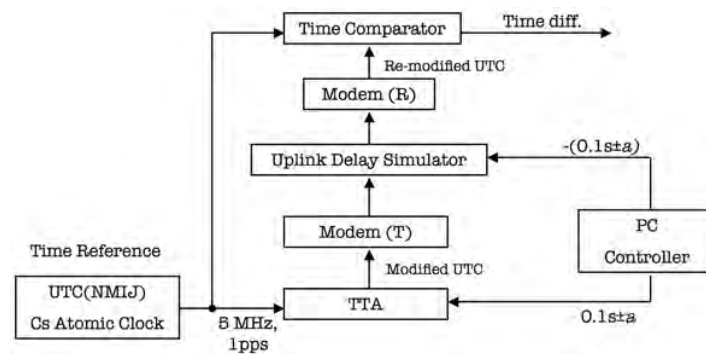


Figure 3.15: Hardware setup for testing the performance of the TTA and the UDS for different values of the imposed time delay  $a$ .

### Fixed Time Delay

In order to test the behavior of the TTA and the UDS, the experimental setup shown in Fig. 3.15 was used. The UTC(NMIJ) time reference was used as a reference and its time information was sent through the chain TTA-Modem(T)-UDS-Modem(R). A constant delay of 0.1 s was set in the UDS and a constant 0.1 s time delay compensation was set in the TTA. In addition to this standard 0.1 s delay an additional delay  $a$  was applied. However, this value is not a constant but is time dependent. In the first experiment  $a$  was set  $1 \mu\text{s}/\text{s}$ . The time comparator embedded inside the modem receiver was used to measure the phase shift between the original UTC signal and the modified UTC signal received by the modem receiver. Fig. 3.16 a) shows the result of the measurement during a 700 s period. The mean value represents the intrinsic delay in the setup equipment chain, which can be compensated for by the TTA, and the deviation after 700 s is approximately 0.7 ns, and is due to an internal delay variation that does not represent a problem because it is easily detectable and compensable by an opportune control of  $a$ . In order to understand the noise processes and their relevant time scales for the chain TTA-Modem(T)-UDS-Modem(R), Fig. 3.16 b) presents the Allan deviation of channel 1 (channel 2 shows very similar behavior). For averaging times below 20 s the level of noise is well below 1 ns, even without compensation of the linear drift that characterize both channels of the chain TTA-Modem(T)-UDS-Modem(R).

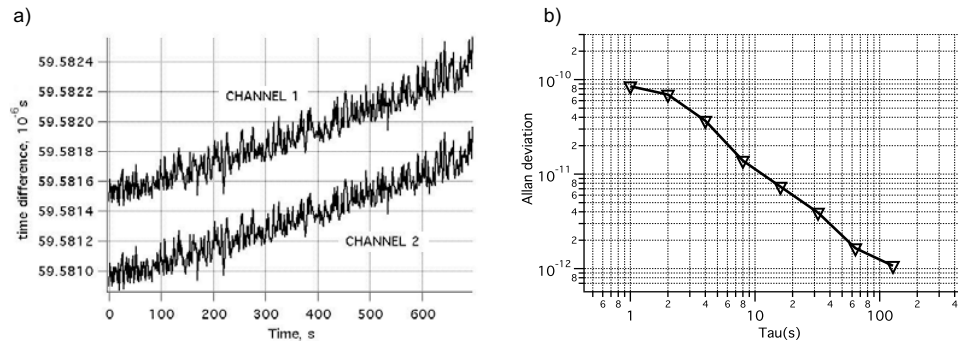


Figure 3.16: a) Time difference variation, over two channels, during a 700 s period when the value of  $a$  is equal to 0. b) Allan deviation of the time difference variation of channel 1. Refer to the experimental setup of Fig. 3.15.

The TTA, the UDS and the modems with a time dependent delay  $a$  were tested because this delay is similar to that of a satellite that varies its relative (to the Earth) flying speed or position, which is the objective of the RESSOX Hardware Simulator test. It is interesting to note the level of white noise, estimated to be well below 1 ns, introduced by the RESSOX communication chain TTA-Modem(Tx)-UDS-Modem(Rx)-Time Comparator.

### Variable Time Delay

With the experimental setup shown in Fig. 3.15, several different time delay values  $a$  were tested. The aim was to investigate the behavior of the TTA and the UDS when the applied delay (in the UDS) and the applied time delay compensation (in the TTA) changes with time over a wider range. Fig. 3.17 shows the average delay over 700 s, measured as in the previous experiment. The time delay  $a$  was varied from  $-1 \mu\text{s}/\text{s}$  to  $1 \mu\text{s}/\text{s}$ . A negative value of  $a$  simulates a satellite that is approaching the Earth, a positive value simulates a satellite that is travelling away.

A study of Fig. 3.17 reveals a proportional intrinsic error in the equipment chain TTA-Modem(T)-UDS-Modem(R) that can be compensated for by an opportune control of the TTA. Future experiments will be needed to understand the precise nature of this instrumental correction.

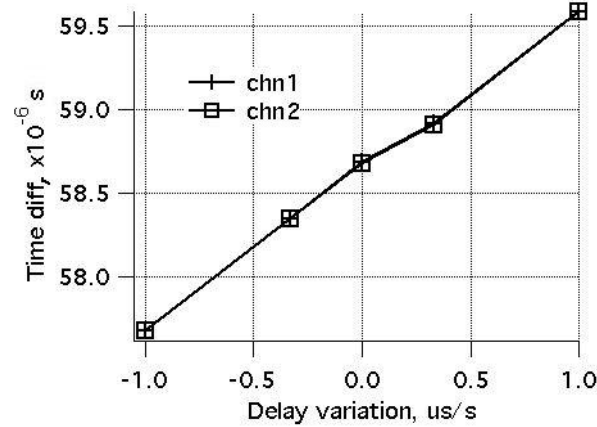


Figure 3.17: Variation of the time difference due to the variation of  $a$ . Refer to the experimental setup of Fig. 3.15.

### 3.5.3 Time Synchronization Performance

Although the whole RESSOX Hardware Simulator had not been completed by the time of writing this thesis, some preliminary experiments for the VCXO control have been carried out. The experimental setup shown in Fig. 3.15 has been modified and a PLL loop similar to the one described in Chapter 4 and in Section 4.3.5 has been developed. The reference signal to which the PLL will lock is the output of the Time Comparator (Fig. 3.15). The experimentally measured white noise generated by the RESSOX uplink channel shown in Fig 3.16 is well below 5 ns (peak to peak amplitude), therefore, at this stage, no particular filter has been adopted.

A proportional control for the PLL on the satellite side has been chosen, implemented and, mainly to test the functionality of the uplink correction signal loop and the behavior of the control, some preliminary experiments were carried out. A constant 0.1 s delay was applied to the uplink delay simulator and a constant 0.1 s time correction signal has been also applied to the TTA. In a setup such as this, the total delay should be completely compensated for and the modified UTC phase should be exactly like the ground station UTC signal phase (total synchronous condition). On the satellite side a basic PLL has been implemented and by means of the satellite side

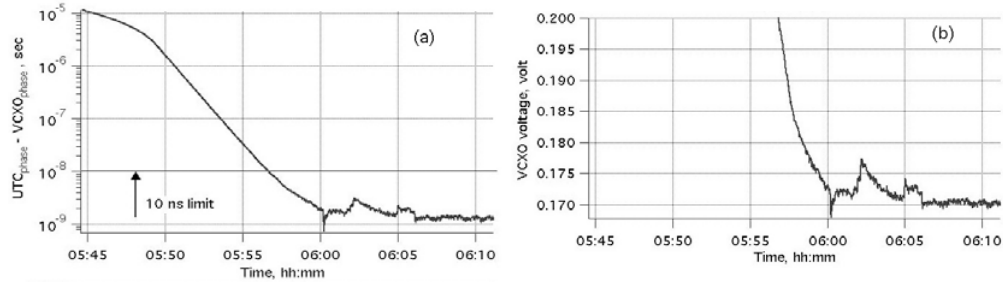


Figure 3.18: *a)*  $UTC_{phase} - VCXO_{phase}$  when the proportional control on the satellite side is active. *b)* VCXO input voltage. The experiment is relative to a 25 minutes period.

controller the following proportional control has been implemented:

$$V_{vcxo} = K_0 \times (P_{vcxo} - P_{utc}) + V_0 \quad 0 < V_{vcxo} < 10 \quad (3.10)$$

where  $V_{vcxo}$  is the input voltage of the VCXO,  $K_0 = -4 \times 10^6$  V/s is the gain of the filter,  $V_0 = 0.1774$  V is the central frequency of the VCXO, and  $(P_{vcxo} - P_{utc})$  is the phase shift, expressed in s, between the VCXO output and the UTC signal.

Fig. 3.18 (a) shows the difference between UTC, used as reference, and the VCXO during a 25 minute period. Fig. 3.18 (b) shows the control command,  $V_{vcxo}$ , of the VCXO (input voltage). Because the experiment started with  $10 \mu\text{s}$  of phase shift (arbitrary choice), about 10 minutes were needed before a phase shift value below 10 ns could be reached. After that time the proportional control was able to keep the phase shift within 10 ns which is indeed the first target requirement of RESSOX.

### 3.5.4 L1/L2/L5 Error Adjustment

Along with the development of the RESSOX hardware, progress in studying the RESSOX architecture has been made. The basic structure of the feedback/feed-forward hardware prototype has been completed. In a recent work a novel error adjustment method for remote synchronization using three different frequency positioning signals (L1/L2/L5) was proposed [62]. By adopting this method, time synchronization was improved by approximately 15% compared with the former method

and an approximate synchronization error of less than 0.77 ns was realized. For more details about this method the reader is referred to [62].

The feed-forward scheme presented in [62] has been combined with the feedback scheme presented in these sections. Preliminary synchronization results of the two combined systems are reported below.

### VCXO PLL loop

For laboratory experimental purposes, two quartz clocks were utilized. Aside from the Oscilloquartz VCXO described in Section 4.3.3, the MINI-OCXO (Oven VCXO) manufactured by C-MAC MicroTechnology (Buckinghamshire, UK) has been employed for specific synchronization tests where feed-forward and feedback schemes have been combined. Due to the scarcity of information on military-designed products, the MINI-OCXO has been characterized by experiments and its behavior is described as follows:

$$f_{vcxo} = f_0 \times (1.0 + f_r \times (V_{in} - V_0)) \quad (3.11)$$

where  $f_{vcxo}$  is the output frequency,  $f_r = 3.2500048 \times 10^{-8}$  1/V is the frequency tuning range and  $V_{in}$  is the applied voltage. Center frequency is  $f_0 = 10.23$  MHz and this frequency can be maintained if  $V_0 = 5.352333$  V, the central frequency of the VCXO. Using the uplinked time information provided by the Time Comparator (Fig. 3.15) a PLL was used to lock the local VCXO. Several tests were carried out, using the proportional controller described in Section 3.5.3. Later a new controller was implemented. In order to be able to have the same controller for both available VCXOs, a proportional integral controller was chosen. Its structure is described by:

$$V_{vcxo,i} = V_0 + K_1 \times (P_{vcxo,i} - P_{utc,i}) + K_2 \times \sum_{j=i}^{i+p} (P_{vcxo,j} - P_{utc,j}) \quad (3.12)$$

where  $V_{vcxo,i}$  is the  $i^{th}$  value of output voltage,  $V_0$  is the central frequency of the VCXO,  $K_1$  is the gain of the proportional component of the phase error ( $P_{vcxo,i} - P_{utc,i}$ ) at the time  $i$ ,  $K_2$  is the gain of the integral component of the phase error ( $P_{vcxo,i} - P_{utc,i}$ ) at the time  $i$ , and  $p$  is the integration time in seconds expressed as multiples of  $i$ . Unlike for classic PLLs [14] the stability of the loop here is not an issue, in fact the

time constant of the PLL loop is recommended to be of the order of 10s of seconds, so that sudden changes due to the possibly noisy (white noise) satellite update link (refer to Fig. 3.16) do not have an associated contribution to the output of the VCXO. Moreover to use an average of the last  $n$ -samples of the different  $P_{vcxo,i} - P_{utc,i}$  is a good way to reduce the white noise contribution. The classic PI controller has been modified so that its inputs (proportional and integral inputs) were the output of a running average of  $l + 1$  samples. However, the number of samples to be used in the running average causes a delay which could cause the PLL to diverge. The filter that gave the best compromise performance is:

$$V_{vcxo,i} = V_0 + \frac{K_1}{l+1} \times \sum_{i=k-l}^k (P_{vcxo,i} - P_{utc,i}) + K_2 \times \sum_{i=0}^{k-l} \int_i^{i+p} (P_{vcxo,i} - P_{utc,i}) \quad (3.13)$$

where  $V_{vcxo,i}$  is the  $i^{th}$  value of output voltage,  $V_0$  is the central frequency of the VCXO,  $K_1 = 7.0 \times 10^6$  is the gain of the proportional component of the phase error ( $P_{vcxo,i} - P_{utc,i}$ ) at the time  $i$ ,  $K_2 = 3.5 \times 10^4$  is the gain of the integral component of the phase error ( $P_{vcxo,i} - P_{utc,i}$ ) at the time  $i$ ,  $p = 2$  is the integration time and  $l = 2$  plus one is the number of samples used by the filter at the time  $i$ .

Additional considerations are discussed in [62]. At this stage, results are preliminary and several hardware problems which arose during these experimental tests are currently under investigation.

### Simulation Results

Several tests were carried out as described in [62]. Details of these experiments are not included here as they are not the work of the author. The atomic standard at the TMS and the on-board crystal oscillator could be synchronized to within 2 ns throughout 90,000 s (25 hours) (Fig. 3.19 a)), even though the noise of the pseudorange has a 1 ns standard deviation. The change of range error during simulations was performed as described in [62]. For the orbit information used at the TMS, which corresponds to Orbit/Delay calculation (with error), an initial error of 5 m for each coordinate component was assumed. The difference in range between actual and measured errors corresponds to the range error. Even though the range error (i.e., orbit estimation) is

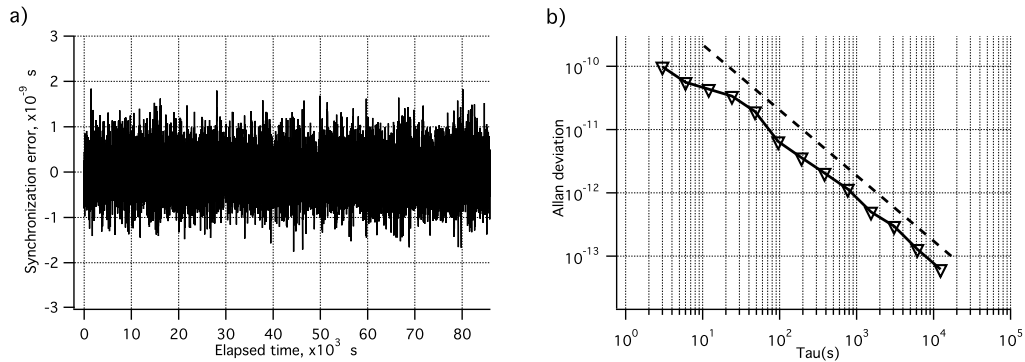


Figure 3.19: Synchronization performance of the RESSOX feedback/feed-forward system. a) Overall synchronization error over 90000 s (25 hours). b) Allan deviation of the synchronization error. The dashed line indicates the  $\sigma = 2$  ns white noise.

large (0~12 m), the proposed method performed well. Fig. 3.19 b) shows the Allan deviation of the synchronization error over 90,000 s (25 hours). For more results and details on the synchronization method the reader is referred to [62].

### 3.6 Conclusions

A novel remote synchronization system for the on-board time reference of the QZSS has been described. The proposed model is a suitable solution for QZSS where continuous base-ground uplink and downlink is indeed feasible. Aimed at satisfying crucial issues such as: 1) improvement of time stability, 2) low cost, 3) low weight and low volumes and 4) low power consumption, this novel system is feasible as a replacement for the traditional on-board timekeeping system adopted by the GPS.

A feasibility study for this novel system has been presented and discussed. A conceptual scheme of the RESSOX was presented and difficulties and restrictions were analyzed. A study of the trajectory estimation error was presented, together with the necessary requirements for the future realization of the RESSOX hardware and software.

The Hardware Simulator for the RESSOX system, which ultimately proves the feasibility from the hardware point of view, is under development. In Section A a

description of the RESSOX Hardware Simulator is presented.

Along with the development of the RESSOX proof-of-concept, a software tool has been developed in collaboration with Mitsubishi Space Software [4]. Section B presents an up to date description of the RESSOX Software Simulator.

The research contribution in this Chapter can be summarized as follows:

- Presentation and discussion of the RESSOX, a novel timekeeping system for the QZSS.
- Analysis of the RESSOX orbit and synchronization signal delays.
- Analysis of RESSOX timing requirements and limitations.
- Development of the basic RESSOX feedback/feed-forward basic scheme.
- Development and test of the RESSOX TTA module.
- Development, design and test of the basic RESSOX on-board VCXO PLL and its controller.
- Test of a large part of the RESSOX Hardware Simulator.

## Chapter 4

# Remote Timekeeping System

A novel synchronization system known as the Remote Timekeeping System (RTKS), for the on-board timekeeping system (TKS) of QZSS is presented. Aimed at offering an alternative architecture to the RESSOX, presented in Chapter 3, the RTKS system consists of a synchronization scheme where an ultra-stable atomic clock, localized at the ground station, is kept synchronized to a second time reference, a VCXO, on-board the QZS. Based on a TWSTFT system, a feedback control signal guarantees the correct synchronization of the on-board time reference and the ground station atomic clock. Compared with the classic GPS TKS, the RTKS scheme offers several advantages in terms of accuracy, cost, weight and power consumption.

In the following Chapter the RTKS structure is described. Particular focus is given to the VCXO control feedback loop, for which a PLL filter is presented and its synchronization performance is discussed through simulations. The VCXO filter algorithm is then tested on a simplified hardware implementation of RTKS. The problem of the detection and mitigation of VCXO frequency jumps is presented and its impact on overall RTKS synchronization is discussed.

### 4.1 Introduction

Generally, to provide positioning signals, GNSS satellites such as GPS satellites need very accurate on-board time references. In fact, in order to achieve high time accuracy,

GPS satellites carry very precise on-board atomic clocks. In such a scenario, the satellite on-board TKS is responsible for the synchronization of the on-board oven VCXO (OCXO) with on-board atomic clocks. These satellites are largely independent from ground station synchronization [85].

As an alternative to the traditional RTK scheme, Chapter 3.3 described the RESSOX synchronization method. This scheme is based on the compensation of the ground station satellite delays through prediction. Fig. 3.4 presented a simplified schematic of the RESSOX system. The precise time available at the ground station (QZS-time) is artificially advanced by means of the TTA and then uploaded to the satellite. A PLL is implemented to steer the local on-board clock, an VCXO, and keep it locked to the received signal. The output of the VCXO is used to construct the QZSS positioning signal that is then broadcast to the user. The key point is to keep the ground station clock and the on-board VCXO synchronized by controlling the TTA so that all communication delays are compensated for. A detailed description of this method can be found in Chapter 3.3 and in [59, 114].

In this Chapter, the feasibility of an alternative method to the RESSOX is investigated. It is a method based on the TWSTFT method, available for QZSS (Chapter 2). This new synchronization method is designed specifically for the QZSS and is characterized by its simplicity. It does not require an on-board atomic clock. Its architecture resembles the structure of the TKS for the classic GPS [92] where, instead, the control voltage that drives the VCXO is processed within a PLL. Moreover, the VCXO control command is processed remotely in the ground station. Hence it has been named the Remote Timekeeping System, RTKS.

In the following sections the RESSOX scheme is used to derive the RTKS basic structure. The TWSTFT method, employed in the RTKS, is presented and its implementation for QZSS is described. The RTKS PLL structure is introduced and an ad-hoc VCXO controller method for the RTKS is proposed. Synchronization quality results are compared with the classic GPS TKS, where a different architecture is implemented. The challenges of detecting frequency and phase jump anomalies are discussed.

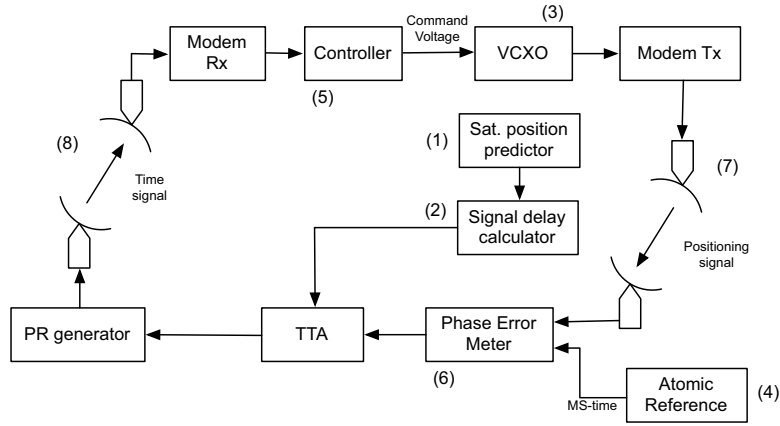


Figure 4.1: Simplified version of the RESSOX synchronization scheme.

The material related to this Chapter has been presented by the author in [113, 110], and included in parallel research activities presented in [107, 61]. The research activity described in this Chapter has led to the development and improvement of the RTKS/RESSOX Hardware Simulator described in the Chapter A.

## 4.2 Remote Timekeeping System for QZSS

### 4.2.1 RESSOX Architecture and its Limitations

The RESSOX synchronization scheme presented in Chapter 3.3 is a synchronization scheme based on satellite-ground station signal delay estimation [59, 114]. As proposed in [107] the construction of the RESSOX (Fig. 4.1 and Fig. 3.4) feed-forward control is based on satellite orbit estimation, geometric detail and troposphere and ionosphere delays (block (1) and block (2), refer to Fig. 3.4). For an acceptable feed-forward control, quasi-real-time determination of these parameters is needed [107]. Moreover, simulations reveal that real-time estimation at meter accuracy level of satellite position is indispensable. Estimation of real-time tropospheric and ionospheric delays is also needed [107].

In the RESSOX architecture, the clock to be remotely controlled, (3), is located on the QZS. The positioning signal, employed to calculate its phase, travels via a path

whose length is time dependent (Chapter 2). The consequence being that if the instant phase shift between (4) and (3) (Fig. 4.1) is required, the instantaneous position of the QZS needs to be calculated. That implies that the phase shift is required with an uncertainty of some ns, the position of the satellite needs to be known with an uncertainty of a few meters (for more details refer to [107]).

Continuous real-time signal delay estimation constitutes a limitation for the RESSOX. Accuracy requirements for such delay estimation is achievable, however, the overall RESSOX scheme (Appendix A) is complex, especially if compared with the classic GPS TKS (Section 2.2.1).

#### 4.2.2 Remote Timekeeping System

Because of the high level of QZS visibility (Section 2.3) a dynamic TWSTFT method (similar to the MILSTAR mission, Section 2.4) could be employed in real-time to produce a feedback signal that can be used to remotely control the QZS clock through the satellite telemetry message.

The clock on-board the QZS can be considered to be similar to the VCXO in a PLL scheme (the classic Phase-Locked Loop scheme was presented by Henry de Bellescise in 1932 [51, 14]). What in the PLL scheme is described as a Phase Detector (PD) is essentially a block that provides the phase shift between the signal reference and the feedback signal [14]. In a classic analog PLL the PD is a mixer, often a multiplier [14]. For QZSS such a PD is the TWTT scheme described in Chapter 2.

Fig. 4.2 shows a simplified representation of the RTKS. The VCXO controller for the RTKS scheme is located at the ground station and its output is delivered to the satellite through a dedicated uplink channel block (8). The whole RTKS functionality relies on the TWSTFT method developed by NICT for QZSS. Because of the TWSTFT system's structure, the phase shift information is delivered to the RTKS ground controller block, (5), with a certain delay. The controller processes the value and calculates the steering voltage almost instantaneously (i.e. it is a real-time process). The steering voltage is then broadcast to the QZS.

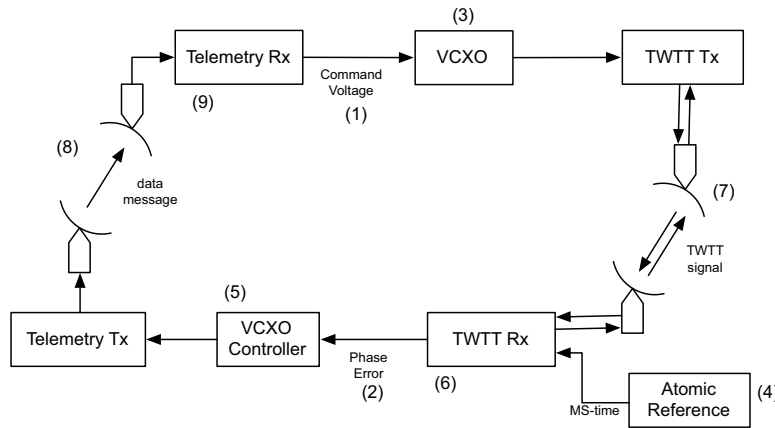


Figure 4.2: Simplified version of the RTKS synchronization scheme.

#### 4.2.3 TWSTFT Method for QZSS

JAXA has planned and launched the ETS-VIII, a multi-service geostationary satellite. The mission of ETS-VIII is not only to improve the quality of digital communications, but also to contribute to the development of fundamental technologies for satellite positioning using a high-precision clock system. The QZSS time comparison equipment, developed by NICT, has been placed on board ETS-VIII and evaluated [87]. This equipment provides time comparison, using the TWSTFT over the S-band, with an accuracy better than 1 ns. In the near future, it will be employed in QZSS to test the performance of the space-borne atomic clocks made specifically for the QZSS. Fig. 4.3 shows how the TWSTFT scheme is adapted for the comparison of clocks on board the QZS (mutual comparison) and for comparison against the ground station clock (master clock). Using this method the phase shift of the on-board clocks could be estimated with a guaranteed accuracy of 1 ns at all times [87]. With the intention of gaining basic knowledge in satellite navigation, JAXA plans to use this architecture to study the basic technology behind on-board atomic clocks and positioning for QZSS.

The RTKS architecture, proposed in this chapter, takes advantage of TWSTFT originally tested for the ETS-VIII mission and now planned to be on board the first QZSS test satellite [87]. Relying on the TWSTFT is a convenient and straightforward way to guarantee the successful test of the QZSS atomic clock-less concept.

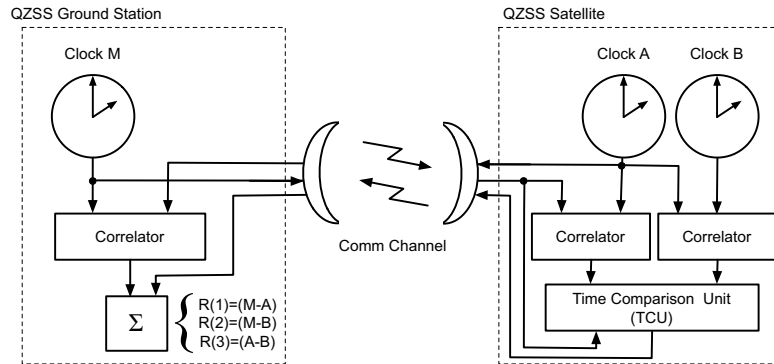


Figure 4.3: Two-way satellite time and frequency transfer scheme for QZSS.

#### 4.2.4 Additional Note About TWSTFT Delay

According to recent developments of the TWSTFT apparatus by NICT, the overall PLL delay should be between 18 s and 19 s. Fig 4.4 shows a detailed representation of the TWSTFT apparatus and of the delay of each single process (delay budget).

Both the RESSOX/RTKS apparatus and the QZSS TWSTFT apparatus require the implementation of significant quantities of hardware and software. AIST and NICT have been working together for the successful implementation of the whole system. The employment of the RTKS architecture should require less hardware than the RESSOX because it relies on the already existing TWSTFT apparatus, Fig 4.4. Therefore RTKS can be a feasible means of testing the feasibility of the atomic clock-less concept.

### 4.3 Remote Timekeeping System Design

The RTKS scheme shown in Fig. 4.2 can be redrawn in Fig. 4.5. However, in doing so, some assumptions have to be made. First, the Phase Detector, block (2), is not located in a specific place; instead its representation is purely abstract [110]. In reality, such a block represents a TWSTFT apparatus, details of which can be found in Chapter 2. The two delay blocks, (5) and (6), are representations of the delay caused by adopting the TWSTFT method. In the following sections the blocks constituting the RTKS scheme are introduced. Particular focus is given to the design of the VCXO controller.

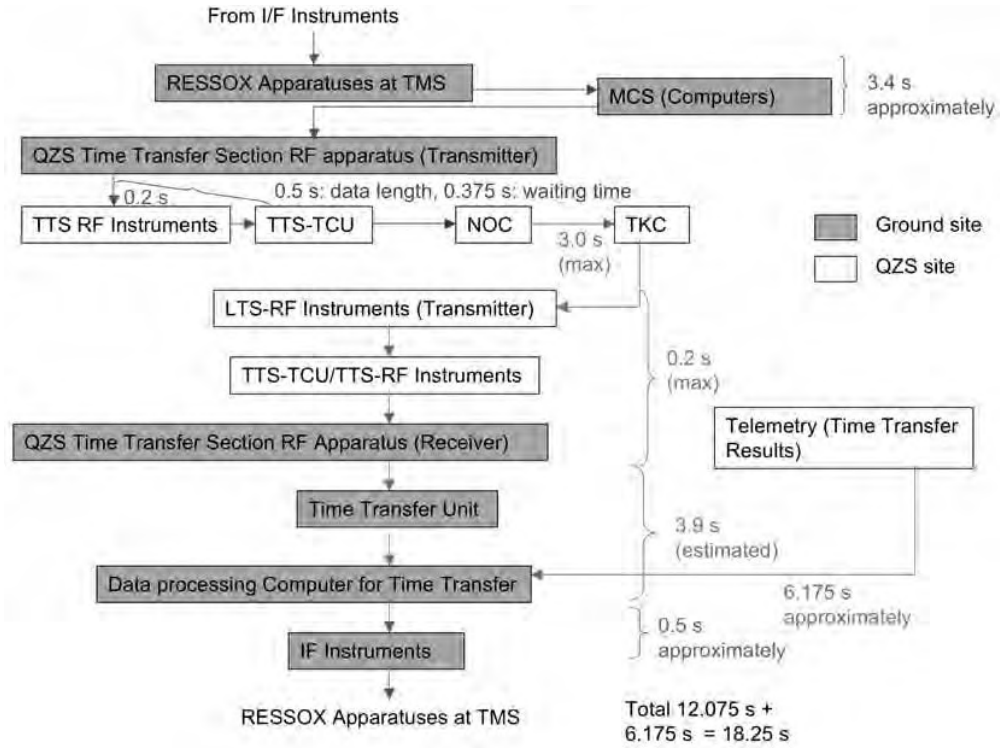


Figure 4.4: QZSS TWSTFT apparatus and its delays.

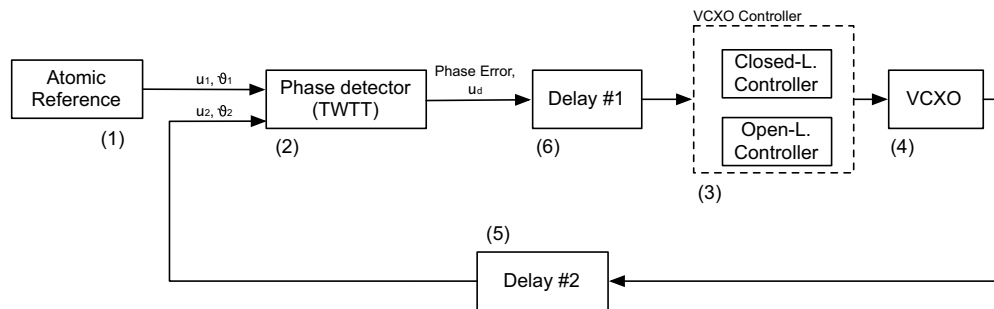


Figure 4.5: RTK Phase-Locked Loop.

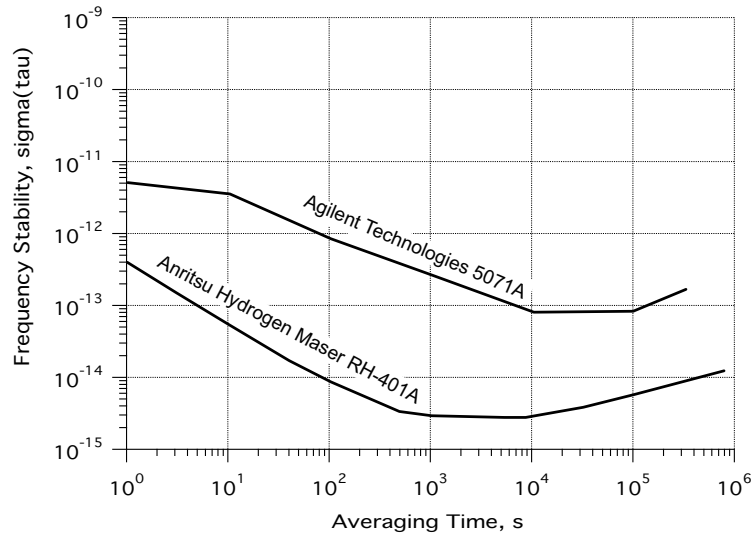


Figure 4.6: Frequency stability of the Anritsu hydrogen maser RH401A and frequency stability of the Cs. Agilent 5071A, now Symmetricom 5071A (planned QZSS ground station clock). Curves are generated accordingly to the specification sheet of both clocks.

### 4.3.1 Ground Station Atomic Reference

For the study of the RTKS synchronization method, the atomic reference (block (4) of Fig. 4.2), was simulated by the behavior (Allan deviation) of the hydrogen maser available in AIST laboratories, the Anritsu hydrogen maser RH401A. Fig. 4.6 shows the frequency stability of the Anritsu hydrogen maser.

### Agilent Cesium Atomic Reference

The actual RTKS apparatus that will likely be experimentally tested with the first QZS will be located in the city of Naha on Okinawa Island, Japan. A dedicated ground station will be built and the Cs atomic reference that is planned to be used for local standard time is the 5071A manufactured by Agilent Technology (now Symmetricom). Fig. 4.6 shows the Allan deviation of the Agilent 5071A.

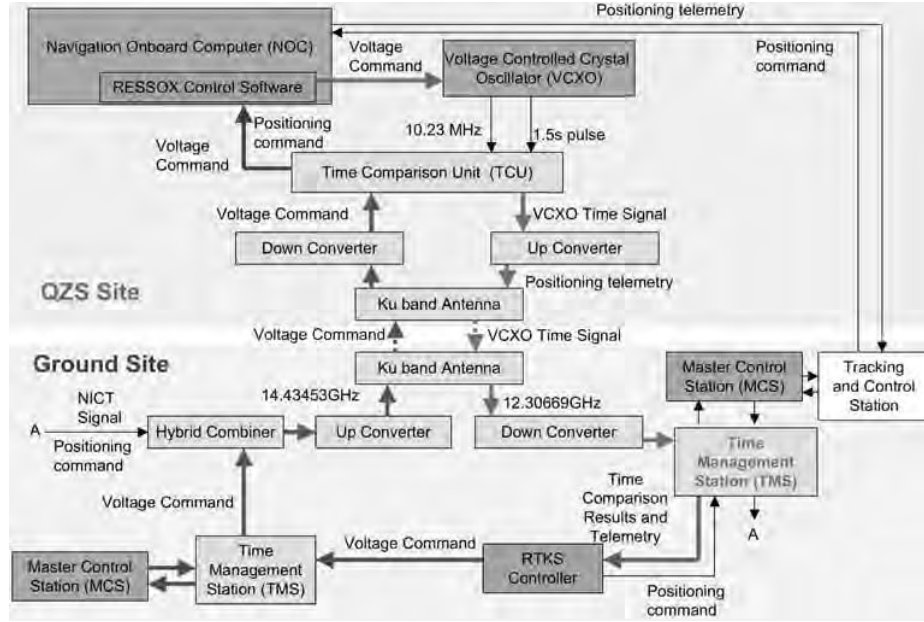


Figure 4.7: Schematic of the RTKS combined with the TWSTFT infrastructure.

#### 4.3.2 Telemetry Interface Blocks

Referring to Fig. 4.2, the Telemetry Interface blocks (8, 9) are the blocks responsible for the communication between the locations where the two clocks are located, that is, in the satellite and in the ground station. They have been considered ideal and no noise or any other disturbing contribution has been considered. Considering that the telemetry block (8) will operate in the  $K_u$  band (12.0 to 18.0 GHz) (Fig. 4.7) it is assumed that the bandwidth available for it does not constitute a limitation for the functioning of RTKS. In addition to telemetry uplink, a data stream could also be modulated on top of the TWSTT link (for example SATRE modems). Such an option could be explored as an alternative route for relaying oscillator control commands.

#### 4.3.3 Voltage-Controlled Crystal Oscillator (VCXO)

For the experiments, the Swiss Oscilloquartz (Swatch Group) 8607-BM was employed. Its frequency deviation due to the input voltage is:

$$\frac{\Delta f_{vcxo}}{f_0} = 6.0 \times 10^{-9} \times \Delta V_{vcxo} \quad f_0 = 5MHz, \quad V_0 = 5.47V \quad (4.1)$$

Table 4.1: Specifications of the Oscilloquartz VCXO 6607-BM employed for this experiment.

Model	VCXO 8607-BM
Manufacturer	Oscilloquartz (Swatch Group)
Nominal frequency	5 MHz
Power Consumption	3 W (10 W max)
Freq. Stability, Allan std. dev. (1s to 30s)	$2.5 \times 10^{-13}$
Aging over 1 day	$2 \times 10^{-11}$
Aging per one month	$5 \times 10^{-12}$
Aging per year	$4 \times 10^{-9}$
Mass (weight)	< 900 g
Dimensions	138 mm X 63 mm X 88 mm
Price	about US\$ 10,000

The characteristics of the VCXO employed in the satellite payload may be slightly different. Given that specific tailoring for a different clock is possible, this should not constitute a problem. A VCXO with similar characteristics can therefore be employed. Table 4.1 lists the characteristics of the VCXO employed for the experiments.

Fig. 4.8 show the frequency stability (Allan deviation) of the VCXO Oscilloquartz 8607-BM when its compared to the Anritsu hydrogen maser RH401A, and when it is compared to an VCXO with similar quality to the 8607-BM.

#### 4.3.4 Phase-Error Measurement

The Phase Detector, (2) of Fig. 4.5, is the block responsible for measuring the phase discrepancy between the QZSS on-board VCXO (block (4)) and the Atomic Reference (block (1)). For the RTKS the PD is the TWSTFT scheme presented in Chapter 2 and in [129]. Fig. 4.7 shows the TWSTFT scheme developed by NICT. Because of the TWSTFT system structure, the phase shift information is delivered by the Time Management Station (TMS) to the RTKS ground controller with a certain delay, typically about 6 s. The controller processes the value and calculates the steering voltage almost instantaneously (i.e. a real-time process). The steering voltage is then broadcast to the QZS with a certain delay, typically 12 s. Data is processed and provided at every epoch (1 s).

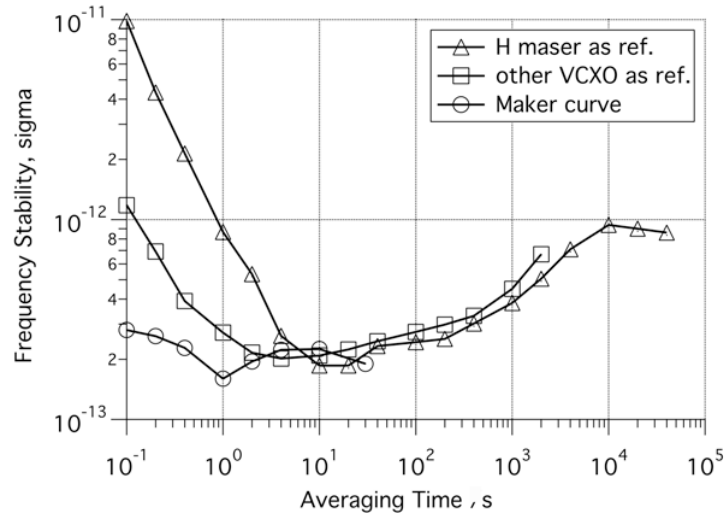


Figure 4.8: Frequency stability (Allan deviation) of the VCXO Oscilloquartz 8607-BM measured against two different reference clocks, the Anritsu hydrogen maser RH401A and an VCXO with similar quality as the 8607-BM. Manufacture’s curve is also provided.

At the time of writing, the QZSS TMS is under investigation at NICT laboratories. For the purposes here it will be assumed that block (2) is an abstract block capable of delivering an output signal that is proportional to the phase difference between its two input signals  $u_1$  and  $u_2$  (Fig. 4.5). Such a block will also contribute a certain white noise to its output signal. Such white noise is the noise contribution of the satellite communication channel block as well as the noise contribution of the TWSTFT apparatus itself [129].

### Phase Detector Block

The TWSTFT apparatus is modeled as a TIC that, provides two input signals,  $u_1$  and  $u_2$ , of frequency  $f_1(t)$  and  $f_2(t)$ , it outputs the absolute phase shift  $\phi(t)$  of the two input signals measured in seconds.

During one gate time,  $T_{gate}$ , an internal circuit measures the change in phase between  $f_1(t)$  and  $f_2(t)$  by counting how many times both signals  $u_1$  and  $u_2$  trigger a fixed threshold. The difference is then calculated. The same measurement is performed at

every consecutive gate time. The final phase difference between  $f_1$  and  $f_2$  is computed by integrating such changes over time.

The model as is does not account for any non-ideal behavior such as measurement quantization due to the use of a discrete counter or phase jitter added by the measurement process. Here the noise that characterizes the TIC has been modeled and injected into the feedback loop right after the ideal output of the TIC.

Based on experimental data utilizing the test bed for the RESSOX project, it was found that the TIC could have a white phase noise with a standard deviation of  $\sigma = 1 \times 10^{-9}$  s. Depending on the quality of the Closed-Loop Controller (block (3)), much higher values of white noise would not create any significant problem for the proper functioning of the system with good filtering at the input. This issue is, however, discussed in the next sections. The Equation that describes the Phase-Error Measurement block is:

$$\frac{d\phi(t)}{dt} = T_{gate} \cdot \frac{f_1(t) - f_2(t)}{f_2(t)} + P_{wn} \quad (4.2)$$

where  $f_1$  and  $f_2$  are the frequency of the atomic reference and the frequency of the VCXO respectively,  $T_{gate}$  is the gate time measured in s (in our experiments  $t_{gate} = 1$  s), and  $P_{wn}$  is a white phase noise with  $\sigma = 1 \times 10^{-9}$  s.

For the experiments (RESSOX/RTKS Hardware Simulator), the universal TIC SR620 from Stanford Research Systems was used. The 1-pps ( $t_{gate} = 1$  s) inputs are used in the TIC for the direct evaluation of synchronization accuracy. An additional white noise generator was also used to simulate the white noise of the RTKS phase detector.

#### 4.3.5 RTKS Loop Controller

The VCXO controller (closed-loop controller) for the RTKS scheme is advantageously located in the ground station. Its output is delivered to the satellite through a dedicated uplink channel. The controller processes the value and calculates the steering voltage almost instantaneously (i.e. it is a real-time process). The steering voltage is then broadcast to the QZS with a certain delay, typically 12 s [110]. The whole RTKS

data processing is done every epoch (1 s or optionally 1.5 s). The RTKS controller has been designed taking into consideration the following:

1. An inevitable delay of about 18 s due to the TWSTFT apparatus must be considered.
2. Taking advantage of the good short-term stability of the VCXO, the TWSTFT white noise can be reduced by choosing an adequate time constant for the RTKS control loop and/or by the adoption of a phase error white noise reduction method.
3. Maximization of the synchronization quality during VCXO free-run, occurring when the satellite is crossing the equatorial region, is essential to reduce phase error drift.
4. Because the reference signal that the RTKS PLL has to follow is the output of a clock, a relative large PLL time constant is recommended (as for the 150 s time constant of the GPS TKS [88]).
5. Relatively fast convergence after VCXO frequency and VCXO phase jumps is desirable (as for the GPS TKS[88]).

Because of the free-run problem, two functioning modes have to be considered, the open-loop mode and the closed-loop mode. During the open-loop mode, the RTKS PLL operates without phase error feedback and the whole controlling capability is handed over to the QZS on-board computer where the Open-Loop VCXO Controller operates. Problems with this mode are discussed in Chapter 5.

In the closed-loop mode, the RTKS PLL is functioning and phase error feedback is provided. The Closed-Loop controller, (block (3)), provides the required command for the VCXO.

#### **Open-Loop VCXO Controller**

The Open-Loop Controller (block (3) of Fig. 4.5) is responsible for properly steering the on-board clock when the PLL feedback is not available due to interruption of satellite-

ground station communications. A detailed description is presented in Chapter 5.

### Closed-Loop VCXO Controller

The closed-loop controller is a PLL controller which uses the TWSTFT Rx output (block (6) of Fig. 4.2) to directly control the VCXO (block (3) of Fig. 4.2). Due to its similarities with the classic PLL the relative stability theory presented in [14] is adopted.

If it is assumed that the PLL has locked and stays locked for the near future, it is possible to develop a linear mathematical model of it. The phase-transfer function  $H(s)$  that relates the phase of the atomic reference  $\theta_1$  and the phase of VCXO  $\theta_2$  is:

$$H(s) = \frac{\mathcal{L}\{\theta_2(t)\}}{\mathcal{L}\{\theta_1(t)\}} = \frac{\Theta_2(s)}{\Theta_1(s)} \quad (4.3)$$

where  $\Theta_1(s)$  and  $\Theta_2(s)$  are the Laplace transforms of the signal  $\theta_1$  and  $\theta_2$  respectively, refer to Fig. 4.5 and Fig. 4.9.

Considering the structure of the PLL and the inherent delay caused by the TW-STFT block,  $H(s)$  becomes:

$$H(s) = \frac{K_d D_1(s) F(s) (K_0/s) D_1(s)}{1 + K_d D_1(s) F(s) (K_0/s) D_2(s)} \quad (4.4)$$

where  $K_d = 2\pi 10 \times 10^6$  is the gain of the phase detector, and the output of the  $K_d$  is then measured in rad.  $D_1(s)$  and  $D_2(s)$  are the delays in the PLL loop (In Laplace domain  $D_1(s)D_1(s) = D(s)$ ). The global delay is assumed to be equal to 18 s (Section 4.2.4).  $K_0$  is the gain of the VCXO expressed in Hz/s, which in this case is  $K_0 = 6 \times 10^{-9} \times 5 \times 10^6$  Hz/s therefore  $K_0 = 30 \times 10^{-3}$  Hz/s. In designing the filter it should not be forgotten that the VCXO outputs its central frequency when its input voltage is about  $V_0 = 5.45V$ , (Section 4.3.3). The value of  $V_0$  was experimentally confirmed but easily subject to change due to the environment (for example GPS TKS VCXO gain monitor routine described in [88]).  $H(s)$  can be simplified to:

$$H(s) = \frac{K_d F(s) (K_0/s) D(s)}{1 + K_d F(s) (K_0/s) D(s)} = \frac{K_d F(s) K_0 D(s)}{s + K_d F(s) K_0 D(s)} \quad (4.5)$$

where

$$K_0 = 3 \times 10^{-2} \quad D(s) = e^{-\tau s} \quad \tau = 18 \quad (4.6)$$

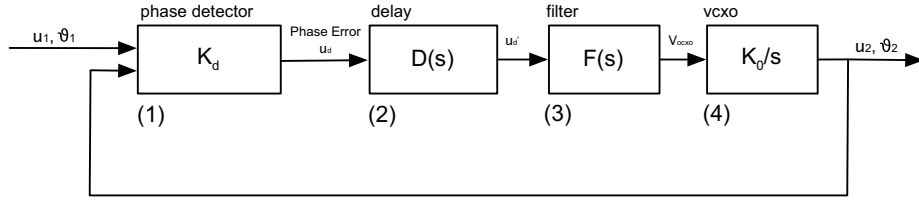


Figure 4.9: Mathematical model for the locked state of the RTKS PLL

$D(s)$  is the Laplace transform of the total RTKS PLL loop delay which is assumed to be 18 seconds (Section 4.2.4). Fig. 4.9 shows a representation of the RTKS PLL loop in the Laplace domain.

#### *Designing the PLL Filter*

The slave clock, the VCXO, is located on board the QZS and therefore subject to gamma ray radiation which can cause, together with aging, the VCXO to change its inner characteristics, its gain  $K_0$  and its voltage offset  $V_0$  (Section 4.3.3). The loop filter responsible for the synchronization of the two clocks in the RTKS network should therefore be able to compensate for these changes. By using not only the absolute value of the output of the PD (proportional filter) but also the integral of it (integral filter), changes in  $K_0$  and in  $V_0$  can be compensated for [14]. A lead-lag filter or a PI filter is therefore proposed. Its transfer function is:

$$F(s) = K_a \frac{1 + s\tau_2}{1 + s\tau_1} \quad (4.7)$$

This filter has a pole at  $s = -1/\tau_1$  and a zero at  $s = -1/\tau_2$ . It also has a gain  $K_a$  which can therefore be greater than one.  $H(s)$  then becomes:

$$H(s) = \frac{K_d K_a \frac{1+s\tau_2}{1+s\tau_1} K_0 e^{-\tau s}}{s + K_d K_a \frac{1+s\tau_2}{1+s\tau_1} K_0 e^{-\tau s}} = \frac{K_d K_a K_0 e^{-\tau s}}{s \frac{1+s\tau_1}{1+s\tau_2} + K_d K_a K_0 e^{-\tau s}} \quad (4.8)$$

The RTKS filter is now developed neglecting the delay. The same filter will then be analyzed when the delay is introduced. The module of  $H(s)$  will not change but the phase of  $H(s)$  will shift, changing the phase margin and therefore influencing the stability of the system. The bandwidth of the original filter will then be chosen so that a maximum delay of about 18 s (Section 4.2.4) can be introduced within the phase margin.

For an optimally flat response a damping ratio  $\xi = 0.707$  is assumed. This gives  $\omega_{3dB} = 2.06\omega_n$  which is about twice the natural frequency. Imposing a value  $\omega_{3dB} = 2\pi \times 1/10$  Hz (smaller than the basic GPS TKS PLL time constant of 40 s with no Adaptive Time Constant (ATC) [88]):

$$\tau_2 = \frac{2\xi}{\omega_n} \quad \tau_1 = \frac{K_0 K_d}{\omega_n^2} \quad F(s) = \frac{1 + s\tau_2}{\tau_1} = \frac{1 + 0.0463828s}{2027.1975} \quad (4.9)$$

The important issue is to choose a PLL time constant low enough that the pole or poles introduced by the intrinsic delay give a contribution which is negligible.

#### *PLL Filter Implementation*

Once the PLL filter  $F(s)$  was designed, it was implemented in the RTKS simulator and tested. An elegant way to do this is to translate the  $F(s)$  into the discrete form making use of the  $z$  transform. The transformation chosen here is:

$$s = \frac{1 - z^{-1}}{\Delta T} \quad (4.10)$$

In the  $z$  domain,  $z^{-1}$  represents a one step sample in the discrete stream.  $F(s)$  then becomes:

$$F(z) = \frac{C_1 + C_2 - C_1 z^{-1}}{1 - z^{-1}} \quad C_1 = \frac{\tau_2}{\tau_1} \quad C_2 = \frac{\Delta T}{\tau_1} \quad (4.11)$$

The discrete implementation of the PLL filter  $F(s)$  then become:

$$y_i - y_{i-1} = (C_1 + C_2)x_i - C_1 x_{i-1} \quad (4.12)$$

Moreover

$$y_i = y_{i-1} + C_1(x_i - x_{i-1}) + C_2 x_i \quad (4.13)$$

where  $C_1 = 2.288026 \times 10^{-5}$  and  $C_2 = 4.9329 \times 10^{-4}$ . Fig. 4.10 shows the response to a 20 ns step of the RTKS PLL when no delay is implemented. Converging time and white noise amplitude are comparable with GPS TKS performance presented in [88, 92].

#### *PLL Filter Characteristics*

Regarding overall PLL behavior, to ensure loop stability, the general requirement is

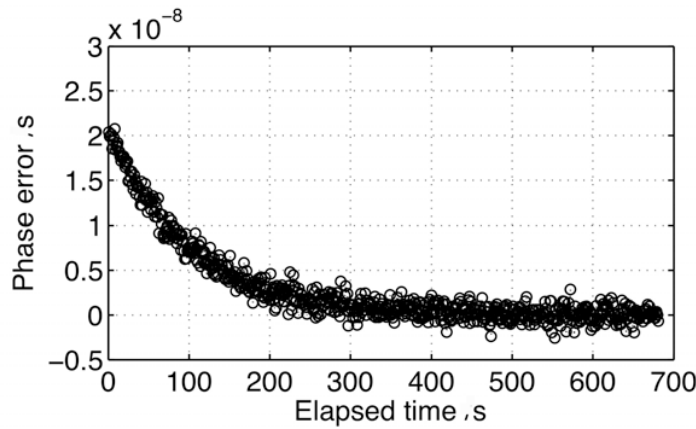


Figure 4.10: RTKS PLL response to a 20 ns phase error step.

that the system should have about 20 degrees of phase margin [14]. Moreover the RTKS PLL will need to have a PLL equivalent bandwidth such that the VCXO will follow the reference (atomic clock). Unlike a classic PLL, this particular requirement is very loose, in fact the phase difference between the two clocks varies over time with a large time constant. Because of the white phase noise introduced by the adoption of the TWSTFT, and because of the intrinsic delay of the TWSTFT apparatus (about 18 sec), a low PLL natural frequency is recommended to ensure PLL stability.

The damping ratio,  $\xi$ , is chosen to be 0.707 to give a good compromise between overshoot and converging time. However, convergence of the order of 150-200 s directly after satellite communication interruption periods (Chapter 5), should be ensured. Fig. 4.11 shows how the RTKS PLL responds to a 50 ns phase step when four different scenarios are assumed; 0 s delay, 10 s delay, 20 s delay and finally 30 s delay (in a 1pps system, 1 epoch is equivalent to 1 s). At 0 s delay, the overshoot is about 20 % which corresponds to a  $\xi = 0.7$  as expected.

Now consider the  $\pm 5$  ns error band in the phase error, and how the PLL settling time is related to the PLL delay. Fig. 4.12 shows (indicative representation) five cases. Note that faster convergence can occur for PLL delays of around 20 ~ 40 s. Larger delays would increase the effect of the pole introduced by the delay giving less stability (i.e. the overshoot would exceed 5 ns) and eventually causing loss of lock. Simulations

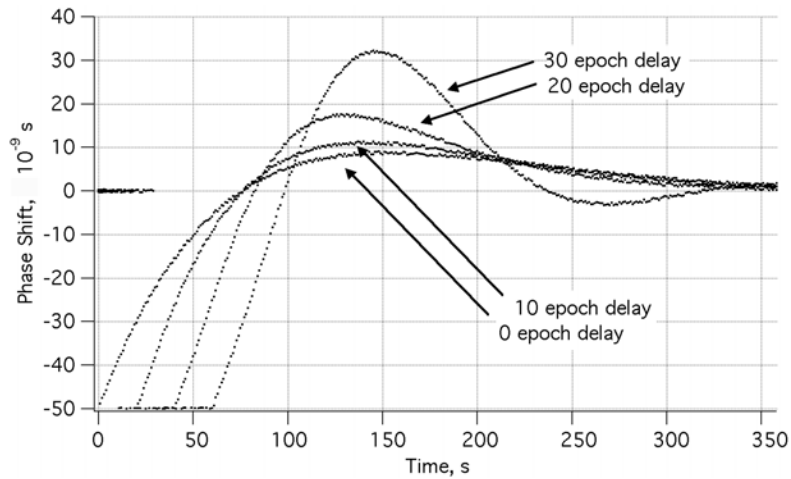


Figure 4.11: RTKS PLL response to a 50 ns phase error step when four different delay scenarios are considered. 1 epoch is equivalent to 1 s delay.

show that if the delay remains below 30 s phase error step response and overall stability are guaranteed.

#### 4.3.6 RTKS Scheme

The following Section describes how the RTKS filter of Equation (4.9) is combined with the RTKS pre-filter and the frequency and phase jump detector to form the whole RTKS scheme.

#### Optimally Unbiased Moving Average

Considering the quality of synchronization of the DTWTT presented in Section 2.5.3 and the TWSTFT synchronization results of the MILSTAR mission presented in the Section 2.4, it is reasonable to assume that the phase error of the QZSS TWSTFT apparatus is likely to be affected by white noise. As also mentioned in [88] for the GPS TKS, if the output of the PD is directly coupled to the RTKS filter (Equation (4.9)), the VCXO output will be quite noisy. The low-pass filtering effect of the RTKS filter will only partially reduce the PD output noise. The same problem occurs with the GPS TKS [88, 91, 125]. The solution proposed by Rawicz [91] and later by Petzinger [88] was to use two modes for the PLL, slow-loop mode and fast-loop mode. A time

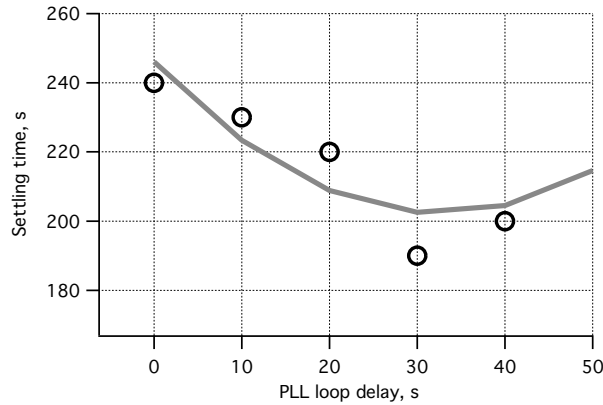


Figure 4.12: Five cases of RTKS PLL settling time versus the length of the delay introduced to the PLL. This particular case refers to a 50 ns phase step. Straight line segments represent the linear fit.

constant of 150-200 s was used for the slow-loop mode (normal functioning) and a time constant of 50 s for the fast-loop mode (for example, to be set during frequency jumps). For the QZSS RTKS a different solution is proposed.

In the field of disciplined clocks [26] a similar problem of phase locking a local VCXO with a highly noisy GPS time signal has been extensively studied. A synchronization method based on an Optimally Unbiased Moving Average (FIR filter) was proposed by Shamaliy [99, 100, 101]. Extensive tests have shown that for  $N < 20$  the best results were achieved with the following filter:

$$\hat{x}_2 = \sum_{i=0}^{n-1} \frac{2N(N-3) + 9 - 6i(N-1)}{N(N^2 + 6)} \xi_{n-1} \quad (4.14)$$

where  $N$  is the length of the filter (in samples) and  $\xi_{n-1}$  is the input of the filter. The FIR filter of Equation (4.14) has been implemented in the RTKS Software Simulator. Fig. 4.13 a) shows the VCXO output for different values of  $N$ . Fig. 4.13 b) shows the improvement due to the moving average (MA) filter, in terms of average absolute phase error over a 1000 s interval.

The Optimally Unbiased Moving Average, Equation (4.14), does however introduce a delay in the PLL that can change the response to a phase step; an issue discussed in Section 4.3.6. The length of  $N$  and therefore the effect of the MA filter has to be chosen carefully as a trade-off between its white noise attenuation effect and its phase

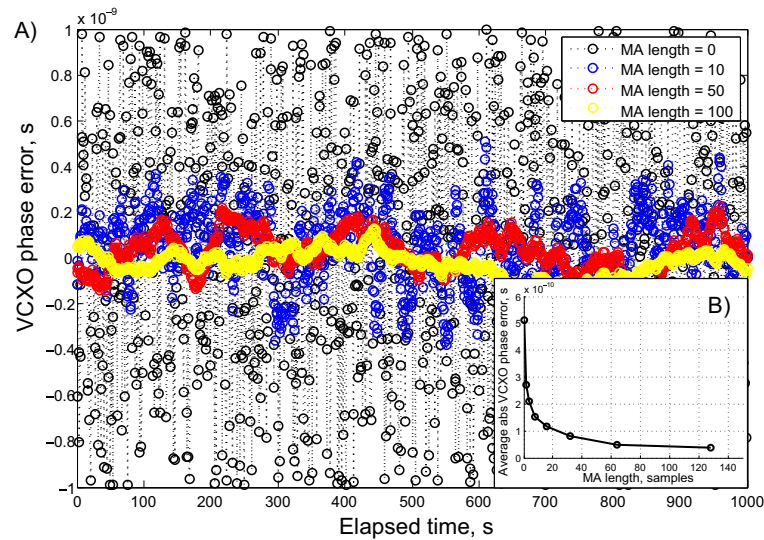


Figure 4.13: a) VCXO phase error over 1000 s when different length  $N$  of optimally unbiased MA filters are used. b) Average absolute VCXO phase error as a function of the optimally unbiased MA filter length.

step settling time. Extensive experiments have shown that  $5 < N < 15$  will guarantee an overall average absolute phase error  $< 0.2$  ns and a settling time (phase error  $< 0.5$  ns) for a 20 ns phase step of about 400 s. Such performance is comparable with the GPS Block IIR results presented in [88, 92].

Another important point in this regard is the intrinsically good short-term timing quality of the RTKS VCXO. Fig. 4.14 shows an experimental measurement of the phase error of the Oscilloquartz 8607-BM when compared to the best reference, the Anritsu hydrogen maser RH401A. For this measurement the VCXO was initially synchronized and then left in free-run mode for about 300 s. The VCXO, if synchronized at the beginning, can maintain an acceptably stable output (phase error  $< 1$  ns) for a period of about 500 s. This implies the following:

- The overall RTKS PLL time constant can be set between 50 s and 200 s (as for the GPS RTK).
- The filter presented in Section 4.3.5 can be coupled with an additional filter designed to reduce the white noise. The overall PLL time constant could be

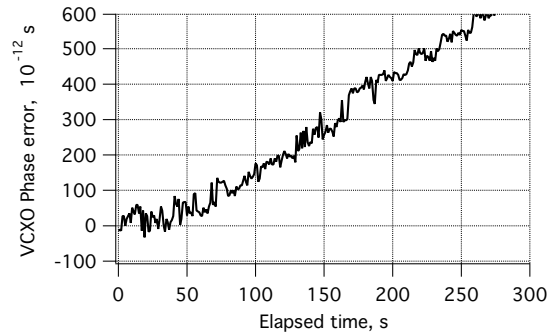


Figure 4.14: Experimental measured phase error of the RTKS VCXO, Oscilloquartz 8607-BM, when left uncontrolled for 300 s.

around 200 s.

- An Adaptive Time Constant (ATC) similar to the GPS TKS could be implemented to speed up and slow down the RTKS PLL.
- Voltage corrections provided to the VCXO could be delivered with a much slower pace than every epoch. For instance, a voltage update rate of one sample per 50 epochs could be acceptable.

It is assumed that in the worst case scenario the RTKS PD will introduce a noise component with an amplitude of  $\sigma_{PD} = 5ns$ , roughly 3 times worse than the GPS TKS PD (Section 2.2.1). From the experimental measurement on what it is considered the RTKS VCXO, refer to Fig. 4.14, it is assumed that the time error introduced by the RTKS VCXO when left in free-run mode has a white noise component of about  $\sigma_{vcxo} = 50 \times 10^{-3} ns$  and, more important, for  $t < 500$  s, a linear drift component of  $ld_{vcxo} = 600 \times 10^{-12} ns/200 ns = 3 \times 10^{-12}$ . The noise introduced by the Anritsu hydrogen maser used as reference to produced the measurement of Fig. 4.14 is negligible as shown by the Anritsu's frequency stability shown in Fig. 4.6.

#### Automatic VCXO Gain Compensation

The RTKS loop filter is designed to reduce the PLL phase error by steering the VCXO command voltage. When the characteristics of the VCXO (e.g. VCXO gain or VCXO

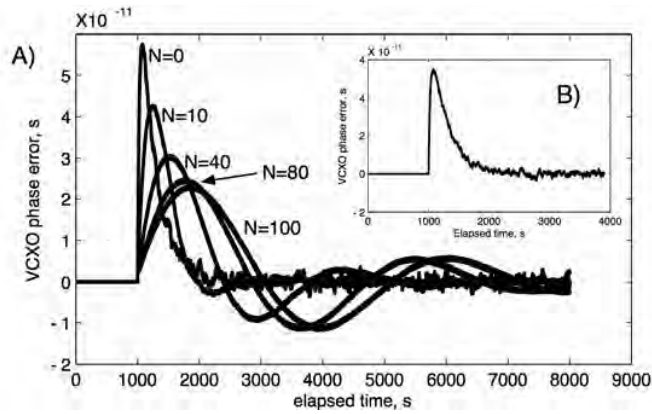


Figure 4.15: A) Oven VCXO phase error over 9000 s for different lengths  $N$  of optimally unbiased MA filters. At  $t=1000$  s a linear phase drift is introduced into the RTKS loop.

central voltage, Section 4.3.3) changed due to environmental reasons, or when a slightly different VCXO is employed for RTKS, synchronization problems may arise. The GPS TKS solves this issue by constantly monitoring the VCXO behavior [88].

In the RTKS scheme, a change in the VCXO central frequency, for instance, has the effect of a bias in the RTKS loop. By adopting a PI filter, such a bias can be detected and compensated for by the integrative action of the PI filter [14]. Moreover, by addressing the problem of a phase/frequency jump (Section 4.3.6) this issue, producing effects of minor magnitude, can be easily addressed. To provide an insight on this matter, an experiment was conducted. In the RTKS loop a sudden change of the VCXO linear drift of  $0.6 \times 10^{-12} \text{ ns}/250 \text{ ns}$  was introduced after 1000 s (refer to Fig. 4.15 B). Fig. 4.15 A) shows how efficiently such a contribution could be compensated for when different values of MA length are considered. For instance, with  $N=10$ , a sudden change in the VCXO drift can be compensated for in about 1000 s. Moreover the overall effect, despite happening suddenly (the worst case scenario) gives an overall contribution of only  $6 \times 10^{-11}$  s, well below the white noise level. Other experiments that have been conducted have confirmed that changes of the VCXO gain do not cause any appreciable problem for RTKS.

### VCXO Frequency and Phase Jumps

An atomic clock or a quartz clock (for example, VCXO) when carried on a satellite will experience phase and frequency jumps due to in-space conditions [88]. The TKS that will govern the functioning of QZSS clocks will, most probably, experience the same problems as the GPS TKS. Petzinger [88] reported a quite comprehensive analysis of the in-space performance of the GPS Block IIR TKS from October 10, 2000 to March 10, 2002. Particular focus was given to frequency and phase jumps of the GPS Block IIR VCXO and its atomic standard during eclipses. From [88, 92] and Section 2.2.1, the following considerations for the GPS TKS can be derived:

- A small VCXO frequency jump has an amplitude of approximately 6 ns.
- In general, frequency jumps have caused phase jumps of approximately 2 ns. Small frequency jumps ( $\Delta f/f = 4 \times 10^{-10}$ ) might occur several times a day for one month out of 6 months.
- In general, a phase jump can have a maximum amplitude of approximately 14 ns.
- There are periods (e.g. beginning of eclipses) of about 30 days during which every 12 hours moderate frequency jumps can happen.
- There are periods of about 14 days, twice a day, when 6 ns phase jumps can happen (max. amplitude < 5 ns).
- GPS TKS fast-loop and slow-loop mode (together with the ATC, Section 2.2.1) is the method used in the GPS TKS to reduce frequency and phase jumps.
- VCXO phase jumps are not instantaneous but build up over about five-minute periods.

A phase jump of 14 ns (worst phase jump) would cause a ranging error of approximately 5 meters. Depending on the geometry of the satellites in view, the positioning error that the user may experience is about 5 meters along its height in the worst case (satellite at the zenith).

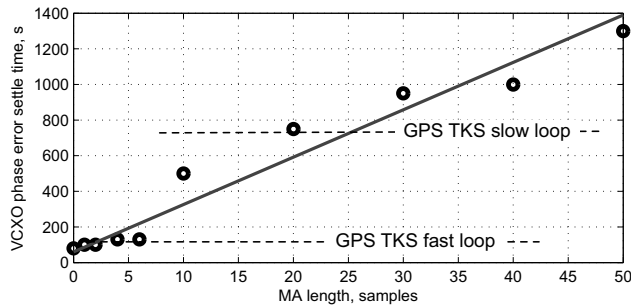


Figure 4.16: VCXO phase error settle (phase error within 0.5 ns) time versus optimum Moving Average length  $N$ . The two lines show the settle time of the GPS TKS for the two modes, slow-loop mode and fast-loop mode.

In order to mitigate the positioning error caused by phase and frequency jumps, the jump needs to be detected and accounted for. Regarding the detection, the delay introduced by the TWSTFT in RTKS (Fig. 4.4) causes a phase/frequency jump detection delay of approximately 12 s. Considering that phase jumps do not happen instantaneously, but rather build up over five minutes, QZSS RTKS can provide detection by monitoring the output of its TWSTFT and therefore be as effective as the GPS TKS. The mitigation, as for the GPS TKS, is provided by a relatively fast response of the RTKS PLL. Simulations show that by choosing the MA length  $5 < N < 25$  the overall response of the RTKS PLL would equal the response of the GPS TKS. Fig. 4.16 shows the VCXO phase error settle time (phase error within  $\pm 0.5$  ns) versus optimum MA length  $N$  for a 20 ns phase jump.

Additionally, since the RTKS reference clock is located on the ground, atomic reference jumps are clearly not happening as in the case of the GPS TKS [88] or are more easily detectable and avoided (clock located on the ground).

The detection of phase and frequency jumps method employed in the QZSS RTKS is implemented by thresholding the output of the TWSTFT and, as for the GPS TKS, an error message is generated if two consecutive values exceed the nominal limit which is fixed, as for GPS, to 2 ns.

Alternatively, the QZSS RTKS could be supplied with a second VCXO (refer to Fig. 4.17) controlled by the same RTKS PLL as in the scheme proposed in [68]. By

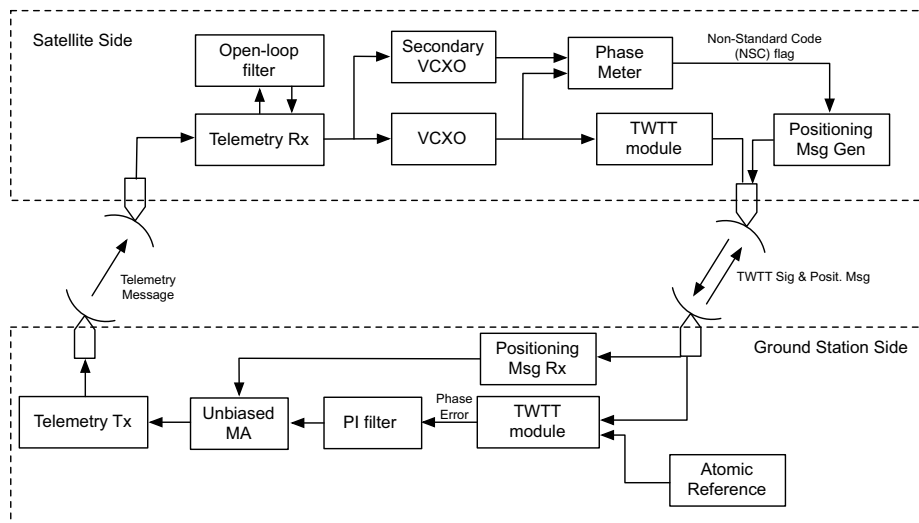


Figure 4.17: QZSS RTKS schematic.

constantly comparing the two satellite VCXOs the frequency/phase jump detection could be achieved within seconds (as for the GPS RTKS). Moreover this method will not only be able to detect phase/frequency jumps that occur in either one of the two VCXOs but also, by comparing consecutive output values, jumps occurring in both clocks can be detected as well. The chance of having two VCXOs experiencing a phase jump at the same time is quite low but is possible. Studies indicate that there is a high occurrence of phase jumps in conditions of high temperature and/or during eclipses [88].

However, a solution based on a double VCXO is only recommended for analysis after in-space testing of the single VCXO RTKS.

### RTKS Scheme

The overall RTKS structure is illustrated in Fig. 4.17. The TWSTFT apparatus provides the phase error at the ground, where the PI filter followed by the Optimally Unbiased Moving Average generate the command voltage which is updated to the satellite via the Telemetry Modem. On board the satellite the VCXO is directly coupled with the Modem Receiver. Therefore no routines will run on the QZSS on-board computer.

An additional Phase Meter could be employed to detect phase and frequency jumps in real-time. This scheme will not only be able to detect phase/frequency jumps that occur on only one of the two VCXO but also by comparing consecutive output values, jumps occurring to both clocks can be detected. The occurrence of such jumps will generate a Non-Standard Code (NSC) in the navigation message, alerting the user. Such information is also used in the ground station to reduce the length  $N$  of the Optimally Unbiased Moving Average so that the whole PLL response is shortened (refer to Fig. 4.16). The Open-loop Filter on board the satellite will intervene during outages of telemetry message, refer to Section 5.

#### 4.4 Long-term Stability of RTKS

To ensure the correct functioning of the RTKS PLL filter, a PI filter was tested utilizing a modified version of the Hardware Simulator originally developed for the RESSOX. Fig 4.18 shows the Hardware Simulator employed for testing. A constant 0.1 s delay that applied to the uplink delay simulator and a constant 0.1 s time correction signal has been also applied to the Transmitting Time Adjuster. In a setup such as this, the total delay should be completely compensated for and the modified UTC phase should be exactly like the ground station UTC signal phase (total synchronous condition). On the satellite side the RTKS PLL scheme has been implemented, and by means of the satellite side controller the RTKS filter was tested.

Fig. 4.19 B) shows the Allan deviation for RTKS when the Cs atomic clock and the hydrogen maser are used as references (Section 4.3.1). In this experiment, no white noise errors introduced by the TWSTFT were considered; the VCXO was controlled in the RTKS loop by adapting the RESSOX Hardware Simulator transmitter/receiver modems and the RTKS PLL filter. Regarding the stability of the Allan deviation over a period of less than 100 s, the stability using the hydrogen maser as the reference was approximately one order of magnitude smaller than using the Cs atomic clock, and is expected to be better than  $1 \times 10^{-14}$  at 100,000 s. This means that the ground station clock used as the reference might affect the properties of RTKS. However, the error introduced by the TWSTFT apparatus for measuring the phase error between

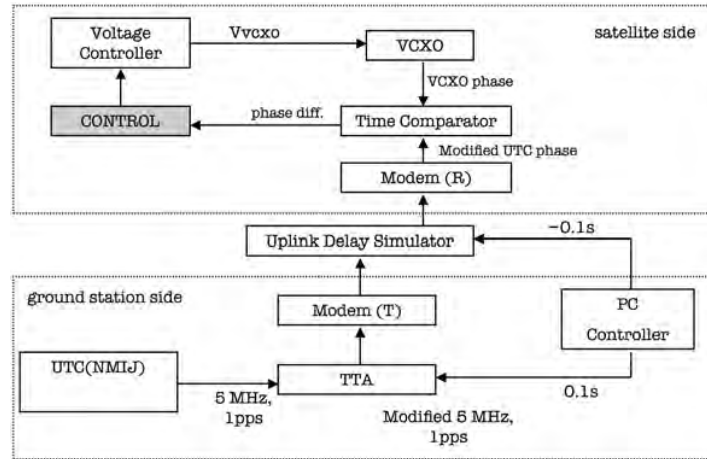


Figure 4.18: Modified version of the RESSOX Hardware Simulator for testing of the RTKS PI filter.

the two clocks is expected to introduce a greater error which will mitigate the ground station atomic clock stability problem.

For averaging time below 100 s the employed VCXO is more stable than the reference therefore the data shown in Fig. 4.19 B) reflect the performance of the reference. At longer time scales the free-running VCXO is less stable than the reference, Fig. 4.19 A) but it is locked to it by the RTKS. The instability of the reference therefore appears in the VCXO and cancel out the difference in common mode. The high stability shown at long times in Fig. 4.19 B) thus relates only to the synchronization loop itself, not to the absolute stability of either reference or VCXO.

## 4.5 Conclusions

A remote synchronization system for the on-board TKS of QZSS has been described. Its structure, and how it was adapted from the already existing TWSTFT apparatus under development by NICT has been presented. The problem related to the inevitable delay introduced by TWSTFT apparatus was described and a PI filter for the RTKS PLL has been presented. Simulations show how the proposed filter will provide the required stability and acceptable convergence time as long as the delay introduced by

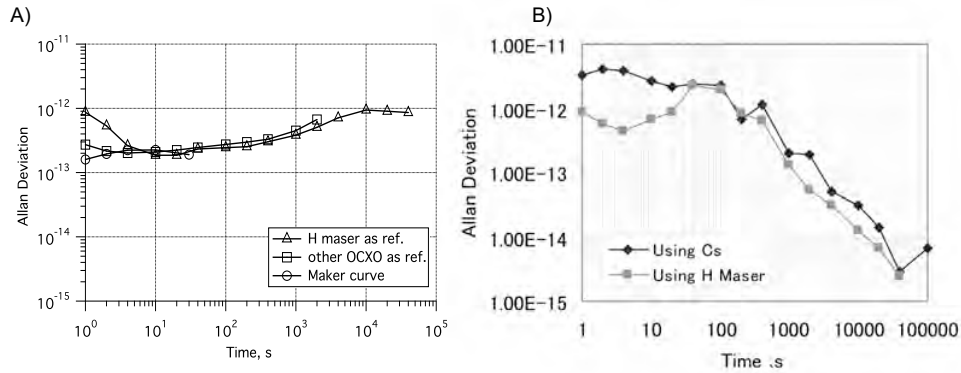


Figure 4.19: A) Frequency stability of the uncontrolled VCXO Oscilloquartz 8607-BM measured against two different reference clocks, the Anritsu hydrogen maser RH401A and an VCXO with similar quality as the 8607-BM. Manufacture's curve is also provided, as in Fig. 4.8. B) Allan deviation for the long-term stability of the RTKS VCXO when the Cs atomic clock and the hydrogen maser were used as references. Stability at 100,000 s was less than  $10^{-14}$ .

the TWSTFT apparatus is guaranteed to be below 30 s.

In order to increase the short-term VCXO stability an Optimally Unbiased Moving Average technique has been presented as an alternative to the GPS TKS Adaptive Time Constant (ATC) approach. Its effects on phase and frequency jumps have been demonstrated. Moreover, the attenuation over the VCXO white noise introduced by the PI filter was analyzed.

The problem of changes in the VCXO characteristics due to environmental effects (for example, space radiation, eclipses, thermal effect) has been identified and solved by the adoption of a PI filter instead of GPS TKS VCXO Gain Tracking.

A real-time detection and mitigation method for frequency and phase jumps based on the adoption of an additional VCXO (of lower quality) was also introduced.

The research contribution in this Chapter can be summarized as follows:

- Presentation and discussion of a novel remote synchronization system, the RTKS, as a candidate for the QZSS timekeeping system.
- Analysis of the inner RTKS delay problem caused by the QZSS TWSTFT apparatus.

- Design of a PI filter for the RTKS.
- Design of a Optimally Unbiased Moving Average technique for the RTKS.
- Analysis of an appropriate detection and mitigation method for RTKS frequency and phase jumps.
- Presentation of a double-VCXO scheme for on-board phase and phase jump detection.



## Chapter 5

# QZSS Satellite Communication Interruption

To provide a proper positioning signal, QZS need stable on-board time references. Instead of using atomic frequency standards, the RTKS method employs a remote synchronization scheme that provides synchronization/correction signal able to keep a master time reference, located on the ground, and the QZS on-board time reference constantly in lock step (refer to Chapter 2.3). One of the critical issues regarding this architecture is the loss of synchronization during satellite communication interruptions. Such losses will inevitably translate into a degradation of positioning when QZSS is employed as an augmentation system for GPS. A hardware-in-the-loop experimental setup has been developed to study the effects on positioning when a space-borne VCXO is employed in the atomic clock-less RESSOX/RTKS architecture. Particular focus is given to the effects of faulty synchronization on positioning, specifically when, because of unavoidable communication interruptions, the QZS clock has to function without ground station assistance. Furthermore, a method for solving the free-run VCXO problem is proposed. A learning algorithm that monitors the satellite on-board clock behavior during its regular functioning has been developed. When synchronization becomes unavailable the QZS on-board clock phase and frequency drifts are kept constrained by using consecutive estimates of clock phase errors. The proposed system has been designed for the RTKS and is characterized by a low hardware requirement,

particularly suitable for the QZS payload. Results show that the proposed phase error compensation method can guarantee enough time accuracy even for communication interruptions of the order of one hour. The relationship between QZSS plus GPS positioning accuracy and QZSS clock quality is discussed.

## 5.1 Introduction

The RESSOX scheme and the RTKS scheme are based on the assumption that if a good location for the MCS is chosen, each QZS could be visible/controllable during its whole orbital period (24 hours). Therefore, a continuous synchronization communication framework could hypothetically guarantee the accurate synchronization of the on-board QZS clock with the master station (master clock).

The RESSOX scheme, as well as the RTKS scheme, represents a way to synchronize two clocks distant from one another. It relies on a master/slave clock synchronization architecture, which can guarantee a certain time synchronization quality as long as the master clock (ground station) and the slave clock (satellite) are able to communicate. The main drawback of this architecture is the inability to guarantee the desired accuracy when satellite uplink communication is not possible. In fact, during these periods the satellite on-board clock cannot be actively steered due to the absence of feedback, and therefore the accuracy depends solely on the quality of the satellite on-board clock. It should be noted that QZS communication interruptions are unavoidable, and the condition of having the QZS operating on its own occurs twice a day when the satellite crosses the equatorial region. Such a condition is necessary for guaranteeing the absence of interference with geostationary telecommunication satellites.

Chapter 6 presents a study of the performance of the RESSOX system when a constant phase error affects the QZS on-board clock due to possible problems in the synchronization. In the same Chapter, studies of short-term and long-term effects are presented, based on results of the RESSOX Software Simulator.

Some of the material related to this Chapter has been published by the author in international conference proceedings [32, 112]. The research activity related has been carried out by means of the RESSOX Software Simulator, described in Appendix B.

The basic idea behind the phase reduction method for RESSOX/RTKS presented in this Chapter has been taken further and a patent is now under examination.

## 5.2 Optimal Clock Prediction

Any two independent clocks will drift away from one another without bound, and the difference between them will exceed any limit given enough time [8]. Because of the backward correlation of the precise-clock noise, it is possible to estimate the future reading of a precise-clock at some precision, which is better than that obtained only from statistical information [11].

For metrology purposes, several algorithms,[12, 123, 132], have been developed to characterize atomic standards and to weight clocks to create an optimum clock ensemble, [46].

In the field of disciplined clocks, e.g. ground station CDMA network (refer to Chapter 2), work has been carried out to improve the performance of the slave clock located on the ground [83, 82, 21, 55]. In principle, an adaptive oscillator model is employed to correct the slave oscillator when the external timing reference is unavailable, [103, 104]. These models differ from the previous in that they consider prediction over time periods of the order of months or years. An accurate method, based on a double Kalman filter algorithm focused on accurate prediction over a relatively short holdover period of 8 and 24 hours, was presented in [82].

The RTKS synchronization scheme, schematically represented in Fig. 5.1, for which this method is proposed, has some unique characteristics. The PLL feedback interruption period length is unknown but generally not longer than 20 minutes, therefore the VCXO phase error reduction has to be maximized for short periods ( $t < 20$  min at worst). Furthermore the slave clock, Fig. 5.1 block (6), is located on board the QZS together with a payload computer with limited memory capability and computational power.

The algorithm proposed here takes advantage of the slave clock statistical knowledge as well as its systematic behavior. Unlike other methods, it is based on the real-time processing of the slave clock command (VCXO command voltage, Fig. 5.1

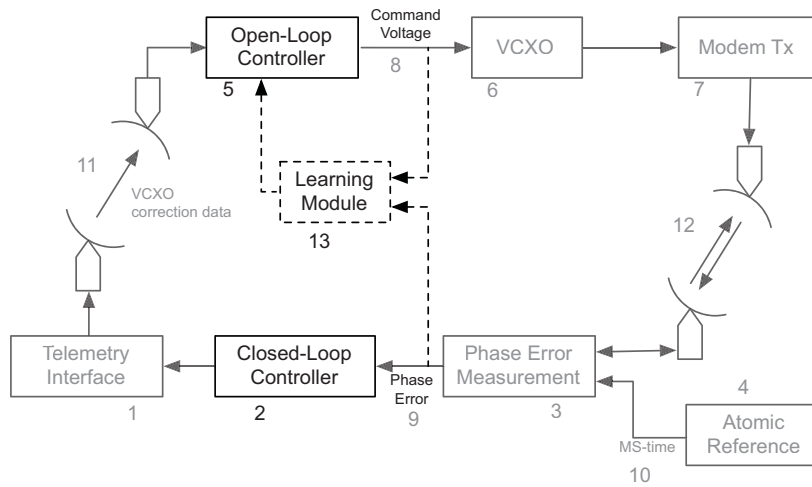


Figure 5.1: Simplified representation of the RTKS for the remote synchronization of QZSS clocks.

block (8)), which is related to phase error measurements. The proposed algorithm analyzes the dynamics of the slave clock in real-time, and uses this to produce the best prediction when the slave clock is in free-run mode.

### 5.3 Clock Synchronization Network

The synchronization scheme for QZSS presented in Section 3.3, and the RTKS, presented in Chapter 4, are fundamentally different. However, both suffer the same basic synchronization problem: proper synchronization cannot be achieved during periods of satellite communication interruption. Fig. 5.1 is a simplified representation of the RTKS scheme for which this method can be better applied. It consists of a PLL synchronization loop where the actual phase error measurement is provided by a TW-STFT scheme. Details of the research on the TWSTFT for QZSS can be found in Chapter 2 and in the recent publication [129].

For a detailed explanation of the RTKS scheme, refer to Chapter 4 and to [110, 112]. For the sake of clarity, the structure of some of the main blocks of the RTKS architecture are discussed.

### 5.3.1 Atomic Reference

For studies of this synchronization method, the atomic reference ((4) of Fig. 5.1), was simulated accordingly to the behavior (Allan deviation) of the hydrogen maser available at the AIST laboratories, the Anritsu Hydrogen Maser RH401A (Section 4.3.1).

### 5.3.2 Telemetry Interface, Modem Transmitter and Communication Blocks

Referring to Fig. 5.1, the Telemetry Interface block (1) and the Modem Transmitter block (7) are responsible for the communication between the two clocks (11) and (12), and they will be considered ideal with no noise or other disturbing contribution.

### 5.3.3 Closed-Loop VCXO Controller

The closed-loop controller is a PLL controller which uses the output (9) to directly control (6). Several methods have been studied and implemented to improve the performance of the Closed-Loop VCXO Controller. [83, 55] are examples of patents of methods to improve closed-loop controller performance for SS-TDMA satellite networks, where a similar problem occurs.

For the purposes here, the Closed-Loop VCXO Controller has been developed as a PI controller, coupled with a running average block suitable for removing the large white noise that affects the input of the Closed-Loop VCXO Controller (2). It is assumed that during closed-loop periods the functioning of the PLL and the Closed-Loop VCXO Controller satisfy the requirements. Details of this controller can be found in Chapter 4 and in [118].

### 5.3.4 Voltage-Controlled Crystal Oscillator (VCXO)

For the experiments the Swiss Oscilloquartz (Swatch Group) 8607-BM presented in Section 4.3.3, has been employed.

## 5.4 VCXO Indirect Phase Drift Prediction

The Least Squares Method gives a prediction of the status of the system, based on past measurements, [8, 103]. The Kalman filter used as the predictive filter takes it one step further, taking advantage of the knowledge of the dynamics of the system (the VCXO clock) to better predict the status of output, in this case the VCXO phase error [82]. Because of the nature of the RTKS, the direct control/monitor of the VCXO command voltage instead of its phase error is preferred (refer to Chapter 4).

The proposed method consists of an algorithm which collects samples of phase error  $PE(t)$ , Fig. 5.1 block (9), and samples of control voltage  $CV(t)$ , Fig. 5.1 block (8), during normal functioning of the PLL. In other words, when the PLL feedback is available and synchronization is achieved ( $0 < t < t_c$ ). As soon as a new sample is available the oldest sample is dumped, as in a stack structure.

A secondary algorithm uses the collected VCXO voltage samples  $CV(t)$  to construct a series of approximation curves  $CV_{apr}(m)$  over the intervals:  $t_c$ ,  $t_c/2$ ,  $t_c/4$ ,  $t_c/8$ , and so on. These curves are approximations of the behavior of the VCXO. As soon as the satellite becomes unavailable to the ground station and synchronization is no longer achievable using the PLL-like scheme, a warning flag is given and the satellite on-board computer will calculate the appropriate VCXO voltage based on the collected data.

At this stage, the curves  $CV_{apr}(m)$  are first order straight line series and the approximation method to generate them is the Least Square Method. Other types of approximation curves could be employed. It is assumed however that, for  $t < 30min$ , the VCXO frequency drift is linear.

The creation of the approximation curves could be done every epoch, e.g. every second, or every several epochs. (The latter is preferred because it is less computationally intensive) Fig. 5.2 show a graphical representation of the generation of the curves. During the period  $t_c$  samples of VCXO control voltage,  $CV_{vcxo}(n)$ , are collected. After  $t_c$  the PLL feedback becomes unavailable and this condition lasts for  $t_{fr}$ . The value of  $V'_{vcxo}$  is the value of voltage that the closed-loop controller should ideally apply. Approximation curves are calculated over the interval  $t_c$ ,  $t_c/2$ ,  $t_c/4$ ,  $t_c/8$ , and so on,

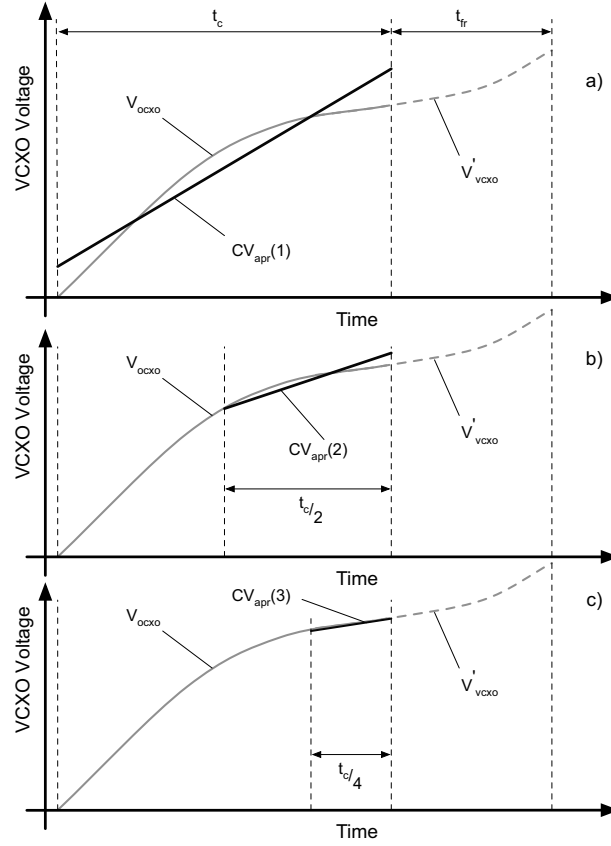


Figure 5.2: Method to generate the the approximation curves  $CV_{apr}(n)$ . Out of the  $t_c$  available samples, a sub-series of them is used to produce approximation curves using the Least Square Method.

where  $t_c/8$  is the most recent interval of VCXO voltage samples. The whole series is stored in the matrix  $CV_{apr}(n)$ .

The series of curves  $CV_{apr}(m)$  is calculated from:

$$y(t)_m = a(m) \times t + b(m) \quad (5.1)$$

where  $y(t)_m$  is the straight line that best approximates the given set of data  $(t, CV(t))$  with  $t = 0 \rightarrow t_{max}$ . The best fitting curve  $y(t)_m$  has the least square error.

Once the approximating curve  $y(t)_m$  is calculated, the array  $CV_{apr}(m)$  is populated with the slope  $a(m)$  of such curves (straight lines) following  $CV_{apr}(m) = a(m)$ .

The first element  $CV_{apr}(1)$  is the slope of the straight line approximating the

collected  $t_{max}$  points. The second element  $CV_{apr}(2)$  is the slope of the straight line approximating the past  $t_{max}/2$  points. The third element  $CV_{apr}(3)$  is the slope of the straight line approximating the past  $t_{max}/4$  points, and soon the scheme is therefore:

$$\begin{aligned}
t = 0 \rightarrow t_{max} &\Rightarrow CV_{apr}(1) = a(1) \\
t = 0 \rightarrow \frac{t_{mak}}{2} &\Rightarrow CV_{apr}(2) = a(2) \\
t = 0 \rightarrow \frac{t_{mak}}{4} &\Rightarrow CV_{apr}(3) = a(3) \\
t = 0 \rightarrow \frac{t_{mak}}{8} &\Rightarrow CV_{apr}(4) = a(4) \\
&\dots \\
t = 0 \rightarrow \frac{t_{mak}}{n} &\Rightarrow CV_{apr}(m) = a(m)
\end{aligned} \tag{5.2}$$

The value of  $m$ , and therefore the number of approximation curves  $CV_{apr}(m)$ , depends on how many  $CV(t)$  samples are available in the first place. Generally if 20,000 is the number of available samples, a value of  $m = 10$  would imply  $n = 2^{m-1} = 512$ , leaving about 39 samples ( $\frac{t_{mak}}{n} = \frac{20,000}{512} = 39$ ) for the approximation curve  $CV_{apr}(10)$ , which is still acceptable.

During the experiments, the number of collected points was 100,000 and the size of the array  $CV_{apr}(m)$  was  $m = 11$ . Fig. 5.3 shows the content of the array  $CV_{apr}(m)$  during three simulated feedback interruptions.

Note that  $CV(t)$  for  $t = 0$  is the most recent value of phase error, therefore this algorithm tends to find a better approximation giving more weight to recent samples. A simplified graphical representation of how the curves  $CV_{apr}(m)$  are calculated for a first order polynomial curve series is given in Fig. 5.2.

In the tests, the process of creating the  $CV_{apr}(m)$  series is performed every epoch. Comparison of new series with old series can give an insight into how the slave clock is performing.

At this stage each element of the curve series  $CV_{apr}(m)$  is just the slope of the first-order polynomial function. More sophisticated functions could be used (higher order polynomial functions, splines, etc.).

Once the  $CV_{apr}(m)$  is created, the learning module is ready to control the VCXO in free-run mode (any time after 100,000 seconds have passed).

#### 5.4.1 The $CV_{apr}(m)$ Array and Its Structure

Generally speaking, by analyzing the trend of  $CV_{apr}(m)$ , it is possible to characterize how the VCXO has been performing during the closed-loop period. Moreover from the trend of  $CV_{apr}(m)$  it is possible to detect the presence of possible interference on the VCXO. Such interference can also be compensated for.

The array  $CV_{apr}(m)$  could be calculated once every epoch, or once every  $\frac{t_{mak}}{n}$  samples, or at any update rate required. It is worth mentioning that even using 100,000 samples of past phase shift, the final size of the vector  $CV_{apr}(m)$  would only require 11 floating point numbers.

The vector  $CV_{apr}(m)$  holds a good approximation of the history of the VCXO and requiring a limited amount of memory. This is one of the strengths of this method. However, the creation and updating of its elements requires significant computational power. This does not constitute a problem; in fact such computational power would be available at the ground station.

The following Section describes an alternative method to store the content of the vector  $CV_{apr}(m)$  where old elements are consecutively stored. Such additional history knowledge can be used for a finer prediction of VCXO voltage values.

#### 5.4.2 The Matrix $\overline{CV}_{apr}(m, h)$ and Its Structure

After  $t = t_{max}$ , the vector  $CV_{apr}(m)$  has been totally populated (following the previous example, after 100,000 samples). From this point on the algorithm is ready to provide an estimate of the behavior of the VCXO and is ready to control the VCXO any moment it is needed.

For  $t > t_{max}$  a new vector  $CV_{apr}(m)$  is calculated using the new  $t_{max}$  samples. The old  $CV_{apr}(m)$  vector, instead of having been dumped, can be stored into a matrix by stacking up newer vectors  $CV_{apr}^h(m)$  from the top. In this way, old vectors  $CV_{apr}(m)$  can be stored and therefore a new matrix populated, called  $\overline{CV}_{apr}(h, m)$ .

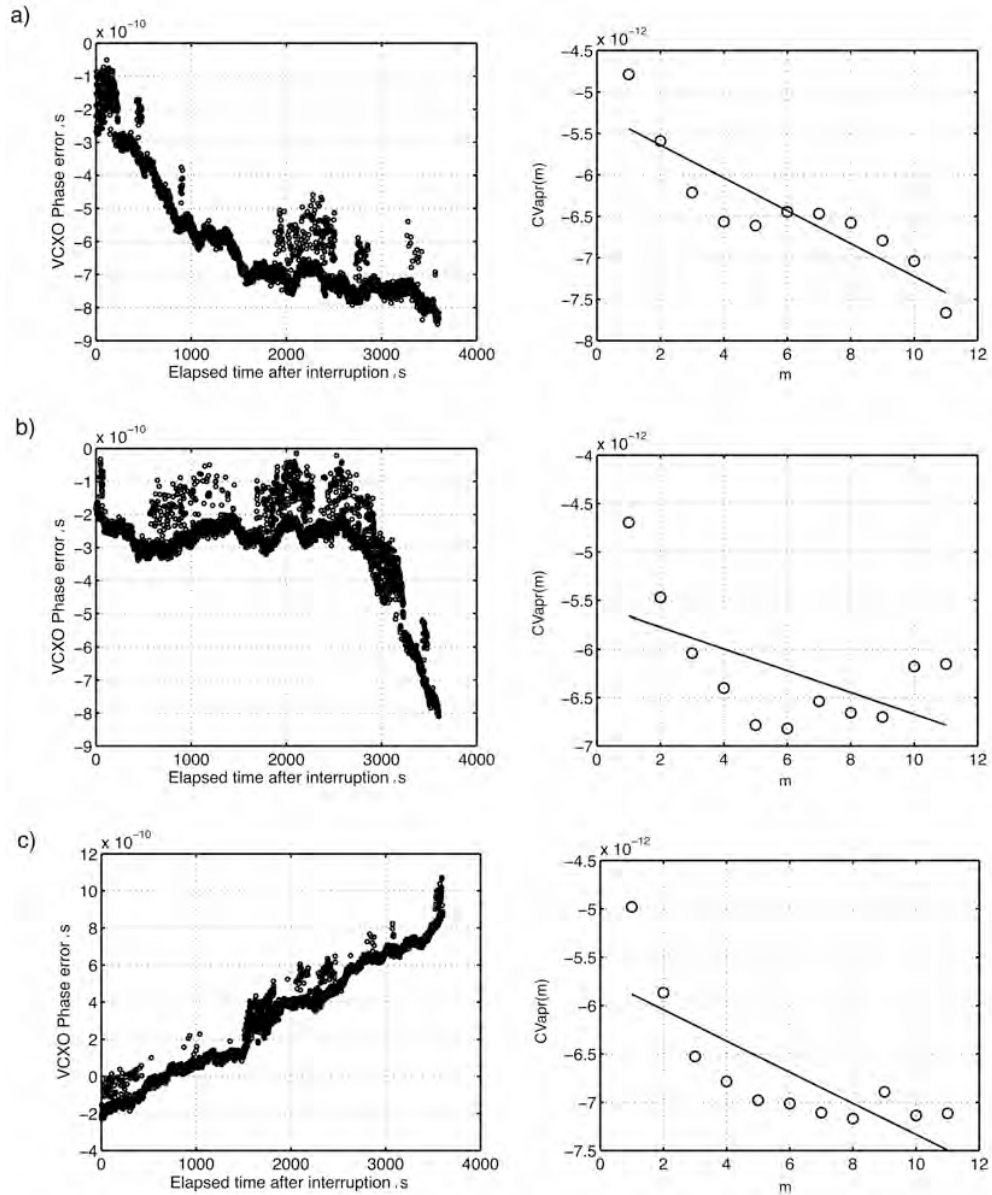


Figure 5.3: Three examples (a, b and c) of VCXO phase error compensation. The algorithm presented has been implemented as a non real-time routine and applied to the phase error shown in Fig. 5.11. Three feedback interruptions have been simulated and 100,000 past samples have been used to create the vector  $CV_{apr}(m)$  and then used to steer the VCXO without feedback. The overall phase error was kept below about 2 ns for feedback interruptions of up to 1 h in length.

$CV_{apr}^1(m)$  refers to the most recent vector  $CV_{apr}(m)$ , and  $CV_{apr}^2(m)$  refers to the vector calculated before  $CV_{apr}^1(m)$ , and so on.

The calculation process repeats and new approximation curves replace old ones. Each row of the matrix  $PE_{apr}(m, h)$  will contain one vector  $CV_{apr}(m)$ . A new row of the matrix  $\overline{CV}_{apr}(h, m)$  is calculated after  $\frac{t_{mak}}{n}$  samples. Following the example before, after  $\frac{t_{mak}}{n} = \frac{20,000}{512} \approx 39$  samples.

$$\overline{CV}_{apr}(h, m) = \begin{pmatrix} CV_{apr}^1(m) \\ CV_{apr}^2(m) \\ CV_{apr}^3(m) \\ \vdots \\ CV_{apr}^h(m) \end{pmatrix} \quad (5.3)$$

where

$$CV_{apr}^h(m) \rightarrow t = t_{max} + \frac{t_{max}}{n} \times (h - 1). \quad (5.4)$$

The value of  $h$  depends on how much of the history of the VCXO is required to be stored. In order to have a satisfactory and homogenous structure of the matrix  $\overline{CV}_{apr}(h, m)$ , a choice of  $h = n$  is recommended.

If the recommended value of  $h = n$  is chosen, after  $t = t_{max} \times 2$  the matrix  $\overline{CV}_{apr}(h, m)$  is totally populated. From then on, new values of the matrix  $\overline{CV}_{apr}(h, m)$  will replace old ones following the same structure as for  $CV(t)$ . For  $t_{max} = 20,000$  the size of the matrix  $\overline{CV}_{apr}(h, m)$  becomes  $32bit \times 10 \times 512 \approx 164KB$  (for a single precision floating point 32 bit system), a memory size that is quite acceptable. If more VCXO behavior history is needed, a greater value of  $t_{max}$  can simply scale the whole model up.

The knowledge stored in the matrix  $\overline{CV}_{apr}(h, m)$  is the complete VCXO behavior history over the last collected samples. Its access is immediate and its size is quite small. For instance, reading the matrix  $\overline{CV}_{apr}(h, m)$  per column, accesses the consecutive approximation curves of the VCXO voltage. In fact the column  $\overline{CV}_{apr}(h, 10)$  contain the coefficients of the first-order approximation curve of the VCXO voltage signal for

$0 < t < t_{max}$  sliced by 39 samples at the time, which is the most accurate reconstruction of the VCXO voltage signal.

Reading the matrix  $\overline{CV}_{apr}(h, 10)$  per column is a useful way to characterize the VCXO in the short-term as well as over the long-term.

### 5.4.3 Construction of the Free-run VCXO Voltage, $V'_{apr}(t)$

As mentioned before after  $t = t_{max}$  the vector  $CV_{apr}(m)$  is full and the system is ready to provide the necessary control voltage as soon as the VCXO falls into the free-run mode.

There are various strategies that can be used for constructing the voltage signal to apply during the period  $t_{fr}$  from the vector  $CV_{apr}(m)$ . The best solution should be chosen according to the structure of the matrix  $CV_{apr}(h, m)$  and a case-by-case study.

A possible solution which has been satisfactory for the experimental setup is presented here. It was found that, the VCXO voltage could be successfully generated using the following formula:

$$V'_{apr}(t) = CV_{str} + \sum_{n=1}^m K_n \times CV_{apr}(n) \times \frac{t}{m} \quad (5.5)$$

where

$$CV_{str} = \sum_{t=1}^{t_{avr}} \frac{CV(t)}{t_{avr}} \quad (5.6)$$

Therefore  $CV_{str}$  is the mean value of the last  $t_{avr}$  samples of the vector  $CV(t)$ . Other methods, such as the use of the coefficients  $b(m)$  (refer to Equation (5.1)), in the approximation of  $CV_{apr}(m)$  could also be used.  $K_n$  is a series of weighting coefficients.

During the closed-loop period ( $t_c$ ) the closed-loop controller applies the voltage  $V_{vcxo}$  and the phase error is assumed to be successfully contained. During the period  $t_{fr}$  the VCXO is free-running, and the VCXO is controlled with a voltage function  $V'_{apr}(t)$  derived from the array  $CV_{apr}(m)$ .

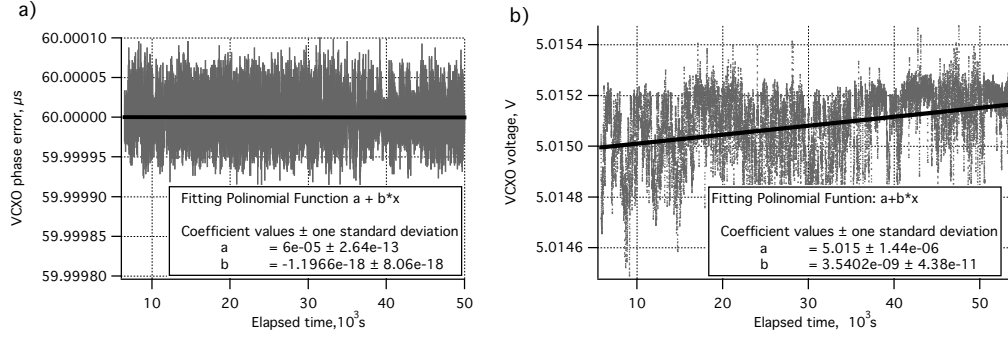


Figure 5.4: a) VCXO phase error, and b) VCXO voltage during a closed-loop controlling period of about 50,000 s.

#### 5.4.4 Choice of the Coefficients $K_n$

The weighting coefficients  $K_n$  are the means of combining the elements  $CV_{apr}(m)$  to get the predicted voltage  $V'_{apr}(t)$ . For voltage prediction, an optimized method for choosing the coefficients  $K_n$  is presented here.

Referring to Fig. 5.5,  $V_{vcxo}$  is the VCXO voltage during a successful synchronization period (closed-loop scenario). At time  $t_1$  the new algorithm is applied and, based on the VCXO voltage history for  $t < t_1$ , the signal  $V_{apr}^1(t)$  is predicted according to the formula:

$$V'_{apr,1}(t) = CV_{str} + \sum_{n=1}^m K_n \cdot CV_{apr}(n) \cdot \frac{t}{m} \quad (5.7)$$

After a time  $t = t_{fr}$ , the same formula is used to calculate  $V'_{apr,2}(t)$ . Because there are  $m = 11$  unknown  $K_n$  coefficients (refer to Section 5.4 and Fig. 5.3), the process is repeated  $m = 11$  times. At this point the mean value of  $V_{vcxo}(t)$  for  $t_1 < t < t_2$  is set equal to the predicted voltage  $V'_{apr,1}(t)$  for  $t = t_1 + t_{fr}/2$ . The eleven  $K_n$  coefficients are then calculated. Solving the formulas:

$$\overline{V'_{apr}}(t_{fr}/2) = CV_{str} - \sum_{n=1}^m K_n \cdot CV_{apr}(n) \cdot \frac{t_{fr}/2}{m} \quad (5.8)$$

$$\left(\overline{V'_{apr}}(m) - CV_{str}(m)\right) \cdot \frac{m}{t_{fr}/2} = \sum_{n=1}^m K_n \cdot CV_{apr}(m, n) = \mathbf{K}(m) \cdot \mathbf{CV}(m, n) \quad (5.9)$$

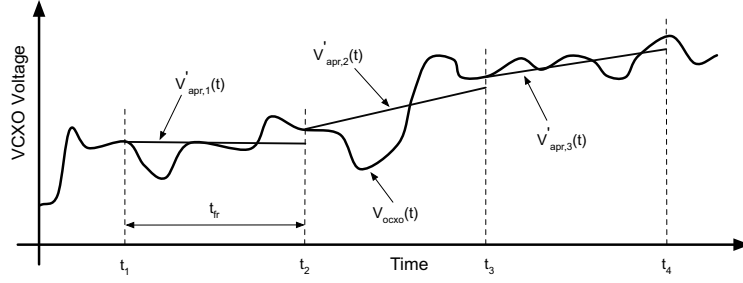


Figure 5.5: VCXO voltage and straight line approximations during a closed-loop controlling period.

where

$$\mathbf{K}(m) = (K_1, K_2, \dots, K_m) \quad (5.10)$$

$$\mathbf{CV}(m, n) = (CV_{apr}(1, n), CV_{apr}(2, n), \dots, CV_{apr}(m, n)) \quad (5.11)$$

therefore

$$\mathbf{K}(m) = (\overline{V'_{apr}}(m) - CV_{str}(m)) \cdot \mathbf{CV}^{-1}(m, n) \cdot \frac{m}{t_{fr}/2} \quad (5.12)$$

The presented algorithm aims to find the  $K_n$  coefficients so that the mean voltage error for  $t = t_{fr}$  is reduced to 0. Other criteria could be used as well. During the experiments it was assumed a  $t_{fr}$  of 30 minutes and  $m = 11$ . Fig. 5.6 show the values of the 11  $K_n$  coefficients for a particular case.

The values of the coefficients  $K_n$  does not resemble any particular distribution, and therefore a uniform average value for all coefficients  $K_n$  of 0.4 was chosen. About 64 different conditions were tested and all of them resulted in a phase error  $< 4ns$  for  $t < 1hour$ . Fig. 5.3 shows three representative cases of successful phase error reduction of the 35 cases analyzed (the experimental results of all 45 cases are given in Appendix C). Overall the choice of the coefficients  $K_n$  is not critical, mainly due to the adaptive nature of the proposed algorithm which tends to use always the newest values of past VCXO voltage commands.

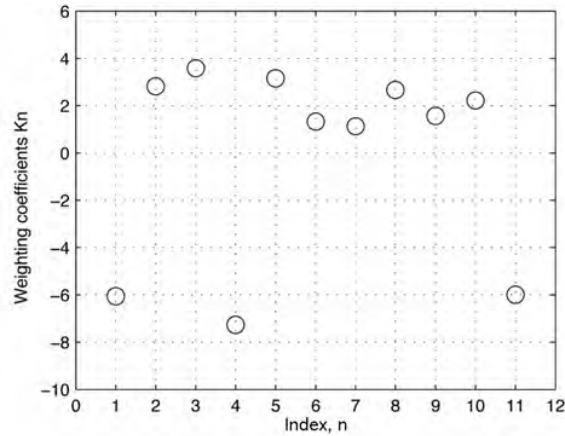


Figure 5.6: Coefficients  $K_n$  calculated by the optimum mean value algorithm.

#### 5.4.5 Algorithm Performance

The proposed algorithm was tested to evaluate its performance under realistic conditions. By means of a modified version of the RESSOX/RTKS Software Simulator (refer to Appendix A), the VCXO was setup to be controlled by the proposed algorithm and its output was compared to an ideal predicted voltage. Utilizing three days worth of data, a controlling scenario was created and 16 VCXO feedback interruptions were simulated. Fig. 5.7 shows two examples where the proposed method is compared against a linear interpolation method. The latter was able to compensate the VCXO phase error, limiting the overall phase error within 1.5 ns (with an interruption period of 3600s). For the same scenario, the proposed method could limit the VCXO phase error within 0.4 ns (interruption period of 3600 s).

Fig. 5.8 is a relative (averaged over one hour) indication of the optimum  $V'_{apr}$  (white circles) together with the  $V'_{apr}$  (black triangles) predicted by the proposed algorithm. The 16 feedback interruption scenarios were 6000 s apart and lasted 3600 s (1 hour). The overall distribution suggests a satisfactory degree of prediction. However to better understand and quantify the performance of the proposed algorithm a second test was conducted.

The same feedback interruptions of 3600 s were repeated 25 times over a two day period. For each period the absolute phase error caused by the drift of the VCXO was

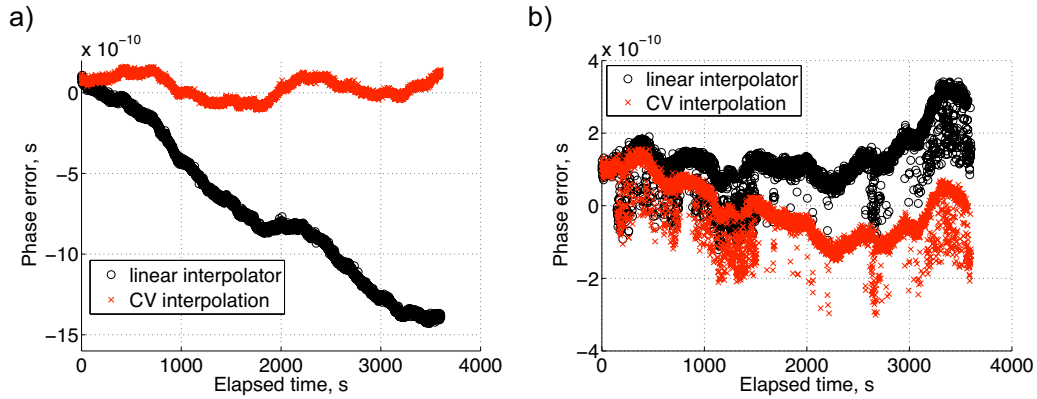


Figure 5.7: Two examples (a and b) of VCXO phase error compensation. The algorithm presented (named CV interpolator) has been compared against the a linear interpolation method. Both methods have been implemented as a non real-time routine and applied to the phase error shown in Fig. 5.11. Two 36000 s feedback interruptions have been simulated and 100,000 past samples have been used to create the vector  $CV_{apr}(m)$  and then used to steer the VCXO without feedback. The linear interpolator method, was able to compensate the VCXO phase error, limiting the overall phase error within 1.5 ns (with an interruption period of 3600s). For the same scenario, the proposed method could limit the VCXO phase error within 0.4 ns (interruption period of 3600 s).

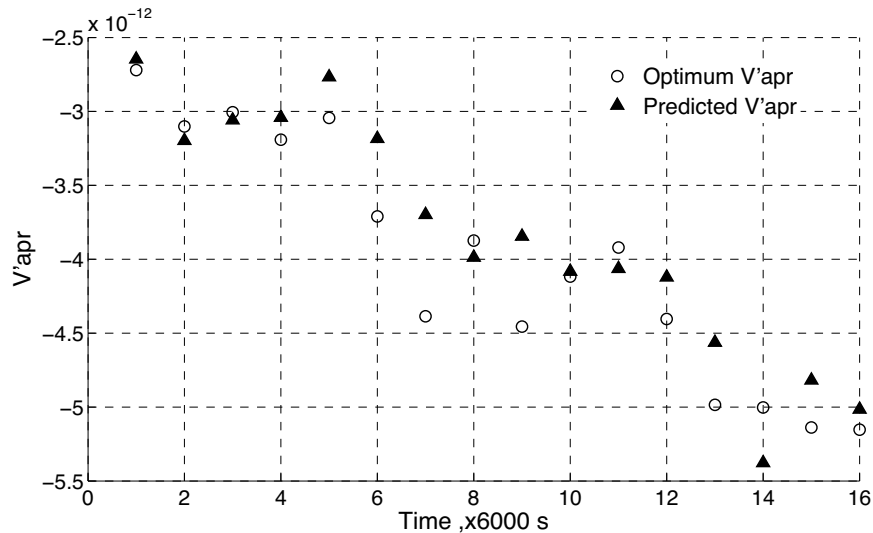


Figure 5.8: Optimum  $V'_{apr}$ .

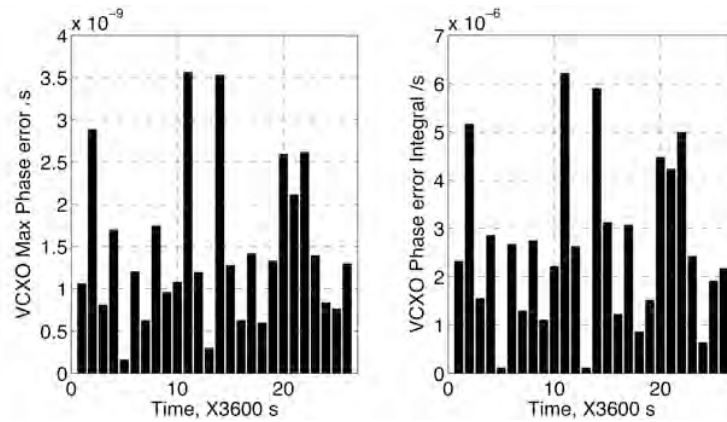


Figure 5.9: Maximum phase error and integral of the phase error for a 3600 s interruption.

measured during two distinct cases; in the first case the ideal prediction was applied, and in the second case the algorithm prediction was applied. Fig. 5.9 shows the difference between the ideal case error, used as a benchmark, and the algorithm error. Results are presented in terms of maximum phase error over one hour of feedback interruption, and integral of the phase error over the same period. Observing the results of Fig. 5.9 it is possible to conclude that when the algorithm is applied for a one hour interruption, the maximum phase error is about 3.6 ns (worst case scenario) and the maximum phase shift error which is likely to occur (mean value) is about 2 ns.

## 5.5 VCXO Phase Compensation, Experimental Results

A set of tests were performed to evaluate the ability of the proposed algorithm to reduce the phase error during free-run. A Hardware Simulator based on a simplified version of the RTKS (Fig. 5.1) was implemented. The TWSTFT apparatus was replaced by a time interval counter. The white noise introduced by the telemetry and communication components have been neglected.

Closed-loop synchronization has been successfully achieved. Fig. 5.4 a) shows the phase error between the VCXO and the atomic reference (10) over a period of about

13 hours. Fig. 5.4 b) shows the VCXO control voltage during the whole 13 hours. At this stage, the effectiveness of the method presented here has been tested through a post-processing method, and the generation of the approximation curves was based on a realistic estimation of past VCXO voltage samples employing the Swiss Oscilloquartz 8607-BM, (Table 4.1).

### 5.5.1 Closed-loop Case

As long as the phase error measured by the block (3) (Fig. 5.1), is fed into the VCXO controller block (5), with an acceptable noise level, synchronization, (phase error  $< 1\text{ns}$ ), has been successfully achieved. Fig. 5.4 a) shows the VCXO phase shift error over a simulation period of 13 hours. The collected VCXO control voltage samples are shown in Fig. 5.4 b). The high level of white noise, visible in the plot, is attributable to the time interval counter which replaces the TWTT block (3). The curve in Fig. 5.4 b) represents the approximation straight line, indicating the aging of the VCXO during the 13 hour period. Details of the closed-loop controller employed for this experiment can be found in the Chapter 4

### 5.5.2 Open-loop Case

After a long enough period ( $t > 20,000$  s) of successful synchronization, the PLL open-loop condition was simulated and the VCXO was left to free-run. Two possible scenarios were considered:

- No VCXO phase error reduction algorithm applied.
- Composite VCXO phase error reduction using the elements of the  $CV_{apr}(n)$  series.

During free-run, the VCXO phase was compared with the accurate hydrogen maser, the Anritsu Hydrogen Maser RH401A. Fig. 5.10 shows the performance of the VCXO for the two scenarios.

Without any compensation, the aging/drift of the VCXO together with the uncertainty of the true Hydrogen Maser central frequency, causes the VCXO phase to drastically drift away very quickly, refer to Fig. 5.11 and Fig. 5.10 a). If the proposed

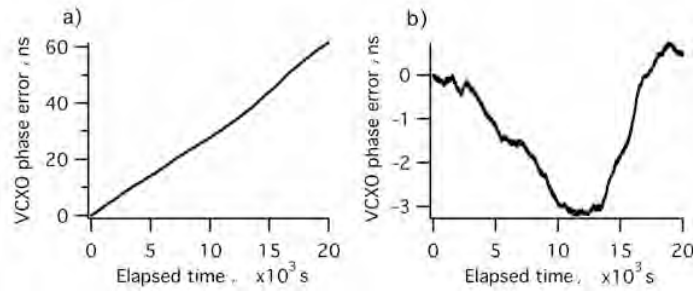


Figure 5.10: Results of a 20,000 s experiment using the Oscilloquartz VCXO 8607-BM with no PLL feedback control. a) The VCXO phase error when no controlling method is applied. b) The VCXO phase error when the proposed algorithm is applied using the approximation function  $CV_{apr}(m)$ .

method is applied, Fig. 5.10 b), the VCXO phase could be contained within about 3 ns over 10,000 s. In this case the main cause of drift is the noise of the VCXO. Furthermore, to prove the robustness of the proposed solution several communication interruptions were simulated and the VCXO was controlled by the proposed algorithm. Fig. 5.3 shows three cases where the VCXO phase error was successfully contained. Three feedback interruptions have been simulated and 100,000 past samples have been used to create the vector  $CV_{apr}(n)$  used to steer the VCXO without feed-back. The overall phase error was kept below 2 ns for feedback interruptions up to 1 h (3600 s) in length.

### 5.5.3 On-board Computer Requirements

The approximation curve  $CV_{apr}(n)$  can be calculated once every epoch, an intensive calculation mode, or less often, e.g. every 50 epochs. The frequency with  $CV_{apr}(n)$  is calculated with an optimum which, through our experiments, does not seem to lead to any computation power problem. During the tests,  $m$  samples of VCXO command voltage haven been continuously collected and the required on-board computer memory size for the vector  $CV_{apr}(n)$  was 40 Bytes (4 bytes X 10 samples) when a single precision floating point 32 bit processing system was used. The memory needed to store the 20,000 samples is located in the ground station computer and therefore does

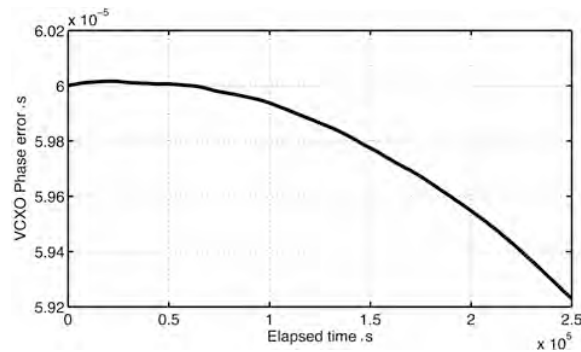


Figure 5.11: Phase error of the VCXO Oscilloquartz 8607-BM left in free-run mode for about 70 hours (250,000 s). After being accurately synchronized (same phase and same frequency) with the atomic standard used as reference, the VCXO has been left to free-run without any control and with a constant voltage of 5.0910 V.

not constitute a problem. The vector  $CV_{appr}(n)$  holds a good approximation of the history of the VCXO requiring a very limited amount of memory. This is definitely one of the strengths of this method. However, the creation and the updating of its elements require significant computational power. If the computational power turns out to be a critical issue, the content of the vector  $CV_{appr}(n)$  can be resized.

The coefficient  $CV_{appr}(n)$  calculated at the ground station will need to be uploaded to the SV every epoch or less often, in accordance to the way the vector is constructed. The proper portion of bandwidth will have to be allocated for this purpose.

## 5.6 Hardware-in-the-loop Experiment

A hardware-in-the-loop experiment setup has been developed to study the effects on positioning when a real space-borne VCXO is employed in the atomic clock-less RESSOX/RTKS architecture.

### 5.6.1 Experimental Setup

The RESSOX Software Simulator employed for the study presented in [112] has been modified to accommodate the integration of a space-borne VCXO in a hardware-in-the-loop configuration. The VCXO employed for this set of experiments is the VCXO 8607-

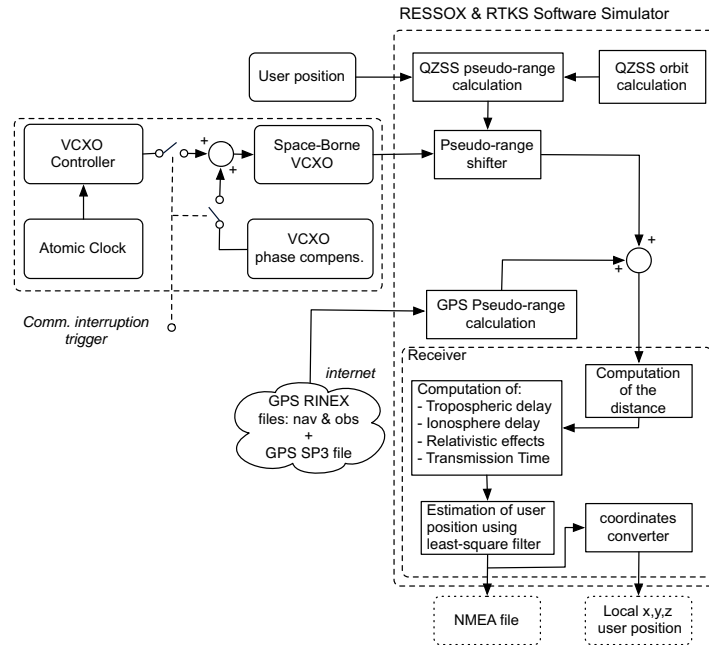


Figure 5.12: RESSOX/RTKS Software Simulator with the space-borne Oscilloquartz VCXO 6607-BM and its phase error compensation algorithm embedded in it.

BM from Oscilloquartz (Table 4.1). An accurate atomic reference (Anritsu RH401A) is employed in the ground station. Two different controllers, the open-loop controller and the closed-loop controller, are used first to achieve synchronization and then to control the VCXO when the atomic reference is not available. Details of both controllers can be found in [112, 118] and in Appendix A. Fig. 5.12 shows the Software Simulator for the RESSOX/RTKS and the clock hardware implementation connected to it.

### 5.6.2 Free-run Experiment

The objective of this set of experiments was to analyze the capability of the Oscilloquartz 8607-BM on board the satellite QZSS-1 remaining stable when not controlled. Results are presented in terms of positioning capability, errors in north/east direction and height. The scenario under test is depicted in Fig. 5.13 and the following configuration was chosen:

- System: GPS plus QZSS.

- User location: Sydney, Australia (lat:-33.0 deg. long:152.0 deg).
- Simulation duration: 5 hours.
- Start time: UTC 23:15, December 31st, 2004.
- Sample ratio: 1 s.
- Receiver mask angle: 26 deg.

Initially, the VCXO of the QZSS-1 is locked to the atomic standard. Such a condition represents the ideal RESSOX scenario. After synchronization is reached the closed-loop condition is intentionally broken and, the open-loop controller is used to reduce the VCXO phase for satellite QZSS-1 (Fig. 5.13). Positioning is then performed for about 5 hours. Three different scenarios are considered.

**Ideal Clock.** This is not a realistic scenario. The VCXO is replaced with an ideal clock with a phase error which is virtually zero. This scenario is used to evaluate the effectiveness of the VCXO phase error compensation algorithm during the whole 5 hours.

**Not controlled VCXO.** Immediately after closed-loop synchronization, a constant voltage is applied to the VCXO (no phase error compensation). This condition is held for the whole simulation period of 5 hours. The applied voltage value is calculated as the average of the last  $n$  voltage samples with  $n=100$ .

**Compensated VCXO.** Immediately after closed-loop synchronization, a variable voltage is applied to the VCXO (phase error compensation). This condition is held for the whole simulation period of 5 hours. The applied voltage value is calculated according to the RESSOX phase error reduction method presented in [112].

## 5.7 Simulation Results and Conclusions

An algorithm that monitors the satellite on-board clock behavior during its regular functioning has been presented. When synchronization becomes unavailable the QZS on-board clock phase and frequency drifts are kept constrained by the proposed algorithm by using consecutive estimates of clock phase errors. Advantages of the proposed method can be summarized as follow:

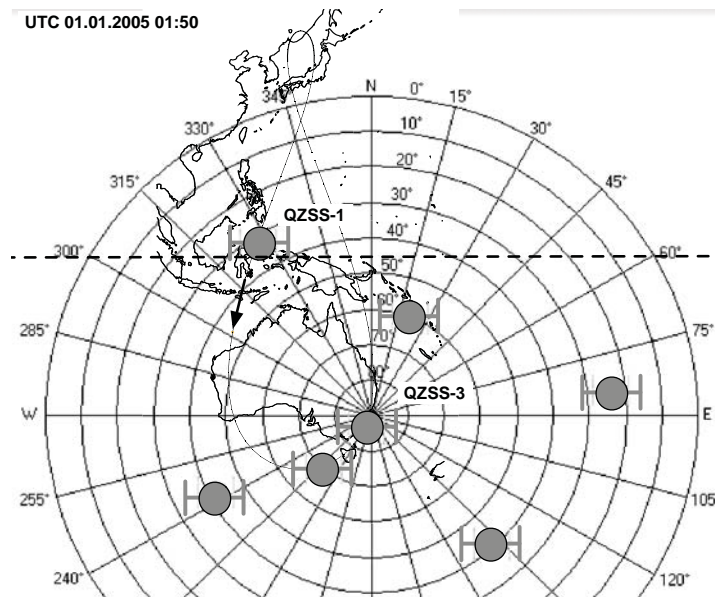


Figure 5.13: Sky-view of the simulated scenario for the combined system GPS&QZSS.

- VCXO aging can be totally compensated for and its effects are negligible even for synchronization interruptions as long as one day.
- Phase errors due to periodic events can be detected and compensated for.
- The approximation curve database is a suitable method to estimate the performance of the on-board time reference.
- The proposed method can be used to detect environmental causes that can alter the output of a time reference. Possible causes could be thermal variation, electromagnetic radiation, gravity changes, etc.
- The proposed method has quite a low hardware requirement which makes it suitable as a component for the payload for the RTKS of the QZSS.

Simulation results show that the VCXO employed during the lab tests can be controlled such that the maximum phase error over a period of 10,000 s can be kept lower than about 3 ns.

Fig. 5.10 a) shows the phase error when the QZSS-1 VCXO is left in free-run mode (no phase compensation). Fig. 5.10 b) shows the phase error when the QZSS-1 VCXO phase is constrained with the method presented in [32]. Fig. 5.14, Fig. 5.15

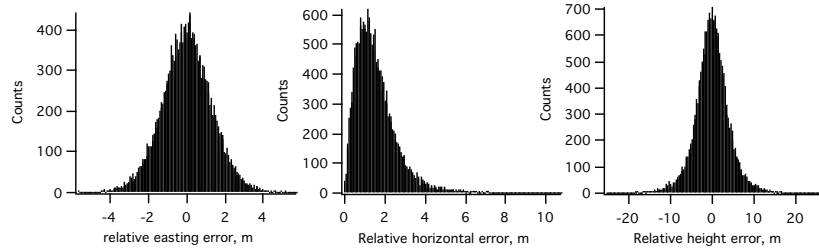


Figure 5.14: Positioning error of the combined system QZSS&GPS over 5 hours. The QZSS on-board clock is an ideal time reference (no drift assumed). 0 m is the true user position.

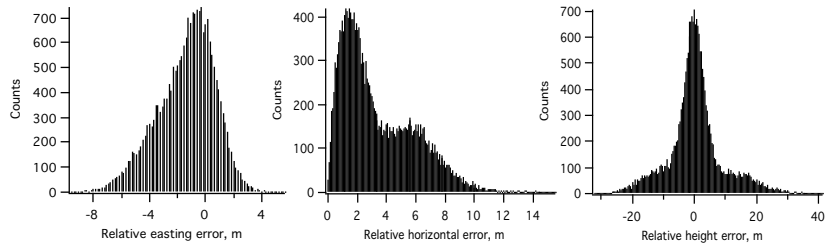


Figure 5.15: Positioning error of the combined system QZSS&GPS over 5 hours. The QZSS on-board clock is the Oscilloquartz VCXO 6607-BM with no drift control. 0 m is the true user position.

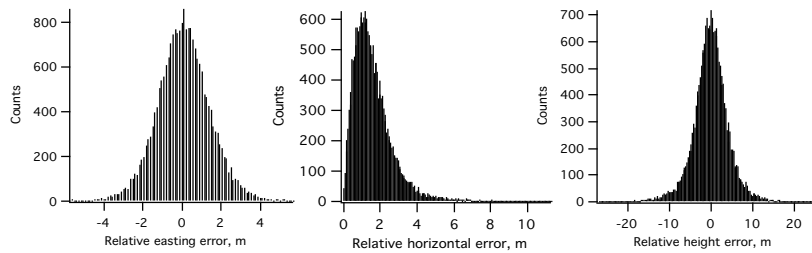


Figure 5.16: Positioning error of the combined system QZSS&GPS over 5 hours. The QZSS on-board clock is the Oscilloquartz with drift compensation control. 0 m is the true user position.

and Fig. 5.16 show the positioning error of the combined GPS plus QZSS for the three scenarios under study. The positioning quality degradation caused by the uncompensated drift on the clock of the satellite QZSS-1 (refer to Fig. 5.13), was successfully reduced. The remaining drift of about 4 ns for the compensated VCXO did not result in an appreciable degradation of the quality of the augmented system QZSS plus GPS. This proves that the RESSOX architecture would have less stringent timing requirements if applied for QZSS; in fact even a 4 ns drift over 5 hours for one QZS does not significantly degrade positioning performance, if compared to the ideal case (of having an atomic reference on board the QZSS-1 satellite). The equatorial communication interruption problem does not seem to be a limitation, for the RESSOX, as long as the phase error reduction method presented earlier is applied. If the Oscilloquartz 8607-BM, or equivalent, is employed as the time reference for QZSSs, satellite communication interruptions and consequently free-run VCXO periods of the order of some hours will not result in positioning degradation with GPS plus QZSS.

After analyzing different VCXO phase shift interruption scenarios (refer to Appendix C), it was found that the choice of the coefficients  $K_n$  is not critical and a simple average of the coefficients  $CV_{apr}(m)$  (by choosing all  $K_n$  equal) does provide adequate phase compensation where the overall drifting phase error does not exceed 4 ns, for  $t < 10,000s$ . The phase error reduction algorithm presented here offers the flexibility of being able to tune the coefficients  $K_n$  so that possible VCXO anomalies (frequency jumps and phase jumps) could eventually be detected. The implementation of a method which takes advantage of the the matrix  $\overline{CV}_{apr}(m, h)$  is part of planned future work.

The research contribution in this Chapter can be summarized as follows:

- Design of a novel method to reduce the phase error of the RTKS/QZSS on-board time reference during synchronization interruptions.
- Evaluation and test of the proposed phase error reduction method by software simulations.
- Development of an hardware-in-the-loop experiment to study the effects of free-run on positioning.



## Chapter 6

# RESSOX and RTKS, Positioning Quality and Timing

A positioning performance analysis of the RESSOX scheme and the RTKS scheme is presented in this chapter. The Software Simulator, described in Appendix B, and the Hardware Simulator, described in Appendix A, have been employed to analyze the positioning quality when GPS is used together with QZSS. The objective of this study is twofold. When QZSS is combined with GPS, positioning quality is improved as long as the QZSS satisfies certain time-accuracy standards. The goal is to understand what these standards are. The second objective is to understand how the positioning quality of the GPS&QZSS system improves or deteriorates if a time phase error is introduced in the RESSOX/RTKS synchronization scheme. This will eventually help in understanding how stringent the RESSOX/RTKS requirements have to be.

In the last part of this Chapter, a free-run clock experiment setup is employed to study the effects on positioning when a VCXO is used in the atomic clock-less RESSOX/RTKS architecture. Particular focus is given to effects on positioning of faulty synchronization specifically when, because of unavoidable communication interruptions, the QZS clock has to function without remote control. Results show that the proposed RESSOX phase error compensation method, discussed in Chapter 5, can guarantee enough time accuracy even for communication interruptions of the order of one hour. The overall relationship between QZSS plus GPS positioning accuracy and

QZSS clock quality will be discussed.

## 6.1 Introduction

The RESSOX presented in Chapter 3 and the RTKS presented in Chapter 4 are two methods that can be employed to keep lock step between an atomic clock located on the ground, and a high-stability VCXO on board each QZS [114, 59]. Ultimately the QZSS is combined with GPS to improve accuracy and satellite availability [87, 65, 126].

One of the important issues regarding the feasibility of either the RESSOX or the RTKS is understanding the required timing quality of the synchronization mechanism responsible for the delicate synchronization of the QZS clock and QZSS ground station clock.

The Software Simulator and Hardware Simulators have been employed to analyze the required accuracy of the RESSOX/RTKS synchronization. Simulators were also used to determine the consequences for the user on positioning if the time reference (remote clock) on board the QZS is left drifting due to RESSOX synchronization problems. The analysis of the timing and positioning error relationship has been carried out considering three different scenarios:

**Constant phase error:** Inside the RESSOX/RTKS synchronization loop a constant phase error was introduced and its effect on positioning quality was studied.

**Software simulated VCXO:** The clock on board the QZS has been simulated using a two-state error model. White phase noise and Random Walk phase noise have been simulated and their effects on positioning quality were studied.

**Free run VCXO:** The clock on board the QZS has been software-simulated and the effect of QZS communication interruptions (the free-run clock condition) on positioning quality was studied.

Through long-term and short-term simulations it is shown how a small time error introduced in the RESSOX synchronization can influence the positioning performance for the GPS&QZSS system.

The free-run VCXO, integrated in the RESSOX/RTKS Software Simulator (communication interruption case), has been used to study the effectiveness of the phase

reduction method presented in [32]. Key results of the GPS&QZSS positioning capabilities using the novel phase reduction method for the RESSOX were presented in Chapter 5.

Most of the material of this Chapter has been published by the author in international conference proceedings, [109, 117, 107], and in a magazine article [113]. The research activity related to this Chapter has been carried out via the RESSOX Software Simulator and the RESSOX Hardware Simulator.

## 6.2 RESSOX/RTKS Software Simulator

A software-implemented QZSS orbit generator, derived from the RESSOX simulator described in Appendix B, and a GPS positioning analysis tool have been integrated in to a single simulator. Fig. 6.1 shows the basic schematic of the simulator. In this study, the objective of this tool is to calculate the user position (NMEA file and Earth fixed-coordinate positioning file) for different scenarios where GPS is combined with QZSS. The simulator can also simulate the RESSOX synchronization by independently de-synchronizing any of the three QZSS clocks, and observing the effect on final positioning [117]. The GPS orbit generator itself is not actually implemented in the simulator and thus the GPS RINEX files and the GPS SP3 file, available on the internet, need to be provided as inputs to the simulator.

The QZSS module is fully implemented and all its orbit parameters can be calculated. From a given position (user position input block), the pseudorange (PR) of each QZS is calculated and modified according to the QZSS clock input file. The PRs of all QZSSs in view and the PRs of the GPS satellites in view are then collected, and the position is computed in the receiver block. Before the PR file is computed a mask angle is applied for both the GPS satellites and QZSSs. Ionospheric, tropospheric and relativistic effects are included in the QZSS orbit calculation and in the positioning calculation. The computed position is output in spherical coordinates (NMEA file) and in Earth fixed-coordinates, where (0,0) represent the true user position.

During the period of research activity related to this Chapter, the RESSOX/RTKS Software Simulator was significantly improved. The current version is capable of gen-

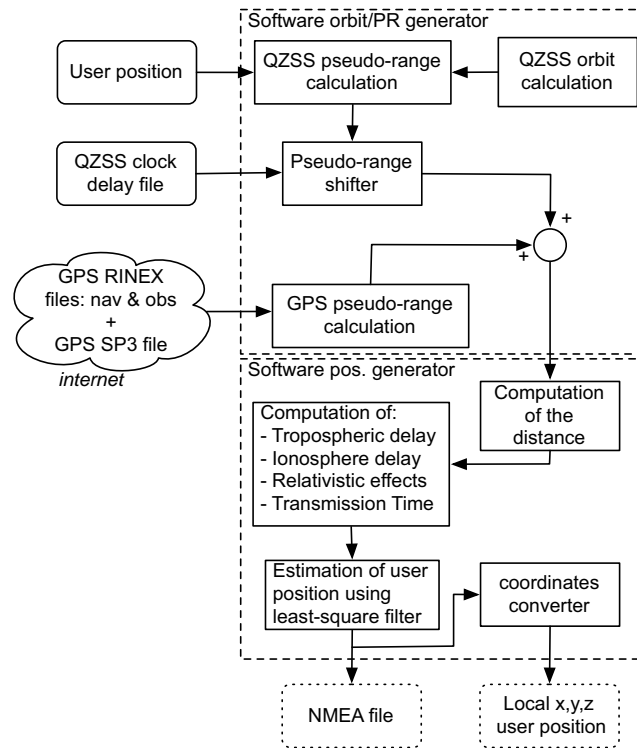


Figure 6.1: RESSOX/RTKS Software Simulator.

erating one positioning solution per second (instead of the previous one solution every 30 seconds). The GPS orbit generator module has been greatly improved as well; GPS RINEX files and the GPS SP3 files are not required anymore because they have been replaced by an internal software GPS orbit generator.

### 6.3 Constant Phase Error

As a first attempt to see how the position accuracy would degrade when the QZSS clocks are lightly de-synchronized, a constant phase error is intentionally introduced and its effects are analyzed. Using the RESSOX Software Simulator, four different simulation scenarios each of nine hours have been considered:

**GPS only:** 24 GPS satellites are considered. The stability of GPS clocks and their synchronization accuracy is dependent on the RINEX files provided.

Table 6.1: Specifications of the simulated scenarios.

Orbit parameters	Values
User location	Okinawa, Japan (lat:26.1946 deg.long:127.67763 deg)
Simulation duration	9 hours
Start time	UTC 23:15, December 31st, 2004
End time	UTC 08:15, January 1st, 2005
Sample ratio	30 seconds
Receiver mask angle	23.0 deg

**GPS&QZSS, phase shift=0 ns:** 24 GPS satellites are simulated together with three QZSSs. The stability of GPS clocks and their synchronization accuracy is the same as in the GPS-only case. The stability of the QZSS clocks is dependent on the VCXO modeled in the simulator. All three clocks are synchronized with respect to each other and synchronized with GPS time.

**GPS&QZSS, phase shift=20 ns:** 24 GPS satellites are simulated together with three QZSSs. The stability of GPS clocks and their synchronization accuracy is the same as in the GPS-only case. The stability of the QZSS clocks is dependent on the VCXO. All three clocks are synchronized with respect to each other but kept 20 ns de-synchronized with respect to GPS time.

**GPS&QZSS, phase shift=50 ns:** 24 GPS satellites are simulated together with three QZSSs. The stability of GPS clocks and their synchronization accuracy is the same as in the GPS-only case. The stability of the QZSS clocks is dependent on the VCXO. All three clocks are synchronized with respect to each other but kept 50 ns de-synchronized with respect to GPS time. Details of the simulation are reported in Table 6.1.

Results for all four cases are presented in Fig. 6.2. Note that the plot of the results of the phase shift equal to 50 ns simulation is at a larger scale.

In order to better understand the results presented in Fig. 6.2, a histogram of each case (presented in Fig. 6.3) was calculated where only the local x Earth fixed-coordinate (Easting direction) was computed. Again, in the last plot of Fig. 6.3 a larger scale is used. The mean x value and the standard deviation for each scale has also been calculated.

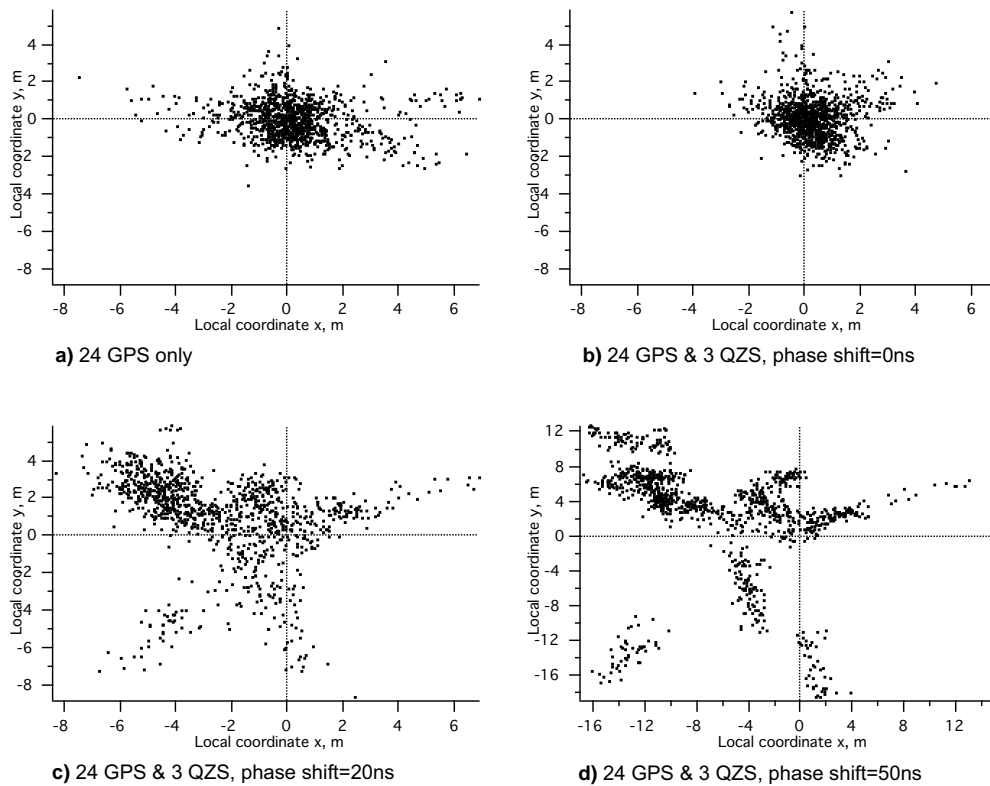


Figure 6.2: Position calculation results of the RESSOX/RTKS Software Simulator. Four scenarios are considered: GPS-only, and 3 cases where GPS is used together with QZSS with 3 different values of phase shift (0 ns, 20 ns and 50 ns). Data is relative to a simulation started at UTC 23:15, 31st of December 2004, and ending at UTC 08:15, 1st of January 2005. Note the scale for the 50 ns case is considerably larger.

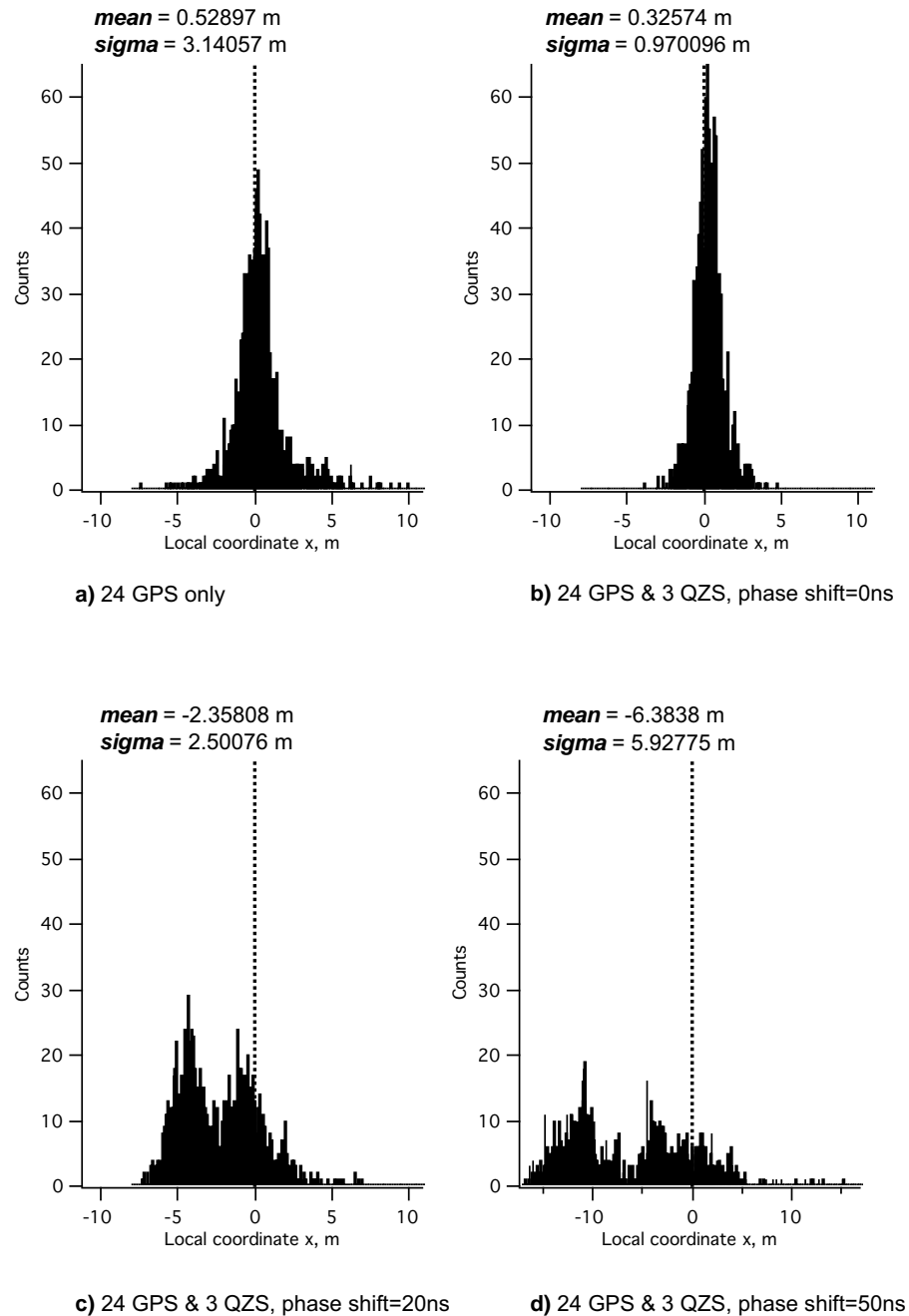


Figure 6.3: Position calculation results of the RESSOX/RTKS Software Simulator represented by histograms. Four scenarios are considered: GPS-only and 3 cases where GPS is used together with QZSS with 3 different values of phase shift (0 ns, 20 ns and 50 ns). Data is relative to a simulation started at UTC 23:15, 31st of December 2004, and ending at UTC 08:15, 1st of January 2005.

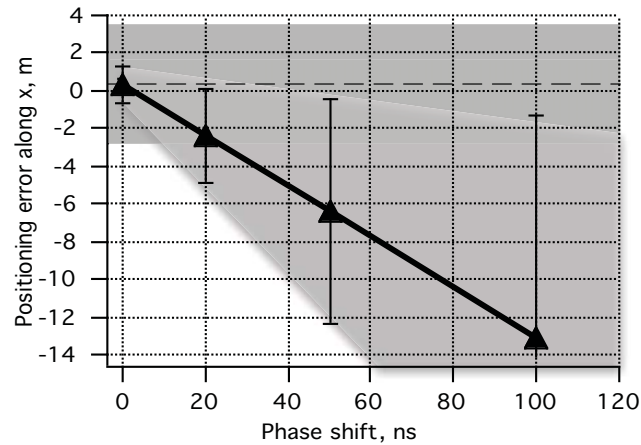


Figure 6.4: Representation of the mean x position (Earth-fixed coordinate system) and its standard deviation for four different level of phase shift (0 ns, 20 ns, 50 ns and 100 ns) over a 9 hour period. The 6.24 m wide dark region centered at 0.52 m represents the GPS-only simulation.

One more case, with the phase shift set to 100 ns, was simulated. The mean value and the standard deviation of all five cases are presented in Fig. 6.4. The 6.24 m wide dark region centered at 0.52 m represents the GPS-only case. The software simulator provides positioning information every 30 seconds because the RINEX observation file used to simulate the GPS has a time interval of 30 seconds. Therefore, for positioning results to be meaningful a long simulation period is required. The results given in Fig. 6.4 are for a nine hour period. For a better understanding of the response observed over a shorter time period it is necessary to run simulations over shorter times using a higher sample rate. To achieve this, the RESSOX/RTKS Hardware Simulator was used. It is worth mentioning that at the time of this study, the RESSOX/RTKS Software Simulator was not able to provide a one positioning solution every second. However the RESSOX/RTKS Software Simulator described in Appendix B, being the latest version, can do this.

### 6.3.1 RESSOX/RTKS Hardware Simulator

The RESSOX Hardware Simulator described in Appendix B was modified so that QZS clocks could be freely de-synchronized. Fig. 6.5 shows a schematic of the experimental

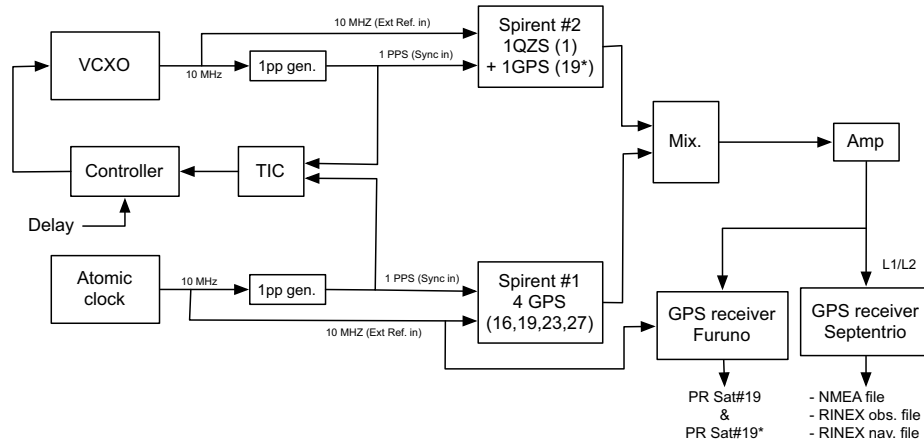


Figure 6.5: Schematic of the Hardware Simulator employed to simulate four GPS satellites and one QZS. The two Spirent GSS4730 devices are independently driven by two different time references (a high-stability VCXO and a hydrogen maser).

setup for this study. Following the same principles of the RESSOX Software Simulator, two Spirent GSS4730 simulators simulate the GPS and the QZSS independently. Each Spirent device is connected to an independent time reference. A GPS receiver (Septentrio PolarRx 2) is employed to compute the navigation solutions. The simulator not only provides more realistic results (real clocks and real GPS receivers are used) but can also provide one positioning solution per second.

The two time references used to steer the two GSS4730 simulators were the hydrogen maser (Anritsu RH401A) for the GPS Spirent, and a high-stability VCXO (Oscilloquartz 8607) for the QZSS Spirent. A PLL keeps them phase-locked. A phase shift module can be set in the VCXO controller. Further details about this simulator can be found in [117].

For the purposes here, only one scenario was considered. Because the Spirent GSS4730 has only four channels, a simple scenario of four GPS satellites and one QZS (the highest in the sky) was simulated. In Fig. 6.6, the sky-view of the chosen scenario at UTC 03:00, 1st of January 2005 is illustrated; user location was Okinawa, Japan (lat:26.1946 deg. long:127.67763 deg). The phase shift between the VCXO and the hydrogen maser was set to 0 ns for the first 8 minutes (case a). It was then set to 20 ns (case b) for 11 minutes. Finally, it was set to 50 ns (case c) for 10

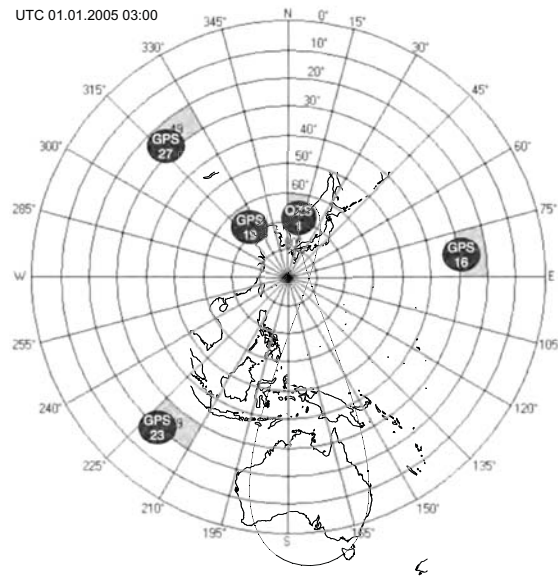


Figure 6.6: Sky-view at the beginning of the 30 minute simulation of the combined GPS and QZSS. Four GPS satellites are combined with one QZSS satellite (QZSS-1). Time : UTC 03:00, 1st of January, 2005. User location, Okinawa, Japan (lat:26.1946 deg, long:127.67763 deg).

minutes. The complete simulation time was about 30 minutes and was completed without interruption. In Fig. 6.7 the positioning results of three consecutive times are presented; UTC 03:05 (case a), UTC 03:16 (case b) and UTC 03:26 (case c). Clearly, from Fig. 6.7, the 20 ns phase shift results in a positioning error of approximately 1 m. A phase shift of 50 ns increases positioning error to approximately 7 m, similar to the average error of the 50 ns case in the Software Simulator results (Fig. 6.3d). The phase shift was changed from 0 to 20 ns and finally to 50 ns, all the while keeping the two Spirent GSS4730 and the Septentrio GPS receiver running. Therefore, these results represent a close to realistic scenario. If the simulation were conducted over a longer period of time, the positioning accuracy would have been influenced by the configuration of the visible satellites and would have changed significantly. The final result would have been similar to Fig. 6.2d.

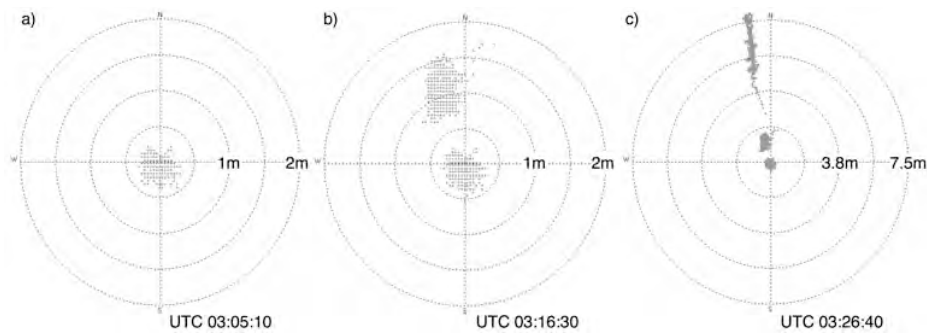


Figure 6.7: Estimated position data obtained during the three periods of the simulation of the combined GPS&QZSS when the phase shift is 0 ns (case a), 20 ns (case b) and 50 ns (case c). Results were obtained using the RESSOX Hardware Simulator. The simulation length was about 30 minutes. Note the larger scale for the 50 ns case.

### Two Spirents GSS4730 Used Simultaneously

The Spirent GSS4730 is a stand-alone 4 channel GPS L1/L2 simulator. This hardware simulator setup employed two of them simultaneously. The first GSS4730 is locked to a hydrogen maser and generated the L1 and L2 signals of the four GPS satellites. The other GSS4730 is locked to a VCXO and generated the L1 and L2 signals for the three QZSSs (Fig. 6.5). The main objective was to accurately steer the VCXO and recreate scenarios where the effect of phase shifts on positioning accuracy could be observed. Using two Spirent GSS4730 simulators together was not a trivial task and several problems arose. Even when the two time references were kept perfectly locked, de-synchronizations in the Spirent internal time reference occurred and no immediate solution could be found. To avoid the problem, a second GPS receiver and a dummy satellite were used (Fig. 6.5). At the beginning of the 30 minute experiment the same satellite (in our case GPS-19) was simulated in both Spirents. The second GPS receiver (Furuno) was used to estimate the PR of GPS-19 from both Spirents. Quite often the PR of the two GPS-19s were not the same, therefore it was necessary to modify the phase shift in the VCXO controller in order to make the PR of the two GPS-19s equal for both Spirents. After this tuning the two Spirents clocks could be considered "synchronized".

## 6.4 Satellite Communication Interruption

As noted a number of times, the positioning performance of the QZSS augmentation system is directly influenced by the quality of the synchronization scheme, whether it is the RESSOX or the RTKS. Fig. 6.4 presents the results of a simplified case where the positioning performance heavily degrades due to a QZS clock with constant de-synchronization. Such a constant phase shift would represent an incorrect synchronization due to a basic malfunction in the RESSOX. Refer to [117] for more details. As noted in that study, the synchronization accuracy of the RESSOX directly influences the performance of the whole QZSS augmentation system. A given anomaly in the synchronization will immediately compromise the positioning performances of the combined system QZSS and GPS. Moreover, there are unavoidable events that could stress the synchronization network. For instance, every time the QZS crosses the equatorial region, communications with the ground station must be shut down for approximately 20 minutes to avoid interference with geostationary communication satellites. During these periods the RESSOX cannot be utilized, and satellite clocks will have to operate in free-run mode.

The following sections present an analysis of the positioning performance when anomalies in the remote synchronization scheme occur. A software simulator of the satellite segment, ground segment and synchronization/correction communication channel is employed to study the behavior of the GPS plus QZSS positioning system during those periods when the RESSOX is not able to provide the necessary synchronization correction.

### 6.4.1 QZSS Satellite On-board VCXO Model

The software-implemented QZSS orbit generator and a GPS positioning analysis tool have been integrated into a single simulator, the RESSOX/RTKS software simulator used for the study described in Section 6.2. The development of this tool has been taken further and a software-implemented VCXO model based on a two-state error model has been integrated within it. Fig. 6.8 shows the basic schematic of the simulator and the VCXO model.

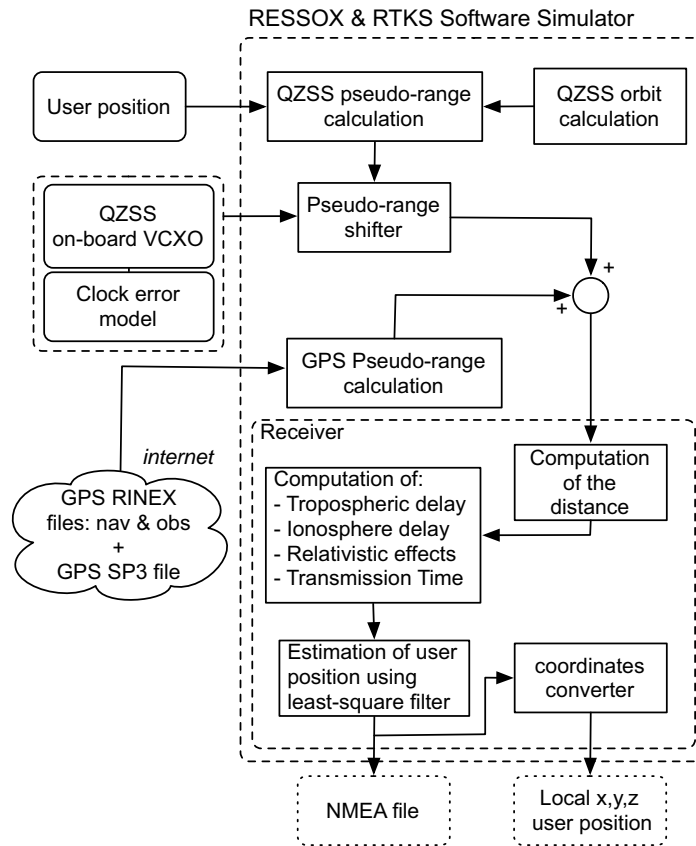


Figure 6.8: Schematic of the RESSOX/RTKS Software Simulator employed for the evaluation of the positioning performance of GPS plus QZSS when QZSS clocks are controlled by two-state model VCXOs.

The block *QZSS on-board VCXO* in Fig. 6.8 represents the VCXO stability in terms of pseudorange changes of a given QZS. Such a block is directly connected to the noise model of the on-board VCXO.

Fig. 6.9 shows how the block representation of the two-state error model has been implemented in ANSI C. The two-state noise model includes the following noise models:

- Frequency Random Walk
- Frequency white noise
- Frequency drift/aging

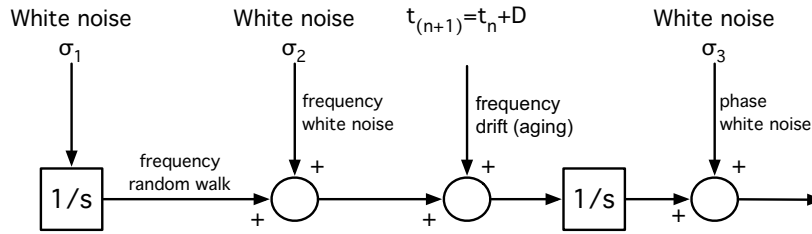


Figure 6.9: RESSOX/RTKS Software Simulator modified to accommodate the two-state error model used to simulate the on-board QZS clock behavior.

Experiment parameter	Value
Simulation start time	01.01.2005 00:00:00
Simulation end time	01.01.2005 04:10:00
User location	Tsukuba, Japan
User Latitude, deg	26.194
User Longitude, deg	127.677
User Height, m	37.67
Satellite select mode	all satellites
Vertical mask angle, deg	40

Table 6.2: Simulation conditions for the free-run experiment.

- Phase white noise

All noise models have been generated according to the real behavior of the VCXO available in the AIST laboratories (for more details refer to [110]).

Fig. 6.10 shows the Allan deviation of the simulated VCXO. The dark region represents the Allan deviation of a typical space-borne VCXO available on the market. The other dark region is the Allan deviation of a typical space-borne Rb clock, normally employed in GPS satellites. It is noticeable how the Rb clock shows a better long-term stability, which is the reason it was chosen as on-board time reference for GPS.

In contrast, the VCXO shows a strong frequency drift (aging) that affects its long-term stability.

## 6.5 Positioning Performance Analysis

Analyzing how bad positioning gets when one QZS on-board clock (simplified case) is left to free-run for a certain interval of time is an attempt to understand what would

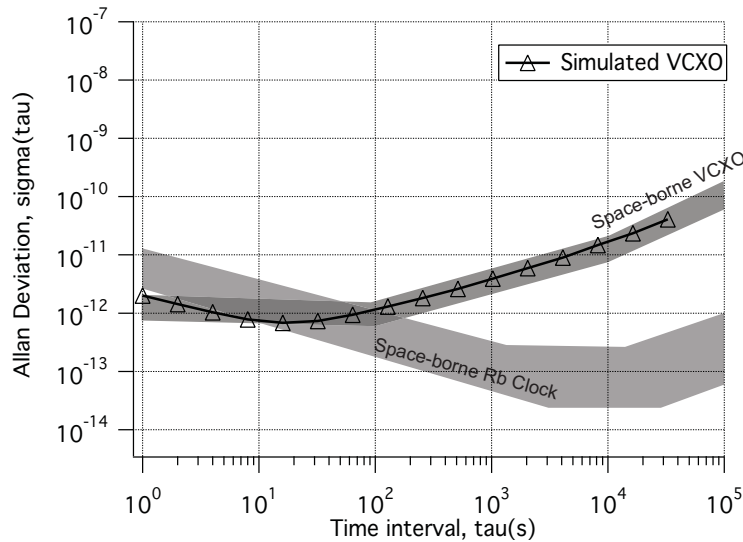


Figure 6.10: Allan deviation of the simulated VCXO. The two dark regions represent the Allan deviation of a typical space-borne Rb clock and the Allan deviation of a space-borne VCXO.

happen during the unavoidable equatorial region interruption. Results could be also used to understand how stable the on-board VCXO has to be if the RESSOX scheme is adopted.

The conditions under which these experiments were conducted are given in Table 6.5. The high mask angle (40 deg) chosen for this experiment represents the conditions when the Japanese QZSS is meant to provide the greatest positioning improvement.

### 6.5.1 Experiment One: Long-term Study

For this experiment the RESSOX was employed to keep all three QZS clocks synchronized for a certain interval of time. Fig. 6.11 shows the positioning performance of GPS+QZSS when no interruption in the RESSOX occurs. This represents the "ideal" case, and it is considered here as the reference case.

A second scenario was simulated. This time, after a period of 20 minutes, the RESSOX responsible for keeping the QZS near the equatorial belt (QZS-3) synchronized was interrupted. The VCXO clock on board QZS-3 was then left to free-run for

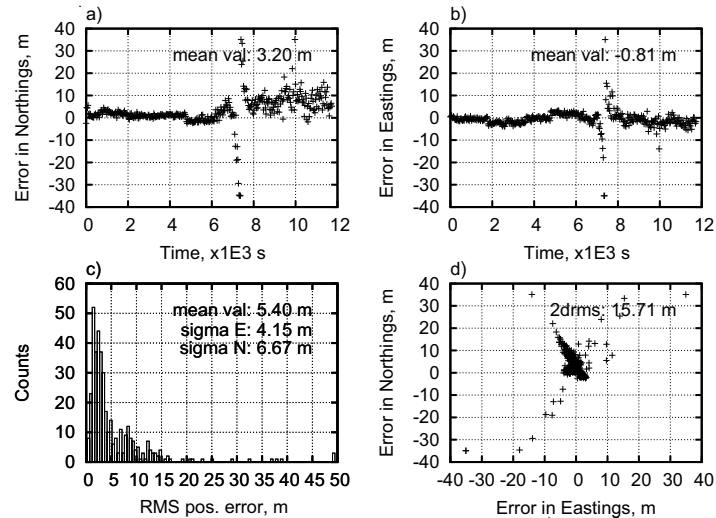


Figure 6.11: Positioning performance of GPS&QZSS when an ideal RESSOX is employed; no synchronization interruptions. a) The error in north direction over time, b) the error in east direction over time, c) the distribution of the RMS positioning error, and d) the scattering plot.

a period of about three and a half hours. Fig. 6.12 shows the positioning performance of GPS&QZSS during the free running period.

Comparing Fig. 6.11 and Fig. 6.12 the effect of having one satellite clock out of four drifting for about three and a half hours is clear. Because of the high mask angle, typical of an urban canyon, after about 7000 seconds a poor GDOP condition creates bad positioning. Such a case cannot be avoided unless more satellites are considered. It is in fact typical of the real-life scenario QZSS is designed to prevent happening.

### 6.5.2 Experiment Two: Short-term Study

For this experiment 26 GPS satellites were combined with three QZSSs. The RESSOX was employed to keep the QZS clocks synchronized for a certain period of time. Fig. 6.13 a) shows the configuration of the satellites, the sky-view, at the beginning of the experiment, and b) shows the sky-view at the end of the experiment.

Two sets of experiments were carried out. For the first experiment the RESSOX was employed to keep all QZS clocks synchronized.

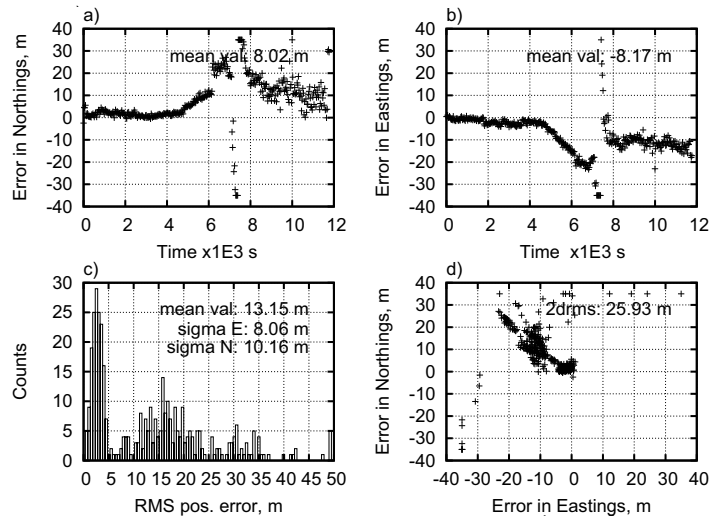


Figure 6.12: Positioning performance of GPS&QZSS when RESSOX is employed and the satellite QZS-3 clock, Fig. 6.13, is left in free running mode. a) The error in north direction over time, b) the error in east direction over time, c) the distribution of the RMS positioning error and d) the scattering plot.

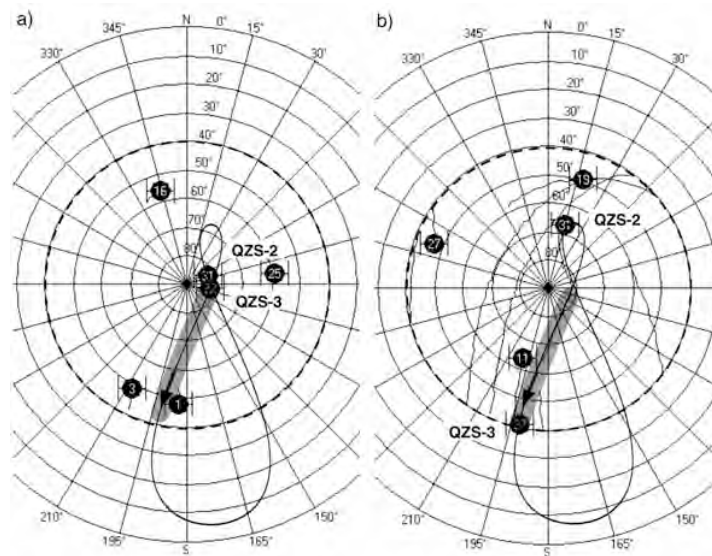


Figure 6.13: Sky-view of the GPS plus QZSS scenario. a) Sky-view starting configuration, b) sky-view end configuration. GPS satellites and QZSs are visible above a 40 deg mask angle. The dark area represents the period (approximately 4h) when the QZS-3 on-board VCXO is left in free-run mode.

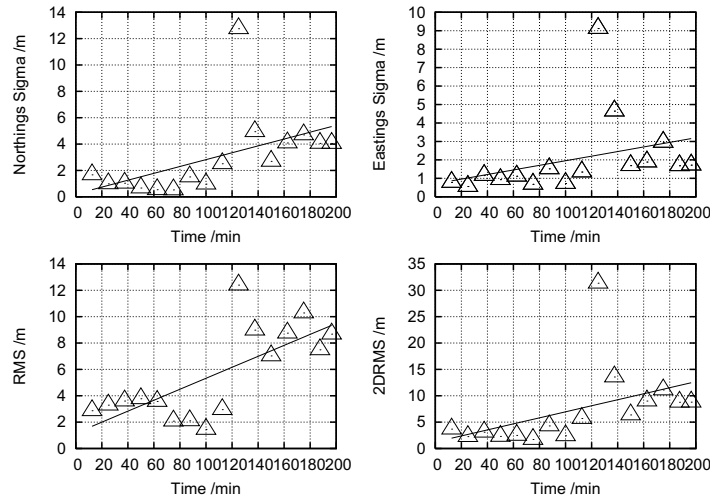


Figure 6.14: Positioning performance of the GPS&QZSS when an ideal RESSOX is employed; no synchronization interruptions. From top left to bottom right: the northings error sigma over time, the eastings error sigma over time, the RMS positioning error sigma over time and the 2DRMS sigma over time. Values of sigma are calculated using the last 10 minutes worth of data at each time.

Fig. 6.14 shows the evolution of the northings error sigma, the eastings error sigma, the RMS positioning error sigma and the 2DRMS sigma over the whole period of about four hours. The sigma values were calculated using the previous ten minutes worth of data. For the second experiment the clock on satellite QZS-3 (refer to Fig. 6.13) was left to free-run after the first 10 minutes. As before, the northings error sigma, the eastings error sigma, the RMS positioning error sigma and the 2DRMS sigma were computed every ten minutes for the whole simulation period of about four hours. Fig. 6.15 shows the results over four hours.

## 6.6 Results and Conclusions

A positioning performance analysis of the RESSOX/RTKS schemes has been presented. By means of a dedicated software simulator, the effect of the combination of GPS with QZSS/RESSOX was analyzed over a nine hour period. Fig. 6.2 and Fig. 6.3 show how the positioning accuracy can be improved when GPS is integrated

with QZSS, and how the accuracy degrades when a phase shift is introduced in the RESSOX synchronization chain. The effect of a 20 ns and 50 ns phase shift on the position accuracy proves that RESSOX could be a worthwhile alternative to the classic on-board atomic clock scheme for the QZSS, as long as the overall synchronization accuracy is kept below 10 ns (a basic requirement of the RESSOX project [114]). Fig. 6.4 shows how the positioning accuracy could decrease when the drift of QZS clocks becomes larger ( $\sigma=2.5$  m for phase shift=20 ns). For a simplified case (four GPS satellites and one QZS), a realistic analysis is carried out by means of a dedicated hardware simulator for the RESSOX. In Fig. 6.7 the change in position accuracy for a 20 ns and a 50 ns phase shift is presented. Here, instead of looking at a statistical analysis of positioning data over a long period, it is clear that a short 20 ns phase-shift jump causes a positioning error of approximately 1 m. Furthermore, if the phase shift is increased to 50 ns the positioning error increases to approximately seven meters, in less than ten minutes. Over a longer period of time the positions of the visible GPS satellites and QZSs obviously change. This causes significant positioning accuracy changes that are difficult to predict. Such changes have been analyzed over a long time (nine hours) with the RESSOX Software Simulator and over a short time (30 minutes) by means of the RESSOX Hardware Simulator. The two methods together show positioning results obtained when QZSS is employed with a RESSOX scheme under different synchronization scenarios. In the second part of this Chapter, a free-run positioning performance analysis of RESSOX/RTKS has been presented. A new ANSI-C clock model, Fig. 6.9, for the on-board VCXO has been developed and integrated into the RESSOX simulator. As shown in Fig. 6.10, the simulated VCXO Allan deviation plot totally overlaps with the Allan deviation plot of the VCXO in the AIST laboratories.

The effect of the combination of GPS with QZSS/RESSOX was analyzed over a four hour period. Fig. 6.11 and Fig. 6.12 show how positioning would degrade when one of the three QZS clocks starts drifting. Experiments have been carried out with a very high mask angle of about 40 degrees (four or five satellites in view). This was done in order to simulate an urban canyon scenario, which is where the Japanese

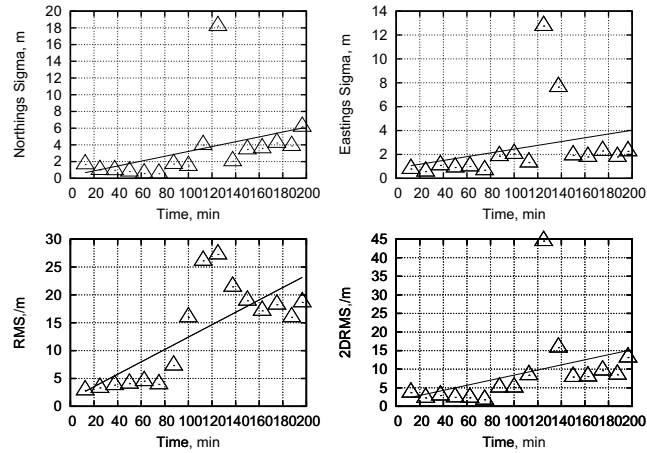


Figure 6.15: Positioning performance of the GPS&QZSS when RESSOX is employed and the satellite QZS-3 clock is left in free-run mode. From top left to bottom right: the northings error sigma over time, the eastings error sigma over time, the RMS positioning error sigma over time and the 2DRMS sigma over time. Values of sigma are calculated using the last 10 minutes worth of data at each time.

QZSS is meant to provide the greatest positioning improvement. Because of that choice, positioning accuracy gets quite bad in periods of high GDOP (Fig. 6.11, after 7000 s). The eastings error and the northings error clearly show the effect of clock drift, Fig. 6.12. Over a period of four hours, the 2DRMS goes up to about 26 m, which is about 10 meters bigger than the reference case where the 2RMS is about 15.7 m, Fig. 6.11.

For a time dependency analysis of the 2DRMS and other parameters, a short-term experiment was carried out. Fig. 6.14 and Fig. 6.15 show what happens to the positioning accuracy (sigma) at ten minute intervals. The bad positioning condition after 110 minutes is due to a bad GDOP value. Neglecting that, it is noticeable that a trend in the RMS positioning error, and for the 2RMS, is directly related to the clock drift of the satellite QZS-3.

Regarding bad satellite pseudorange detection, it is worth remembering that because of the high mask angle, the number of visible satellites is generally about four or five and therefore RAIM techniques would not be suitable for detecting the faulty satellite (QZS-3).

The research contribution in this Chapter can be summarized as follows:

- Study of the QZSS positioning quality when the RESSOX/RTKS is employed.
- Study of the positioning performance improvement of the combined QZSS plus GPS.
- Study of the timing requirement for RESSOX/RTKS and the effect of synchronization problems on the global positioning quality.
- Study of the effects of employing the RESSOX/RTKS for QZSS during faulty synchronization scenarios and satellite communication interruptions.
- Improvement of the RESSOX/RTKS software and hardware simulators.



## Chapter 7

# Regional Synchronized GNSS

In this Chapter a new concept for a satellite-based navigation system which does not require on-board atomic references is presented. This concept evolves naturally from the ideas presented in earlier Chapters and shows how some of the QZSS concepts can be incorporated into other applications. This novel concept consists of a constellation of compact low-Earth orbit positioning satellites that are equipped with on-board steerable clocks, that is voltage controlled crystal oscillators. An appropriate ground-satellite synchronization network is responsible for keeping clocks on board the visible satellites synchronized with a master atomic reference located on the ground. Regional/local clock synchronization, low-weight satellites and low manufacturing cost are some of the unique aspects of this system. Key issues such as number and spatial location of the required synchronization stations, clock de-synchronization issues and positioning accuracy are discussed. A Software Simulator specifically developed for studying its feasibility is under development together with a plan to develop a micro-satellite payload to demonstrate the feasibility of such system.

### 7.1 Introduction

The concept behind the synchronization schematic presented in Chapter 3 and Chapter 4 could be extended to a worldwide positioning system. The system will rely on a ground-satellite synchronization network which keeps on-board steerable satellite

clocks aligned with a master clocks located on the ground.

## 7.2 Regional Synchronized GNSS

### 7.2.1 Orbit Design and LEO Satellite Visibility

A satellite system which does not require atomic clocks could be implemented with compact LEO satellites, as proposed in 2006 by Der-Ming Ma [33]. The coverage of the system will depend on the number of satellites and on the design of the orbit.

When a user wants a position solution, their receiver will attempt to track signals from all satellites in view at that location. Thus, satellites visible to the user will need a coherent on-board time. A network of ground stations will guarantee the correct synchronization of all satellites visible in the area of interest. To do this, ground stations must be properly distributed over the territory.

To investigate the number of ground stations needed, and their locations, consider the Australian territory. The Australian continent is, roughly, a rectangle 4000 Km wide by 3000 km high centered at 26.19 deg South and 134.56 deg East. Assume what is required is a guaranteed positioning service for the whole Australian continent. One configuration is to assume four ground stations, each located at the corner of this rectangle. Any user near one ground station will roughly see as many satellites as the ground station, therefore clock synchronization of satellites over the ground station does not constitute a problem. However, moving away from this ground station, satellite visibility could be an issue. With the simple geometry considered here, the most critical point is the synchronization of satellites located above the center of the rectangle. Fig. 7.1 shows a simplified 2-dimensional representation of the ground station, user and the satellite. The approximate formula that gives the length of the path between the satellite and the ground station is:

$$l(t) = \sqrt{(R_{GS} + h)^2 + R_{GS}^2 - 2R_{GS}(R_{GS} + h)\cos\omega t} \quad (7.1)$$

When the user is between two ground stations, the satellites at the zenith, for the user, are the most difficult to see for the ground station. In that specific case:

$$\beta = \pi/2, \quad \tan(\alpha) = \frac{l'}{d} \quad (7.2)$$

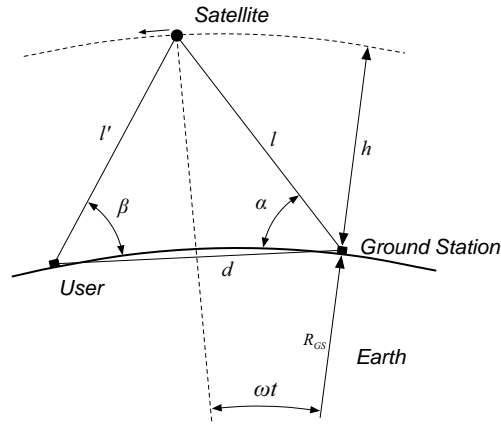


Figure 7.1: Simplified bi-dimensional representation of synchronization ground station, user and satellite for the proposed system.

Considering that the typical orbit of a LEO satellite is about 800 km altitude, and assuming that ground stations are approximately 4000 km apart, the visibility of satellites which are at the zenith of the user in between two ground stations is guaranteed by:

$$\alpha = \arctan\left(\frac{h}{d}\right) = 21 \text{ deg} \quad (7.3)$$

This means that each ground station would be geometrically able to synchronize all satellites with ground tracks located within a 2000 km radius and elevation angles greater than 21 deg. Furthermore, assuming a cut off angle of 15 deg, ground station synchronization capability is guaranteed even further, across a larger area.

For a territory as vast as Australia (4000 Km by 3000 km), several ground stations will be needed. Assuming that each ground station can guarantee the synchronization of all satellites visible within a 2000 Km radius and that is possible for an elevation angle greater than 21 deg. and that there was enough overlapping of adjacent coverage areas, it would be reasonable to say that six ground stations located 1500 km apart and evenly placed over the Australian territory could guarantee the minimum synchronization requirement for all visible satellites over Australia (Fig. 7.2). On the other hand, if only one station is employed and located in the center of Australia (for example, at Alice Springs), all satellites right over the Australian territory will indeed be visible to it. However, all satellites not directly over the Australian territory but

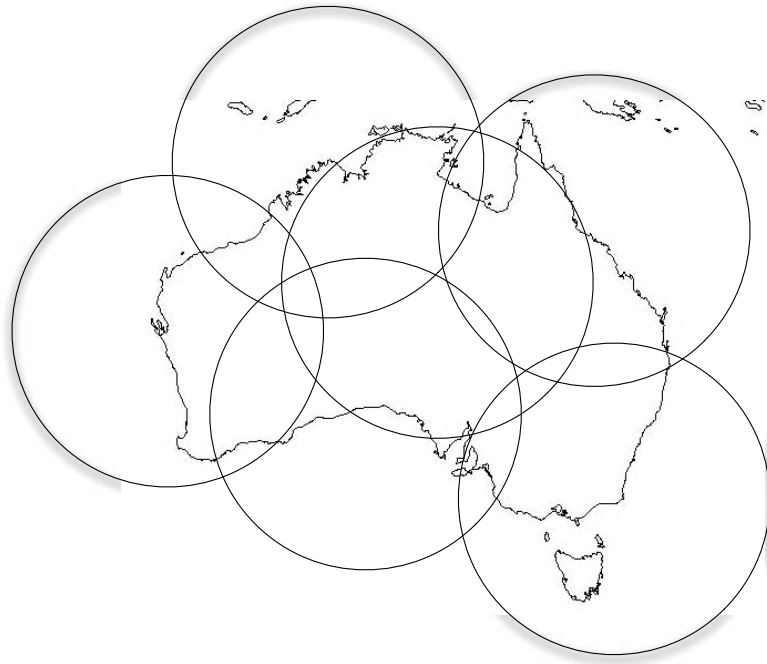


Figure 7.2: Australian territory and six ground stations.

visible to users located along the Australian coast, will not be usable. This would give an average Australian user the ability of utilizing, at worst, half the number of satellites visible to their receiver.

### 7.2.2 LEO Satellite Velocity and Doppler Shift

Due to the lower altitude, LEO GNSS satellites orbit the Earth at a velocity much higher than GPS satellites. Therefore, the period of time in which a given LEO GNSS satellite remains visible to the ground station or to the user is quite limited. Considering that a typical LEO satellite orbits the Earth in about 90 minutes, satellite ground station contact periods of the order of ten min are to be expected. During this short time, satellite clock and ground station clock synchronization will have to happen.

Unlike for MEO systems like QZSS or GPS, satellite ground station contact periods of ten hours are expected. For a LEO GNSS such a period is greatly reduced and

therefore initial handshake process will have to be established in a period of time of the order of 30 s. This will represent a challenge.

Because of the high LEO GNSS satellite velocity which is, generally speaking, of the order of 27,000 km/h (8 km/s), about three times higher than QZSS, the Doppler shift that communication and synchronization signals would experience will impose a more stringent timing requirement for the TTA module in the RESSOX system (refer to Section 3.2.2).

Regarding the satellite clock synchronization aspect of the atomic clock-less LEO GNSS, the previous experience with the RESSOX/RTKS for QZSS will certainly help. However the different orbit design of the LEO GNSS will require design reconsideration of some fundamental RESSOX subsystems such as the TTA, UDS and TX/RX modems.

### 7.2.3 Advantages of the Proposed System

The concept of a GNSS with no on-board atomic clocks would offer several advantages over current designs in terms of satellite cost, life expectancy and satellite power consumption. This concept is applicable to low Earth orbit, micro satellite-based positioning systems, where satellite weight is clearly a critical issue. The proposed satellite system would be synchronized by an Australian ground segment, so the system would initially work only in Australia. However, as the satellite system orbits about the Earth, Australia will be able to provide such functionality to other countries that by themselves would not have the capability of building a satellite-based positioning system. With such a system Australia could be independent of the US military or European civilian GNSS operators. Aside from the economic benefits mentioned above, a LEO satellite-based positioning system which does not require a high quality on-board atomic frequency standard is in itself a very interesting system, both from the research and the engineering points of view. Such a system may lead to research achievements that could have applicability in fields such as clock design, network synchronization and time transfer.

## 7.3 Experimental Synchronization Payload

### 7.3.1 Host Satellite, ALMASat-I

The University of Bologna, Italy, has been active in the research field of microsatellite design, manufacturing and operations in space since 2003. The first step of this activity at the microsatellite laboratory located at the II School of Engineering in Forlì was the design, assembly and integration of a fully automated amateur-radio ground station, at first working only at VHF and UHF bands. In 2005 the ground station was upgraded to S-band downlink capabilities, enabling the reception of spacecraft (S/C) signals at higher data-rates (up to 153600 bps). Since then, the ground station has been fully operational and routinely used for the downlink of amateur radio satellite telemetry information, Earth images, and store-and-forward packet communication. In early 2004, the same group of faculty, PhD, graduate and undergraduate student started the design of a low-cost, highly modular microsatellite platform. The S/C was later named ALMASat (ALma MAter Satellite). The first prototype of this microsatellite platform, ALMASat-I, is planned for launch in early 2008 and will qualify all S/C subsystems for the flight in space.

ALMASat-I is a three-axis stabilized cubic S/C, weighing about 12 kg, whose dimensions are 300X300X300 mm (see Fig. 7.3). Its structure is made of six stackable shop-machined Al trays, each containing a single subsystem. The lower tray (the one pointing toward the Earth) contains the S-band subsystem and the on-board power control electronics. The second tray carries the Attitude Determination and Control System while the third is devoted to the micro-propulsion. The upper two trays carry the on-board electronic systems (modem, telemetry and on-board computer, and the VHF-UHF receivers and transmitters, respectively). The fourth tray, ideally left unoccupied for possible payloads, is filled with the Li-Ion battery packs for the first mission, in order to avoid the S/C being unbalanced in terms of position of the centre of mass and moments of inertia. Digital information is exchanged throughout the S/C using a CAN (Controller Area Network) bus protocol, which easily allows the introduction of new systems and electronic boards without the need for changes to the overall architecture.

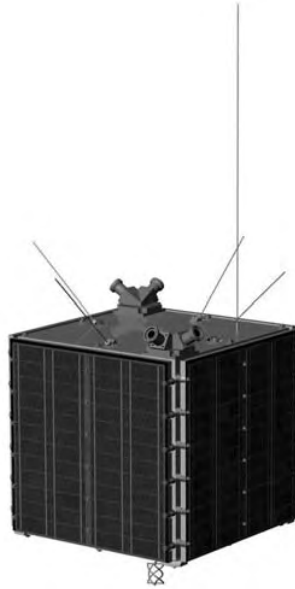


Figure 7.3: Drawing of the microsatellite ALMASat-I developed by the microsatellite laboratory, in the II School of Engineering, University of Bologna, Italy.

The modular architecture of the ALMASat bus easily allows its adaptation to payloads with different needs in terms of mass, size and necessary power. Hence, the idea is to consider it as the baseline bus for the on-board remote clock control experiment. Actually, once the GNSS payload characteristics are fully specified, it will be clear if the nominal size of a single tray will suffice to host the flight hardware of the navigation experiment. In case more space will be required, the S/C size can be increased in height by adding as many trays as needed or, alternatively, increasing the height of the single payload tray. As far as the on-board power is concerned, low-cost Si cells are being used for the ALMASat-I mission but more efficient and reliable triple-junction Ga-As space qualified cells can be used for the ALMASat mission carrying the navigation payload, if needed. The last issue to be considered for hosting the GNSS payload, strictly connected to its interaction with the ground infrastructure, is the amount of data to be exchanged during the ground station contact. At the moment, the combination of the ground station installed in Forlì and the flight hardware installed on-board the ALMASat-I mission allow a data rate, at S-band, of the order of 112

kbps. The development of an X-band communication system has already started; the goal being to develop a system capable of downlink data rates up to 1 Mbps from LEO.

### 7.3.2 Payload and Ground Station Synchronization Test

For a LEO satellite orbiting at a nominal altitude of 800 km, the maximum visibility time to a ground station is of the order of 15 minutes. This estimate assumes a zenith pass over the ground station and a zero-elevation cut-off angle. By assuming non-zero mask angle (say of the order of 5-10 deg, to avoid excessive contamination from ionospheric and tropospheric effects on signal propagation) and a non-zenith pass, the contact time to the ground station reduces drastically. A typical nominal contact time of no more than 10 minutes has to be expected. Thus, the design of the payload-to-ground station synchronization tests must take into account these constraints. In particular, a highly automated acquisition sequence for the payload signals transmitted to the ground must be implemented, as well as an automated reply from the ground station which will start transmitting its synchronization signals to the on-board clock. If more than a single ground station is available for the real on-orbit tests, hand-over procedures must also be investigated, implemented and tested. As a reference, one could make use of the procedures already successfully used for the hand-over of uplink signals to a distant deep-space S/C, being tracked for navigation purposes by two deep-space stations on Earth. In particular, when a ground station loses visibility of the S/C, it must cease transmitting its uplink carrier frequency, as the transmission will start from another ground station that is in view of the S/C. Similar procedures must be studied for the GNSS payload described above, in order to avoid a synchronization signal being simultaneously received by the satellite, as transmitted by two ground control stations.

## 7.4 Conclusions

In this Chapter an analysis of the main time synchronization issues for a regional satellite-base positioning system has been described. In the proposed system, LEO

---

satellites equipped with low-cost time references provide a positioning signal based on accurate time built on the ground. The synchronization scheme proposed for this system is a modified version of the one described in Chapter 3 and Chapter 4. The proposed LEO satellite positioning system would require a minimum of six control stations for a territory as large as Australia.

This Chapter presents the basis of a possible direction where the research presented in this thesis can be extended to. Therefore, it does not need to be “complete”.

The microsatellite ALMASat, under development at the University of Bologna, is possibly a good in-space testbed for a simplified version of the proposed synchronization scheme.



## Chapter 8

# Conclusions and Future Works

The results of the preceding Chapters are summarized here. The aim of this dissertation was to investigate a novel satellite timekeeping system (TKS) for the Japanese QZSS where no on-board atomic clocks are employed. This thesis describes two possible architectures to realize this.

### 8.1 The Context of the Results

The work associated with this thesis is part of a larger research activity carried out by the Space Technology Group of AIST, the University of New South Wales and several other Institutions and Industrial partners which have collaborated over the years for the realization of a novel TKS for QZSS.

This dissertation focuses on some research topics and on some system level engineering implementation issues rather than dealing with the whole QZSS time synchronization research project.

Because of the nature of a PhD thesis, the author omitted detailed explanations of the contributions not made by him. However, a substantial contribution was made by him in the design and development of indispensable tools, described in the Appendix A and Appendix B, without which experimentation could have not been possible. Great effort has also been invested in planning, designing and testing particular subsystems (e.g the TTA module, described in Section A.1.1) because they will eventually consti-

tute part of the QZSS ground station timing facility useful for in-space testing together with the first QZS; refer to Section 8.4 for more details.

## 8.2 Summary of the Results

The broad objective of this dissertation is to assess the feasibility of a low-cost TKS which would reduce manufacturing costs of QZSs and spacecraft launching costs; this is interesting from both the research and the engineering points of view.

Chapter 3 presents an optimal architecture for realizing the atomic clock-less concept for QZSS. An analysis of the delays that the proposed system has to account for was presented. The development of the necessary software tools (refer to Appendix A.1 for more details) for realizing the feed-forward control command has been developed alongside the main research activity. Design and test of the components for the Hardware Simulator have also been carried out in parallel with it. The last part of the Chapter describes a partial hardware/software implementation of the feed-forward and feedback RESSOX scheme. A novel VCXO control loop is combined with the RESSOX feedback command (refer to Section 3.3) and synchronization results were presented. Initial synchronization accuracy better than 10 ns was achieved. Furthermore, by means of the implementation of the RESSOX feed-forward and feedback scheme, synchronization accuracy better than 4 ns within 24 hours was achieved.

The synchronization scheme proposed in Chapter 3 is characterized by a high level of complexity. Its functioning depends heavily on the precise satellite position prediction algorithm and on precise delay prediction calculations. In Chapter 4 an alternative to RESSOX, named RTKS, was presented. Based on the TWSTFT system, under development by NICT (refer to Section 2.5), RTKS is a simpler and more reliable architecture. The overall RTKS functioning, its scheme and its subsystems are presented. A novel VCXO control algorithm that deals with the NICT TWSTFT apparatus was presented. The design of both open-loop controller and closed-loop controller were presented. Convergency performance as well as overall synchronization accuracy were presented by means of computer simulations. An absolute phase synchronization accuracy better than 1 ns was achieved. A phase step convergency

time of around 300 s for a 20 ns phase jump was achieved. The problem of VCXO frequency and phase jump was introduced and evaluated by means of in-space raw data available in literature. A double VCXO scheme able to detect and mitigate frequency and phase jumps was proposed. The proposed RTKS VCXO control algorithm was tested by means of a modified version of the RESSOX HS, An overall synchronization accuracy analysis (Allan deviation) was performed.

One of the critical issues regarding the RESSOX or RTKS architecture is the loss of synchronization during satellite communication interruptions. Such losses will inevitably translate into a degradation of positioning when QZSS is employed as an augmentation system to GPS. Chapter 5 presented a hardware-in-the-loop experimental setup which has been developed to study the effects on positioning when a real space-borne VCXO is employed in the atomic clock-less RESSOX/RTKS architecture. Particular focus was given to the effects of faulty synchronization on positioning, specifically when, because of unavoidable communication interruptions, the QZS clock has to function without ground station assistance. Furthermore, a method for solving the free-run VCXO problem was proposed. The relationship between QZSS plus GPS positioning accuracy and QZSS clock quality was discussed.

The study of the relationship between positioning quality and synchronization quality, presented in Chapter 6, defined the requirements for the whole synchronization method. It also assessed the impact of synchronization loss, technically the main drawback of this system. Studying the relationship between QZSS time quality and QZSS plus GPS positioning capabilities with the focus on time synchronization loss addresses some problems for the specification of the crystal clock to employ for the proposed scheme. This study represents an important contribution because it defines the timing requirements for the RESSOX architecture as well as the RTKS architecture. Along with the development of this study, a contribution has been made to the development of the Software Simulator described in Appendix B.

Aside from strictly technical contributions, the development of this study has been a tremendous opportunity for strengthening the international research relationship between the University of New South Wales and the Space Technology Group of AIST.

The contributions of this dissertation can therefore be summarized in the following five main points:

**RESSOX feasibility study.** An optimal synchronization architecture known as the RESSOX for realizing the atomic clock-less concept for QZSS was presented and its feasibility was studied. The overall RESSOX system design and subsystem definition was presented. An analysis of the ground station satellite communication delays was proposed. The design of the feed-forward and feedback block, the core of RESSOX, was presented. Through a simplified version of the RESSOX hardware, results of a synchronization experiment of the feed-forward and feedback architecture was presented.

**Remote timekeeping system, RTKS.** A novel synchronization scheme known as RTKS, an alternative to RESSOX, was presented. The structure of the TWSTFT scheme, the core of RTKS, was explained and the closed-loop and open-loop problem, related to the VCXO PLL for RTKS was evaluated and a design for the PLL controller was proposed. Computer simulations allowed for an assessment of the synchronization performance of the proposed filter to be made. The general problem of VCXO frequency and phase jump was discussed.

**QZSS clock, the free-run problem.** The problem of timing accuracy degradation, which results from a lack of ground communication, was addressed by presenting a VCXO control method which reduces the satellite on-board time error during communication outages. Hardware-in-the-loop simulations were used to prove the effectiveness of the proposed method.

**QZSS, positioning quality and timing.** The relationship between QZSS timing quality and QZSS plus GPS positioning quality was investigated. RESSOX and RTKS subsystems' timing requirements were derived. The influence of the QZSS clock accuracy on the overall positioning when QZSS is combined with GPS was investigated. Through computer simulations, the effect of satellite-ground station communication outages on QZSS plus GPS positioning was evaluated and discussed.

**Simulation tools development.** Along with the research activity that has led to the writing of this thesis, direct contributions in the development of the RESSOX/RTKS

Hardware Simulator as well as of the RESSOX/RTKS Software Simulator have been made. Details on the RESSOX/RTKS Software and Hardware simulators were presented in the appendices.

### 8.3 Regional Synchronized GNSS

As a natural extension to this work, the author has spent the last period of his PhD working on an extended version of the atomic clock-less architecture, which would enable a new concept for a satellite-based navigation system which does not require on-board atomic references. This novel concept consists of a constellation of compact low-Earth orbit positioning satellites that are equipped with on-board steerable clocks. An appropriate ground-satellite synchronization network is responsible for keeping in lock step clocks on-board the visible satellites with a master time reference located on the ground. The system is a regional satellite system with the capability of providing coverage over a region, as long as a synchronization ground station network is available and enabled to control the satellites.

A description of this concept can be found in [111]. This new concept of regionally enabled availability has been investigated. The microsatellite ALMASat, [111], under development in the University of Bologna, could represent an in-space testbed host for a simplified proof of concept.

### 8.4 Future Work

The research activity which has led to the writing of this dissertation is still ongoing. The incomplete RESSOX/RTKS Hardware Simulator is still under development.

The first QZS, named QZSS-1, scheduled to be launched in the first half of 2009, will go through a 2 year in-space test period. During the first half of the test period QZSS-1 will be used to host the necessary hardware to run tests on either the RESSOX or the RTKS synchronization architecture. Because of the simpler structure, and because it relies on the already existing TWSTFT apparatus, the RTKS architecture is likely to be tested instead of RESSOX.

Experiments where the VCXO is kept in phase lock for a long time in space will have to be run. They will give an indication of how problematic it is for QZSS to rely only on an VCXO. Overall time synchronization quality will also need to be tested.

The problem of frequency and phase jumps for the RESSOX/RTKS VCXO in space will have to be defined by collecting raw phase data by means of the QZSS on-board TKS. Experimental data will have to be compared to the problem definition described in Section 4.3.6. The proposed solution will have to be confirmed. Alternatively the behavior of RESSOX/RTKS to phase and frequency jumps will have to be determined by in-space experiments.

The consequence of absent synchronization commands during satellite interruptions will have to be tested, especially equatorial crossing and artificial interruption of time synchronization command scenarios. The algorithm presented in Section 5 will need to be tested on board QZSS-1.

Since the actual VCXO to be employed on QZSS-1 has not yet been selected, it will be necessary to run simulations using the simulator described in Appendix B.

Despite its limited capabilities, QZSS-1 will be able to confirm the synchronization/positioning quality results presented in Chapter 6. By computing positioning results using GPS and GPS plus QZSS-1 during good synchronization scenarios, and progressively degraded scenarios, the results from Chapter 6 will need to be further confirmed.

Regarding the regional synchronized GNSS project presented in Chapter 7 and in [111], the AlmaSat-I microsatellite developed by the University of Bologna is an opportunity for further investigation of this concept.

## Appendix A

# Appendix - RESSOX/RTKS

## Hardware Simulator

Along with the research activity described in this thesis, a great deal of effort has been spent on the study, design and implementation of a hardware and software prototype. The objective of both tools is to test, in as realistic as possible, the atomic clock-less architecture and its requirements.

These appendices present a description of the RESSOX/RTKS Hardware Simulator as well the RESSOX/RTKS Software Simulator. The last Section contains extensive results of the experiments for testing the free-run algorithm presented in Chapter 5.

The development of both experimental tools has been carried out mainly by the author, together with Dr. Iwata and some other collaborators. The actual implementation of the submodules of the Hardware Simulator was commissioned to private Japanese companies. The author has collaborated with Mr. Nakajima of Mitsubishi Space Software in the development of the Software Simulator.

### A.1 RESSOX/RTKS Hardware Simulator

Fig. A.1 shows the structure of the RESSOX simulator as described in Section 3.3. Most of the hardware components have been designed following the structure of Fig. 3.4. However, some special components and software are required to simulate

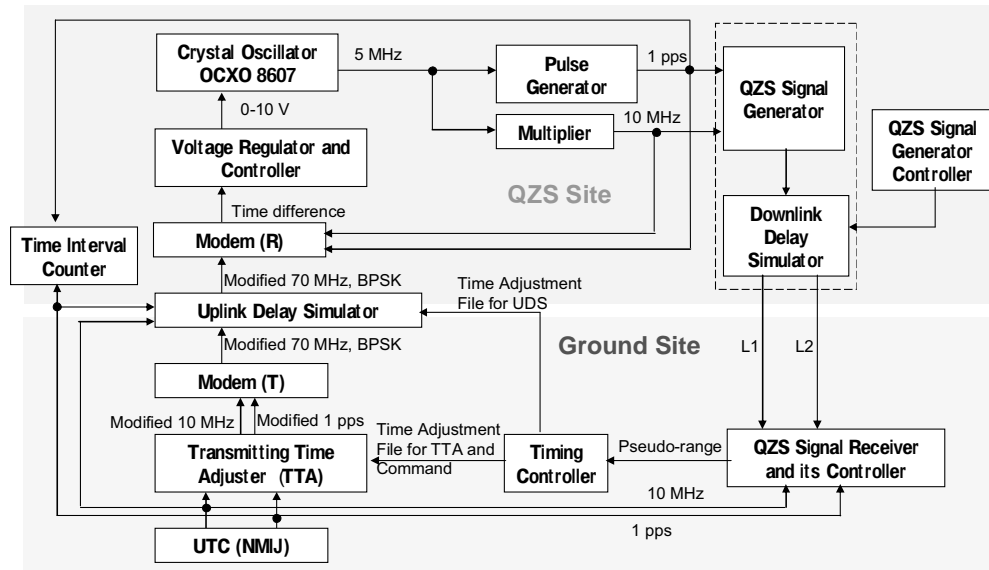


Figure A.1: RESSOX/RTKS Hardware Simulator.

the delay between the TMS and the QZS.

### A.1.1 Transmitting Timing Adjuster and Timing Controller

The TTA is an apparatus that generates advanced time to compensate for the delay between the TMS and the QZS. The commands for the TTA are generated by the timing controller connected to a PC through TCP/IP. The time adjustment files are prepared by calculated delay models, and the time adjustment commands are given by the PC as feedback information from the QZS receiver in real-time. The TTA delays or advances the input signal by  $0.1 \text{ s} \sim 0.2 \text{ s}$ . This will compensate for the signal delay due to the distance between the TMS and the QZS. The delay change rate varies from  $-1 \mu\text{s}/\text{s}$  to  $1 \mu\text{s}/\text{s}$ , which corresponds to a rate ranging from  $-300 \text{ m}/\text{s}$  to  $300 \text{ m}/\text{s}$ . To realize these specifications, a Direct Digital Synthesizer (DDS) is used.

Fig. A.2 shows the block diagram of the TTA and timing controller for the ground test bed. To operate the TTA, first, the Ku-band estimated time advance file that describes the advanced time at a broadcasting UTC at the TMS is prepared by orbit calculation and other delay simulations (this file is assumed to be generated from

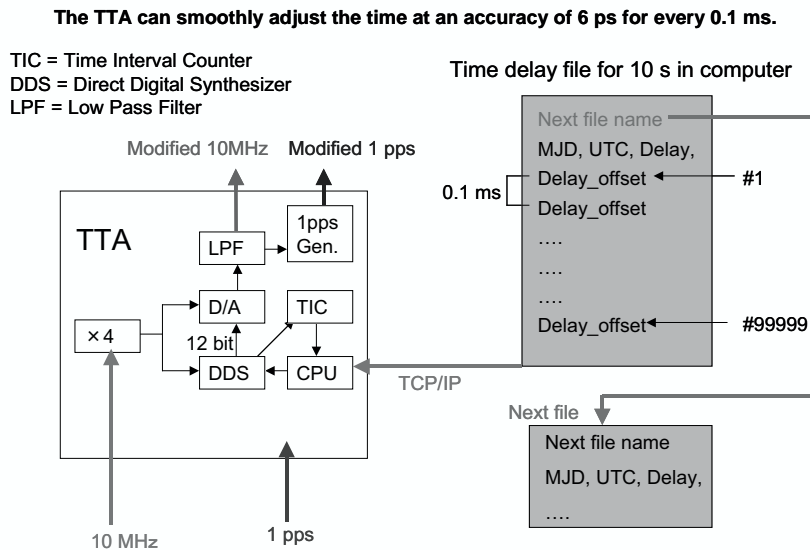


Figure A.2: Block diagram of the TTA.

the estimated orbit information in actual operations). Using the Ku-band estimated time advance file, time adjustment files for TTA are prepared with a utility program. Details of the structure of the adjustment file can be found in [58].

In the ground testbed, the TTA receives 10 MHz and 1 pulse per second (pps) from UTC(NMIJ), (NMIJ stands for National Metrology Institute of Japan, one of the institutes in AIST). UTC(NMIJ) is used as the time standard for the ground testbed instead of the QZSS Time. The time adjustment commands are also given as changes of the coefficients. The database of L1 and L2 delays was prepared beforehand through orbit and delay calculations and compared with the pseudorange measured by the QZS signal receiver. The differences between them are accumulated, and, using the least-mean-squares filter, the error to be compensated is calculated and output as the change of the coefficients to be adjusted.

### A.1.2 Modems (PN-Code Generator and Time Comparator)

The modem at the TMS is a PN-code generator and the modem on-board the satellite is a time comparator. The modem at the TMS is known as the transmitter modem

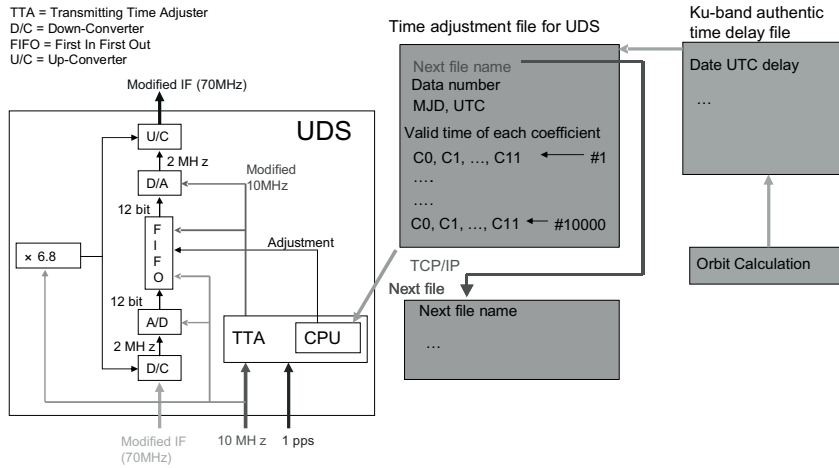


Figure A.3: Block diagram of the UDS.

(Modem (T)) and that on the satellite is known as the receiver modem (Modem (R)). The RESSOX control signal is modulated and demodulated using the PN code (M-sequences), and then transmitted via the 70 MHz carrier.

### A.1.3 Uplink Delay Simulator (UDS)

The UDS is a Hardware Simulator used in the ground testbed. Fig. A.3 shows the block diagram of the UDS. The UDS assigns offset values to the first-in/first-out (FIFO) memory according to the Ku-band authentic time delay files for the UDS that have the same format as those for the TTA. These files are assumed to be the authentic delay of the Ku-band signal. Then, the UDS adjusts the time information of the modified 10 MHz generated by the TTA. The UDS is based on DDS technology of the TTA and FIFO memory control techniques. It receives an intermediate frequency (IF) signal that includes time information (central frequency of 70 MHz, bandwidth of 2.5 MHz), down-converts the frequency to 2 MHz, downloads the waveform of time information into FIFO memory in real-time, and reads out the FIFO memory data using the modified 10 MHz generated by the TTA inside the UDS. The UDS up-converts the frequency to 70 MHz, and outputs the modified IF signal using the time adjustment files for the UDS.

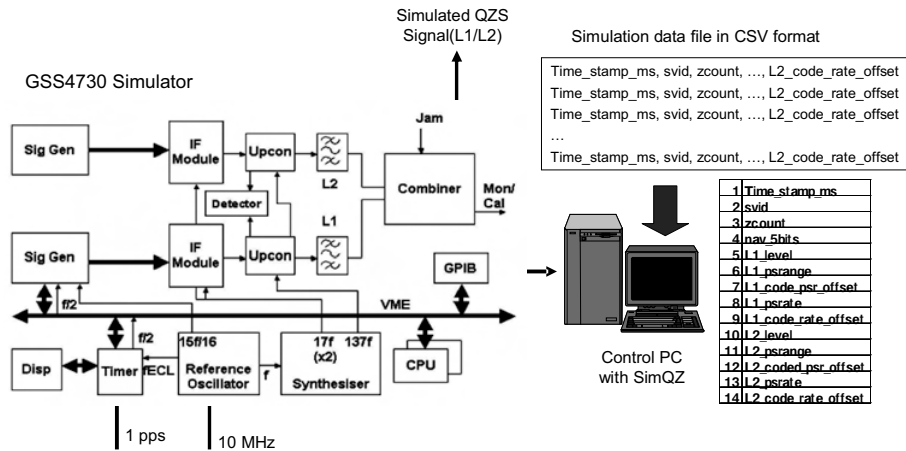


Figure A.4: Block diagram of the QZS signal generator.

#### A.1.4 QZS Signal Generator and Controller

In the ground testbed, the QZS signal generator is required to simulate the positioning signal coming from the QZS. Although QZSS will broadcast L1C/A, L1C, L2C, and L5 signals, and since there is no generator generating all signals at the the time of the investigations, a GPS signal generator (Spirent GSS4730) with four channels of L1C/A and L2P positioning signals was used. To simulate one QZS, only one channel of L1 C/A and L2P signals is used. Because commercially available software that controls the GSS4730 supports only simple orbit models and ionosphere delay, we have developed a new delay simulation method called SimQZ that uses the simulation data file specifically made for this simulator. The simulation data file includes the 14 data values described in Fig. A.4, with one time step record per line. The time step is 100 ms and the file is in the comma separated value (CSV) format. The simulation data files are read by SimQZ in real-time, and SimQZ controls the signal generator hardware (Spirent GSS4730) to output the simulated QZS signal.

#### A.1.5 QZS Signal Receiver and Controller

Because the QZS signal includes time information of the onboard crystal oscillator, the time information coming from the QZS is adopted as the pseudorange. To calculate

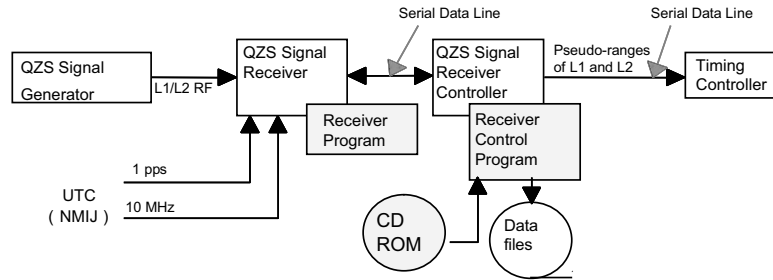


Figure A.5: Block diagram of the QZS signal receiver.

the pseudorange, a custom-made QZS signal receiver was used. The block diagram of the QZS signal receiver is shown in Fig. A.5. The QZS signal receiver calculates the pseudorange using UTC (NMIJ) and outputs it to the timing controller. The timing controller generates the time adjustment commands using the pseudorange.

#### A.1.6 VCXO

Two different crystal oscillators were used for the ground experiments. The first one was the BVA-type VCXO manufactured by Oscilloquartz S.A., and the other was an engineering model of the onboard VCXO (with the same specifications as the onboard VCXO) manufactured by C-MAC Micro Technology. The former was selected because it was one of the most stable crystal oscillators in the world at the time of the investigations and when the specifications of the on-board crystal oscillators were not determined. More details on both OCXOs can be found in Chapter 3.3. More discussion about the VCXO can also be found in Chapter 5.

#### A.1.7 Time Interval Counter (TIC)

To measure and evaluate the time difference between the VCXO 8607 or the PLL/MINI-OCXO and the ground atomic clock, the universal time interval counter (TIC) SR620 of Stanford Research Systems is used. One-PPS signals are input to the TIC directly for the evaluation of synchronization accuracy. The TIC is used to estimate the overall time accuracy of the clock. In Chapter 5 it is also used to test the validity of the algorithm that control the VCXO.

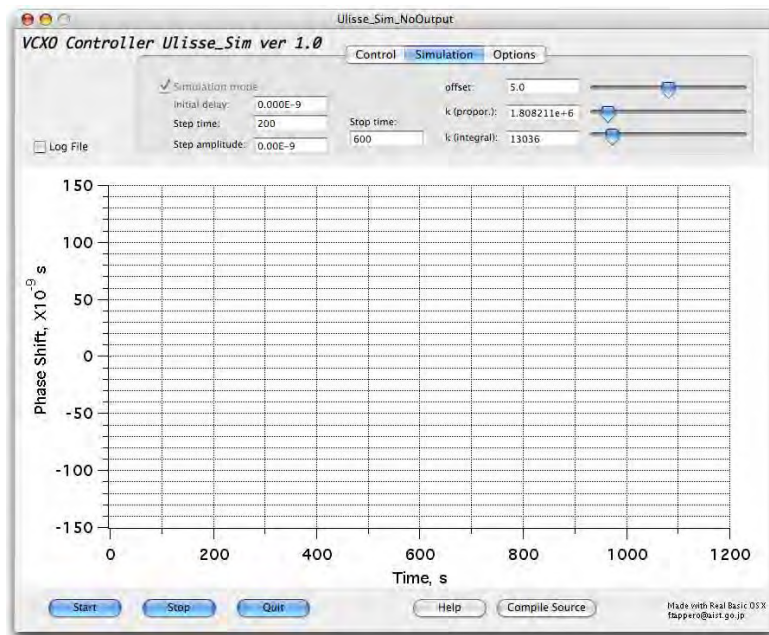


Figure A.6: VCXO Controller interface running on a standard PC.

### A.1.8 VCXO Controller Interface

In the RESSOX/RTKS Hardware Simulator, Fig. A.1, the actual control of the VCXO is by means of an ANSI-C routine (VCXO controller) running on a standard PC. The phase shift error provided by the SR620 TIC, or alternatively by the QZSS Modem Rx (refer to Section A.1.2), is fed to the routine through a GPIB connection. The output of the routine is then fed to a precise Voltage Generator through a RS-232 serial port connection. Fig. A.6 shows the interface that controls the GPIB input port and the RS-232 serial port. Note how the parameter of the VCXO Controller can be changed while the whole system is running. A real-time graphical representation of the VCXO phase error is also provided. The VCXO Controller running inside the interface can also be modified while the whole QZSS clock loop is running.

### A.1.9 Additional Note

Aside from the development of the RESSOX/RTKS Hardware Simulator, other hardware tools have been developed to test subsystems and algorithms such as those pre-

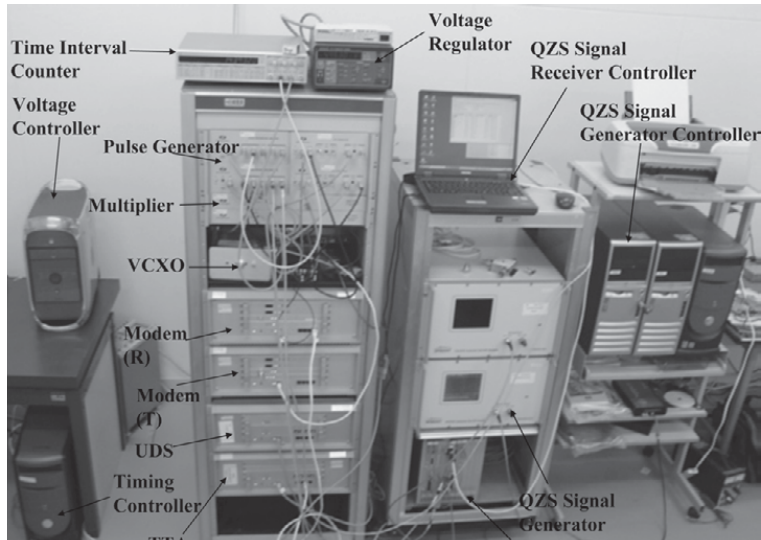


Figure A.7: RESSOX/RTKS Hardware Simulator.

sented in Chapter 4 and for the synchronization quality study presented in Chapter 6. Section 6.3.1 of Chapter 6, presents an overview of a standalone simulator used to study the positioning quality of the combined system GPS plus QZSS. Fig. A.7 shows the RESSOX/RTKS Hardware Simulator at the AIST labs.

#### A.1.10 Contribution from the Author

Within the development of the RESSOX/RTKS Hardware Simulator presented in this chapter, the author has contributed in part of the development and testing of the TTA module presented in Section A.1.1 and in the development of the module presented in Section A.1.8.

## Appendix B

# Appendix - RESSOX/RTKS Software Simulator

### B.1 RESSOX/RTKS Software Simulator

The remote timekeeping system Software Simulator, RTKSsim, is a software tool written in ANSI C specifically for investigating the concept of an atomic clock-less GNSS.

Its final implementation, version 1.0, is capable of simulating the two schemes so far proposed, the RESSOX scheme and the RTKS scheme.

RTKSsim, is compilable and usable under Microsoft Windows, Macintosh OS X and Linux operating systems. Development was primarily carried out under OS X 10.4 and compiled with gcc 4.0. Small incompatibility issues may arise when RTKSsim is compiled and/or used in the MS Windows environment.

#### B.1.1 RTKSsim Structure

The main objective of RTKSsim version 1.0 is to simulate the GPS satellite constellation together with the Japanese augmentation system QZSS. RTKSsim is capable of calculating satellite position, user receiver pseudorange data and user position. The phase shift of clocks on board each satellite, GPS and QZSS, is controllable and configurable inside the software.

The RTKSsim version 1.0 schematic is presented in Fig. B.1. In its early devel-

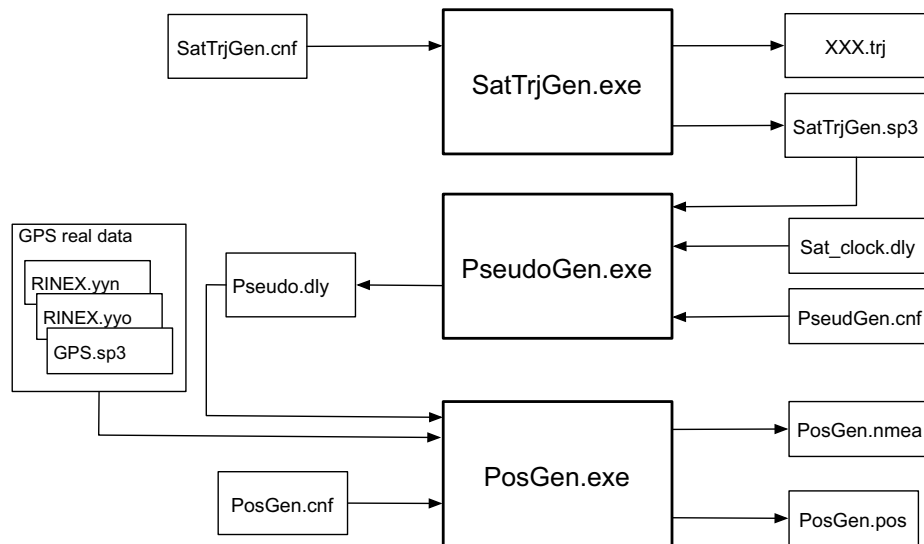


Figure B.1: Basic schematic of the RTKSsim Software Simulator.

opment RTKSsim was incapable of simulating any closed loop control. However its functionality is already good enough for utilization as the main tool for this thesis.

RTKSsim version 1.0 consists of three independent executable files:

- Satellite Trajectory Generator - SatTrjGen
- Pseudorange Generator - PseudoGen
- Positioning Generator - PosGen

RTKSsim is configurable and controllable by three configuration files:

- SatTrjGen.cnf
- PseudoGen.cnf
- PosGen.cnf

RTKSsim simulator is capable of generating:

- SatTrjGen.sp3., The SP3 format file with the precise positions of the satellites specified in the configuration file SatTrjGen.cnf.

- Pseudo.dly, The pseudorange data for the satellites specified in the configuration file SatTrjGen.cnf.
- PosGen.pos, The position of the user determined using the satellites specified in the configuration file SatTrjGen.cnf.
- PosGen.nmea, NMEA file of the position of the user determined using the satellites specified in the configuration file SatTrjGen.cnf.

### What RTKSsim Does

RTKSsim is capable of simulating several aspects of a GNSS. Essentially, given a satellite constellation configuration file, "SatTrjGen.cnf", RTKSsim can generate the SP3 file with the positions of each satellite at defined epochs. More information can be found in Section 10.1.2.

The satellite position information is then used in the second procedure, "PseudoGen", to compute the pseudorange data for each epoch given an arbitrary user position. The on-board clock shift of each satellite in the constellation is specified at each given moment in the file "Sat-clock.dly". More information can be found in Section 10.1.3.

The pseudorange information is then used by the "Position Generator" to compute the position of the user. At this level, any possible constellation combination can be specified:

- GPS constellation
- GPS plus QZSS constellation
- GALILEO constellation
- GPS plus GALILEO plus QZSS constellation

### GPS Raw Data

RTKSsim works on simulated data. However, the procedure "PseudoGen" has been designed to also work with GPS raw data. With RTKSsim it is in fact possible to

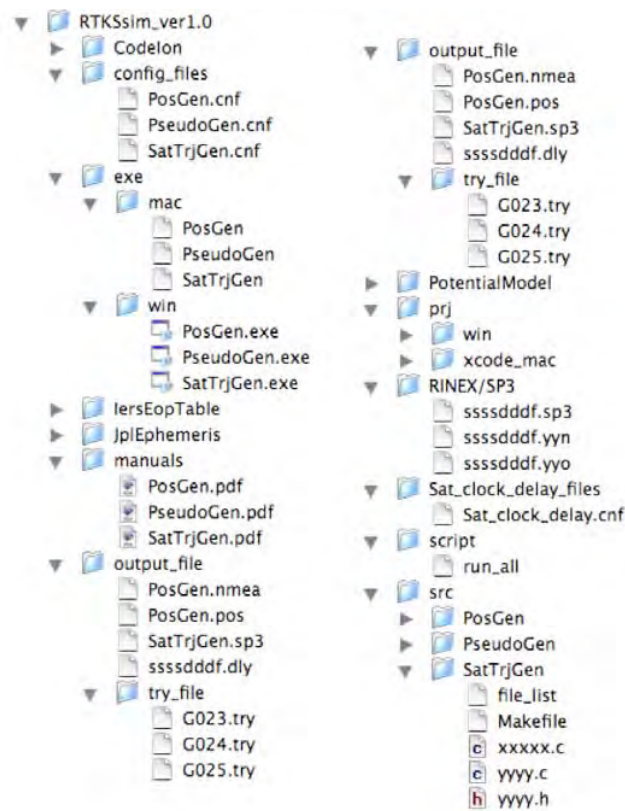


Figure B.2: Directory structure of RTKSsim.

combine simulated data with GPS raw data (RINEX and SP3 files) and evaluate the position.

More details can be found in Section 10.1.3.

### Directory Structure

The RTKSsim directory structure is presented in Fig. B.2. The structure of the directories cannot be changed but it can be moved, as it is, in any location of the HD (Macintosh, Linux or Windows version). In the program, directories are specified with a relative path (e.g `.././exe/`). Refer to the file `directory.h` in the `src` folder for details.

A description of the directory structure is presented below.

```

+-RTKSsim_ver1.0/      folder that contain the whole RTKSsim simulator
|
+-CodeIon/            directory that contains the ... files
|
+-config_files/       directory that contains the configurations files necessary to run the executables
| |
| +-PosGen.cnf         configuration file that specify the parameters for the calculation of the position
| |
| +-PseudoGen.cnf     configuration file for the pseudorange generation routine
| |
| +-SatTrjGen.cnf     configuration file that specify the satellite constellation under test
|
+-exe/                directory containing the executable files, macintosh/linux and windows version
| |
| +-mac/              |
| | |                |
| | +-PosGen          executable file, macintosh/linux version
| | |                |
| | +-PseudoGen       executable file, macintosh/linux version
| | |                |
| | +-SatTrjGen       executable file, macintosh/linux version
| |
+-IersEopTable/       Earth rotation parameters (EOP) data, Refer to http://hpiers.obspm.fr/eop-pc/
|
+-JplEphemeris/       file relative to the Planetary ephemeris DE405
|
+-manuals/            directory with manuals
|
+-output_file/        |
| |
| +-PosGen.nmea        position file, nmea format. Useful with the free software "u-blox"
| |
| +-PosGen.pos         positioning file, custom format. Very useful for producing custom made plots
| |
| +-SatTrjGen.sp3      satellite positioning file, velocity vector in ICRF/ITRF
| |
| +-try_file/          folder containing satellite positioning files, useful for producing custom made plots
| |
| | +-G023.try         | |
| | |                 |
| | +-G024.try         |
| |
+-PotentialModel/     file specifying the Earth geopotential coefficients
|
+-prj/                folder containing project folders
| |
| +-win/               borland project folder. Windows 2000 version
| |
| +-xcode_mac/         xcode project folder Macintosh OS X 10.4 version
| |
+-RINEX:SP3/          folder containing GPS raw data
| |
| +-ssssddf.sp3        GPS sp3 data file
| |
| +-ssssddf.yyn        RINEX navigation file, raw data
| |

```

```

| +-ssssddf.yyo      RINEX observation file, raw data
|
+-Sat_clock_delay_files/  folder containing files for the satellite clocks phase shift
| |
| +-Sat_clock_delay.cnf  satellite clock phase shift file
|
+-src/                  folder containing the source files
|
+-PosGen/               folder containing the source files for the routine PosGen
|
+-PseudoGen/           folder containing the source files for the routine PseudoGen
|
+-SatTrjGen/           folder containing the source files for the routine SatTrjGen
|
+-file_list            list of the source files
|
+-Makefile             makefile to compile the executable SatTrjGen
|
+-xxxx.c               source file

```

### B.1.2 Satellite Trajectory Generator - SatTrjGen

SatTrjGen is a multiple satellite orbit generator. This tool includes the implementation of the following models.

- Non-spherical geopotential effect (JGM3 or EGM96)
- Newtonian point mass effect of planets, the Moon and the Sun (DE405)
- Solar pressure effect (plane, GPS-T20, GPS-T30 model)
- Solid Earth tide effect
- General relativity effect

SatTrjGen outputs a SP3 format file. Input and output files for SatTrjGen are described below.

#### SatTrjGen.cnf Format

SatTrjGen.cnf is the input file that defines the conditions by which SatTrjGen runs. SatTrjGen.cnf consists of two parts: the common parameters part and the satellite parameters part. To generate multiple satellite simulations, the satellite parameters section has to be repeated. Fig. B.3 shows SatTrjGen.cnf in detail. The first column

```

### COMMON PARAMETERS #####
01. NUMBER OF SATELLITES           :31:                      (*1)
02. SIM. START UTC DATE            :20050101000000.000:
03. SIM. STOP  UTC DATE            :20050102000000.000:
04. LEAP SECONDS TAI-UTC           :32.000:
05. INITIAL ORBIT UTC EPOCH        :20050101000000.000:          (*2)
06. GEOPOTENTIAL MODEL             :1:(=1;JGM-3,=2;EGM96)
07. INTEGRATION STEPSIZE IN SEC    :60:
08. OUTPUT INTERVAL COUNTER        :15:                      (*3)
09. OUTPUT DIRECTORY NAME          :case0001:                  (*4)

#(*1) max. 80 satellites
#(*2) It is preferable that START DATE and ORBIT EPOCH are corresponding.
#(*3) In this case, output interval is 900 sec(60x15).
#(*4) All output results are stored into the directory(output_files/case0001/).
# Blank between ":" and "." is not permitted (bad exp. : case0001 :).

### SATELLITE 001 #####
01. SATELLITE ID+PRN               :G001:                      (*5)
02. ORBIT TYPE                     :2: (=1;CART,=2;KEP+MA,=3;KEP+EA,=4;KEP+TA)
03. COORDINATE TYPE                :3: (=1;ICRF,=2;TOD;=3;ITRF)
04. UNIT                           :3: (=1;M,S,DEG,=2;KM,S,DEG,=3;M,S,RAD)
05. ELEMENT1 X or A                : 2.656155094102e+07:
06. ELEMENT2 Y or E                : 7.033917238005e-03:
07. ELEMENT3 Z or I                : 9.569095335459e-01:
08. ELEMENT4 VX or AN              :-4.077031924019e+01:
09. ELEMENT5 VY or AP              :-1.756225839570e-03:
10. ELEMENT6 VZ or MA/EA/TA        : 2.544766500781e+00:
11. CLOCK ERROR TOC                :1,0.0e-00,6.9421716e-05,1.3187673e-11,0.0e+00: (*6)
12. POTENTIAL DEG.(N) & ORD.(M)    :4,4:
13. PLANETS,MOON & SUN              :0,0,0,0,0,0,0,0,0,1,1:          (*7)
14. SOLAR PRESSURE                  :2,1.200: (=0;NONE,=1;CR;=2;T20,=3;T30)          (*8)
15. SOLID EARTH TIDE                :0: (=0;not consider,=1;consider)
16. RELATIVITY EFFECT              :0: (=0;not consider,=1;consider)
17. ATMOSPHERE                      :0,2.3: (=0;NONE,=1;US76&CD,=2;MSIS&CD,=3;JR&CD) (*9)
18. MASS & AREA IN KG,SQ.M         :986.580,0.000:
19. NUMBER OF IMPULSIVE DV          :0: (not used;always zero)

# repeat this satellite parameter part

#(*5) 1 character + 3 digits (PRN)
#(*6) If you simulate the satellite clock error, you must setup 5 parameters.
# 1st ; consideration flag (=0;not consider,=1;consider)
# 2nd ; one sigma value of random noise component in second
# 3rd ; GPS clock error model [a0+a1*(t-TOC)+a2*(t-TOC)^2] first coeff a0 in sec.
# 4th ; GPS clock error model second coeff. a1 in sec/sec.
# 5th ; GPS clock error model second coeff. a2 in sec/sq.sec.
#(*7) The order of this flag is Mercury,Venus,Earth,..,Pluto,Moon and Sun.
#(*8) If you select CR model(flag=1), you must setup (18. MASS & AREA IN KG,SQ.M).
#(*9) The altitude of the Current positioning satellite system is over 1000km. Therefore,
# ATMOSPHERE option should be zero.

```

Figure B.3: Example of SatTrjGen.cnf.

indicates the comment line (return key is ignored), and parameters must be defined between “:”.

## Output Files of SatTrjGen

### crf/trfwwwwd.sp3

SatTrjGen generates the satellite orbit in SP3 format, in both coordinate datums ITRF and ICRF. The ICRF SP3 output is used as input to PseudoGen in order to calculate accurately the Sagnac effect. Refer to the following URL for detail of the SP3 format.

[http://www.ngs.noaa.gov/GPS/SP3\\_format.html](http://www.ngs.noaa.gov/GPS/SP3_format.html)

### XXXX.trj Format

First, SatTrjGen will generate the SP3 output file and the XXXX.trj trajectory file. Both describe the satellite positions for the whole simulation. The format of the XXXX.trj file is as follows:

```
# CREATION JST DATE ; 2006/06/15 19:33:50.000   date and time when the simulation is run
# INPUT FILE ; ../../config_files/SatTrjGen.cnf  path of the input file
# SIM. START GPS DATE ; 2000/12/31 23:15:00.000  simulation start time
# SIM. START GPST MJD ; 51909.968750000000000   simulation end time
SEC          PAST EPOCH simulation time (s)
X(m)        satellite position X component in ICRF
Y(m)        satellite position Y component in ICRF
Z(m)        satellite position Z component in ICRF
VX(m/s)     satellite velocity X component in ICRF
VY(m/s)     satellite velocity Y component in ICRF
VZ(m/s)     satellite velocity Z component in ICRF
SMA(m)      semi-major axis
ECC         eccentricity
INC(deg)    inclination in ICRF
AN(deg)     ascending node in ICRF
AP(deg)     argument of perigee
MA(deg)     mean anomaly
EA(deg)     eccentric anomaly
TA(deg)     true anomaly
R(m)        geocentric range
LAT(degN)   geodetic latitude
LNG(degE)   longitude
HEIGHT(m)   ellipsoidal height
RELATIVITY DRIFT(s/s)  drift effect due to relativity
RELATIVITY ECC(sec)   eccentricity effect due to relativity
```

SatTrjGen will generate one XXXX.trj file for each satellite. The SP3 file instead will be only one for the whole simulation.

### B.1.3 Pseudorange Generator - PseudoGen

PseudoGen generates the L1 and L2 pseudorange values for multiple user positions. This tool considers the following error models.

- Ionospheric model (CODE GIM)
- Tropospheric model (Saastamoinen and Niell mapping function,etc.)
- Relativity model (Sagnac, eccentricity effect)
- Satellite clock error
- Receiver clock error

The user position it calculates considers the displacement due to the solid Earth tide (based on IERS96). The input and output files of PseudoGen are described below.

#### PseudoGen.cnf Format

PseudoGen.cnf is the input file that defines the running conditions for PseudoGen. PseudoGen.cnf consists of two parts: the common parameters part, and the station parameters part. To use multiple stations, the station parameters for each station need to be defined. Fig. B.4 shows the contents of PseudoGen.cnf. In this file, the first column indicates the comment line, and the parameters must be defined between “:”.

#### Output Files of PseudoGen

PseudoGen outputs the file ssssdddfyy.csv. Here ssss is the four character station name designator (defined in PseudoGen.cnf), ddd is the day of the year of the first record, f is file sequence number and yy is the last two digits of the year. This file is the input for the next routine PosGen. The structure of the file ssssdddfyy.csv is as follows:

```

Station Information
sta name      :sydn:
itrfr xyz (m) : -4648240.38128, 2560636.51828, -3526318.54915:
# RUN DATE   : 2006/10/ 2 11:13:16 JST
# RUN FILE    : _ObservGen_Input.Copy
# Definition of parameters (one line consists of the following items)

```

```

### COMMON PARAMETERS #####
01. CASE ID (same as SatTrjGen) :case0001: (*1)
02. SIMULATION START UTC :20041231235947.000: (*2)
03. SIMULATION STOP UTC :20050101235947.000: (*2)
04. LEAP SECOND TAI-UTC :32.000:
05. MEASURE. INTERVAL IN SEC :30.000:
06. EARTH MODEL :1:
# ----- 1= GRS80 model -----
# ----- 2= WGS84 model -----
07. NUMBER OF ION FILE :3: (*3)
# ----- 0= not consider -----
:COD13035.ION:
:COD13036.ION:
:COD13040.ION:
08. NUMBER OF STATIONS :2: (*4)

#(*1) you set the directory name into output_files include "crfwwwd.sp3".
# and the all output results of PseudoGen are stored in this directory.
#(*2) you should be set the offset date (UTC-GPS) seconds. In this processing,
# the start time of output is xx:xx:00.000 GPS time.
#(*3) you should prepare corresponding the day before of the day and later data.
#(*4) no limitation (depend your PC)

### EACH STATION PARAMETERS #####
### 1ST STATION - DOWNLINK CASE

01. STATION NAME :sydn: (*5)
02. LOCATION TYPE :1:
# ----- 1= LAT(deg), LNG(deg), HGT(m) -----
# ----- 2= X(m), Y(m), Z(m) -----
03. LOCATION - X or GEO.LAT :-33.78087941:
04. - Y or LONGITUDE :151.15037921:
05. - Z or ELLIP. H : 85.67708224:
06. EL CUTOFF ANGLE IN DEG : 5.000:
07. RECEIVER CLOCK ERROR : 0.e-00,0.e-00,0.e-00,0.e-00:
# ----- 1st noise (sec) -----
# ----- 2nd polynomial 0th (s) -----
# ----- 3rd polynomial 1st (1/s) -----
# ----- 4th polynomial 2nd (1/s2) -----
08. UP/DOWN LINK, FREQ (MHZ) :2,1575.420: (*6)
# ----- 1= uplink -----
# ----- 2= downlink -----
09. TIDAL DISPLACEMENT :1: (*7)
# ----- 0= not consider -----
# ----- 1= solid earth tide -----
# ----- 2= ocean tide -----
# ----- 3= solid earth & ocean tide -----
10. TROPOSPHERIC DELAY MODEL :4:
# ----- 1= Hopfield -----
# ----- 2= modified Hopfield -----
# ----- 3= Saasatamoinen -----
# ----- 4= 3 include mapping function -----
11. TROPO. MAPPING FUCTION :2:
# ----- 1= Marini & Murray -----
# ----- 2= Niell -----
12. METEO. DATA POINTS :0: (*8)
# ----- 0= T(15),P(1013.25),RH(70) -----
# ----- unit Temperature T(Cels.) -----
# ----- unit Pressure P(hPa) -----
# ----- unit Relative Humidity RH(%) -----

```

Figure B.4: Example of PseudoGen.cnf.

```

# yyyy      : 4 digits year (GPST)
# mm        : 2 digits month (GPST)
# dd        : 2 digits day (GPST)
# hh        : 2 digits hour (GPST)
# mn        : 2 digits minute (GPST)
# sec       : 6.3f type second (GPST)
# GPST week : 4 digits gps week
# GPST days  : 1 digit days past gps week
# GPST seconds : 16.8f type seconds past week
# simt      : 16.8f simulation time in sec
# n         : 2 digits number of visible satellites
# PRN       : 2 digits satellite PRN number
# C1        : 18.8f type C/A code pseudorange (meter)
# P2        : 18.8f type P2 code pseudorange (meter)
# CE        : 14.6f type satellite clock error (microsec)
# Repeat n times from PRN to CE

```

### B.1.4 Positioning Generator - PosGen

PosGen is the precise point positioning tool based on the ICD-GPS-200 specifications using L1, or L1 and L2, pseudorange data (two frequency ionospheric correction). The main models included in this routine are:

- Tropospheric delay correction
- Ionospheric delay correction (Klobuchar, C1/P2 two frequency)
- Selection of satellites (specific PRNs, optimal GDOP due to 4 sat.)
- Addition of random noise
- Addition of QZS clock error (one second interval).

PosGen can be executed using the following data.

- Actual data mode:
  - rinex obs. file + rinex nav. file
  - rinex obs. file + rinex nav. file (for sat. clock error) + SP3 file
  - rinex obs. file + SP3 file (include sat. clock error)
- Simulation data mode:
  - sp3 file crfwwwwd.sp3 (generated by SatTrjGen)
  - obs. file sssdddfyy.csv (generated by PseudoGen)

## Input Files

### PosGen.cnf Format

PosGen.cnf is the input file for the execution of PosGen. Two samples of PosGen.cnf files are shown here, one is the simulation mode and the other is the actual data mode.

#### (1) Sample of simulation mode:

```

Type                :s:(s or S=simulation,a or A=actual data) (*1)
Directory           :case0001:      (*2)
RINEX file?        :n:              (*3)
RINEX OBS File     :sydn0010.05o.csv: (*4)
RINEX NAV File     ::                (*5)
Start Time         :2005/01/01, 00:00:00:(yyyy/dd/dd, hh:mm:ss)
End Time          :2005/01/01, 12:59:30:(yyyy/dd/dd, hh:mm:ss)
PRNs of GPS (1to50) :01,03,04,05,.....,27,28,29,30: (*6)
    QZS (3 satellites) :41,42,43: (*7)
Position Coordinate :1: (*8)
Latitude (deg)     : 26.194594805:
Longitude (deg)    : 127.677626853:
Height (m)         : 37.671397076:
Satellite Select Mode :0:=0 all satellits, =1 Min GDOP, =2 High Elevation QZS
Precise orbit?     :y: (*9)
SP3 orbit filename :trs13036.sp3: (*a)
2 frequency?      :y: (*b)
Broadcast ionosphere? :n:
Tropo?            :y:
Vert cut (deg)     :15.0:
Data Interval Counter :1: (*c)
Out Files (NMEA)   :y:
Clock Delay of QZS :y: (*d)
    filename of QZS1 :qzs01.delay:
    filename of QZS2 ::
    filename of QZS3 ::
C1 noise (1 sigma, m) :5.0: (*e)
P2 noise (1 sigma, m) :1.0: (*e)

```

- (\*1) if you want to run by simulation mode, input s or S.
- (\*2) PosGen output directory ( output\_files/case0001/ ). and in the simulation mode, the generated sp3 and observation file must be in this directory.
- (\*3) in the simulation mode, this flag must be n.
- (\*4) observation file name generated by PseudoGen.
- (\*5) in the simulation mode, not use this line.
- (\*6) set all GPS satellites PRN include into sp3 file.
- (\*7) if QZS exist, set all QZS PRN include into sp3 file.
- (\*8) if you input 1, station location is ITRF spherical coordinate.  
if you input 0, station location is ITRF Cartesian x,y,z in meter.
- (\*9) in the simulation mode, this flag must be y.
- (\*a) sp3 file name generated by SatTrjGen.
- (\*b) in the simulation mode, this flag must be y.
- (\*c) output interval is (Data Interval Counter)\*(sampling of observation file).
- (\*d) if you simulate the influence of QZS clock error,  
you set this flag y and QZS clock error file into Sat\_clock\_delay\_files.
- (\*e) in the simulation mode, you should input the non-zero value.

#### (2) Sample of actual data mode:

```

Type                :a:(s or S=simulation,a or A=actual data) (*1)
Directory           :case0001:      (*2)
RINEX file?        :y:              (*3)
RINEX OBS File     :sydn0010.05o:    (*4)
RINEX NAV File     :sydn0010.05n:    (*5)
Start Time         :2005/01/01, 00:00:00:(yyyy/dd/dd,hh:mm:ss)
End Time           :2005/01/01, 12:59:30:(yyyy/dd/dd,hh:mm:ss)
PRNs of GPS (1to50) :01,03,04,05,.....,27,28,29,30: (*6)
    QZS (3 satellites) :41,42,43:    (*7)
Position Coordinate :1:          (*8)
Latitude (deg)     : 26.194594805:
Longitude (deg)    : 127.677626853:
Height (m)         : 37.671397076:
Satellite Select Mode :0:=0 all satellits, =1 Min GDOP, =2 High Elevation QZS
Precise orbit?     :y:          (*9)
SP3 orbit filename :igs13036.sp3:    (*9)
2 frequency?      :y:          (*a)
Broadcast ionosphere? :n:          (*a)
Tropo?            :y:
Vert cut (deg)    :15.0:
Data Interval Counter :1:          (*b)
Out Files (NMEA)   :y:
Clock Delay of QZS :n:          (*c)
    filename of QZS1  ::
    filename of QZS2  ::
    filename of QZS3  ::
C1 noise (1 sigma, m) :0.0:      (*d)
P2 noise (1 sigma, m) :0.0:      (*d)

```

(\*1) if you want to run by actual data mode, input a or A.  
(\*2) PosGen output directory (output\_files/case0001 ).  
(\*3) in the actual data mode, this flag must be y.  
(\*4) actual rinex observation file name into the directory RINEX&SP3/.  
(\*5) in the actual data mode, actual rinex nav. file name into the directory RINEX&SP3/.  
(\*6) set all GPS satellites PRN include into rinex nav. or sp3 file.  
(\*7) QZS dose not exist in actual data, therefore this line is no data ::  
(\*8) if you input 1, station location is ITRF spherical coordinate.  
if you input 0, station location is ITRF Cartesian x,y,z in meter.  
(\*9) in the actual data mode, you can set both y and n. if you set y,  
in the next line is actual sp3 file name into the directory RINEX&SP3/.  
(\*a) in the actual data mode, you can set both y and n.  
(\*b) output interval is (Data Interval Counter)\*(sampling of rinex obs. file).  
(\*c) in the actual data mode, this flag must be n.  
(\*d) in the actual data mode,  
you must set 0.0, because the random noise has already existed in the actual data.

## Delay File Format

This file simulates the influence of the positioning accuracy due to the QZS clock error.

The format of this delay file is as follows:

- Time delay unit is seconds.
- Line by line represents one second.

- First line corresponds to the start time of PosGen simulation.

For example, if the simulation time span is one day, the delay file will need to have 86401 lines.

### Output Files

Output file is of two types: (1) NMEA format (extension of output file is .nmea, for the details of this format refer to (<http://www.gpsinformation.org/dale/nmea.htm>)). (2) CSV (format extension of output file is .pos) used for post-analysis. CSV file includes the following parameters:

tsec, : seconds past epoch  
nobs, : number of visible satellites  
x, : x component of station position in ITRF (m)  
y, : y component of station position in ITRF (m)  
z, : z component of station position in ITRF (m)  
lat, : latitude of station position in ITRF (deg)  
lon, : longitude of station position in ITRF (deg)  
height, : geodetic height of station position (m)  
GDOP, : GDOP value  
PDOP, : PDOP value  
HDOP, : HDOP value  
VDOP, : VDOP value  
errc, : receiver clock error in meter  
grx, : x component station position error in ITRF (m)  
gry, : y component station position error in ITRF (m)  
grz, : z component station position error in ITRF (m)  
lrx, : north direction station position error (m)  
lry, : east direction station position error (m)  
lrz : up direction station position error (m)



Figure B.5: RTKSSim graphical user interface, GUI.

### B.1.5 How to Run RTKSSim

To simplify the process of using, modifying, recompiling and rerunning one or all three routines SatTrjGen, PseudoGen, PosGen a GUI was developed. Fig. B.5 show a screenshot of the GUI. Its use is straightforward: the main text window shows the content of the configuration files, the tick box allows selection of which routine to run (each routine can be run independently) using the RUN button. The COMPILATE button permits compilation of the source package of the selected routine.

### B.1.6 VCXO TKS Controller Implementation

In parallel with the development of RTKSSim, a PLL for the RTKS scheme was implemented by the author. Fig. B.6 gives an overview of the implemented models. A fully modular architecture is noticeable. The RTKS modules were written in standard ANSI C and compiled on a Macintosh/Unix machine. Xcode was used under OS X, and Borland Builder 6 was used under Windows 2000. The structure of the directories

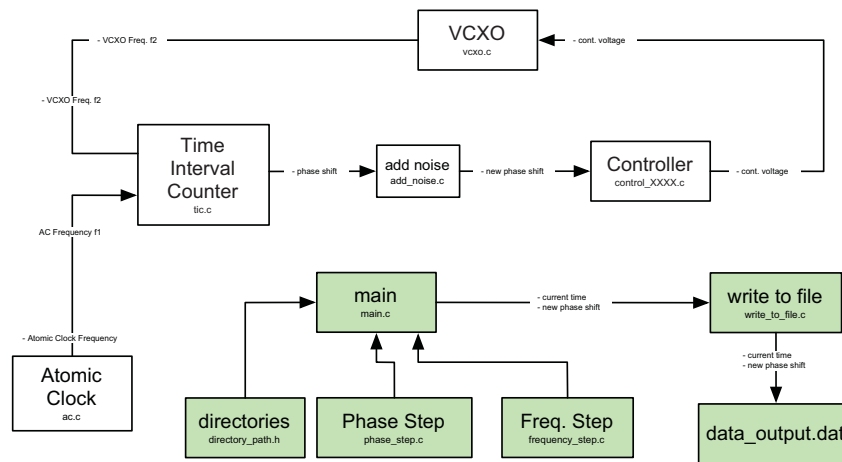


Figure B.6: Block scheme of the VCXO TKS developed in ANSI-C.

is shown in Fig. B.7. Once completed, each single module can be connected to the rest of the RESSOX environment and a complete RESSOX/RTKS software tool under a real-time closed loop control is possible.

**documentation:** Contains the documentation of the C source and the schematic of the VCXO TKS simulator. Some pdf files with simulation results and algorithm comparison results are also present.

**exe:** Contains the executable files, generated by Xcode and Borland Builder.

**Igor-graph:** Contains a project where the output file data-output.dat can be read and results can be printed (a program called gor is necessary).

**noise-files:** Contains the files produced with Stable-32 and used to simulate the noises in the TKS.

**old:** Contains old files, not used anymore.

**output:** Contains the output file data-output.dat of the VCXO TKS simulator.

**project-mac:** Contains the project for compiling the VCXO TKS simulator with Apple XCode.

**project-win:** Contains the project for compiling the VCXO TKS simulator with Borland Builder 6 on Windows 2000.

**source:** Contains ALL the source files used to implement the schematic in Fig. B.6.

The RESSOX VCXO control algorithm presented in Chapter 3, as well as the

documentation	Today, 1:43 PM	Folder
exe	Today, 1:44 PM	Folder
project_mac	Today, 1:32 PM	16 KB Unix Executable File
Project_win.exe	Today, 11:23 AM	12 KB Rar File
Project_win.tds	Today, 11:24 AM	64 KB Document
lgor_graph	Today, 1:38 PM	Folder
noise_files	Today, 11:18 AM	Folder
Allan_Variance.png	Feb 16, 2005, 2:59 PM	72 KB Portable ...hics Image
note.txt	Feb 16, 2005, 2:59 PM	4 KB Plain text document
VCXO_tic_ac_noise.dat	Feb 16, 2005, 2:59 PM	2.5 MB TextEdit Document
old	Today, 11:18 AM	Folder
output	Today, 11:24 AM	Folder
data_output.dat	Today, 11:25 AM	2 MB TextEdit Document
project_mac	Today, 11:18 AM	Folder
build	Today, 11:18 AM	Folder
project_mac.1	Feb 16, 2005, 2:59 PM	4 KB Document
project_mac.xcode	Today, 1:38 PM	Xcode Project File
README.txt	Feb 17, 2005, 3:00 PM	4 KB Plain text document
project_win	Today, 11:24 AM	Folder
obj	Today, 11:22 AM	Folder
Project_win.-bpr	Today, 11:23 AM	8 KB Document
Project_win.bpf	Feb 16, 2005, 5:07 PM	4 KB Document
Project_win.bpr	Today, 11:24 AM	8 KB Document
README.txt	Feb 17, 2005, 3:17 PM	4 KB Plain text document
source	Today, 11:25 AM	Folder
ac.c	Feb 16, 2005, 2:59 PM	4 KB C Source File
add_noise.c	Feb 17, 2005, 2:46 PM	4 KB C Source File
control_iwata.c	Today, 11:16 AM	4 KB C Source File
control_p.c	Feb 18, 2005, 5:00 PM	4 KB C Source File
control_tappero.c	Today, 11:25 AM	4 KB C Source File
directory_path.h	Feb 17, 2005, 2:58 PM	4 KB C Header Source File
frequency_step.c	Today, 11:13 AM	4 KB C Source File
main.c	Today, 11:16 AM	4 KB C Source File
phase_step.c	Today, 11:13 AM	4 KB C Source File
tic.c	Feb 18, 2005, 6:45 PM	4 KB C Source File
vcxo.c	Feb 21, 2005, 7:37 PM	4 KB C Source File
write_to_file.c	Feb 17, 2005, 2:46 PM	4 KB C Source File

Figure B.7: Structure of the VCXO RTKS simulator.

RTKS PLL algorithm presented in Chapter 5, were tested with this simulator. The positioning study presented in Chapter 6 was carried out merging this simulator with parts of the Hardware Simulator (hardware-in-the-loop study).

### B.1.7 RTKSim Tool Used for Subsystem Development

As for the Hardware Simulator, RTKSim has been used in combination with other subsystem developed for the RESSOX project with the aim of developing subsystems or test algorithms useful for the development of this project. Section 5.6 describes the use of this Software Simulator for the study of the satellite communication interruption problems.

### B.1.8 Contribution from the Author

Within the development of the RESSOX/RTKS Software Simulator presented in this chapter, the author has contributed in the definition of the RTKSim software structure presented in Section B.1.1, in the development of the graphical user interface (GUI)

that control RTKSsim presented in Section B.1.5 and in its interface with the RTKSsim routines.

The author has fully contributed to the development and testing of the VCXO TKS controller software implementation and its PLL presented in Section B.1.6.

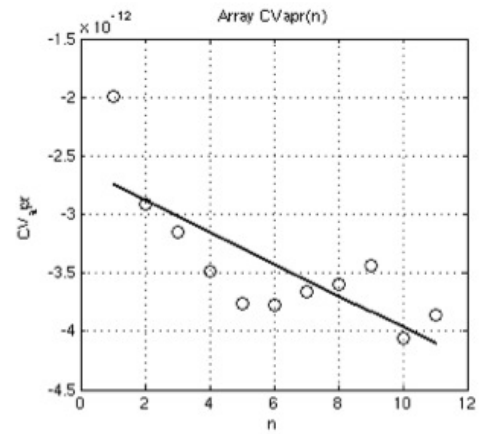
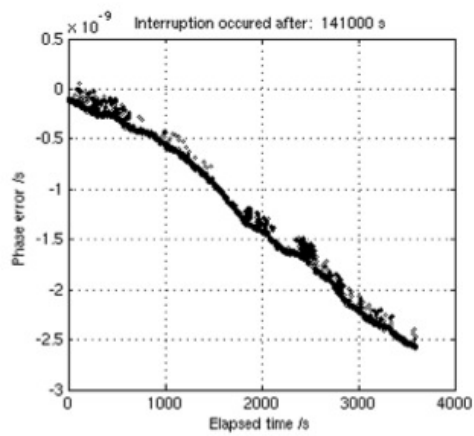
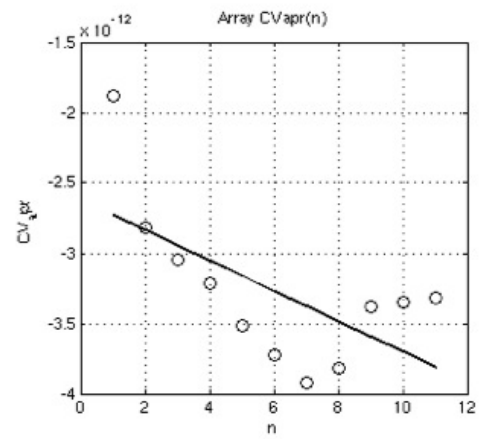
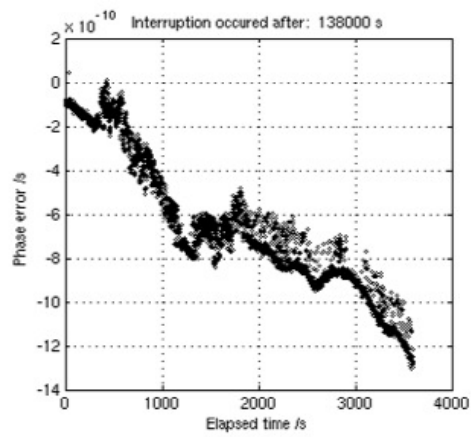
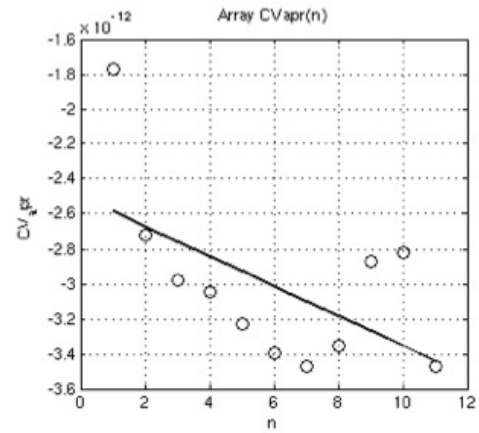
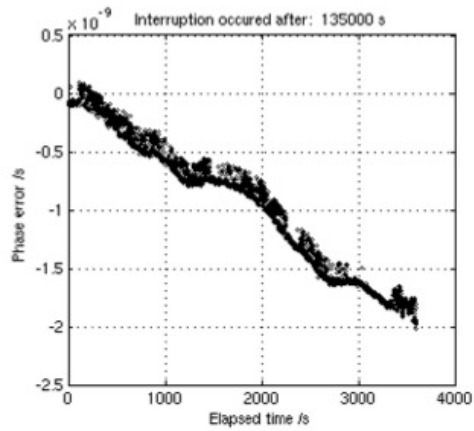
## Appendix C

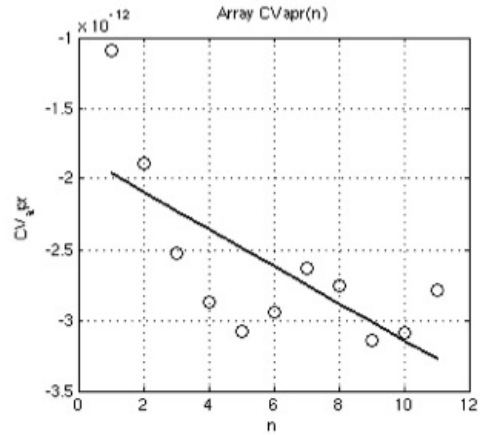
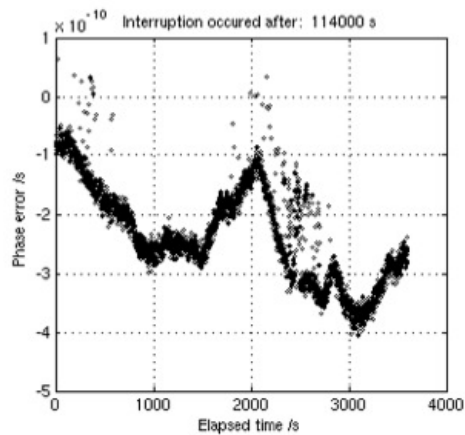
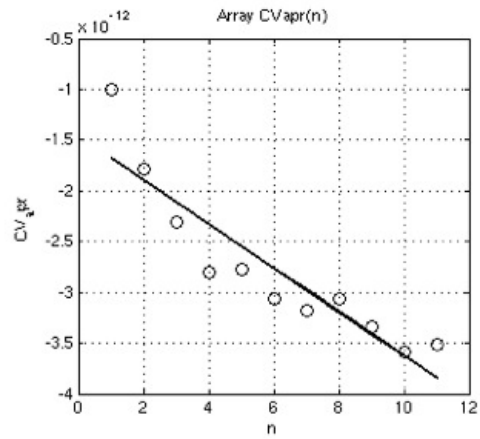
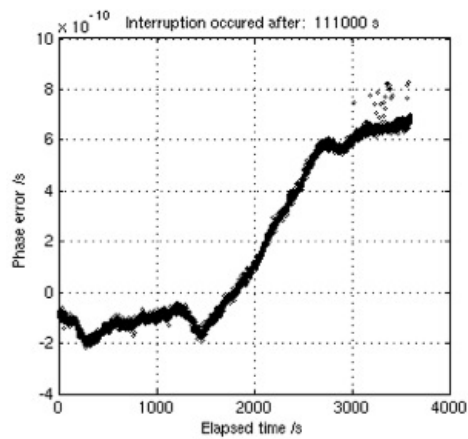
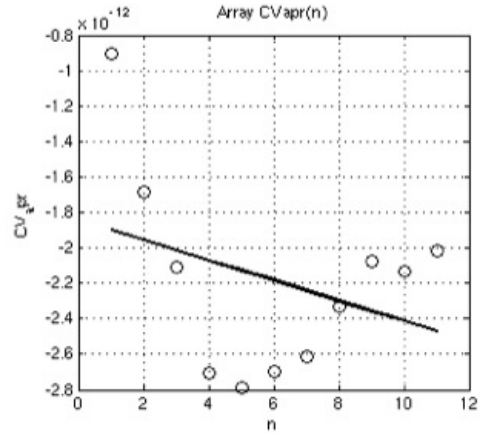
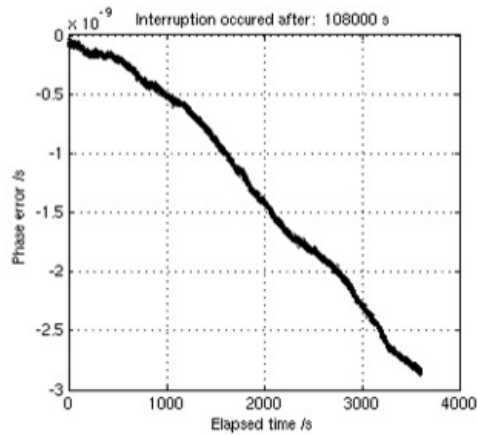
# Appendix - Feedback Interruption, Experimental Results

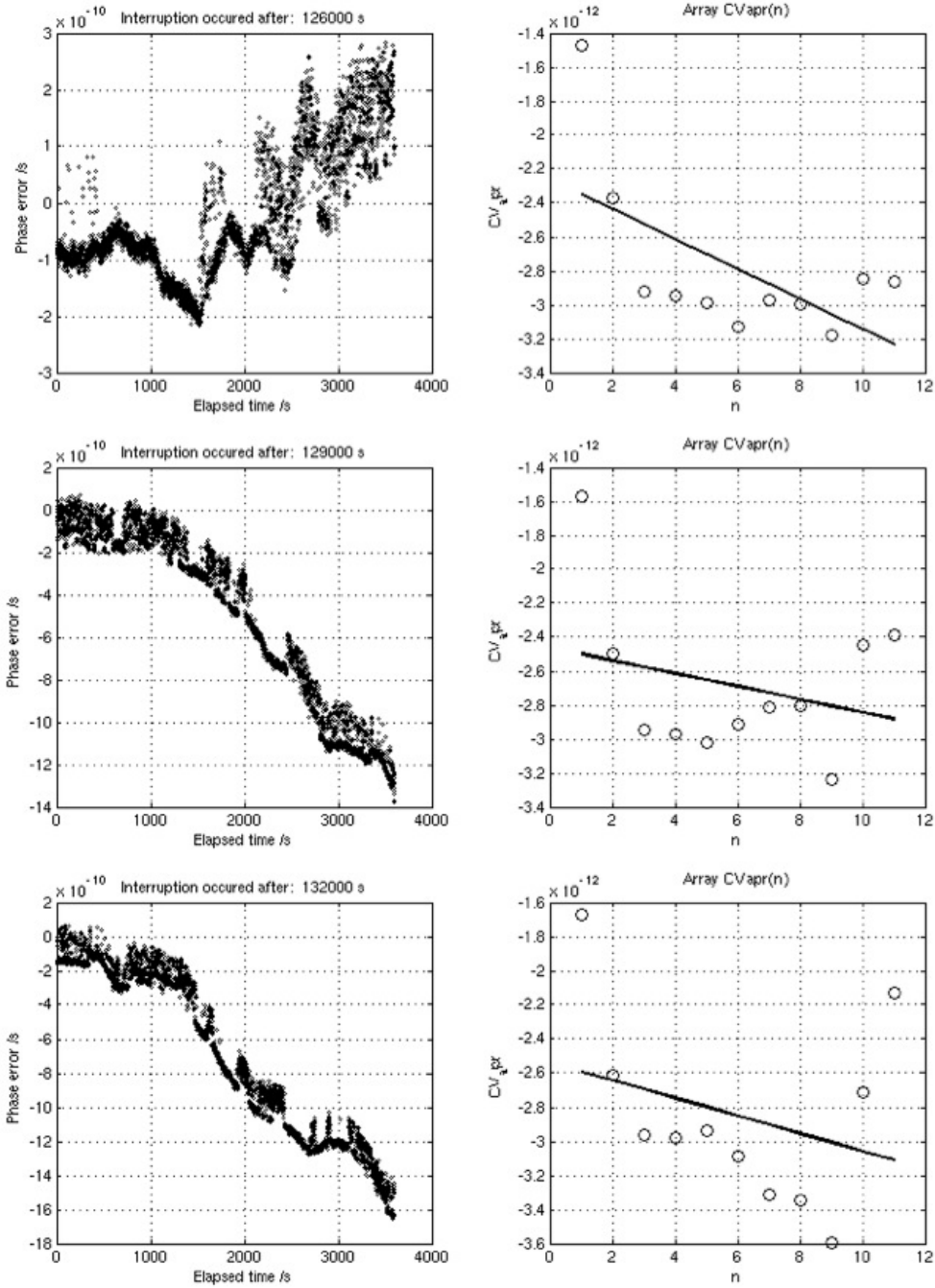
In order to test the effectiveness of the free-run interruption algorithm presented in Chapter 5 under realistic conditions, the raw VCXO data presented in Fig. 5.11 have been embedded into a non-real time software routine. Such a routine would generate several satellite communication interruptions from which the VCXO will behave in accordance to the raw data. The objective is to analyze how the free-run interruption algorithm will behave during these outages by opportunely compensating the VCXO.

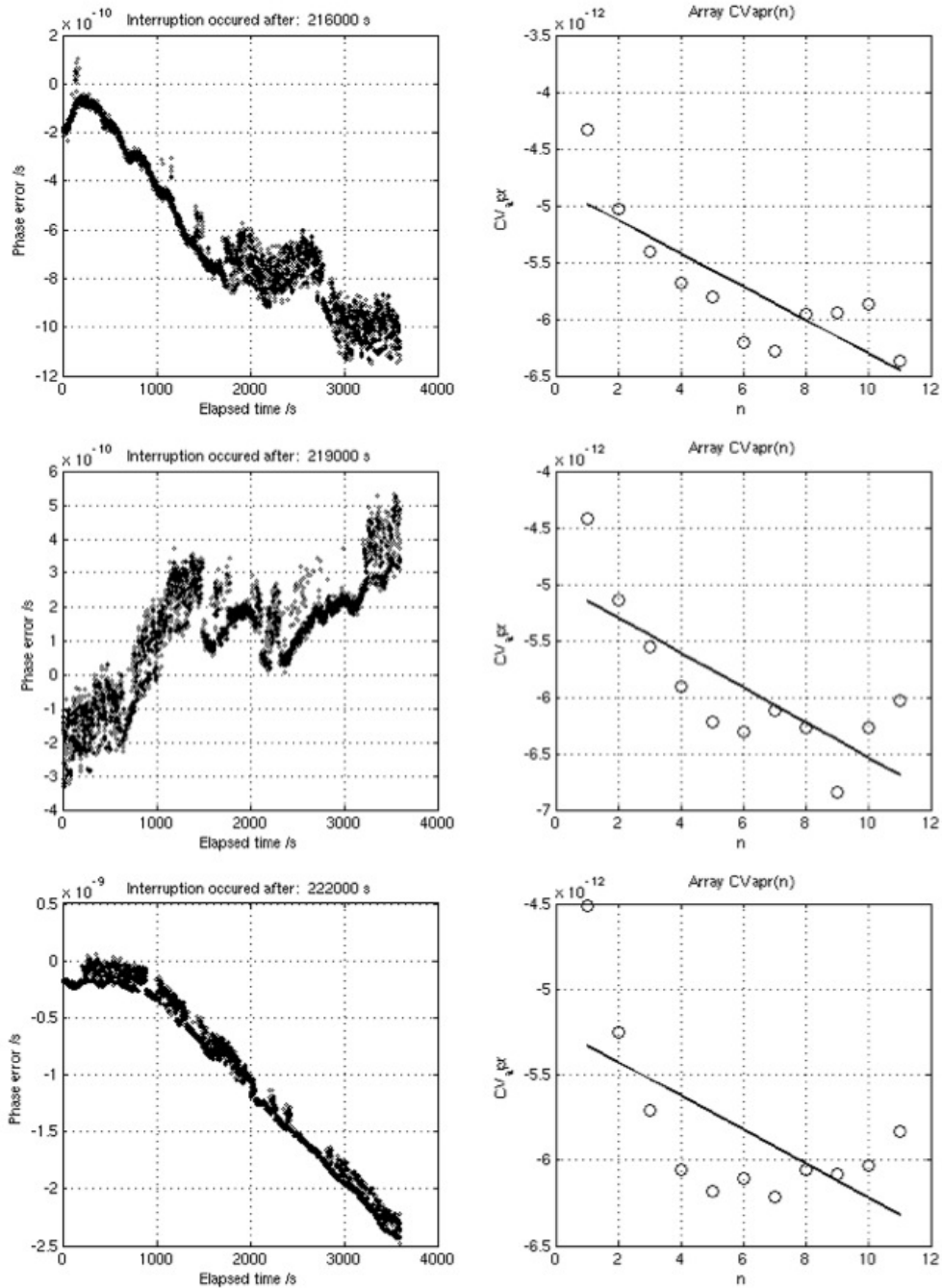
The algorithm is put under test by generating 45 independent feedback interruptions. One hundred thousand past (always different) samples are used by the algorithm to create the vector  $CV_{apr}(m)$ , and are then used to steer the VCXO that otherwise would drift.

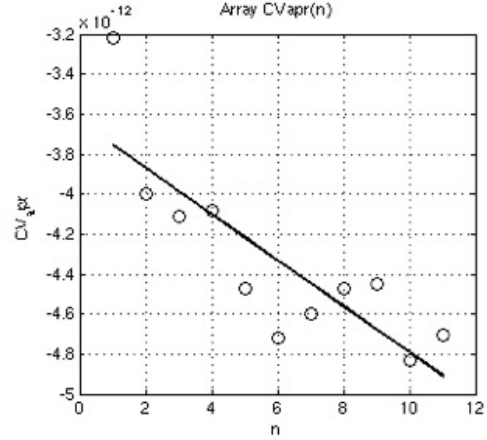
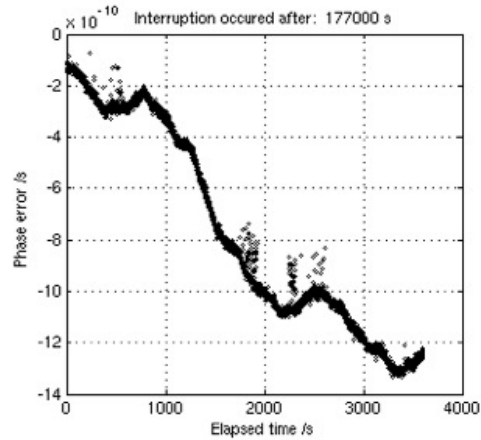
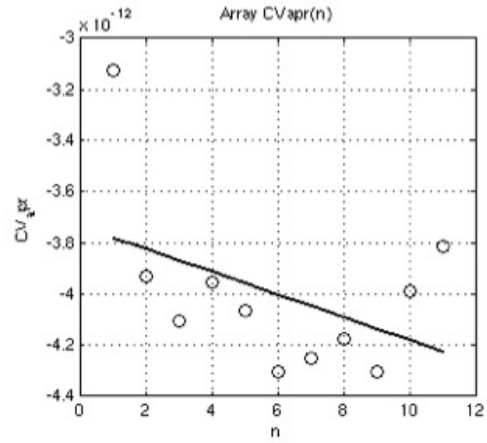
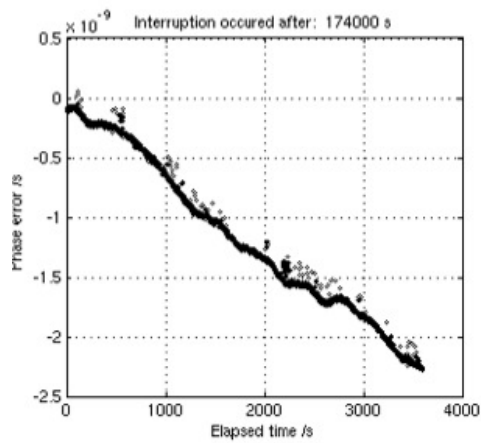
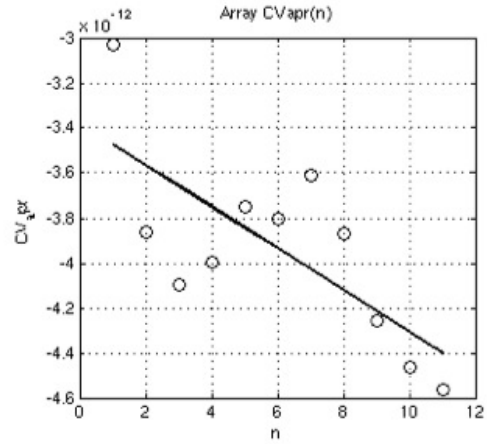
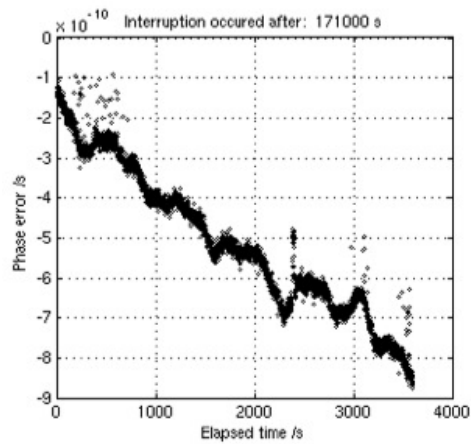
The following 45 pairs of plots show 3600 s worth of compensated VCXO phase shift after the satellite communication interruption for each case. Moreover, for each interruption the vector  $CV_{apr}(m)$  is also shown.

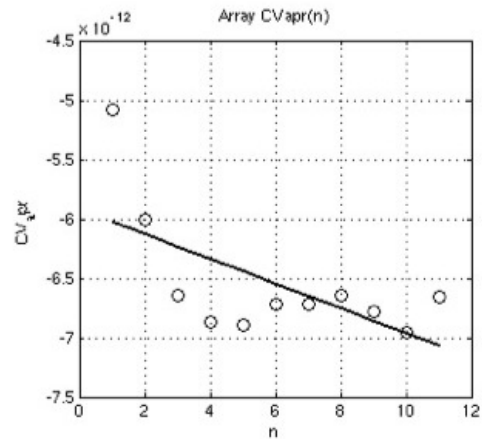
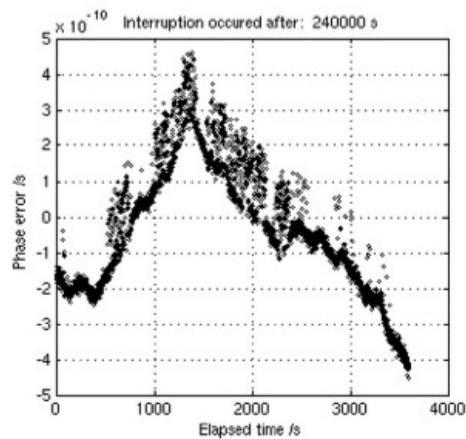
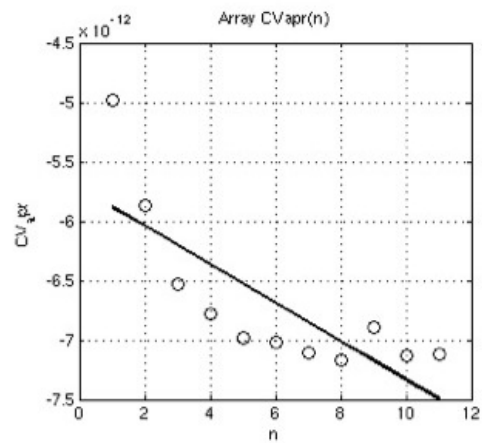
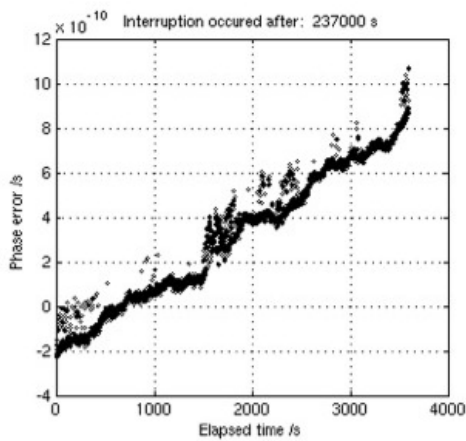
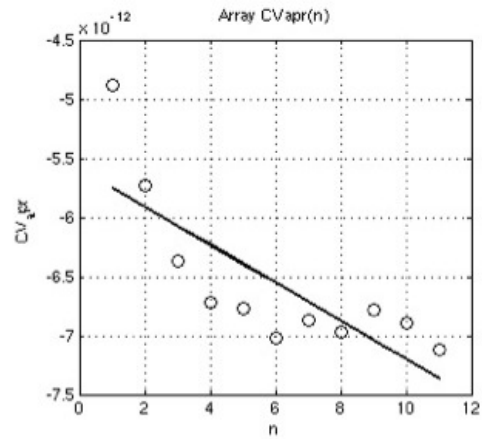
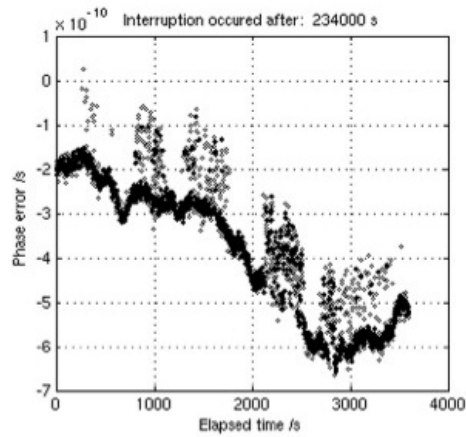


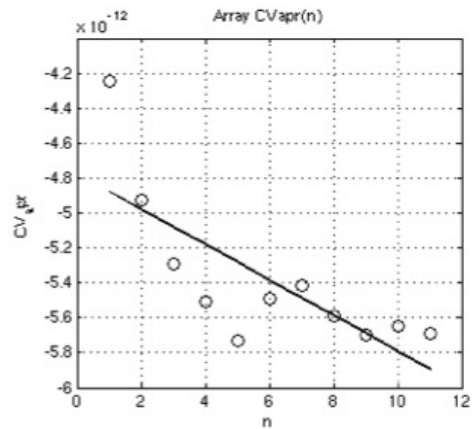
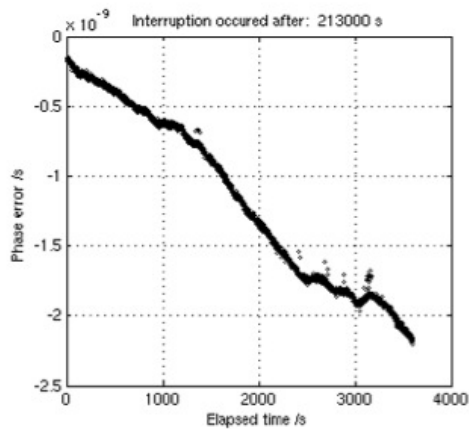
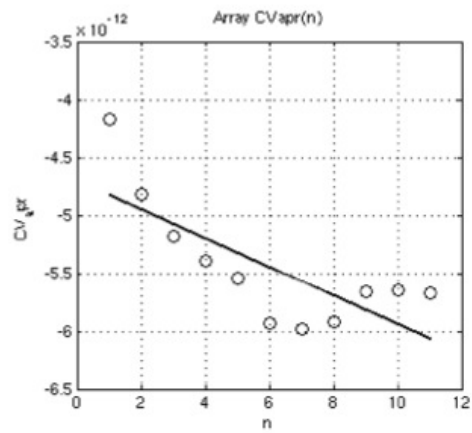
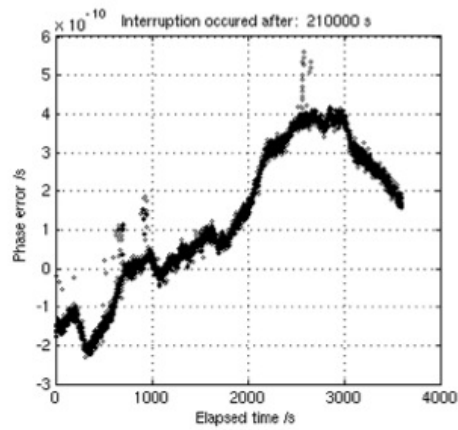
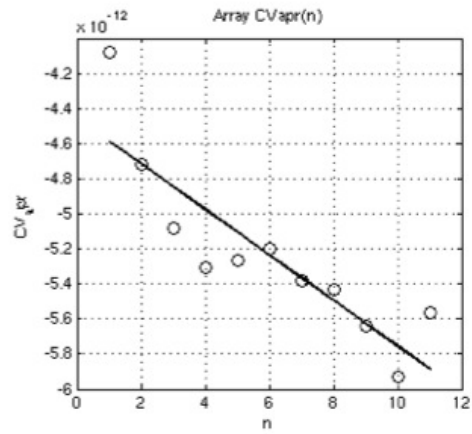
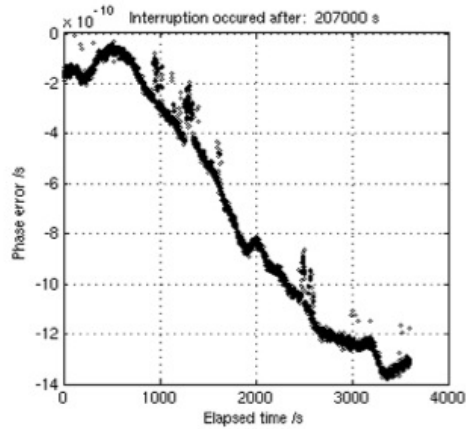


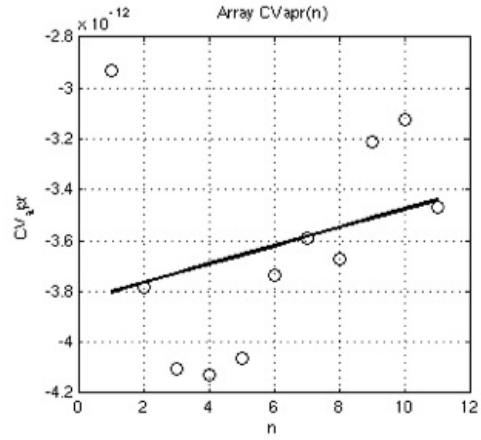
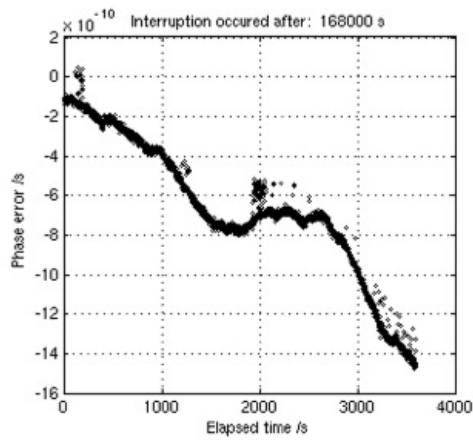
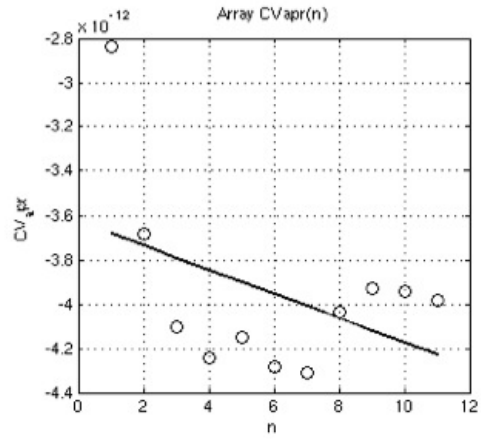
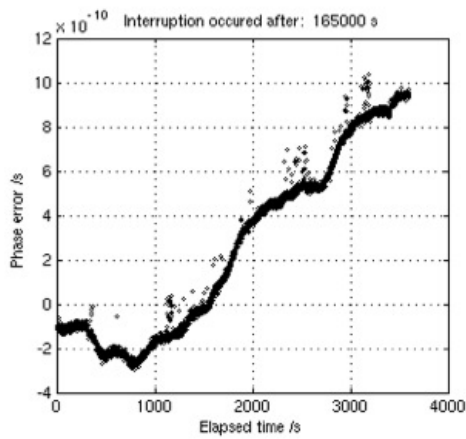
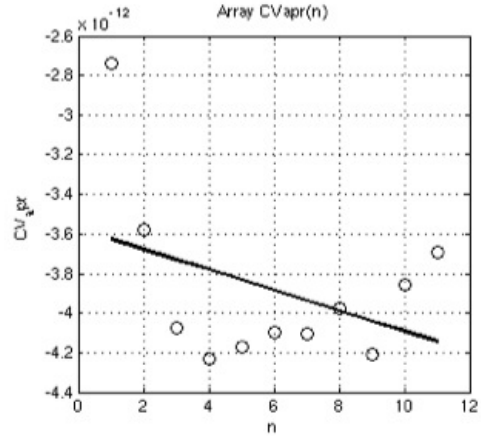
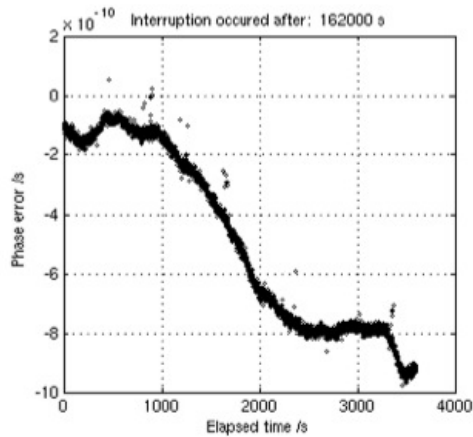


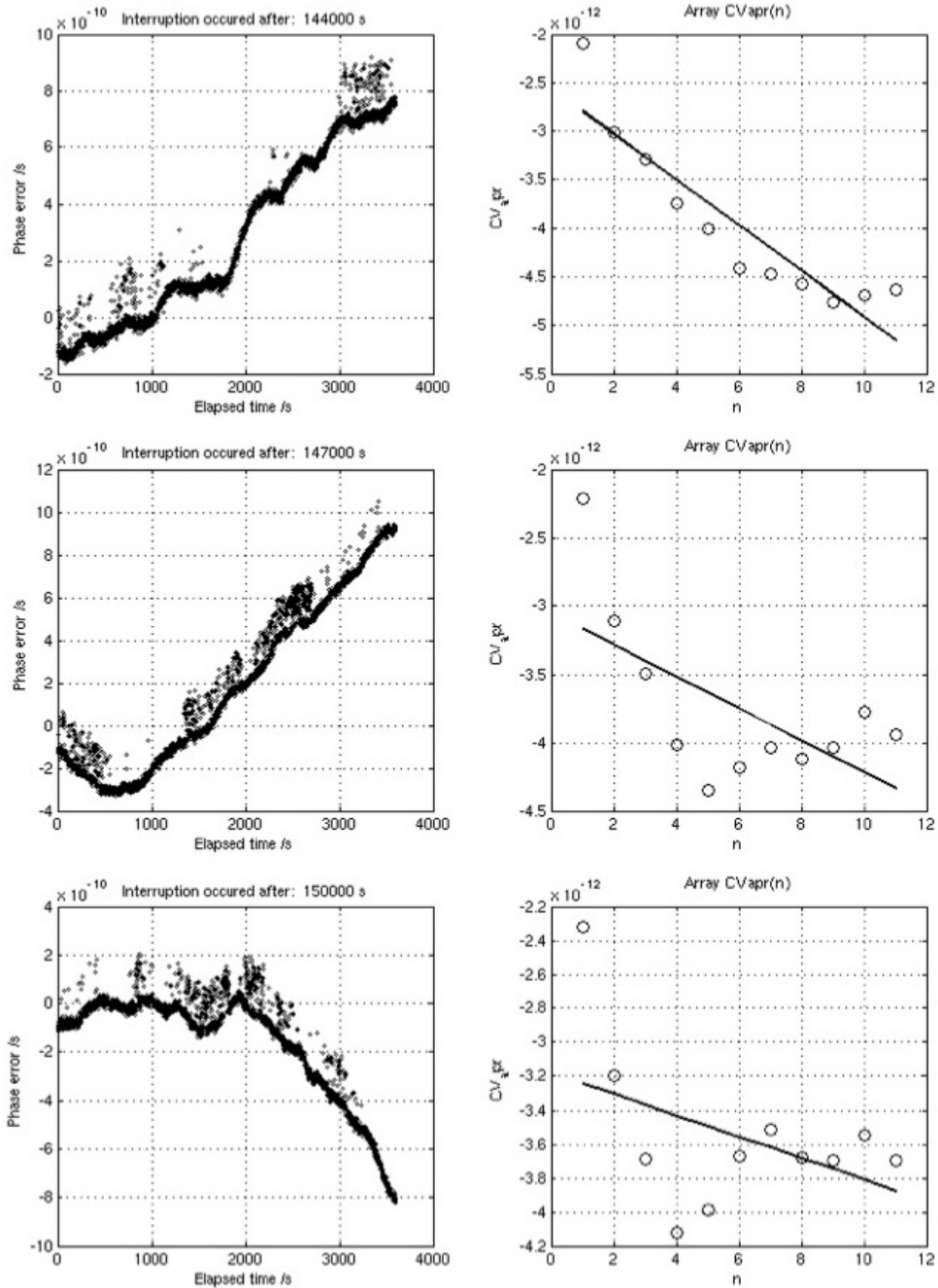


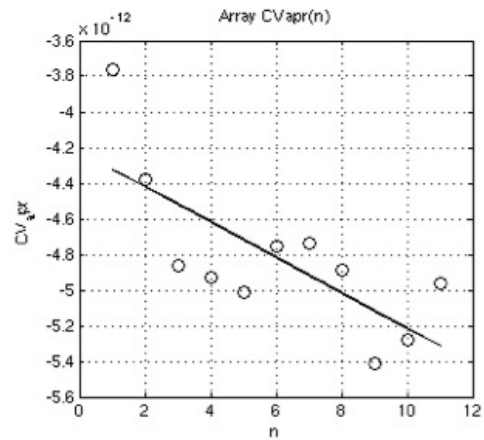
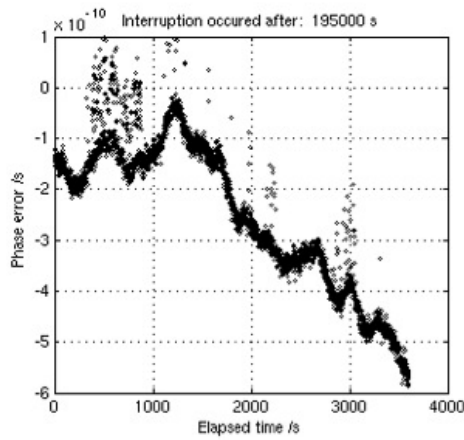
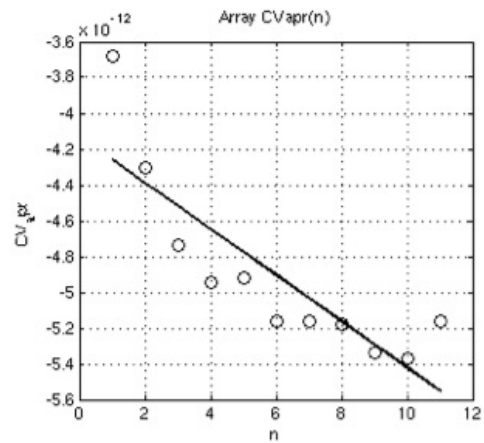
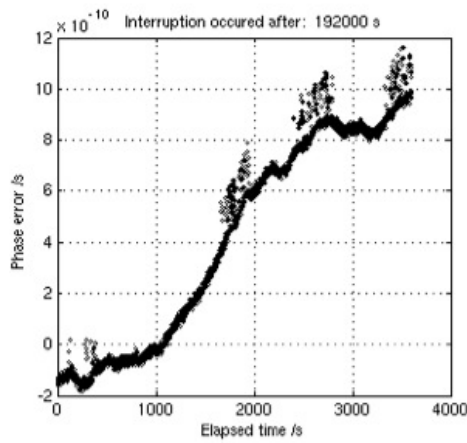
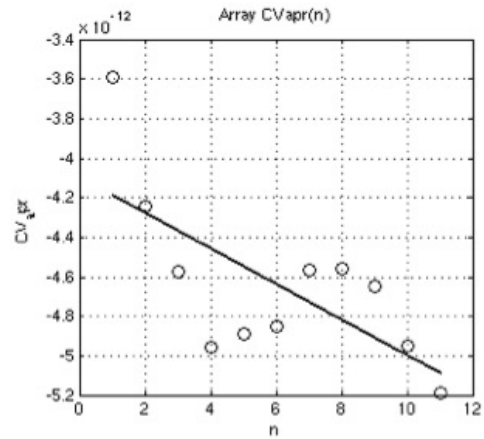
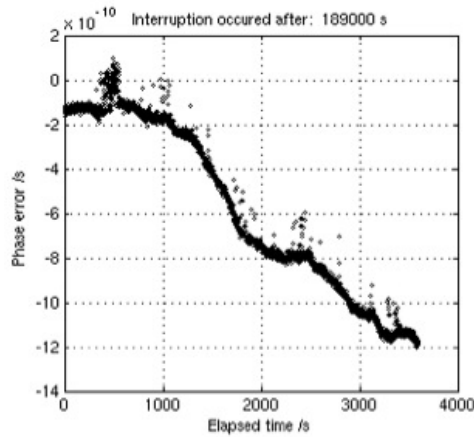


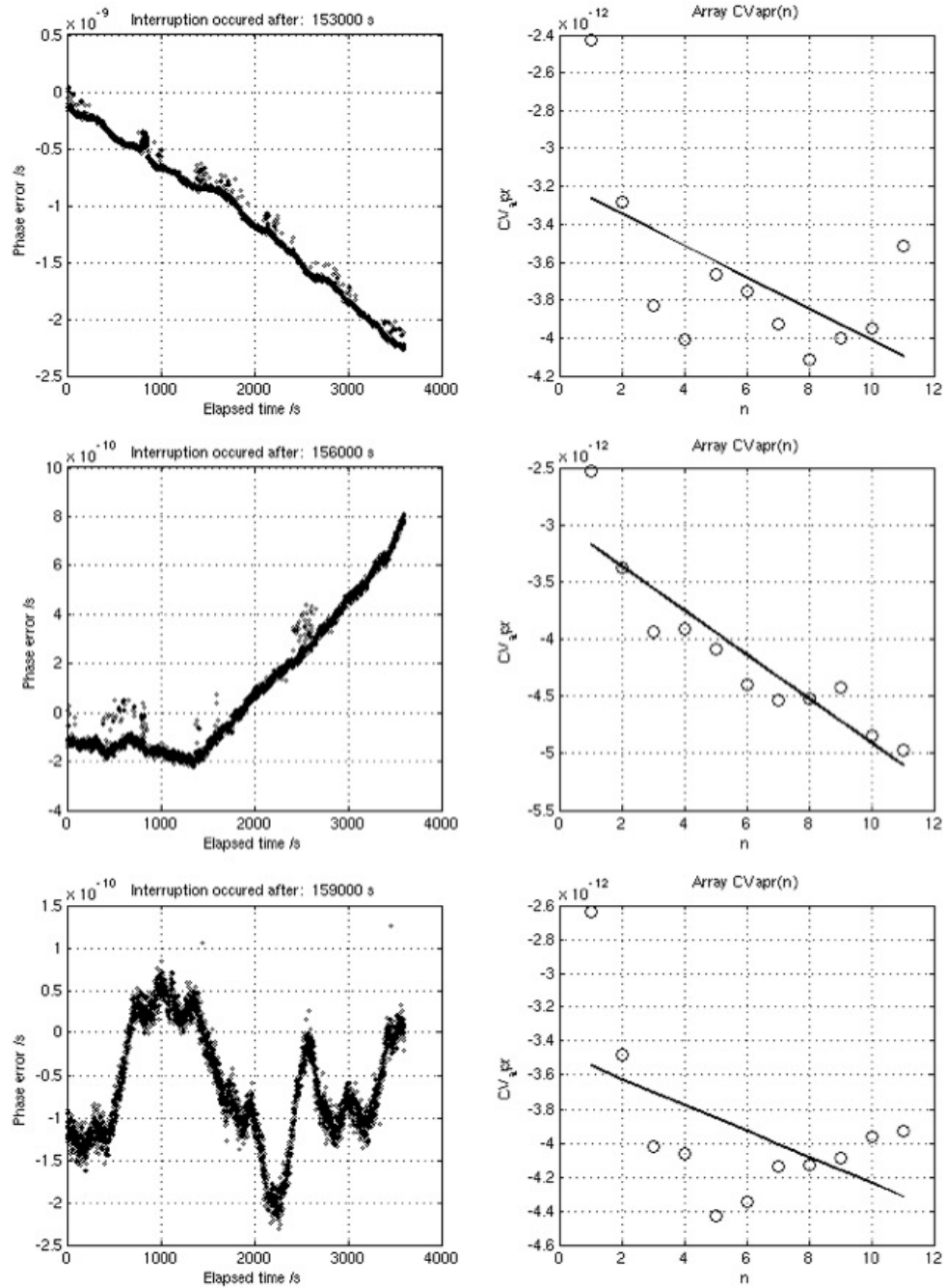


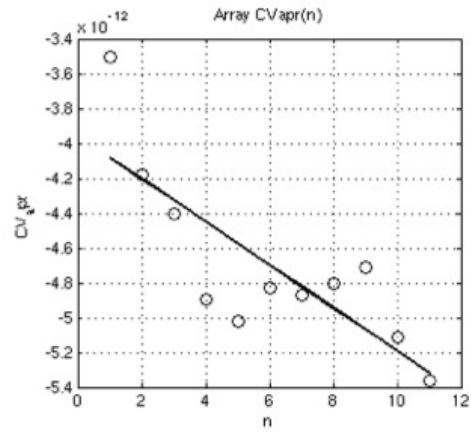
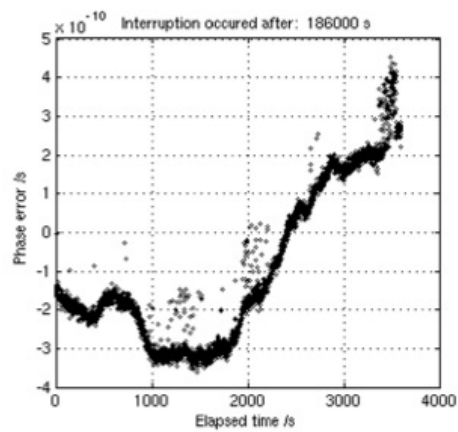
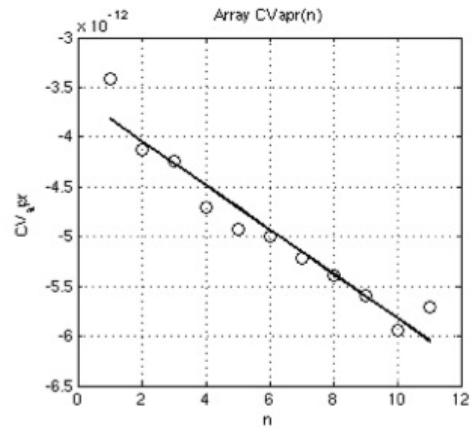
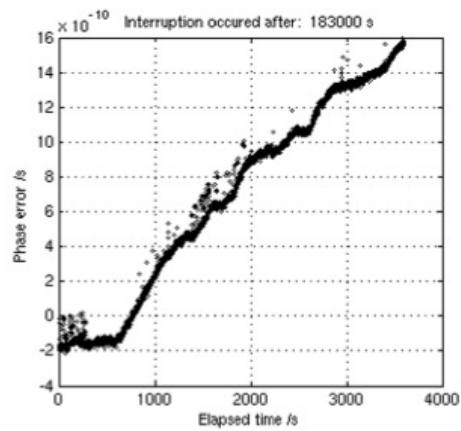
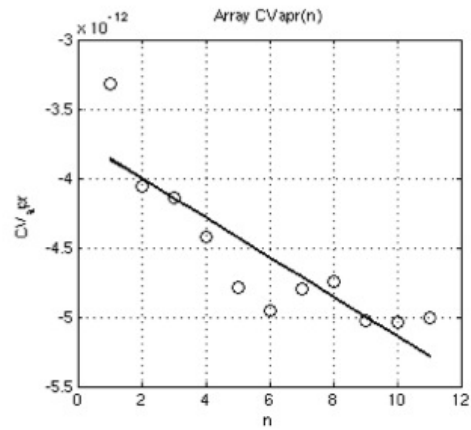
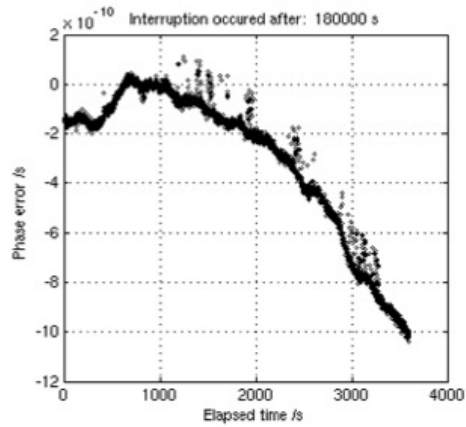


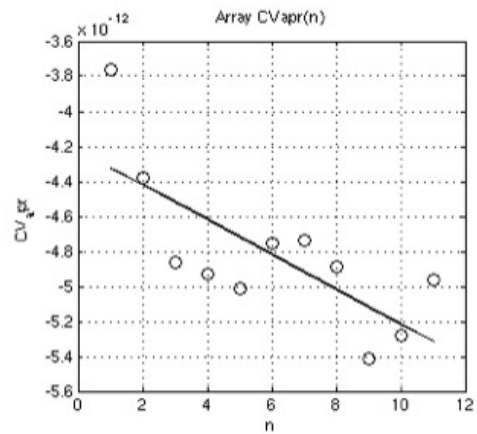
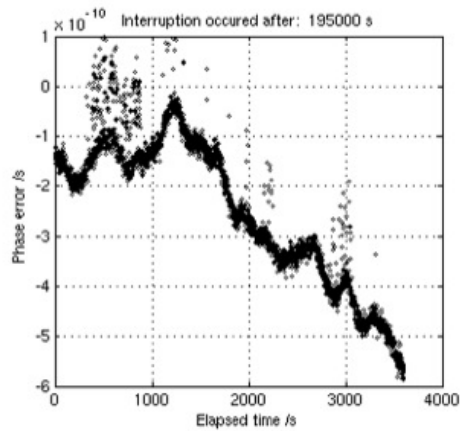
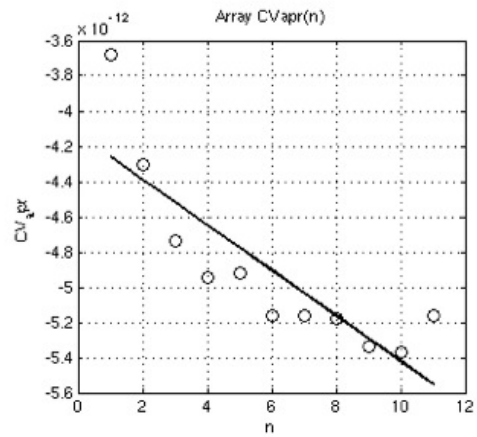
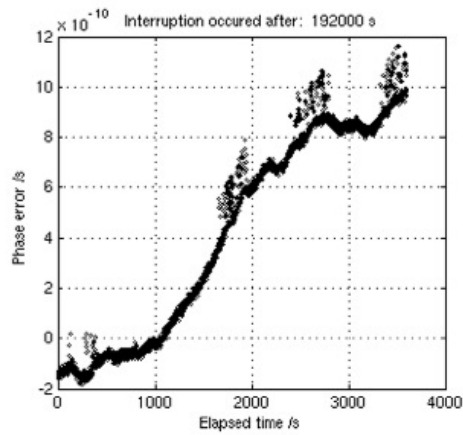
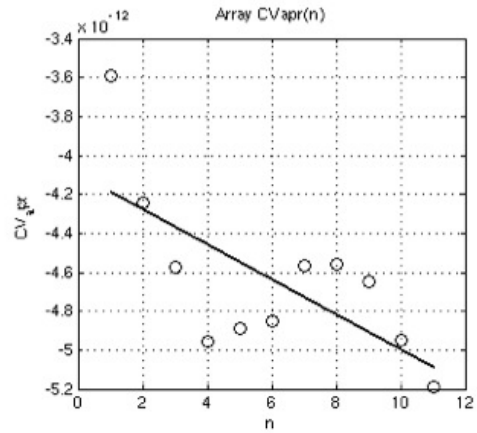
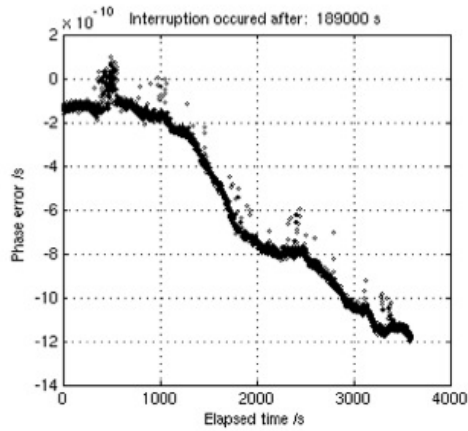


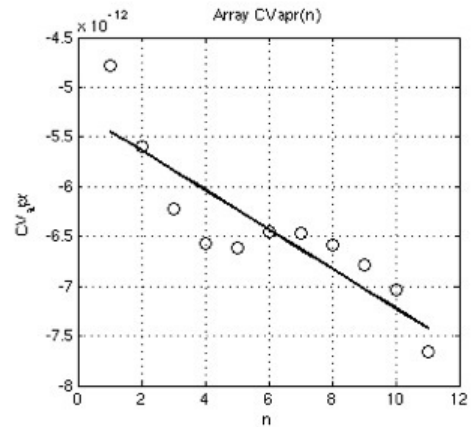
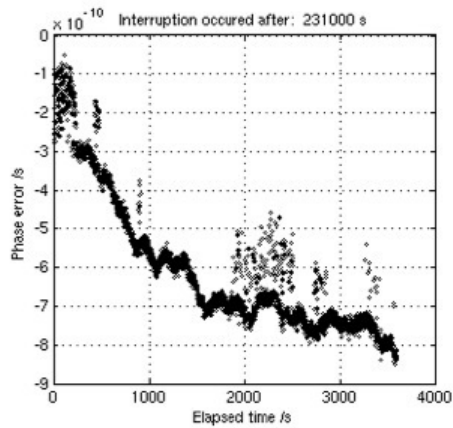
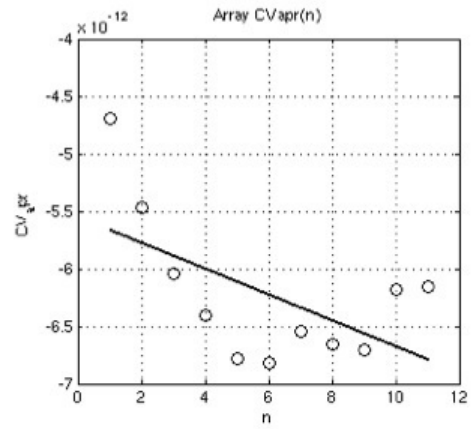
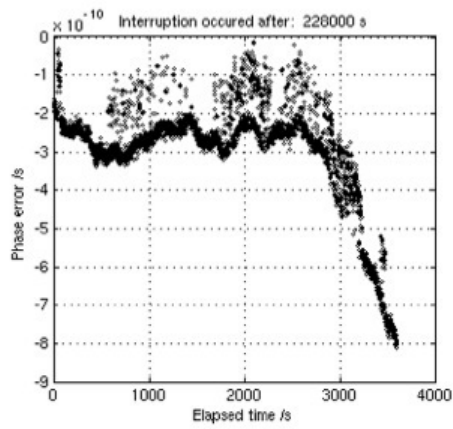
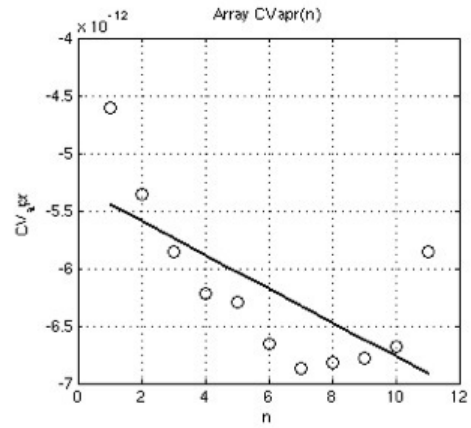
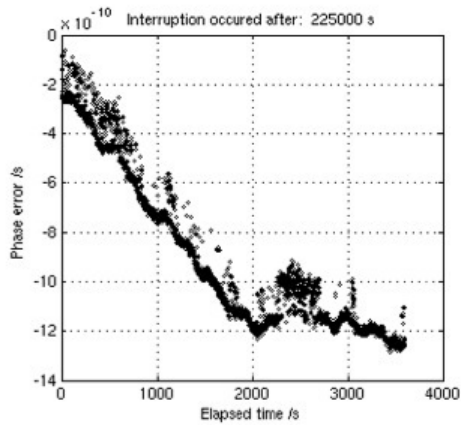


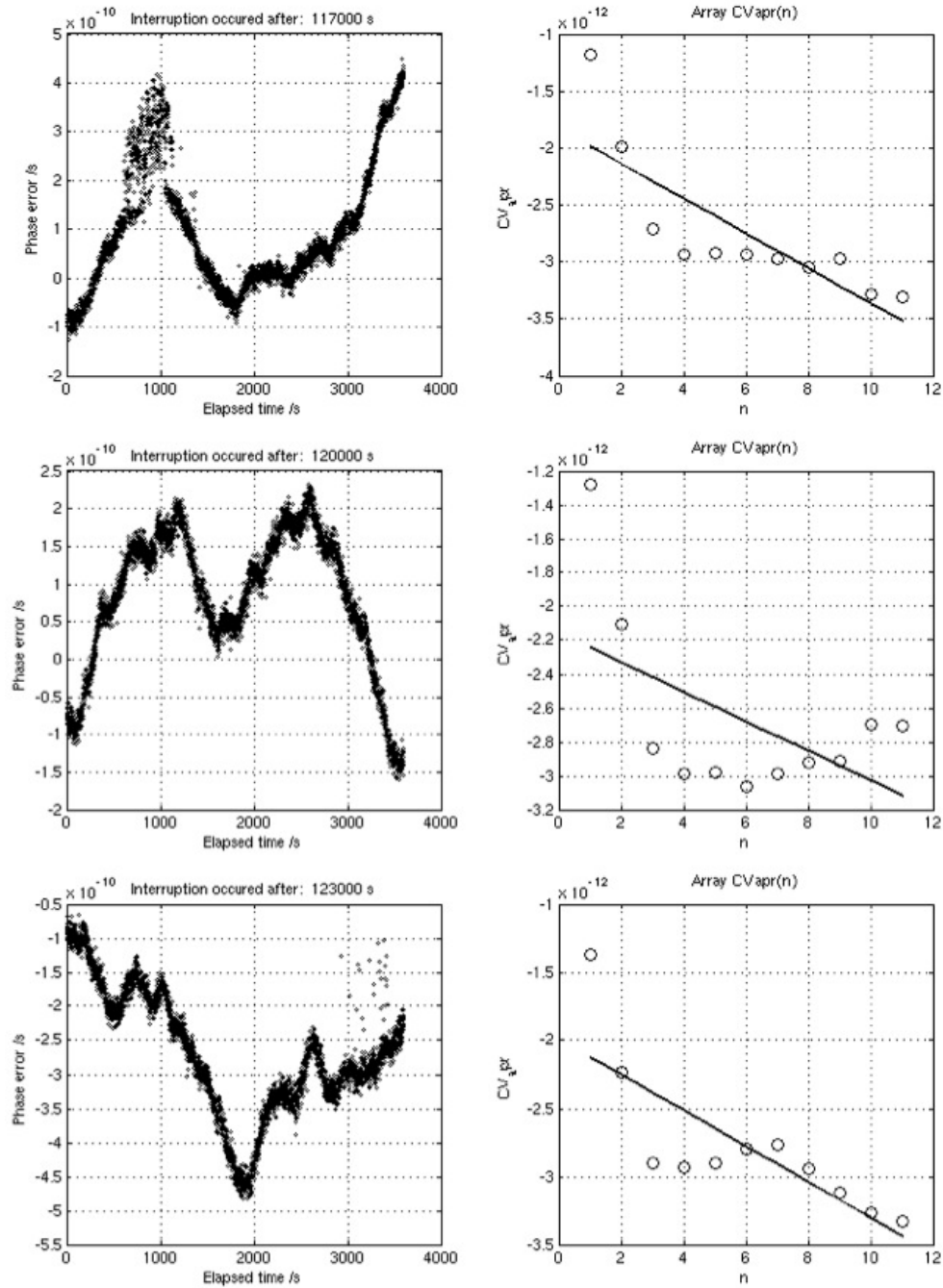












# Bibliography

- [1] AIST, National Institute of Advanced Industrial Science and Technology. [Online]. Available: <http://www.aist.go.jp>
- [2] Centre of Orbit Determination (CODE). [Online]. Available: <http://www.aiub.unibe.ch>
- [3] JAXA, Japan Aerospace Exploration Agency. [Online]. Available: <http://www.jaxa.jp>
- [4] Mitsubishi Space Software. [Online]. Available: <http://www.mss.co.jp/en/index.html>
- [5] Russian Space Agency. [Online]. Available: <http://www.glonass-ianc.rsa.ru/pls/htmldb/f?p=202:20:4969607893141445194::NO>
- [6] J. I. Ababneh and M. H. Bataineh, "Linear phase FIR filter design using particle swarm optimization and genetic algorithms," *Digital Signal Processing*, vol. 18, no. 4, pp. 657–668, 2008.
- [7] M. A. Aldajani, "Logarithmic quantization in the least mean squares algorithm," *Digital Signal Processing*, vol. 18, no. 3, pp. 321–333, May 2008.
- [8] D. W. Allan, "Device and method for providing accurate time and/or frequency," *US Patent 5,274,545*, December 1993.
- [9] F. G. Ascarrunz, S. Jefferts, and T. E. Parker, "A delay calibration system for two-way satellite time and fequency transfer," *Proceedings of the IEEE International Frequency Control Symposium*, pp. 250–253, May 1998.

- [10] N. Ashby, "Relativity in the Global Positioning System," *Living Reviews in Relativity*, <http://relativity.livingreviews.org/Articles/lrr-2003-1/>, vol. 6, no. 1, 2003.
- [11] J. Barnes, "Characterization of frequency stability," *IEEE Transactions on Instrumentation and Measurement*, vol. 20, no. 2, pp. 105–120, May 1971.
- [12] J. A. Barnes and D. W. Allan, "An approach to the prediction of Coordinated Universal Time," *Precision Measurement and Calibration*, vol. 5, p. 242, June 1972.
- [13] M. Belanger, *Digital Processing of Signals: Theory and Practice*. Wiley, ISBN: 978-0-471-97673-8, May 2000.
- [14] R. E. Best, *Phase-locked Loops: Design, Simulation and Applications*. McGraw-Hill, ISBN 0-07-141201-8, 2003.
- [15] H. Bethke, D. Ringer, and M. V. Melle, "Rubidium and cesium frequency standards status and performance of the GPS program," *Proceedings of the 16th Annual Precise Time and Time Interval (PTTI) Applications and Planning Meeting. Goddard Space Flight Center, Greenbelt, MD.*, pp. 127–141, November 1984.
- [16] M. B. Bloch, J. Ho, T. McClelland, M. Meirs, N. D. Bhaskar, L. Mallette, and J. Hardy, "Performance data on the MILSTAR rubidium and quartz frequency standards: comparison of ground tests in a simulated space environment to results obtained on orbit," *Proceedings of the IEEE International Frequency Control Symposium*, pp. 1057–1065, ISBN: 0-7803-3309-8, 5-7 June 1996.
- [17] M. B. Bloch, J. C. Ho, C. S. Stone, A. Syed, and F. L. Walls, "Stability of high quality quartz crystal oscillators: an update," *Proceedings of the 43rd Annual Symposium on Frequency Control. Denver, CO, USA*, pp. 80–84, 1989.
- [18] S. Boutiouta and A. H. Belbachir, "Monitoring the ionosphere activity from GPS data," *International Journal of Remote Sensing*, vol. 28, pp. 5617–5625, 2007.

- [19] G. Busca, L. G. Bernier, H. Schweda, N. Kardashev, V. Andreianov, I. W. Roxburgh, and S. Polnarev, “The CRONOS hydrogen maser clock redshift experiment on Radioastron,” *Advances in Space Research*, vol. 32, no. 7, pp. 1421–1428, 2003.
- [20] L. Cacciapuoti, N. Dimarcq, G. Santarelli, P. Laurent, P. Lemonde, A. Clairon, P. Berthoud, A. Jornod, F. Reina, S. Feltham, and C. Salomon, “Atomic clock ensemble in space: Scientific objectives and mission status,” *Nuclear Physics B - Third International Conference on Particle and Fundamental Physics in Space*, vol. 166, pp. 303–306, April 2007.
- [21] J. C. Campanella, “Satellite clock system,” *US Patent 4,792,963*, December 1988.
- [22] J. C. Camparo and R. P. Frueholz, “Monte Carlo simulations of precise timekeeping in the MILSTAR communication satellite system,” *The 26th Annual Precise Time and Time Interval (PTTI) Applications and Planning Meeting. San Diego, California, USA*, pp. 291–303, May 1995.
- [23] J. C. Camparo, R. P. Frueholz, and A. P. Dubin, “Demonstration of synchronization between two geosynchronous satellites without ground intervention,” *Annual Precise Time and Time Interval (PTTI). Naval observatory Washington DC, USA*, vol. 28, pp. 169–178, 1996.
- [24] J. C. Camparo and R. Frueholz, “Precise timekeeping in MILSTAR: the aerospace corporation’s Monte Carlo simulations,” *Aerospace Report*, vol. 15, no. 3, pp. 135–139, 15 May 1994.
- [25] T. Celano, J. Warriner, S. Francis, and A. Gifford, “Two-way time transfer to airborne platforms using commercial satellite modems,” in *Annual Precise Time and Time Interval (PTTI) Meeting. Reston, VA, USA*, December 2002.
- [26] P. Chu, “GPS reference clock generator,” *Patent number: 5717402*, Feb 10, 1998.
- [27] W. Cochran, “The clock paradox,” *Vistas in Astronomy*, vol. 3, pp. 78–87, 1960.

- [28] P. Colmenarejo, E. Di Sotto, and V. Barrena, "Low-cost relative navigation sensing: GNSS-like devices hosted on deployed tethers," *Acta Astronautica*, vol. 59, no. 8-11, pp. 873–881, 2006.
- [29] T. Dass, G. Freed, J. Petzinger, J. Rajan, T. J. Lynch, and J. Vaccaro, "GPS clocks in space: Current performance and plans for the future," *34 Annual Precise Time and Time Interval (PTTI) Meeting. Reston, VA, USA*, December 2002.
- [30] J. Davis, W. Lewandowski, J. De Young, D. Kirchner, D. Hetzel, P. Parker, W. Klepczynski, G. De Jong, A. Soring, F. Baumont, K. Bartle, H. Ressler, R. Robnik, and L. Veenstra, "Comparison of two-way satellite time and frequency transfer and GPS common-view time transfer during the INTELSTAT field trial," *European Frequency and Time Forum, EFTF. Brighton, UK*, pp. 382–387, March 1996.
- [31] R. V. de Moraes, A. A. da Silva, and H. K. Kuga, "Simple orbit determination using GPS based on a least-squares algorithm employing sequential givens rotations," *Mathematical Problems In Engineering*, Article ID 49781, July 2007.
- [32] A. G. Dempster, F. Tappero, and T. Iwata, "Positioning performance study of the RESSOX system with hardware-in-the-loop clock," in *International Global Navigation Satellite Systems Society. IGNSS Symposium. The University of New South Wales, Sydney, Australia*, 4-6 December 2007.
- [33] M. Der-Ming, Z. Shen-You, S.Huan-Ein, and F.-B. Hsiao, "Positioning system using low Earth orbit constellations," *Proceedings of Cospar Colloquium on Microsatellites as Research Tools*, vol. Volume 10, pp. 314–323, 1999.
- [34] H. Dittus, C. Lammerzahn, A. Peters, and S. Schiller, "OPTIS - a satellite test of special and general relativity," *Advances in Space Research*, vol. 39, no. 2, pp. 230–235, 2007.
- [35] M. Dornheim, "MILSTAR-2 brings new program role," *Aviation Week and Space Technology*, pp. 63–64, 16 November 1992.

- [36] F. Droz, "On board GALILEO atomic clocks," *GIM International*, vol. 19, no. 11, November 2005.
- [37] F. Droz, G. Barmaverain, Q. Wang, F. Emma, and P. Waller, "Galileo rubidium standard, lifetime data and GIOVE-A related telemetries," *Frequency Control Symposium, 2007 Joint with the 21st European Frequency and Time Forum. IEEE International*, May 2007.
- [38] F. Droz, P. Mosset, G. Barmaverain, P. Rochat, Q. Wang, M. Belloni, L. Mattioni, U. Schmidt, T. Pike, F. Emma, and P. Waller, "The on-board Galileo clocks: Rubidium standard and passive hydrogen maser current status and performance," *20th European Frequency and Time Forum, Braunschweig, Germany*, pp. 27–30, March 2006.
- [39] L. Essen, "The measurement of time," *Vistas in Astronomy*, vol. 11, pp. 45–67, 1969.
- [40] J. Fawcette, "MILSTAR: hotline in the sky," *High Technology*, pp. 62–67, November 1983.
- [41] E. Frayssinhes and E. Lansard, "Mission analysis of clusters of satellites," *Acta Astronautica*, vol. 39, no. 5, pp. 347–353, 1996.
- [42] R. P. Frueholz, J. C. Camparo, and A. P. Dubin, "Precise time synchronization of two MILSTAR communications satellites without ground intervention," *International journal of satellite communications*, vol. 15, pp. 135–139, 1997.
- [43] D. Gambis, "Allan Variance in Earth rotation time series analysis," *Advances in Space Research*, vol. 30, no. 2, pp. 207–212, 2002.
- [44] Gao and Yu-ping, "Applications of IGS products in GPS time comparisons," *Chinese Astronomy and Astrophysics*, vol. 29, no. 2, pp. 213–222, 2005.
- [45] F. Gonzalez and P. Waller, "Short term GNSS clock characterization using short term GNSS clock characterization using one-way carrier phase," *IEEE Interna-*

- tional Frequency Control Symposium, Joint with the 21st European Frequency and Time Forum.*, pp. 517–522, May 2007.
- [46] C. A. Greenhall, “A Kalman filter clock ensemble algorithm that admits measurement noise,” *Metrologia*, vol. 43, pp. 311–321, 2006.
- [47] D. W. Hanson, “Fundamentals of two-way time transfer by satellite,” *43rd Annual Frequency Control Symposium. Denver, CO, USA*, pp. 174–178, 1989.
- [48] H. Hassanpour, “A time-frequency approach for noise reduction,” *Digital Signal Processing*, pp. 728–738, 2008.
- [49] H. Hellwig, “Microwave time and frequency standards,” *Radio Science*, vol. 14, p. 561, 1979.
- [50] S. Hongwei, M. Imae, and T. Gotoh, “Impact of satellite motion on two-way satellite time and frequency transfer,” *Electronics Letters*, vol. 39, no. 5, pp. 482–483, March 2003.
- [51] <http://en.wikipedia.org/wiki>, “Wikipedia.”
- [52] U. Hugentobler, S. Schaer, and P. Fridez, “Bernese GPS software, version 4.2,” Astronomisches Institute, Universitat Bern (AIUB),” Software simulation tool, 2001.
- [53] Y. Ikemoto, T. Iwata, M. Imae, T. Suzuyama, F. Tappero, A. Iwasaki, and H. Murakami, “Study on control of remote synchronization system for on-board crystal oscillators during communication interruption. (Japanese),” in *Symposium on Space Technology. Hiroshima, Japan*, vol. 49, 9 November 2005.
- [54] M. Imae, M. Hosokawa, K. Imamura, H. Yukawa, Y. Shibuya, N. Kurihara, Y. Nakadan, and K. Hagimoto, “Two-way satellite time and frequency transfer networks in pacific rim region,” *IEEE Trans. Instrum. Meas.*, vol. 50, p. 559, 2001.
- [55] T. Inukai, “Onboard clock correction by means of drift prediction,” *US Patent 4,602,375*, July 1986.

- [56] A. Iwasaki, T. Iwata, Y. Fukuyama, F. Tappero, K. Hagimoto, T. Ikegami, and H. Murakami, "Software concept for remote synchronization system for on-board crystal oscillator of quasi-zenith satellite," in *24th International Symposium on Space Technology and Science, ISTS*, Miyazaki, Japan, 30 May 2004.
- [57] T. Iwata, Y. Ikemoto, M. Imae, T. Suzuyama, F. Tappero, A. Iwasaki, and H. Murakami, "Feedback control experiments of remote synchronization system for onboard crystal oscillators. (Japanese)," in *Symposium on Space Technology*, vol. 49, no. S0277B, Hiroshima, Japan, 9 November 2005, pp. 2–15.
- [58] T. Iwata, M. Imae, T. Suzuyama, Y. Kawasaki, N. Takasaki, K. Kokubu, A. Iwasaki, S. Fukushima, Y. Hashibe, F. Tappero, and A. G. Dempster, "Ground experiments of remote synchronization for onboard crystal oscillator of quasi-zenith satellites - use of multiple positioning signals for feedback control," in *38th Annual Precise Time and Time Interval (PTTI) Systems and Applications Meeting. Reston, Virginia, USA*, Article ID 462062, 5-7 December 2006.
- [59] T. Iwata, A. Iwasaki, Y. Fukuyama, T. Ikegami, H. Murakami, and K. Hagimoto, "Remote synchronization system for on-board crystal oscillator of quasi-zenith satellite system," *International Symposium on GNSS/GPS. The University of New South Wales, Sydney, Australia*, pp. 375–380, 17 November 2003.
- [60] T. Iwata, A. Iwasaki, Y. Fukuyama, F. Tappero, K. Hagimoto, T. Ikegami, and H. Murakami, "Ground tested for quasi-zenith satellite remote synchronization system for on-board crystal oscillator," in *24th International Symposium on Space Technology and Science, ISTS*, Miyazaki, Japan, 30 May 2004.
- [61] T. Iwata, Y. Kawasaki, M. Imae, T. Suzuyama, H. Murakami, F. Tappero, A. G. Dempster, N. Takasaki, A. Iwasaki, Y. Takahashi, and J. Amagai, "Design of tools and plan for remote synchronization system for quasi-zenith satellites," in *International Global Navigation Satellite Systems Society. IGNSS Symposium. Holiday Inn Surfers Paradise, Australia*, 17-21 July 2006.

- [62] T. Iwata, T. Suzuyama, A. Iwasaki, F. Tappero, and A. G. Dempster, "Remote synchronization simulation of onboard crystal oscillator for QZSS using L1/L2/L5 signals for error adjustment," *International Journal of Navigation and Observation*, p. 7, Article ID: 462062, 2008.
- [63] T. Iwata, F. Tappero, M. Imae, T. Suzuyama, H. Murakami, Y. Kawasaki, N. Takasaki, and A. Iwasaki, "Simulation and ground experiments of remote synchronization system for onboard crystal oscillators of quasi-zenith satellites," *Navigation: Journal of the Institute of Navigation*, vol. 53, no. 4, pp. 231–235, 2006.
- [64] D. G. Jablonski, W. M. Middleton, and M. E. Valkenburg, "Radio navigation systems," *Reference Data for Engineers (Ninth Edition)*, pp. 1–9, 2002.
- [65] JAXA, "Interface specification for QZSS," JAXA, Tech. Rep. ver 0.0, January 2007.
- [66] C. Jayles and M. Costes, "Ten centimeters orbits in real-time on-board of a satellite: DORIS-DIODE current status," *Acta Astronautica*, vol. 54, no. 5, pp. 315–323, 2004.
- [67] L. Jian-xun, K. Xi-zheng, and D. De-qiang, "A time-scale algorithm based on wavelet entropy," *Chinese Astronomy and Astrophysics*, vol. 31, no. 3, pp. 322–331, 2007.
- [68] H. Kato, "Double PLL device," in *Patent number: 5194828*, 1993.
- [69] W. Kester, *Mixed-signal and DSP Design Techniques*. Burlington: Analog Devices Inc., Engineering Staff, December 2002, vol. pp. 368.
- [70] D. Kirchner, "Two-way time transfer via communication satellites," *Proceedings of the IEEE*, vol. 79, no. 7, pp. 983–990, July 1991.
- [71] P. Koppang and R. Leland, "Linear quadratic stochastic control of atomic hydrogen masers." *IEEE Transactions on Ultrasonics, Ferroelectrics, and Frequency Control*, vol. 46, no. 3, pp. 517–522, 1999.

- [72] O. K. Kwon, W. H. Kwon, and K. S. Lee, "FIR filters and recursive forms for discrete-time state-space models," *Automatica*, vol. 25, no. 5, pp. 715–728, 1989.
- [73] K. M. Larson and J. Levine, "Time transfer using the phase of the GPS carrier," *IEEE transactions on ultrasonics, ferroelectrics, and frequency control*, vol. 45, no. 3, pp. 539–540, 1998.
- [74] K. M. Larson, J. Levine, L. M. Nelson, and T. E. Parker, "Assessment of GPS carrier-phase stability for time-transfer applications," *IEEE Transactions on Ultrasonics, Ferroelectrics, and Frequency Control*, vol. 47, no. 2, pp. 484–494, 2000.
- [75] J. Levine, "Time transfer using multi-channel GPS receivers," *IEEE Transactions on Ultrasonics, Ferroelectrics, and Frequency Control*, vol. 46, no. 2, pp. 392–398, 1999.
- [76] J. Levine and K. M. Larson, "Carrier-phase time transfer," *IEEE Transactions on Ultrasonics, Ferroelectrics, and Frequency Control*, vol. 46, no. 4, pp. 1001–1012, 1999.
- [77] J. Liang, B. Ji, J. Zhang, S. Wang, and F. Zhao, "Recursive least squares-like algorithms for the adaptive second-order lattice notch filter," *Digital Signal Processing*, vol. 18, no. 3, pp. 291–306, May 2008.
- [78] H. Madjid and J. M. Myers, "Adjustability as a requirement of ideal clocks," *Annals of Physics*, vol. 158, no. 2, pp. 421–432, 1984.
- [79] E. M. Mattison, "Ultra stable clocks for use in space," *Advances in Space Research*, vol. 9, no. 9, pp. 13–19, 1989.
- [80] O. Montenbruck and E. Gill, *Satellite Orbits Models, Methods and Applications*. Springer, ISBN: 978-3-540-67280-7, 2005.
- [81] D. J. Nelson and D. C. Smith, "A linear model for the distribution of signals in time and frequency with a historical perspective of conventional time-frequency distributions," *Digital Signal Processing*, vol. 18, no. 2, pp. 81–102, 2008.

- [82] C. Nicholls, "Reference timing signal oscillator with frequency stability," *US Patent 6,711,230*, March 2004.
- [83] J. S. Nielsen, "Oscillator stability monitoring and compensation system," *US Patent 6,194,970*, August 1999.
- [84] J. Oaks and M. Largay, "Global Positioning System constellation clock performance," in *34 Annual Precise Time and Time Interval (PTTI) Meeting. Reston, VA, USA*, December 2002.
- [85] B. W. Parkinson, J. J. Spilker, P. Axelrad, and P. Enge, *Global Positioning System: Theory and Applications*. American Institute of Aeronautics and Astronautics (AIAA), ISBN: 156347249X, 1996, vol. 1.
- [86] G. Petit, C. Thomas, Z. Jiang, P. Uhrich, and F. Taris, "Use of GPS ASHTECH Z12T receivers for accurate time and frequency comparisons," *IEEE Transactions on Ultrasonics, Ferroelectrics, and Frequency Control*, vol. 46, no. 4, pp. 941–949, 1999.
- [87] P. Petrovski, "QZSS - Japan's new integrated communication and positioning service for mobile users," *GPS World*, vol. 14, no. 6, pp. 24–29, 2006.
- [88] J. Petzinger, "Enhancement to the GPS block-IIR timekeeping system," in *34 Annual Precise Time and Time Interval (PTTI) Meeting. Reston, VA, USA*, December 2002.
- [89] R. Prasad and M. Ruggieri, *Applied satellite navigation using GPS, GALILEO, and augmentation systems*. Boston: Artech House, ISBN: 1580538142, 2005.
- [90] J. D. Prestage and L. Maleki, "Precision clocks in space and [alpha]-variations," *Nuclear Physics B - Proceedings Supplements*, vol. 134, pp. 163–170, 2004.
- [91] H. C. Rawicks, M. A. Epstein, and J. A. Rajan, "The timekeeping system for GPS block-2R," in *34 Annual Precise Time and Time Interval (PTTI) Meeting. Reston, VA, USA*, December 2002.

- 
- [92] H. Rawicz, "The time keeping system for GPS block-IIR," in *24th Annual Precise Time and Time Interval Meeting. McLean, VA, USA*, December 1992.
- [93] O. Robert, "Overview of digital signal processing algorithms," *IEEE Instrumentation and Measurement Magazine*, pp. 59–121, April 2002.
- [94] A. Rowe, R. Mangharam, and R. Rajkumar, "RT-link: A global time-synchronized link protocol for sensor networks," *Ad Hoc Networks*, vol. 6, no. 8, pp. 1201–1220, 2008.
- [95] L. J. Rueger, J. R. Norton, and P. T. Lasewia, "Long-term performance of precision crystal oscillators in a near-Earth orbital environment," *IEEE International Frequency Control Symposium. Hershey, Pennsylvania, USA*, pp. 465–469, 27-29 May 1992.
- [96] U. Sachmid, "Synchronized Universal Time Coordinated for distributed real-time systems," *Control Engineering Practice*, vol. 3, no. 6, pp. 877–884, 1995.
- [97] S. Scheithauer, C. Lammerzahl, H. Dittus, S. Schiller, and A. Peters, "The optis satellite, improved tests of special and general relativity," *Aerospace Science and Technology*, vol. 9, no. 4, pp. 357–365, 2005.
- [98] U. Schmid, "Synchronized UTC for distributed real-time systems," *Annual Review in Automatic Programming*, vol. 18, pp. 101–107, 1994.
- [99] Y. S. Shamaliy, "A simple optimally unbiased MA filter for timekeeping," in *IEEE Transactions on Ultrasonics, Ferroelectrics, and Frequency Control*, vol. 49, no. 6, June 2002.
- [100] Y. S. Shamaliy and O. Ibarra-Manzano, "An unbiased FIR filter for TIE model of a local clock in applications to GPS-based timekeeping," in *IEEE Transaction On Ultrasonics, Ferroelectrics and Frequency Control*, vol. 53, no. 5, May 2006, pp. 862–870.
- [101] Y. S. Shamaliy, O. IbarraManzano, R. Rojas-Laguna, and R. Vazquez-Bautista, "Studies of an optimally unbiased MA filter intended for GPS-based timekeep-

- ing,” in *33th Annual Precise Time and Time Interval Meeting. Long Beach, California, USA*, 2001.
- [102] Y. S. Shmaliy, J. Munoz-Diaz, and L. Arceo-Miquel, “Optimal horizons for a one-parameter family of unbiased FIR filters,” *Digital Signal Processing*, vol. 18, no. 5, pp. 739–750, 2008.
- [103] Y. S. Shmaliy, “GPS-based optimal Kalman estimation of time error, frequency offset and aging,” *31st Annual Precise Time and Time Interval (PTTI) Meeting. Reston, Virginia, USA*, pp. 431–440, 1999.
- [104] S. R. Stein, “Kalman filter analysis for real time applications of clocks and oscillators,” *42nd Annual Frequency Control Symposium. Baltimore, Maryland, USA*, pp. 446–452, 1-3 June 1988.
- [105] D. B. Sullivan, N. Ashby, E. A. Donley, T. P. Heavner, L. W. Hollberg, S. R. Jefferts, W. M. Klipstein, W. D. Phillips, and D. J. Seidel, “Parcs: NASA’s laser-cooled atomic clock in space,” *Advances in Space Research*, vol. 36, no. 1, pp. 107–113, 2005.
- [106] Symmetricom, “Chip scale atomic clock development,” *III-Vs Review*, vol. 18, no. 7, p. 19, September 2005.
- [107] N. Takasaki, A. Iwasaki, T. Iwata, M. Imae, T. Suzuyama, F. Tappero, and H. Murakami, “Quasi-real-time signal delay estimation using internet database,” in *25th ISTS*, Kanazawa, Japan, 4-11 June 2006.
- [108] N. Takashi, A. Iwasaki, T. Iwata, M. Imae, T. Suzuyama, F. Tappero, H. Murakami, and K. Nakajima, “End-to-end simulation of remote synchronization system for on-board crystal oscillators. (Japanese),” in *Symposium on Space Technology*, Hiroshima, Japan, 9 November 2005.
- [109] F. Tappero, A. G. Dempster, and T. Iwata, “Anomalies influence analysis of the remote synchronization system RESSOX for the Japanese Quasi-Zenith Satellite System,” in *57th International Astronautical Congress, IAC*, Valencia Spain, 2-6 October 2006.

- [110] F. Tappero, A. G. Dempster, T. Iwata, M. Imae, and Y. Takahashi, "Remote control system for the quasi-zenith satellite crystal oscillator based on the two-way time transfer method," in *International Global Navigation Satellite Systems Society. IGNSS Symposium. Holiday Inn Surfers Paradise, Australia*, 17-21 July 2006.
- [111] F. Tappero, A. G. Dempster, T. Iwata, and P. Tortora, "Low Earth orbit satellite positioning system with remotely controlled on-board clocks," in *The 3rd Workshop for Space, Aeronautical and Navigational Electronics, WSANE2007*, Perth, Western Australia, 15-18 April 2007.
- [112] F. Tappero, A. G. Dempster, and T. Iwata, "Phase error reduction method for free-run QZSS clock," in *IEEE International Frequency Control Symposium, IEEE-FCS*, Geneva, Switzerland, 29 May 2007.
- [113] F. Tappero, A. G. Dempster, and T. Iwata, "Satellite augmentation system with ground-based atomic reference," *Location*, vol. 2, no. 1, p. 46, January 2007.
- [114] F. Tappero, T. Iwata, A. G. Dempster, M. Imae, T. Ikegami, Y. Fukuyama, A. Iwasaki, and K. Hagimoto, "Proposal for a novel remote synchronization system for the on-board crystal oscillator of the Quasi-Zenith Satellite System," *Navigation: Journal of the Institute of Navigation*, vol. 53, no. 4, pp. 219–229, December 2006.
- [115] F. Tappero, T. Iwata, M. Imae, Y. Fukuyama, A. Iwasaki, K. Hagimoto, T. Ikegami, and H. Murakami, "Control algorithm of the hardware simulator for a remote synchronization system for the Japanese Quasi-Zenith Satellite System," in *ION NTM*, San Diego, USA, 24-26 January 2005.
- [116] F. Tappero, T. Iwata, M. Imae, Y. Fukuyama, A. Iwasaki, K. Hagimoto, T. Ikegami, K. Nakajima, and H. Murakami, "Software simulator for a remote time reference synchronization system of satellite-based positioning system," in *8th International Workshop on Simulation for European Space Programs, SESP*, Noordwijk, The Netherlands, 21 October 2004.

- [117] F. Tappero, T. Iwata, M. Imae, T. Suzuyama, Y. Fukuyama, and A. Iwasaki, "Positioning performance evaluation of the remote synchronization system RESSOX for the Japanese Quasi-Zenith Satellite System," in *International Symposium on GNSS/GPS. Hong Kong*, Hong Kong, 8-10 December 2005.
- [118] F. Tappero, T. Iwata, A. Iwasaki, M. Imae, Y. Fukuyama, K. Hagimoto, T. Ikegami, and H. Murakami, "Hardware experimental setup for the remote synchronization system of on board crystal oscillator," in *Symposium on Space Technology, Fukui, Japan*, 4 November 2004.
- [119] F. Taris, P. Urich, G. Petit, Z. Jiang, R. Barillet, and F. Hamouda, "The BNM-LPTF software for the frequency comparison of atomic clocks by the carrier phase of the GPS signal," *IEEE Transactions on Ultrasonics, Ferroelectrics, and Frequency Control*, vol. 47, no. 5, pp. 1140–1146, 2000.
- [120] R. F. C. Vessot, "Clocks and spaceborne tests of relativistic gravitation," *Advances in Space Research*, vol. 9, pp. 21–28, 1989.
- [121] C. H. Volk and R. P. Fmeholz, "The role of long-tern lamp fluctuation in the random-walk of frequency behavior of the rubidium frequency standard: A case study," *Journal of Applied Physics*, vol. 57, 980, 1985.
- [122] Wang and Zheng-ming, "The reduction and analysis of GPS common view data," *Chinese Astronomy and Astrophysics*, vol. 25, no. 4, pp. 490–498, 2001.
- [123] G. Wei, "Analysis of atomic clock noise," *MS thesis of Shaanxi Astronomical Observatory*, 1986.
- [124] Z. Wei-qun, L. Chuan-fu, Y. Shuang-lin, W. Guan-zhong, Z. Yi-ping, Y. Pei-hong, and Z. Jian, "A study and performance evaluation of hydrogen maser user in Chinese mobile VLBI stations," *Chinese Astronomy and Astrophysics*, vol. 25, no. 3, pp. 390–397, 2001.
- [125] A. Wu, "Investigation of the GPS block IIR timekeeping system anomalies caused by the voltage-controlled crystal oscillator (VCXO)," in *31th Annual Precise Time and Time Interval Meeting (PTTI). Reston, Virginia, USA*, 1999.

- 
- [126] F. Wu, N. Kubo, and A. Yasuda, "Performance evaluation of GPS augmentation using Quasi-Zenith Satellite System," *IEEE transactions on aerospace and electronic systems*, vol. 40, no. 4, pp. 1249–1261, October 2004.
- [127] K. Xi-zheng, L. Xiao-hui, L. Zhi-ying, and D. Fang-lin, "Stability analysis of a time scale algorithm," *Chinese Astronomy and Astrophysics*, vol. 26, no. 2, pp. 245–253, 2002.
- [128] Y. Xu-hai, H. Yong-hui, L. Zhi-gang, L. Xiao-hua, and X. wu Zheng, "An algorithm for a near real-time data processing of GPS common-view observations," *Chinese Astronomy and Astrophysics*, vol. 27, no. 4, pp. 470–480, 2003.
- [129] S. Yokota, "Accuracy of two-way satellite time and frequency transfer via non-geostationary satellites," *Metrologia*, vol. 42, pp. 344–350, May 2005.
- [130] G. Yu-ping and W. Zheng-ming, "Application of network adjustment to the GPS common-view time links for TAI computations," *Chinese Astronomy and Astrophysics*, vol. 27, no. 2, pp. 217–225, 2003.
- [131] Z. Zhao, K. Dong, and C. Xu, "Data block adaptive filtering algorithms for [alpha]-stable random processes," *Digital Signal Processing*, vol. 17, no. 4, pp. 836–847, 2007.
- [132] S. Zhu, "Optimum precise-clock prediction and its applications," *IEEE International frequency control symposium, Orlando, FL, USA*, pp. 412–417, 28-30 May 1997.